



Universitat Autònoma de Barcelona

ADVERTIMENT. L'accés als continguts d'aquesta tesi queda condicionat a l'acceptació de les condicions d'ús establertes per la següent llicència Creative Commons:  http://cat.creativecommons.org/?page_id=184

ADVERTENCIA. El acceso a los contenidos de esta tesis queda condicionado a la aceptación de las condiciones de uso establecidas por la siguiente licencia Creative Commons:  <http://es.creativecommons.org/blog/licencias/>

WARNING. The access to the contents of this doctoral thesis it is limited to the acceptance of the use conditions set by the following Creative Commons license:  <https://creativecommons.org/licenses/?lang=en>

Targeting of Breast Cancer Stem Cells to improve the Treatment of Triple Negative Breast Cancer

PhD thesis presented by

Patricia Cámara Sánchez

To obtain the degree of

PhD for the Universitat Autònoma de Barcelona (UAB)

PhD thesis carried out in the Functional Validation and Preclinical Research Group,
at Vall d'Hebron Research Institute (VHIR)

Thesis affiliated to the Department of Biochemistry and Molecular Biology from the UAB,
in the PhD program of Biochemistry, Molecular Biology and Biomedicine

Universitat Autònoma de Barcelona, September 26th 2021

Director

Dr. Ibane Abasolo Olaortua

PhD candidate

Patricia Cámara Sánchez

Tutor

Dr. Ana Meseguer Navarro

Abstract

Triple negative breast cancer (TNBC) is a heterogeneous disease distinctly aggressive, with higher rates of relapse and metastasis and shorter overall survival than other breast cancer (BC) types. Upon the lack of targeted therapies, conventional chemotherapy remains the primary treatment for TNBC. Unfortunately, most patients relapse quickly after initial remission and the acquisition of drug resistances greatly limit their treatment options. Accumulating evidences indicate that the cancer maintenance, metastatic dissemination and drug resistance are sustained by a small subpopulation of cancer cells with stem cell-like properties, termed cancer stem cells (CSCs). Interestingly, TNBC shows high numbers of CSCs, a fact that has been linked to the high rate of relapse in this subtype. The recent concepts of CSC phenotypic plasticity and the dynamic bidirectional interconversion between CSCs and non-CSCs, represent an important breakthrough in understanding tumor heterogeneity and have important therapeutic implications. Based on this knowledge, strategies to circumvent tumor relapse should carefully consider not only eliminating potential aggressive CSCs within tumors, but also targeting those signaling pathways responsible for the interconversion capacity of non-CSCs to new CSCs. Of all the therapeutic modalities currently under investigation, drug combination approaches and nanotechnology-based drug delivery systems have opened a window to more personalized and individually tailored anticancer therapies.

In this thesis, we provided two additional CSC fluorescent models of TNBC cell lines, in which these dynamic phenotypic changes could be observed both *in vitro* and *in vivo*. Thereby, expanding the battery of available cell line models for the preclinical validation of CSC-specific therapeutics before the clinical phase. From an initial subset of 17 compounds initially identified by drug repurposing studies, 8-Quinololinol (8Q) and Niclosamide (NCS) emerged as potential candidates for CSC targeting by affecting essential stemness hallmarks in different TNBC cell lines. The combination of 8Q and NCS with the chemotherapeutic drug Paclitaxel (PTX) was studied, identifying synergistic ratios with which the proliferation of bulk cancer cells and the viability of CSCs are both efficiently inhibited, counteracting the pro-CSC activity of PTX whilst reducing cell viability by inhibiting CSC essential signaling pathways. The anti-CSC activity of drug-combination was remarkably enhanced when encapsulated into polymeric micelles (PM) in addition to providing evidence of a chemosensitizing effect to PTX.

In summary, the results achieved in this thesis highlight the potential anti-CSC role of 8Q and NCS drugs in combination with PTX – either free or (co)encapsulated into PM – opening the way to a more efficacious treatment of TNBC.

Resumen

El cáncer de mama triple negativo (CMTN) engloba un grupo de tumores muy agresivos heterogéneos y que a diferencia de otros subtipos de cánceres de mama (CM), suele estar asociado a un mayor riesgo de recaída y de metástasis, y por lo tanto, a un pronóstico más desfavorable. Ante la actual falta de terapias dirigidas, la quimioterapia sigue siendo el tratamiento más utilizado para tratar este subtipo de CM. Sin embargo, la mayoría de las pacientes experimentan recidivas y desarrollan quimio-resistencia, limitando sus opciones de tratamiento. En los últimos años se ha identificado una subpoblación celular con características de célula madre que parece ser la responsable de originar y mantener los tumores. Estas células madre cancerosas (CMC), se caracterizan por su notable resistencia a tratamientos convencionales y su elevado potencial metastásico, lo que favorece la progresión tumoral y el desarrollo de recurrencia. La plasticidad celular confiere a las células tumorales poder transitar de forma reversible y dinámica entre estados epiteliales y estados mesenquimales. Estas observaciones suponen un gran avance en el conocimiento y comprensión de la heterogeneidad tumoral, además de tener importantes implicaciones terapéuticas. En este sentido, las nuevas terapias antineoplásicas no solo deben de eliminar de forma eficiente las CMC potencialmente agresivas, sino también impedir la dediferenciación de células tumorales y la consecuente adquisición de propiedades de CMC. De entre todas las disciplinas terapéuticas actualmente en investigación, tanto la terapia combinada como la nanotecnología representan una gran oportunidad en el área de la medicina personalizada y adaptada al paciente.

En esta tesis, se han desarrollado dos modelos fluorescentes de CMC en dos líneas celulares de CMTN. Ambos modelos permiten estudiar la transición dinámica celular in vitro e in vivo, además de servir como modelos preclínicos para testar la eficacia de terapias antitumorales. Con el fin de identificar fármacos con actividad anti-CMC, se hizo un cribado de un total de 17 compuestos, de los cuales finalmente se seleccionaron dos, el 8-quinolinol (8Q) y la niclosamida (NCS). Ambos compuestos mostraron la capacidad de afectar varias propiedades de las CMC, además de mostrar un potente efecto sinérgico al combinarlos con el quimioterapéutico paclitaxel (PTX) a determinados ratios. El tratamiento combinado contrarresta la actividad pro-CMC de PTX a la vez que reduce la viabilidad celular mediante la inhibición de vías de señalización. Este efecto se ve aún más potenciado si la combinación se encapsula en micelas poliméricas (MP).

En conclusión, los resultados de esta tesis demuestran el potencial efecto anti-CMC de los fármacos 8Q y NCS en combinación con PTX, y respaldan el uso de sistemas micelares como potencial herramienta para mejorar el tratamiento de CMTN.

Resum

El càncer de mama triple negatiu (CMTN) engloba un grup de tumors molt agressius heterogenis i que a diferència d'altres subtipus de càncers de mama (CM), sol estar associat a un major risc de recaiguda i de metàstasi, i per tant, a un pronòstic més desfavorable. Davant l'actual falta de teràpies dirigides, la quimioteràpia segueix sent el tractament més utilitzat per tractar aquest subtipus de CM. No obstant això, la majoria de les pacients experimenten recidives i desenvolupen quimio-resistència, limitant les seves opcions de tractament. En els últims anys s'ha identificat una subpoblació cel·lular amb característiques de cèl·lula mare que sembla ser la responsable d'originar i mantenir els tumors. Aquestes cèl·lules mare canceroses (CMC), es caracteritzen per la seva notable resistència a tractaments convencionals i el seu elevat potencial metastàtic, que afavoreix la progressió tumoral i el desenvolupament de recurrència. La plasticitat cel·lular confereix a les cèl·lules tumorals poder transitar de forma reversible i dinàmica entre estats epitelials i estats mesenquimals. Aquestes observacions suposen un gran avenç en el coneixement i comprensió de l'heterogeneïtat tumoral, a més de tenir importants implicacions terapèutiques. En aquest sentit, les noves teràpies antineoplàsiques no només han d'eliminar de forma eficient les CMC potencialment agressives, sinó també impedir la desdiferenciació de cèl·lules tumorals i la consegüent adquisició de propietats de CMC. D'entre totes les disciplines terapèutiques actualment en investigació, tant la teràpia combinada com la nanotecnologia representen una gran oportunitat en l'àrea de la medicina personalitzada i adaptada al pacient.

En aquesta tesi, s'han desenvolupat dos models fluorescents de CMC en dues línies cel·lulars de CMTN. Tots dos models permeten estudiar la transició dinàmica cel·lular in vitro i in vivo, a més de servir com a models preclínic per testar l'eficàcia de teràpies antitumorals. Per tal d'identificar fàrmacs amb activitat anti-CMC, es va fer un cribratge d'un total de 17 compostos, dels quals finalment es van seleccionar dos, el 8-quinolínol (8Q) i la niclosamida (NCS). Tots dos compostos van mostrar la capacitat d'afectar diverses propietats de les CMC, a més de mostrar un potent efecte sinèrgic al combinar-los amb el quimioterapèutic paclitaxel (PTX). El tractament combinat contraresta l'activitat pro-CMC de PTX alhora que redueix la viabilitat cel·lular mitjançant la inhibició de vies de senyalització. Aquest efecte es veu encara més potenciat si la combinació s'encapsula en micel·les polimèriques (MP).

En conclusió, els resultats aconseguits en aquesta tesi demostren el potencial efecte anti-CMC dels fàrmacs 8Q i NCS en combinació amb PTX, i donen suport a l'aplicació de sistemes micel·lars com a eina potencial per millorar el tractament de CMTN.

Table of contents

ABSTRACT	I
RESUMEN	II
RESUM	III
TABLE OF CONTENTS	IV
LIST OF FIGURES	VIII
LIST OF TABLES	XII
ABBREVIATIONS	XIII
INTRODUCTION	2
1.1. BREAST CANCER	2
1.1.1. Epidemiology and risk factors.....	2
1.1.2. Breast anatomy and breast cancer origin	5
1.1.3. Current methods for breast cancer screening and diagnosis	5
1.1.4. Classification of breast cancer	8
1.1.4.1. Traditional classification.....	9
1.1.4.1.1. Histological classification and staging	9
1.1.4.1.2. Biological classification	11
1.1.4.2. Gene expression-based classification of breast cancer.....	12
1.1.4.2.1. Luminal A and B.....	15
1.1.4.2.2. HER2-enriched	16
1.1.4.2.3. Basal-like.....	16
1.1.4.2.4. Normal-like	19
1.2. TRIPLE NEGATIVE BREAST CANCER	20
1.2.1. Triple negative breast cancer classification	20
1.3. MODELS OF TUMOR HETEROGENEITY AND CANCER PROPAGATION	23
1.4. BREAST CANCER STEM CELLS	27
1.4.1. Breast cancer stem cells properties.....	27
1.4.2. Cancer stem cell markers	29
1.4.3. Cancer stem cell identification and isolation.....	32
1.4.4. Signaling pathways regulating breast cancer stem cells	37
1.4.5. Implications of the EMT and the dynamic CSC/non-CSC conversion	41
1.5. TREATMENT OF TRIPLE NEGATIVE BREAST CANCER.....	45
1.5.1. Chemotherapy	45
1.5.1.1. Guidelines for the treatment of triple negative breast cancers	46
1.5.2. Targeted therapies in triple negative breast cancer.....	49
1.6. THERAPEUTIC TARGETING STRATEGIES AGAINST CANCER STEM CELLS	55
1.6.1. Combination therapy against cancer stem cells	63

1.7.	NANOTECHNOLOGY-BASED DRUG DELIVERY SYSTEM.....	65
1.7.1.	Targeted drug delivery systems in cancer therapy.....	65
1.7.2.	Currently used nanomedicine in breast cancer treatment and novel nanoformulations targeting CSC.....	67
	HYPOTHESIS AND OBJECTIVES.....	72
	MATERIALS AND METHODS.....	75
3.1.	MATERIALS	75
3.1.1.	Reagents and compounds	75
3.1.2.	Cell lines and culture conditions	75
3.2.	METHODS	77
3.2.1.	Generation of cell line models with fluorescently labelled CSC.....	77
3.2.1.1.	Lentiviral transduction	77
3.2.1.2.	DNA plasmid transfection	78
3.2.1.3.	CSC line validation	78
3.2.2.	In vitro bioluminescence assay for luciferase reporter proteins.....	79
3.2.3.	Anti-CSC drugs selection.....	79
3.2.3.1.	Cell viability assays by MTT in standard cultures.....	80
3.2.3.2.	Drug combination analysis.....	80
3.2.4.	Cell sorting and flow cytometry assays.....	81
3.2.4.1.	Fluorescence-activated cell sorting (FACS).....	81
3.2.4.2.	Flow cytometry assays for tdTomato+ and tdTomato- evaluation	81
3.2.4.3.	Flow cytometry assays for treatment evaluation in CSC	81
3.2.5.	Mammosphere assay.....	82
3.2.6.	Colony formation assay (anchorage-independent growth)	82
3.2.7.	Wound healing assay.....	83
3.2.8.	Matrigel cell invasion assay.....	83
3.2.9.	CSC reversion assay	84
3.2.10.	Stemness gene expression-based analysis	84
3.2.10.1.	Total RNA purification and quantification	84
3.2.10.2.	Retrotranscriptase polymerase chain reaction (RT-PCR).....	85
3.2.10.3.	Quantitative real time PCR (qRT-PCR)	85
3.2.11.	Western blot.....	86
3.2.11.1.	Protein extraction from cell cultures.....	86
3.2.11.2.	Determination of protein concentration and sample preparation.....	87
3.2.11.3.	Protein separation by SDS-PAGE and protein wet transfer.....	87
3.2.12.	In vivo studies	88
3.2.12.1.	In vivo tumorigenic and metastatic capacity assay	88
3.2.12.2.	Stem cell isolation and detection from mice blood samples	89
3.2.12.3.	In vivo therapeutic efficacy assay	90
3.2.13.	Analysis of tdTomato expression in solid tumors	91

3.2.14.	Immunohistochemistry analysis.....	92
3.2.15.	Statistical analysis	92
RESULTS	94
4.1.	GENERATION OF TNBC REPORTER CELL LINES WITH CONSTITUTIVE EXPRESSION OF LUCIFERASE AND FLUORESCENTLY LABELLED CANCER STEM CELLS	94
4.1.1.	Luciferase reporter expression in HCC-1806 and MDA-MB-468 TNBC cells	94
4.1.2.	In vitro characterization of ALDH1A1-tdTomato expressing HCC-1806 and MDA-MB-468 TNBC cells	96
4.1.3.	In vivo characterization of TNBC ALDH1A1-tdTomato cell models.....	100
4.1.3.1.	HCC-1806-Red-Fluc.ALDH1A1-tdTomato model in vivo.....	100
4.1.3.2.	MDA-MB-468-Fluc.ALDH1A1-tdTomato in vivo	103
4.1.4.	MDA-MB-468-Fluc-ALDH1A1-tdTomato in vitro reversion	107
4.2.	IDENTIFICATION OF COMPOUNDS WITH POTENTIAL ANTI-CSC ACTIVITY	110
4.2.1.	Identification of compounds with described anti-CSC preferential activity by compound library screening	110
4.2.2.	Identification of potential candidates with a high anti-proliferation activity against human breast cancer cell lines	111
4.2.3.	Identification of potential candidates with selective anti-CSC activity	115
4.2.4.	8-Quinololinol and Niclosamide affect specific stem cell-like features of breast CSC subpopulation.....	120
4.3.	COMBINED THERAPY OF ANTI-CSC DRUGS WITH CHEMOTHERAPY AS A NOVEL STRATEGY TO ENHANCE THEIR ANTI-CANCER EFFICACY FOR TNBC TREATMENT	122
4.3.1.	8Q and NCS display a synergistic effect when combined with PTX at specific ratios in different TNBC cell lines.....	122
4.3.2.	Combination of 8Q or NCS with PTX increases the anti-CSC efficacy of the drugs..	128
4.3.3.	The combination of 8Q and NCS inhibits NF- κ B and Wnt/ β -catenin signaling pathways	134
4.4.	NEW DESIGNED POLYMERIC MICELLAR SYSTEMS FOR ANTI-CANCER DRUG DELIVERY.....	138
4.4.1.	PTX-loaded Glu-decorated polymeric micelles for PTX delivery in vitro.....	138
4.4.1.1.	Physicochemical characterization of PTX-loaded glycosylated micelles.....	139
4.4.1.2.	PTX-loaded micelles enhance chemotherapeutic antitumor activity in vitro	140
4.4.1.3.	The encapsulation of PTX within glycosylated micelles improves its anti-CSC effect in vitro	141
4.4.1.4.	Evaluation of glycosylated micelles internalization in CSCs	143
4.4.2.	Evaluation of the therapeutic efficacy in vivo of PTX-loaded glycosylated micelles towards free PTX in TNBC tumor-bearing mice	145
4.4.2.1.	Anti-tumor proliferation efficacy of PTX-loaded glycosylated micelles in TNBC tumor-bearing mice.....	146
4.4.3.	Physicochemical characterization of drug-loaded Pluronic® F127 polymeric micelles	148

4.4.3.1.	Combination of 8Q or NCS with PTX within the same PM increases the efficacy of the free drugs	150
4.4.3.2.	Combination of 8Q or NCS with PTX within the same PM increases their anti-CSC efficacy	152
4.4.4.	Evaluation of the therapeutic efficacy in vivo of combination of drugs, either free or within polymeric micelles	155
4.4.4.1.	The administration of PTX in combination with free NCS enhances the anti-tumor proliferation efficacy in TNBC tumor-bearing mice	156
4.4.4.2.	The administration of PTX in combination with NCS reduces both intermediate and advanced stage of the metastatic process in vivo	159
DISCUSSION		163
5.1.	CLINICAL CHALLENGES IN THE MANAGEMENT OF TNBC	163
5.2.	CANCER STEM CELLS AND THEIR CONTRIBUTION TO TNBC HETEROGENEITY AND TREATMENT FAILURE	163
5.3.	RELEVANT CELL-BASED STRATEGIES FOR THE ISOLATION AND ENRICHMENT OF CSCs	165
5.4.	PRECLINICAL FLUORESCENT CSC MODELS OF TNBC CELL LINES FOR CSC IDENTIFICATION AND ISOLATION	167
5.5.	REPURPOSED DRUGS FOR ANTI-CSC TREATMENT	170
5.6.	COMBINED THERAPY OF ANTI-CSC DRUGS WITH THE REFERENCE DRUG PTX LEADS TO A SYNERGIC ANTI-CSC EFFECT AT SPECIFIC RATIOS	173
5.7.	THE SYNERGISTIC COMBINATION THERAPY PREVENTS PTX INDUCED CSC ENRICHMENT VIA INHIBITION CRUCIAL CSC SIGNALING PATHWAYS	176
5.8.	DRUG DELIVERY SYSTEMS TO OVERCOME DRUG RESISTANCE OF CSCs	179
5.9.	CO-ENCAPSULATION OF SYNERGISTIC DRUG RATIOS INCREASES ITS ANTI-CSC EFFICACY IN VITRO AND IN VIVO	180
5.10.	PROMISING PTX-TARGETED BC CHEMOTHERAPY TO OVERCOME MDR BASED ON GLYCOLYTIC PM	181
CONCLUSIONS		185
REFERENCES		187

List of figures

FIGURE 1. ESTIMATED NUMBER OF NEW CANCER CASES AND DEATHS AMONG WOMEN WORLDWIDE IN 2020.	2
FIGURE 2. DISTRIBUTION OF ESTIMATED BC CASES AND DEATHS AMONG WOMEN BY WORLD REGION IN 2018.....	3
FIGURE 3. MODIFIABLE AND NON-MODIFIABLE RISK FACTORS FOR BC DISEASE	4
FIGURE 4. GENERAL ANATOMY OF FEMALE BREAST	5
FIGURE 5. TRIPLE ASSESSMENT IN BREAST CARCINOMA.....	7
FIGURE 6. PROGRESSION AND HISTOLOGICAL EVOLUTION OF BC.	10
FIGURE 7. CLINICAL STAGING FOR BC ACCORDING TO TNM SYSTEM.....	11
FIGURE 8. INTRINSIC OR MOLECULAR CLASSIFICATION OF BC.....	14
FIGURE 9. MULTIDISCIPLINARY APPROACH FOR BC CLASSIFICATION.....	15
FIGURE 10. OVERLAP AMONG BASAL-LIKE, TRIPLE-NEGATIVE AND BRCA1-MUTANT BC.....	18
FIGURE 11. TRIPLE NEGATIVE BREAST CANCER MOLECULAR SUBTYPES, MAIN INVOLVED PATHWAYS AND PROMISING THERAPIES	21
FIGURE 12. MODEL OF THE HUMAN MAMMARY EPITHELIAL HIERARCHY LINKED TO CANCER SUBTYPE.....	23
FIGURE 13. MODELS OF TUMOR HETEROGENEITY AND CANCER PROPAGATION.....	25
FIGURE 14. INTERCONVERSION MODEL EXPLAINING TUMOR HETEROGENEITY.....	26
FIGURE 15. SCHEMATIC PRESENTATION OF ESSENTIAL STEMNESS CSC CHARACTERISTICS AND FUNCTIONS	28
FIGURE 16. CURRENT APPROACHES IN IDENTIFICATION AND ISOLATION OF CANCER STEM CELLS.....	34
FIGURE 17. SCHEMATIC DIAGRAM OF PLENTI6_ALDH1A1/TDTOMATO-BASED PLASMID	36
FIGURE 18. SIGNALING PATHWAYS AND EPIGENETIC AND TRANSCRIPTIONAL MECHANISMS RELEVANT FOR CSCS IN TNBC	38
FIGURE 19. EPITHELIAL-TO-MESENCHYMAL TRANSITION (EMT) AND THE REVERSE MESENCHYMAL-TO-EPITHELIAL TRANSITION (MET) PROCESS IN CELLS	42
FIGURE 20. SCHEMATIC REPRESENTATION OF THE PARTICIPATION OF CTC IN MULTIPLE STAGES OF METASTASIS.....	43
FIGURE 21. CHEMOTHERAPY TREATMENTS FOR TNBC AND THEIR MECHANISM OF ACTION.....	45
FIGURE 22. ESMO GUIDELINES-RECOMMENDED TREATMENT REGIMENS FOR NEWLY DIAGNOSED EARLY-STAGE AND REFRACTORY TNBC	47

FIGURE 23. MAIN ANTINEOPLASTIC AGENTS ACCORDING TO THE CELL CYCLE STAGE IN WHICH THEY ARE MOST EFFECTIVE	48
FIGURE 24. EMERGING THERAPEUTIC TARGETS IN TNBC.....	53
FIGURE 25. THERAPEUTICS STRATEGIES USED TO TARGET CSCS	56
FIGURE 26. EXPERIMENTAL PROTOCOL SCHEDULE FOR THE IN VIVO THERAPEUTIC EFFICACY ASSAY IN MICE	91
FIGURE 27. BIOLUMINESCENCE CHARACTERIZATION OF LUCIFERASE-TRANSDUCED TNBC CELL LINES.....	95
FIGURE 28. SCHEMATIC DIAGRAM OF PLENTI6_ALDH1A1/TDTOMATO-BASED PLASMID	96
FIGURE 29. HCC-1806- AND MDA-MB-468-TDTOMATO MODELS.....	97
FIGURE 30. STEM CELL-LIKE GENE EXPRESSION PROFILE OF ENRICHED CSC AND NON-CSC SUBPOPULATIONS FROM TNBC FLUORESCENT MODELS MEASURED BY QRT-PCR.....	98
FIGURE 31. MAMMOSPHERE CULTURE OF TDTOMATO+ AND TDTOMATO- CELLS.....	99
FIGURE 32. TUMOR INITIATION CAPACITY OF TDTOMATO+ AND TDTOMATO- IN HCC-1806.REDFLUC.ALDH1A1-TDTOMATO MODEL.....	101
FIGURE 33. PRESENCE OF TDTOMATO+ CELLS IN HCC-1806.REDFLUC.ALDH1A1-TDTOMATO TUMORS.....	102
FIGURE 34. TUMOR INITIATION CAPACITY OF TDTOMATO+ AND TDTOMATO- IN MDA-MB-468.FLUC.ALDH1A1-TDTOMATO MODEL.....	104
FIGURE 35. EVALUATION OF LUNG METASTASIS IN MDA-MB-468.FLUC.ALDH1A1-TDTOMATO MODEL	105
FIGURE 36. PRESENCE OF TDTOMATO+ CELLS IN MDA-MB-468.FLUC.ALDH1A1-TDTOMATO TUMORS.....	106
FIGURE 37. SCHEMATIC REPRESENTATION OF IN VITRO CELL REVERSION EXPERIMENTS PERFORMED IN MDA-MB-468.FLUC.ALDH1A1-TDTOMATO FLUORESCENT CSC MODEL.	107
FIGURE 38. MONITORING OF CSC REVERSION IN THE MDA-MB-468.ALDH1A1.FLUC-TDTOMATO FLUORESCENT MODEL.....	109
FIGURE 39. DETECTION OF CSC REVERSION BY TDTOMATO- CELLS OF THE MDA-MB-468 FLUORESCENT MODEL	109
FIGURE 40. SELECTED ANTI-CSC DRUGS (PART I).....	110
FIGURE 41. SELECTED ANTI-CSC DRUGS (PART II).	111
FIGURE 42. DIFFERENTIAL RESPONSES OF MCF-7 AND MDA-MB-231 CELL LINES TO TESTED COMPOUNDS.....	113

FIGURE 43. STEM CELL-LIKE GENE EXPRESSION PROFILE OF ENRICHED CSCS AND NON-CSCS FROM MDA-MB-231 FLUORESCENT MODEL MEASURED BY QRT-PCR	115
FIGURE 44. SELECTIVE ANTI-CSC ACTIVITY OF SCREENED DRUGS IN CSC AND NON-CSC MDA-MB-231 CELLS GROWN IN ATTACHMENT CONDITIONS.....	116
FIGURE 45. ANTI-CSC ACTIVITY OF SELECTED COMPOUNDS IN THE MDA-MB-231 CSC POPULATION CULTURED UNDER LOW ATTACHMENT CONDITIONS	117
FIGURE 46. EFFECT OF DRUGS IN MAMMOSPHERE FORMATION ABILITY (MSF) IN OTHER TNBC CELL LINES.....	119
FIGURE 47. EFFICACY OF 8Q AND NCS INHIBITING MIGRATION, TUMORIGENICITY AND INVASION IN MDA-MB-231 CELL LINE	121
FIGURE 48. ANALYSIS OF THE COMBINED THERAPY OF PTX WITH 8Q AND NCS ANTI-CSC DRUGS IN MDA-MB-231 CELLS	123
FIGURE 49. EFFECT OF THE COMBINATION OF 8Q AND NCS WITH PTX IN THE CELL VIABILITY OF MDA-MB-231 CELLS.....	124
FIGURE 50. SYNERGISM OF 1:2 PTX-NCS RATIO IS CONCENTRATION-DEPENDENT IN MDA-MB-231 CELLS.....	125
FIGURE 51. THE ANTI-CSC DRUGS 8Q AND NCS DISPLAYED A SYNERGISTIC INHIBITION OF CELL VIABILITY WHEN COMBINED WITH THE CHEMOTHERAPEUTIC DRUG PTX IN HCC-1806 CELL LINE	127
FIGURE 52. COMBINATION OF 8Q OR NCS ANTI-CSC DRUGS WITH PTX ENHANCES THEIR SYNERGISTIC CYTOTOXIC EFFECT IN MDA-MB-468 CELLS.....	128
FIGURE 53. ANTI-CSC ACTIVITY OF 8Q AND NCS IN COMBINATION WITH PTX IN MDA-MB-231 FLUORESCENT CSC MODEL	129
FIGURE 54. ANTI-CSC ACTIVITY OF 8Q AND NCS IN COMBINATION WITH PTX IN TNBC FLUORESCENT CSC MODELS	131
FIGURE 55. EFFECT OF THE COMBINATION OF 8Q OR NCS WITH PTX IN MDA-MB-231 MAMMOSPHERES.....	133
FIGURE 56. COMBINATION OF 8Q OR NCS ANTI-CSC DRUGS WITH PTX ENHANCES THEIR SYNERGISTIC ANTI-CSC ACTIVITY IN LOW ATTACHMENT CONDITIONS IN OTHER TNBC CELL LINES.....	134
FIGURE 57. EFFECT OF THE COMBINATION OF 8Q OR NCS WITH PTX IN NF-KB AND WNT/B-CATENIN SIGNALING PATHWAYS IN MDA-MB-231 CELLS.....	135
FIGURE 58. EFFECT OF 8Q AND PTX TREATMENTS IN THE NF-KB SIGNALING PATHWAY IN MDA-MB-231 CELLS	136

FIGURE 59. EFFECT OF NCS AND PTX TREATMENTS IN THE WNT/B-CATENIN SIGNALING PATHWAY IN MDA-MB-231 CELLS	137
FIGURE 60. MORPHOLOGICAL CHARACTERIZATION AND MACROSCOPIC APPEARANCE OF PTX-LOADED GLYCOSYLATED MICELLES	140
FIGURE 61. EVALUATION OF THE ANTI-PROLIFERATION ACTIVITY OF EGM AND PTX-GM USING MDA-MB-231 CELLS	141
FIGURE 62. THE ENCAPSULATION OF PTX WITHIN GLYCOSYLATED MICELLES REMARKABLY ENHANCED ITS ANTI-CSC ACTIVITY IN LOW ATTACHMENT CONDITIONS IN MDA-MB-231 CELLS	142
FIGURE 63. INTERNALIZATION STUDIES OF LABELLED 5-DTAF-GM IN CSC AND NON-CSC CELL SUBPOPULATIONS IN ATTACHMENT AND LOW ATTACHMENT CONDITIONS.....	144
FIGURE 64. FLOW CYTOMETRY GATING ANALYSIS STRATEGY FOR INTERNALIZATION STUDIES USED IN BOTH CELL CULTURE CONDITIONS AT TIME 0 AND AFTER 15 MIN OF MICELLES INCUBATION.....	145
FIGURE 65. EXPERIMENTAL PROTOCOL SCHEDULE FOR THE IN VIVO THERAPEUTIC EFFICACY ASSAY IN MICE OF GM-PTX	146
FIGURE 66. IN VIVO THERAPEUTIC EFFICACY OF FREE PTX AND PTX-LOADED GLYCOSYLATED MICELLES IN TNBC TUMOR-BEARING MICE	147
FIGURE 67. BODY WEIGHT CHANGE (%) FROM ALL THREE-STUDY GROUPS THROUGHOUT THE EXPERIMENT.....	147
FIGURE 68. PHYSICOCHEMICAL CHARACTERIZATION OF THE POLYMERIC MICELLES (PM).	149
FIGURE 69. THE ANTI-CANCER EFFICACY OF PM-PTX-8Q AND PM-PTX-NCS IN MDA-MB-231 CELLS.....	151
FIGURE 70. COMBINATION OF 8Q OR NCS WITH PTX WITHIN THE SAME PM ENHANCED THEIR SYNERGISTIC ANTI-CSC ACTIVITY IN LOW ATTACHMENT CONDITIONS IN MDA-MB-231 CELL LINE	153
FIGURE 71. ANTI-CSC ACTIVITY OF PM-PTX-8Q AND PM-PTX-NCS IN THE MDA-MB-231 FLUORESCENT CSC MODEL.....	154
FIGURE 72. IN VIVO THERAPEUTIC EFFICACY OF PTX IN COMBINATION WITH NCS, EITHER FREE OR ENCAPSULATED IN MICELLES IN TNBC TUMOR-BEARING MICE.....	157
FIGURE 73. BODY WEIGHT CHANGES FROM ALL FOUR-STUDY GROUPS THROUGHOUT THE THERAPEUTIC EFFICACY STUDY IN ORTHOTOPIC TNBC MICE MODEL.....	159
FIGURE 74. ANALYSIS OF INTERMEDIATE AND ADVANCED STAGE OF METASTASIS AFTER TREATMENTS.....	161

List of tables

TABLE 1. MOLECULAR INTRINSIC SUBTYPES OF BC.....	13
TABLE 2. ASSIGNMENT OF TNBC CELL LINES TO SUBTYPES BY GENE EXPRESSION ANALYSIS.....	22
TABLE 3. SUMMARY OF BREAST CSC MARKERS.....	31
TABLE 4. ADVANTAGES AND DISADVANTAGES OF CSC ISOLATION METHODS.....	35
TABLE 5. TARGETS OF TNBC UNDER ACTIVE CLINICAL EVALUATION.	51
TABLE 5. TARGETS OF TNBC UNDER ACTIVE CLINICAL EVALUATION.	52
TABLE 6. REPURPOSED DRUGS SELECTED AS POTENTIAL CANDIDATES FOR ANTI-CSC SELECTIVE TARGETING IN TNBC.....	60
TABLE 7. A SUMMARY OF THE KEY LIMITATIONS TO BC DRUG THERAPY AND THE WAYS NANOMEDICINE CAN BE USED TO OVERCOME THESE CHALLENGES.....	66
TABLE 8. FDA-APPROVED NANOMEDICINES IN ROUTINE CLINICAL USE FOR BREAST CANCER TREATMENT.....	68
TABLE 9. NANOMEDICINE FOR BREAST CSC THERAPY.....	70
TABLE 10. PRIMER SEQUENCES USED IN QRT-PCR ASSAYS.....	86
TABLE 11. LIST OF ANTIBODIES USED FOR PROTEIN DETECTION IN WESTERN BLOT ASSAYS....	88
TABLE 12. LIST OF ANTIBODIES USED FOR IMMUNOHISTOCHEMISTRY (IHC) ASSAYS.....	92
TABLE 13. SUMMARY OF THE CONCENTRATIONS TESTED IN CELL VIABILITY ASSAYS OF ALL COMPOUNDS IN MDA-MB-231 AND MCF-7 CELL LINES.....	112
TABLE 14. CYTOTOXIC EFFICACY OF SELECTED COMPOUNDS ASSESSED BY MTT ASSAYS.....	114
TABLE 15. MAMMOSPHERE FORMATION INHIBITION OF SELECTED DRUGS IN CSC.....	119
TABLE 16. MICELLAR SIZE AND SIZE DISTRIBUTION (PDI, POLYDISPERSITY INDEX) OF GLYCOSYLATED MICELLES IN THE ABSENCE (EGM) AND PRESENCE (PTX-GM) OF PTX.....	139
TABLE 17. SUMMARY OF THE MAIN CHANGES PERFORMED AND THEIR CONSEQUENCES IN THE PREPARATION PROTOCOL OF CO-LOADED MICELLAR SYSTEMS TO ENHANCE THEIR LOADING CAPACITY.....	156
TABLE 18. SUMMARY OF THE MAIN SIDE-EFFECTS DETECTED AMONG THE EXPERIMENTAL GROUPS DURING TREATMENT.....	158

ABBREVIATIONS

#	3D	Three-dimensional
	5-FU	5-fluorouracil
	6-SHO	6-shogaol
	8Q	8-quinolinol
A	ABCG2	ATP-binding cassette super-family G member 2
	AC	Adenocarcinoma
	ACE	Acetaminophen
	ADCs	Antibody-drug conjugates
	ALDH	Aldehyde dehydrogenase
	ALDH1	Aldehyde dehydrogenase 1
	ALDH1A1	Aldehyde dehydrogenase 1A1
	AR	Androgen receptors
	ASCC	Acantholytic squamous cell carcinoma
	ATP	Adenosine triphosphate
ATRA	All-trans retinoic acid	
B	BC	Breast cancer
	BL1	Basal-like 1
	BL2	Basal-like 2
	BLI	Bioluminescence imaging
	BME	Basal medium eagle
	BRCA	Breast cancer susceptibility genes
	BSA	Bovine serum albumin
C	CAFs	Cancer-associated fibroblasts
	CDH1	Cadherin 1
	CDK	Cyclin-dependent kinase
	cDNA	Complementary DNA
	CHEK2	Checkpoint Kinase 2
	CIT	Citral
	CIT	Combination index
	CK	Cytokeratins
	CMKLR1	Chemerin chemokine-like receptor 1
	COX-2	Cyclooxygenase-2
	CS	Carcinosarcoma
	CSC	Cancer stem cell
	CTC	Circulating tumor cells
CXCR1	Chemokine receptor 1	

D	DAB	3,3'-diaminobenzidine
	DAPI	4',6-Diamidino-2-phenylindole dihydrochloride
	DBT	Digital breast tomosynthesis
	DC	Ductal carcinoma
	DCIS	Ductal carcinoma in situ
	DDS	Drug delivery systems
	Dhh	Desert hedgehog
	DFT	Defactinib
	DLL1	Delta-like ligands
	DLS	Dynamic light scattering
	DMSO	Dimethyl sulfoxide
	DNA	Deoxyribonucleic acid
	DOX	Doxorubicin
	DSF	Disulfiram
	E	ECM
EDTA		Ethylenediaminetetraacetic acid
EGF		Epidermal growth factor
EGFR		Epidermal growth factor receptor
eGM		Empty glycosylated micelles
EMT		Epithelial-mesenchymal transition
EpCAM		Epithelial cell adhesion molecule
EPR		Enhanced permeability retention
ER		Estrogen receptor
ESMO		European Society for Medical Oncology
EVE	Everolimus	
F	FACS	Fluorescence-activated cell sorting
	FBS	Fetal bovine serum
	FDA	Food and Drug Administration
	FGF2	Fibroblast growth factor-2
	FLU	Flubendazole
	FZD	Frizzled domain
G	GAPDH	Glyceraldehyde 3-phosphate dehydrogenase
	gBRCAm-BC	Germline BRCA mutation associated breast cancer
	GFP	Green fluorescent protein
	GLA	Glabridin
	GLI	Glioma-associated oncogene
	Glu	Glucose
	GLUT	Glucose transporter membrane proteins
GSK3	Glycogen synthase kinase 3	

H	H&E	Hematoxylin and eosin stain
	HDAC	Histone deacetylase
	HEPES	4-(2-hydroxyethyl)-1-piperazineethanesulfonic acid
	HER2	Human epidermal growth factor receptor 2
	Hh	Hedgehog
	HIFs	Hypoxia-inducible factors
	HPLC	High performance liquid chromatography
	HR	Hormone receptor
	HRP	Horseradish peroxidase
I	i.m.f.p.	Into the mammary fat pad
	IBC	Invasive breast cancer
	IC₅₀	Half inhibitory concentration
	ICIs	Immune checkpoint inhibitors
	IDC	Invasive ductal carcinomas
	IHC	Immunohistochemical
	Ihh	Indian hedgehog
	IM	Immune modulator
	ISO	Isoliquiritigenin
J	JAG	Jagged proteins
	JAK	Janus kinase
K	KLF4	Krüppel-like factor 4
L	LAR	Luminal androgen receptor
	LEF	Lymphoid enhancer-binding factor
	LRP	Low-density-lipoprotein
M	M	Mesenchymal
	MACS	Magnetic cell sorting
	MAPK	Mitogen-activated protein kinase
	MDR	Multidrug resistance
	MET	Mesenchymal-epithelial transition
	MET	Metformin hydrochloride
	miRNAs	MicroRNAs
	MRI	Magnetic resonance imaging
	mRNA	Messenger RNA
	MSF	Mammosphere-forming efficiency
	MSL	Mesenchymal stem-like
	MSV	Mammosphere viability
	mTOR	Mammalian target of rapamycin
	MTT	3-(4,5-dimethylthiazol-2-yl)-2,5-diphenyltetrazolium bromide
	MUC1	Transmembrane glycoprotein mucin 1

N	Nab	Nanoparticle albumin-bound	
	NCCN	National Comprehensive Cancer Network	
	NCS	Niclosamide	
	NIPAM	N-isopropyl acrylamide	
	NIT	Nitidine hydrochloride	
	NPs	Nanoparticles	
	NRQ	Normalized relative quantities	
	NSAIDs	Non-steroidal anti-inflammatory drugs	
	NST	No-special-type	
O	OXPHOS	Oxidative phosphorylation	
	PALB2	Partner and localizer of BRCA2	
	PARP	Poly(ADP-ribose)polymerase	
	PARPi	PARP inhibitors	
	PBS	Phosphate buffered saline	
	pCR	Pathological complete response	
	PD-L1	Programmed-death ligand 1	
	PDGFR	Platelet-derived growth factor receptor	
	PdI	Polydispersity index	
	PEG	Polyethylene glycol	
	PET/CT	Positron emission tomography/computed tomography	
	Pgp	P-glycoprotein 1	
	P	PI3K	Phosphoinositide 3-kinase
		PIP₃	Phosphatidylinositol-3,4,5-trisphosphate
		PM	Polymeric micelles
		PM-NCS	PTX-loaded polymeric micelles
		PNB	Panobinostat
		POU5F1/OCT4	POU class 5 homeobox 1
		PPM	Precision and personalized medicine
		PR	Progesterone receptor
		PTCH	Protein patched homolog 1
		PTEN	Phosphatase and tensin homolog
PTX		Paclitaxel	
PTX-GM		PTX-loaded glycosylated micelles	
Q		qRT-PCR	Quantitative real time PCR
		RAD51C	RAD51 paralog C
R	RT	Room temperature	
	RT-PCR	Reverse transcription polymerase reaction	
	RTKs	Receptor tyrosine kinases	

S	SAL	Salimomycin
	SD	Standard deviation
	SEM	Standard error of the mean
	Shh	Sonic hedgehog
	SMO	Smoothened
	Soluplus	Polyvinyl caprolactam–polyvinyl acetate–polyethylene glycol
	SP	Side population
	SSEA-3	Stage-specific embryonic antigen-3
	STAT	Signal transducer and activator of transcription
	STK11	Serine/Threonine Kinase 11
T	TBS-T	Tris-buffered saline with 0.1% Tween 20
	TCF	T-cell factor
	TDLUs	Terminal ductal-lobular units
	tdT	tdTomato
	TEM	Transmission electron microscopy
	TGF-β	Transforming growth factor β
	TME	Tumor microenvironment
	TNBC	Triple negative breast cancer
	TNM	Tumor-node-metastasis
	TP53	Tumor protein 53
	TPGS	D-α-tocopheryl polyethylene-glycol 1000 succinate
U	UV	Ultraviolet
V	VEGFR	Vascular endothelial growth factor
	VHIR	Vall d'Hebron Institut de Recerca
	VP	Vinylpyrrolidone
	VS	VS-5584
Y	YM	YM-155 hydrochloride
*	β-OH-CDs	Hydroxypropyl-β-cyclodextrines

INTRODUCTION

INTRODUCTION

1.1. Breast cancer

1.1.1. Epidemiology and risk factors

Breast cancer (BC) is the most frequently diagnosed cancer among women worldwide, with an estimated 2.3 million new cases in 2020, representing 24.5% of total new female cancer cases [1] (**Figure 1**). Thus, female BC is nowadays the leading cause of global cancer incidence (11.7%), surpassing lung cancer (11.4%). In terms of mortality, BC is the fifth leading cause of cancer death worldwide and the first among women, being responsible for 684,996 deaths in 2020, 15.5% of all female cancer deaths [1] (**Figure 1**).

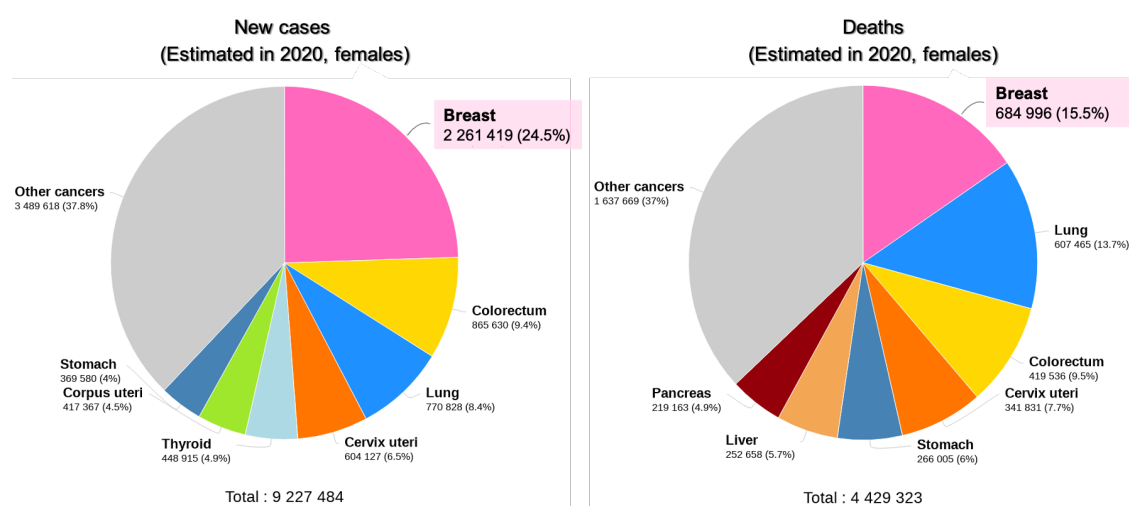


Figure 1. Estimated number of new cancer cases and deaths among women worldwide in 2020. Data source GLOBOCAN 2020 (International Agency for Research on Cancer, World Health Organization).

According to the American Cancer Society' estimations, 1 in 8 U.S. women (13%) will be diagnosed with BC at some point during their lifetime [2]. The global incidence of BC has been increasing since 1980, going from 641,000 cases to nearly 2.3 million in 2020, reflecting both growth and ageing of the population as well as changes in the prevalence and distribution of risk factors. However, since 2000s, incidence rates dropped or almost stabilized in many developed regions, including Northern America, Europe and Oceania [1]. As shown in **Figure 2**, there are large variations in estimated incidence rates worldwide. Lifetime risk of BC among females in high-income countries can be up to three times that in low-income countries. In 2018, the highest incidence rates registered in developed regions were those of Australia/New Zealand (94 cases per 100,000 female

population), Europe (90) and North America (85), whereas in low and middle-income regions, as Middle Africa (28) and South-Central Asia (26), were considerably lower.

Unlike female BC, breast carcinoma in men is a rare disease, accounting for about 1% of all patients with BC. The reason of the low incidence rate in male population is the relatively low amount of breast tissue along with the difference in their hormonal environment. In 2021, about 2,650 men are expected to be diagnosed with the disease, and an estimated 530 men are expected to die from BC. A man's lifetime risk of BC is about 1 in 833 [3].

Female BC incidence and mortality rates in 2018

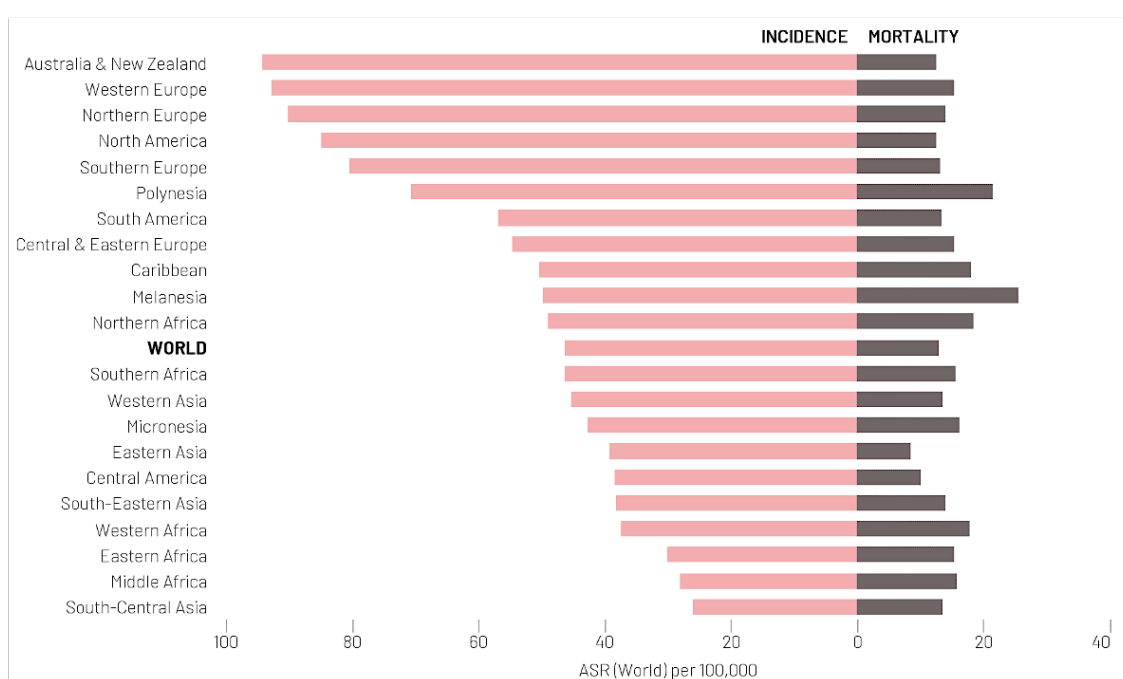


Figure 2. Distribution of estimated BC cases and deaths among women by world region in 2018. Data source Cancer Atlas book (American Cancer Society).

These variations observed in BC incidence across countries can be partly explained by differences associated with the prevalence and distribution of the major risk factors as well as to BC diagnosis at earlier stages. As such, incidence rates are often higher in developed countries that implement BC screening programs. As regards the BC mortality rates, geographic variation is less pronounced. Notably, some countries in Europe, North America, and Oceania have among the lowest mortality rates despite their high incidence rates. The mortality rates in low-income regions meet and, in some cases even exceed, those of the more developed areas, mainly attributed to delayed presentation, late stage at diagnosis and limited access to anticancer treatments [4]. However, exist other factors

that are associated with an increased risk of developing BC, including established factors that cannot be changed, such as gender, older age, ethnicity and reproductive factors (early menarche and late-onset menopause), while others are modifiable, which are mainly associated to lifestyle and environmental exposures, some of which are potentially avoidable, such as obesity, alcohol consumption, physical inactivity, hormone therapy and hormonal contraceptives [5] (**Figure 3**). Indeed, around 20% of BC cases worldwide have been attributed to these modifiable risk factors [6].

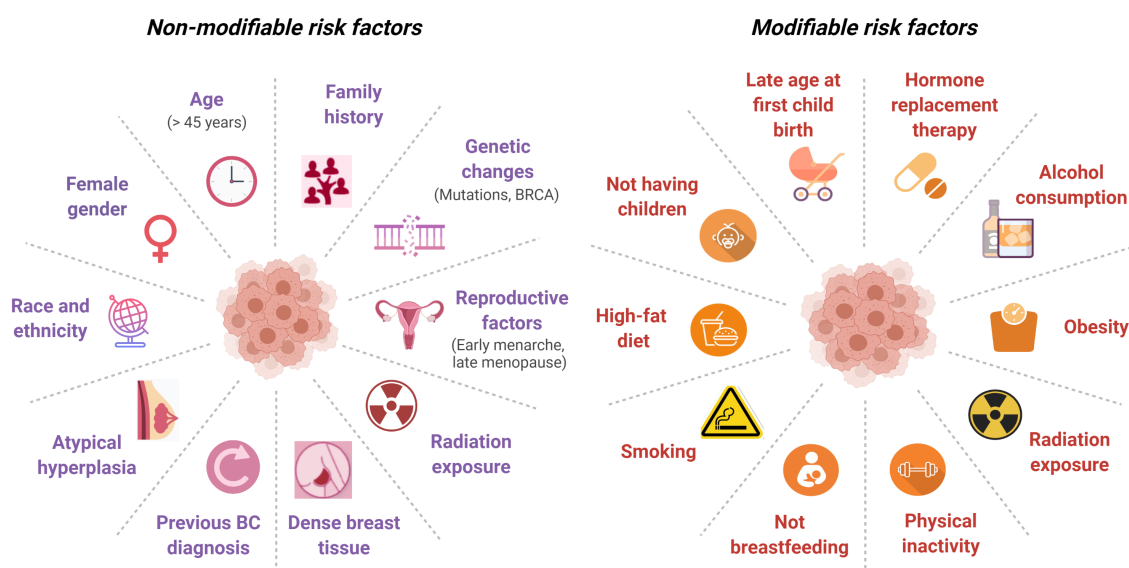


Figure 3. Modifiable and non-modifiable risk factors for BC disease. Created with BioRender.com.

BC is a multifactorial disease, and therefore, its manifestation is reliant on the interplay between lifestyle and environmental risk factors, but genetic predisposition plays a crucial role as well. Approximately 10% of BC cases are inherited and associated with a family history. Most inherited BC cases have been associated with mutations in some genes, which have been identified as drivers of the development of this disease. Mutations in two tumor suppressor genes, the breast cancer susceptibility genes BRCA1 and BRCA2, whose main functions include DNA repair and transcriptional regulation in response to DNA damage, are likely to be the only major high-penetrance genes underlying BC [7], since the cumulative risk of developing BC by the age of 80 years is 72% and 69% for BRCA1-and BRCA2 -mutation carriers, respectively [8]. However, mutations in other genes have also been identified as drivers of BC, such as TP53 (tumor protein 53), PTEN, STK11, CDH1 (cadherin 1), PALB2, CHEK2, ATM and RAD51C, which are considered rare cancer genes or moderate-penetrance genes [7].

1.1.2. Breast anatomy and breast cancer origin

The breast consists for the most part of adipose and connective tissue, enclosing a smaller proportion of glands. The glandular tissue consists of the lactiferous ducts that radiate around the nipple and the so-called terminal ductal-lobular units (TDLUs), which are the morphological and functional unit of the mammary gland (**Figure 4**). TDLUs comprise a lobule responsible for producing milk during lactation with secretory function, and a terminal duct connecting it to the duct system [9]. Most breast carcinomas arise in the TDLUs, and hence, are considered the most predominant site of BC origin [10]. Although the exact cause of BC remains unknown, several theories and etiologic factors have been proposed. Indeed, much effort has been made during the past decades to molecularly characterize BC and delineate its formation and progression, as well as for a better understanding of the natural history of this lesion. Among all breast malignancies, adenocarcinomas are the most common malignant lesion, which accounts for more than 95% of all BC, although different types of sarcomas and lymphomas have also been identified [11].

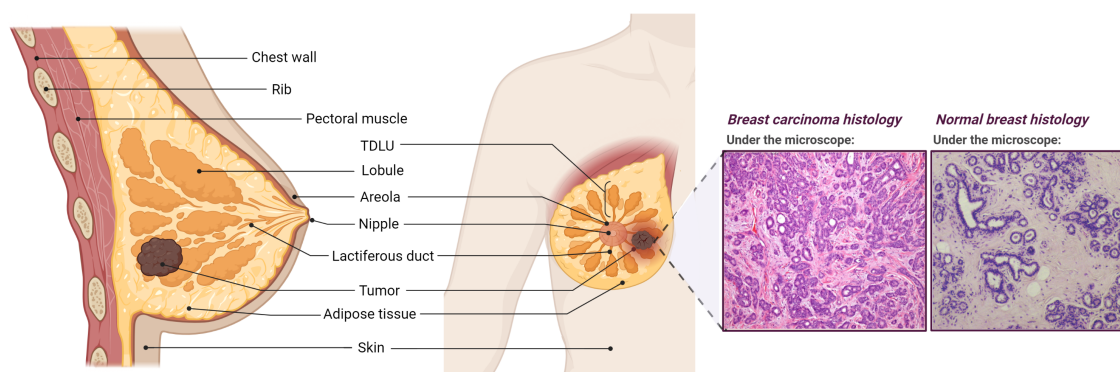


Figure 4. General anatomy of female breast. Cross section and front view of the mammary gland showing breast tumor. Histological comparison of normal and cancerous breast tissue (20x magnifications). Created with BioRender.com.

1.1.3. Current methods for breast cancer screening and diagnosis

Early diagnosis strategies have been the key to improve patients' survival and outcome of this disease, by providing an accurate identification of early-stage BC as well as greater insight regarding the most appropriate and effective therapeutic strategy for each case. Moreover, improved screening and diagnostic tools together with the development of more effective cancer treatment regimens have contributed to noticeably reducing the death rate of BC over the last decade [12,13].

Breast screening is periodically performed in women before any evident symptoms or signs appear, so that disease can be detected as early as possible. Early detection of BC has been associated with an increase in the survival rate of patients, since tumors measuring less than 2 cm in size have a 10-year survival rate of approximately 85%, while tumors larger than 5 cm, which generally correspond to a more advanced BC stage, that rate is below 60% [14]. The components of a breast screening evaluation depend on patient age and other factors, such as medical and family history, and normally include breast awareness, physical breast examination, risk assessment and imaging evaluation. By contrast, diagnostic BC evaluation is used to evaluate an existing lesion or abnormalities, primarily breast changes or breast symptoms, such as the appearance of a lump (dominant mass), discharge from the nipple, localized breast pain or skin irritation and/or skin changes [15].

BC diagnosis is based on a triple test comprising clinical examination, imaging evaluation and needle biopsy (**Figure 5**). Among the different diagnostic procedures used for BC detection, clinical examination is the most readily available mode of diagnosis, mainly because it is a simple form of early BC detection allowing the detection of tumors of at least 1-2 cm, depending on the tumor location and the breast size. To this day, it remains the most common way breast tumors are first detected, and in some cases, are identified by the affected women herself via a breast self-examination [14]. With regard to early diagnosis and systematic BC screening modalities, a variety of imaging techniques exist for the screening and evaluation of the breast, which provide the diverse characteristics of BC. The most widely used and studied modality for BC diagnosis has been film mammography, which has been the gold standard diagnostic method for BC detection for several decades. There is good evidence that the use of mammography as a diagnostic tool has resulted in a reduction of both BC specific mortality and cancer stage at time of diagnosis for women ages 50 years and older. Nonetheless, the benefits versus risks vary based on the individual's age, risk factors, and frequency of screening, and its use as imaging tool has been associated with false-positives results and over-diagnosis for some cases, by detecting small tumors on screening that would not lead to clinical significance [13,16]. In this context, there is an ongoing search for new imaging diagnostic tools in BC, such positron emission tomography/computed tomography (PET/CT), the digital breast tomosynthesis (DBT), ultrasonography and magnetic resonance imaging (MRI) (**Figure 5**). PET/CT is a well-established imaging technology commonly used for BC diagnosis and staging by using iodine-based contrast medium for breast examination [16,17]. However, due to its radioactivity and low sensitivity, is not as commonly used as other imaging methods. By contrast, DBT is a three-dimensional

(3D) approach which improves digital mammography providing a 3D image of the breast, increasing detection rate of malignant lesions and allowing an adequate evaluation of microcalcifications [16,17]. Although ultrasonography is not typically used as an initial screening modality for BC, it has been used as a supplemental tool in addition to mammography for further evaluation of suspicious areas, to assess localized symptoms, to identify and characterize screen-detected abnormalities, and above all, for certain high-risk groups, primarily women with dense breasts [16]. Importantly, ultrasonography is the primary imaging modality for guiding interventional procedures such as imaging-guide percutaneous biopsy, cyst aspiration, preoperative needle localization and drainage. Finally, MRI has been widely used for screening, detection and staging high risk BC patients as a complementary imaging technique to mammography and ultrasonography [16]. Besides, MRI is normally used under specific clinical indications, such as in women for whom conventional imaging tests have been equivocal, inconclusive or discordant, but also for evaluating women with breast implants and for evaluating women with axillary nodal metastases but no detectable or occult breast tumors [4].

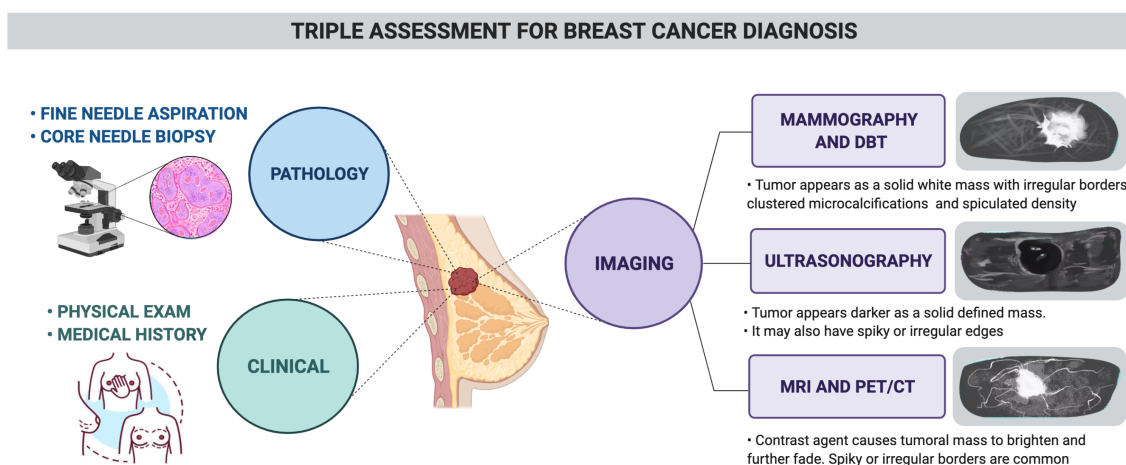


Figure 5. Triple assessment in breast carcinoma. In a patient who presents a breast lump or other symptoms suspicious of carcinoma, the diagnosis should be made by a combination of three different procedures, clinical assessment, imaging techniques and tumor tissue biopsy for histological evaluation. Created with BioRender.com.

When a lesion is detected during screening, the next step consists in accurately evaluating and diagnosing the abnormality detected as benign or malignant based on the results of a number of diagnostic procedures, including imaging techniques and microscopic examinations [14]. The vast majority of breast abnormalities found are classified as benign, meaning that the abnormal tissue is localized in the breast and has

not spread further. Both mammography and ultrasonography imaging procedures in addition to allowing the detection of small tumors in the breast, also enable to distinguish between benign and malignant lesions. However, tumor biopsies of the breast tissue are required to provide an accurate diagnosis and tumor malignancy confirmation (**Figure 5**). Indeed, tumor biopsy is still the gold standard technique that confirms if a tumor is benign or malignant via histopathology analysis and molecular evaluation. Thereafter, anatomical staging is combined with prognostic staging which comprises tumor grading, receptor status and genomic testing for a more complete diagnosis, prognosis and cancer management. In this regard, the use of suitable biomarkers for diagnosis could provide insights into BC pathogenesis, define BC molecular subtypes and contribute to a better prognosis and therapeutic approaches, as well as to a more personalized cancer management [12].

Much effort has been made during the past decades to improve BC screening and help in the assessment of breast lesions. As a result of such improvement, more cases of pre-invasive breast lesions and small tumors are detected, raising BC survival rates. However, many challenges are still need to be solved in order to differentiate benign from malignant masses at early stages, with the ultimate aim of avoiding unnecessary surgery, over-diagnosis and overtreatment.

1.1.4. Classification of breast cancer

BC is a heterogeneous disease, comprising multiple entities with different biological, histopathological and molecular properties, clinical presentation and behavior, response to treatments and outcome [18]. Traditional classification systems have been based on histopathological assessment, including histological type and grade, clinical staging and morphology to divide tumors into separate categories. However, their clinical utility in prognosis determination and risk assessment of an individual BC patient remained quite limited [19]. In this regard, a major effort has been done in the past decades to devise more clinically meaningful classification schemes, mainly based on the immunohistochemical characterization and study of the molecular basis for heterogeneity of BC. Unfortunately, the 'perfect' classification of BC still has not been reached. Herein, the different schemes developed for BC classification will be addressed with an historical perspective, from the more traditional histopathological subtypes to the newer molecular classes.

1.1.4.1. Traditional classification

1.1.4.1.1. Histological classification and staging

From a histological point of view, BC can be classified according to the histological type, grade and stage. The histological type classification categorizes breast carcinomas based on architectural features and growth patterns. BC is broadly divided into *in situ* carcinoma and invasive (infiltrating) carcinoma, depending if tumor is limited to the epithelial component of the breast or has already penetrate the surrounding stromal breast tissue (**Figure 6**). Both types can be further classified as ductal or lobular depending on the tumor cytoarchitectural features, and no for its precise location within the breast tissue, as first proposed [11]. The so-called invasive ductal carcinoma of no-special-type (NST) is the most common breast carcinoma, accounting for up to 75% of all BC cases, while the rest are classified either as lobular carcinomas (10-14%) or as special types (including different rare histotypes and their subclassifiers) [4,18]. Therefore, NST is a diagnosis of exclusion and comprises those carcinomas that cannot be classified in one of the specific histological types because they do not present sufficient morphological features. As a result, the NST subtype comprises tumors with a wide scope of morphological variation and clinical behavior, stressing the limited clinical utility of this histopathological classification in clinics [20]. Therefore, new systems were developed in order to allow clinicians to monitor their patients better, mainly based on the assessment of the histological grade of the tumor.

The histological grade classification is based on the degree of tumor differentiation (the proportion of cells that are in tubule formation), the variation of nuclear size and shape between the cells (nuclear pleomorphism) and the cell mitotic rate (cell divisions). According to this approach, BC can be classified into low, intermediate and high grade, each subtype associated with different clinical outcomes. Tumor grade has shown to reflect the potential aggressiveness of the BC and a proven ability as prognostic factor [19,21].

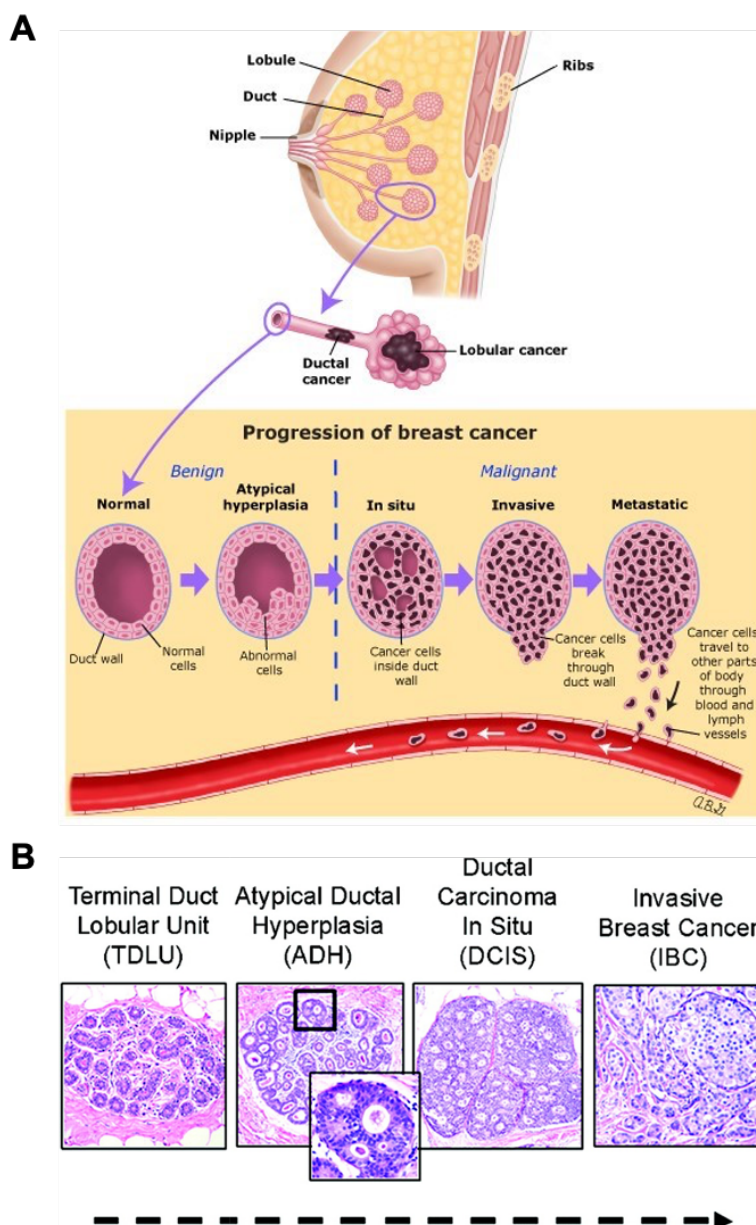


Figure 6. Progression and histological evolution of BC. A) Breast anatomy and progression of BC from breast ductal carcinoma in situ (DCIS) to invasive breast cancer (IBC). DCIS is a pre-invasive lesion with malignant atypical cells that grow within ducts and lobules that have not yet invaded the surrounding breast tissue. In order to become invasive ductal carcinoma, cancer cells have to break out of the glands and ducts and enter the stroma, thereby enabling them to spread beyond the ducts or lobules of the breast into the nearby tissue. When cancer cells reach blood and lymph vessels, they have the ability to travel and spread to distant tissues, becoming metastatic. **B)** The histologic evolution of ductal carcinoma shows the natural progression and histological continuum from hyperplasia to IBC, with DCIS immediately preceding invasive cancer. Hematoxylin and eosin (H&E)-stained tissue sections at 100x original magnification. Adapted from [22].

Staging of BC also provides valuable prognostic information for patients. The most widely used system for staging breast carcinoma is the TNM classification (TNM classification system of malignant tumors), an anatomically based system that records the extent of cancer at the primary site (tumor or T), the status of the regional lymph nodes (nodes or N) and the absence or presence of metastases (metastases or M) [21]. In this method, each category is appended with a number to specify the degree of extent and malignancy of the tumor. Most often, the higher the number assigned, the larger the cancer tumor and the more it has spread into nearby tissues. According to this system, BC is staged into five stages (from 0 to 4) by combining these T, N and M categories, of which stage 0 corresponds to non-invasive ductal carcinoma in situ, while stages 1 through 4 are used for invasive BC (explained in detail in **Figure 7**).

STAGES OF BREAST CANCER

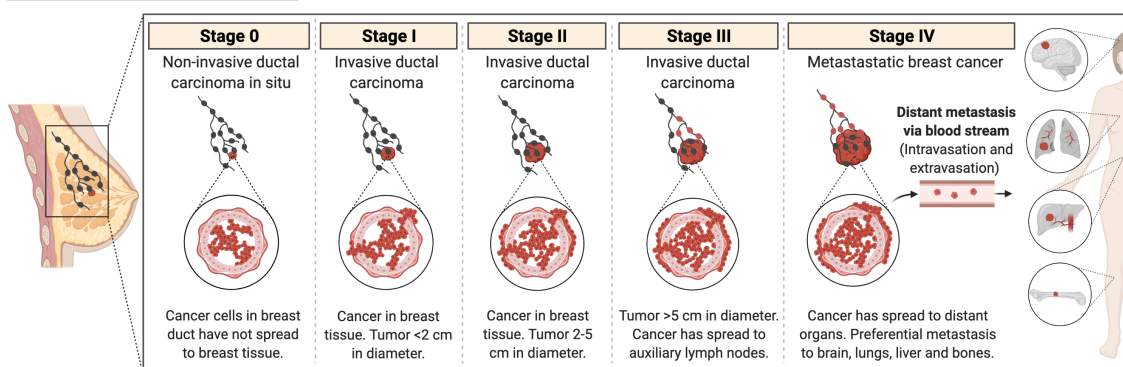


Figure 7. Clinical staging for BC according to TNM system. Progression of BC from breast ductal carcinoma in situ (DCIS) – stage 0 – to invasive ductal carcinoma (stage 1 to 3). Stage 1 corresponds to early-stage breast carcinomas smaller than 2 cm where lymph nodes are not involved (T1N0M0). Stage 2 refers to tumors in the breast tissue of 2-5 cm across, which may also spread to auxiliary lymph nodes. Stage 3 is when breast tumor is larger than 5 cm across with extensive spread to auxiliary or nearby lymph nodes. Stage 4 is when cancer has spread outside the breast and lymph nodes to distant parts of the body, like lungs, liver, brain and even bones, becoming metastatic (any T, any N, but M1). Adapted from BioRender.com.

1.1.4.1.2. Biological classification

Biological classification methods for BC were defined based on predictive biomarkers, including hormone receptors expression (estrogen -ER- and progesterone receptors -PR-) and human epidermal growth factor receptor 2 (HER2) status, to predict response to systemic treatment and as a prognostic factor for early recurrence and long-term outcome [21,23]. The immunohistochemical (IHC) determination of the ER, PR and HER2 status classifies BC into three main groups i) hormone receptor (HR)-positive ii)

HER2-positive and iii) triple-negative tumors (HR- and HER2-negative). At BC diagnosis, they are routinely tested by IHC on the formalin-fixed paraffin embedded tissue samples obtained from pre-surgical core biopsies. However, the significant differences detected among HR-positive patients in response to endocrine treatment and of patients with HER2 overexpression to trastuzumab treatment, besides those obtained in long-term survival rates, pointed out the importance of providing a more precise BC classification to tailor individualized treatment options [24].

1.1.4.2. Gene expression-based classification of breast cancer

The role of traditional classification systems in capturing the BC heterogeneity and in determining prognosis and risk of cancer of an individual patient remains quite limited, since patients with similar combination of features may have very different clinical outcomes [18,20]. For this reason, great effort has been focused on developing new molecular analytical methods to deal with the constraints identified of traditional classification systems. Molecular biology studies, such as gene expression profiling, have had a considerable impact on our understanding of BC biology, since have shown that response to treatment is not determined by anatomical factors (such as tumor size or lymph node status), but rather by intrinsic molecular characteristics of the tumor. Accordingly, the traditional classification methods have been refined and complemented with new molecular parameters [25–27].

The pioneering work by Perou, Sørlie *et al.* classified BC molecularly into distinct subtypes based on similarities in the gene expression profiles using the complementary (cDNA) microarray technology [25,26]. In this study, BC was classified into five relevant intrinsic molecular subtypes according to various gene expression: **luminal A** and **luminal B**, both reflecting ER, ER responsive genes and other genes normally expressed in luminal breast epithelial cells, but with distinct histological grade and clinical outcomes; **HER2-enriched**, reflecting tumors with HER2 (ERBB2) gene amplification and overexpression, and are mostly high-grade; **basal-like**, mostly reflecting ER, PR, and HER2 negative tumors (hence, “*triple-negative*”) together with the expression of genes expressed in normal breast basal and/or myoepithelial cells; and **normal breast-like**. These BC subtypes not only differ in terms of their gene expression patterns, but also in terms of clinical and biological features, response to treatment, patient survival and disease prognosis [25,26,28]. Besides, molecular intrinsic classification into those BC subgroups correspond reasonably well to clinical characterization on the basis of ER, PR and HER2 status, as well as cell proliferation markers (such as Ki-67) or histological grade (**Table 1**).

Table 1. Molecular intrinsic subtypes of BC.

Intrinsic subtype	Molecular characteristics (by IHC)				Grade	TP53 mutations	Outcome
	ER	PR	HER2	Ki-67			
Luminal A	+	±	-	Low <14%	1 2	Low	Good
Luminal B	+	- or low	-	High	2 3	Intermediate	Intermediate
	+	Any	Overexpressed or amplified	Any			Poor
HER2-enriched	Absent	Absent	Overexpressed or amplified	Any	2 3	High	Poor
Basal-like	-	-	-	Any	3	High	Poor
Normal-like	-	-	-	Low <14%	1 2 3	Low	Intermediate

ER, estrogen receptor; PR, progesterone receptor; HER2, human epidermal growth factor receptor 2.

Further research demonstrated a relation between intrinsic subtypes and response to various therapeutic modalities in adjuvant and neoadjuvant settings, showing the potential of this classification as a valuable tool to predict clinical outcomes and prognosis. This genetic information based on molecular profiling is more clinically useful in guiding therapy and defining prognosis in an individual BC patient than morphology alone [29]. Currently, clinical practice typically uses a surrogate classification of five subtypes on the basis of histological and immunohistochemical biomarkers (ER/PR/HER2/Ki-67) and molecular characteristics (**Figure 8**).

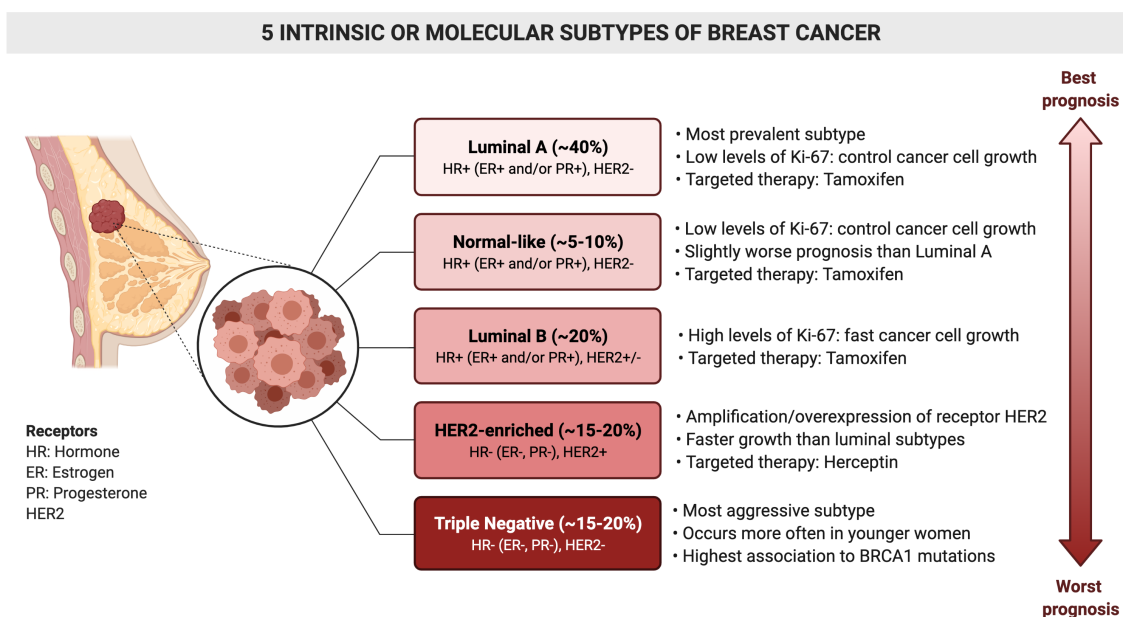


Figure 8. Intrinsic or molecular classification of BC. BC subtypes can be categorized based on their expression of hormone receptors (estrogen receptor (ER) and progesterone receptor (PR)), the proliferation marker Ki-67, and the receptor tyrosine kinase HER2. Targeted therapies, such as Herceptin® (aimed at the HER2 protein) and Tamoxifen (aimed at the ER), can be used in the treatment of certain BC subtypes. Prognosis varies based on the subtype of BC. Reprinted from "Intrinsic and Molecular Subtypes of Breast Cancer", by BioRender, 2021.

Gene expression profiling of breast tumors was closely followed by the development of high-throughput microarray-based commercial assays to improve risk stratification and accurate prognosis determination based on the gene quantification of multiple genes. These assays use a collection of genes rather than individual genes to identify a particular tumor in relation to its biological behavior. The three commercially available multigenic assays are i) Prosigna® (PAM50), ii) MammaPrint® and iii) Oncotype DX® assay [30–32]. The application of microarray-based gene-expression analysis has helped to uncover multi-gene expression markers that were independent of classical anatomical markers, and thus, led to the development of a BC classification system based on tumor biology rather than morphology. Likewise, the application of genomic and expression profiling studies also evidenced that BC is a complex and molecularly heterogeneous disease with different clinics containing different gene expression patterns that influence prognosis, response to therapy and tumor aggressiveness [33–35]. Hence, the translation of gene-expression profiling technology into clinical practice would improve the current conventional IHC-based clinical subtyping approach, allowing the execution of more personalized treatment plans for each subset of BC patients (Figure 9).

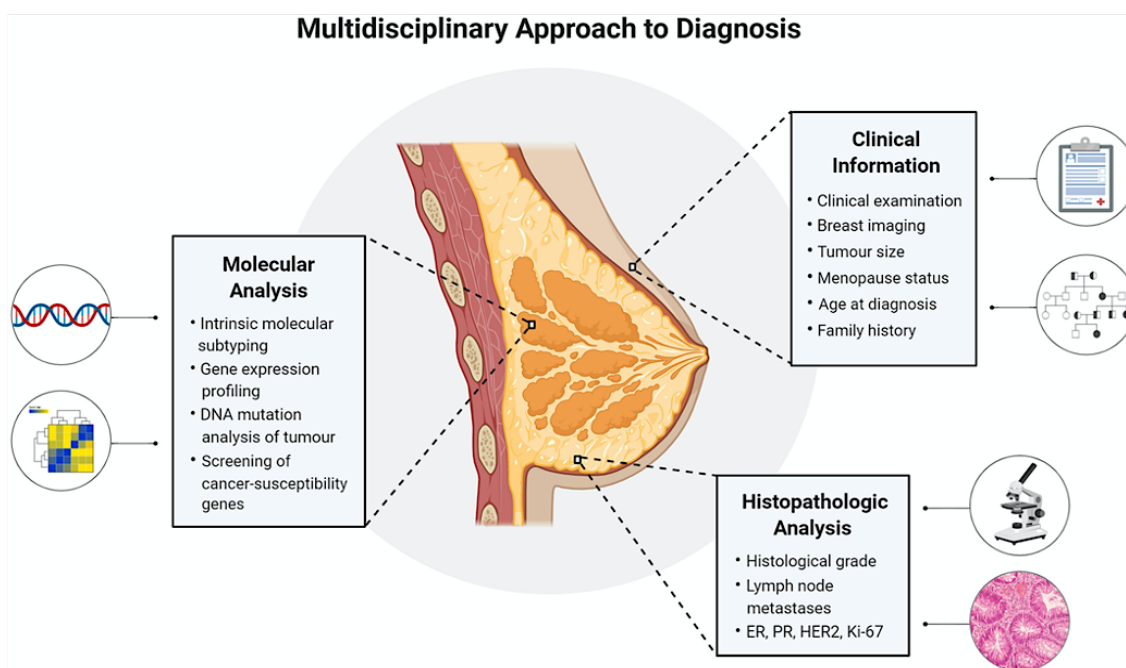


Figure 9. Multidisciplinary approach for BC classification. Integration of clinical information with histopathological and molecular analysis would result in a better diagnosis and patient monitoring, and tailoring treatment to the individual patient. Taken from [36].

1.1.4.2.1. Luminal A and B

These tumors have characteristics of luminal epithelial cells of the breast, including high expression of low molecular weight cytokeratins (CK7/8/18/19), hormone receptors and associated genes. The expression status of proliferation linked genes is one of the most important factors of the difference between luminal A and luminal B breast cancers [37]. Luminal A is the most common intrinsic subtype representing 40% of newly diagnosed BC cases. This subtype was defined as ER-positive, high expression of PR, HER2-negative and low levels of proliferation associated genes, such as Ki-67 (<14%). Luminal A tumors usually have a low histological grade, are associated with a highly favorable prognosis and good outcome, and generally show less lymph node involvement (**Table 1** and **Figure 8**) [11,38]. On the other hand, the luminal B subtype accounts for 20% of all BC cases. Luminal B is IHC defined as ER/PR-positive, while HER2 expression is variable, hence, this subtype can be further categorized into luminal B HER2-negative (ER-positive, PR-negative, HER2-negative with high levels of Ki-67) and HER2-positive (ER-positive, HER2-positive and low/high levels of both PR and Ki-67). Moreover, luminal B cancers usually have a high histological grade and a more aggressive phenotype than subtype A (**Table 1** and **Figure 8**) [11,37].

Patients with both luminal subtypes are treated with endocrine therapy, either based on selective estrogen receptor modulators (tamoxifen) or aromatase inhibitors (anastrozole), although the degree of response differs depending on subtype. The luminal B subtypes are linked with a significantly worse prognosis when compared with the luminal A. This difference is mainly due to variations in response of luminal A and B breast cancers to endocrine anti-estrogen treatment, being higher for the luminal A subtype. For this reason, luminal B tumors usually benefit from chemotherapy added to endocrine therapy [39,40]. Therefore, treatment for luminal B cancers is challenging and much effort needed to find new pathways involved to target them.

1.1.4.2.2. HER2-enriched

This group of cancers is characterized by the overexpression and/or amplification of the HER2 gene located in the 17q12 chromosome, and by its low expression of ER and associated genes. HER2-enriched cancers constitute about 15-20% of all new diagnosed BC cases. These cancers express low levels of luminal genes and their IHC profile is defined as ER-negative and HER2-positive (**Table 1** and **Figure 8**) [11,28]. It is worth mentioning that not all HER2 amplified or overexpressing tumors fall under the HER2-enriched intrinsic category, because if the tumor is also positive for ER expression will then fall within the luminal B subtypes [27]. Generally, HER2-enriched subtype is more likely to be high histological grade, lymph node metastasis positive, highly proliferative (high Ki-67 expression) and is characterized by a more aggressive biological and clinical behavior, leading to short disease-free survival and worse prognosis [11,24]. They have increased sensitivity to certain cytotoxic agents such as doxorubicin, relative resistance to hormonal agents and a propensity to metastasize to the brain and visceral organs. However, targeted anti-HER2 therapies such as trastuzumab (Herceptin[®]) have been substantially developed during last decade, improving the survival of patients with both metastatic and primary cancers [41].

1.1.4.2.3. Basal-like

The basal-like cancer is an aggressive molecular subtype that represents up to 15% of all breast carcinomas, and is so named due to its pattern of expression that is similar to basal epithelial cells of the normal breast. Basal-like tumors are typically characterized by a high expression of basal cytokeratins (CK5/6, CK14, CK17), CD44, epidermal growth factor receptor (EGFR) and/or c-kit positive, P-cadherin expression, low or no expression of ER and PR and their associated genes, and low levels of HER2 amplification (**Table 1**) [29,42,43]. Generally, basal-like tumors are characterized by

having an onset at a younger age, a high histological grade, a high frequency of lymph node infiltration and a larger tumor size at diagnosis [44]. Furthermore, high rate of mutations in tumor protein 53 (TP53) gene and genomic instability are common in this subtype, together with a high proliferation rate (high Ki-67 expression), features that could explain their enormous aggressiveness and poor prognosis [11,43]. Germline mutation in BRCA1 gene give rises to sporadic BC, which approximately 70% cluster with the basal-like subtype (**Figure 10**) [44]. This indicates that a mutation in this gene predisposes for the development of basal-like cancer subtype and is associated with the lack of expression of ER and poor prognosis. The BRCA1 gene is located on chromosome 17 and is related with both inherent DNA damage sensing processes and DNA repair mechanisms. Importantly, its inactivation leads to the accumulation of errors and genetic instability favoring the growth of tumors [43,44].

Histologically, basal-like BC are generally invasive ductal carcinomas (IDC) with a high nuclear grade and mitotic rate, pushing margin of invasion and lack of tubule formation. This subtype of tumors often presents necrotic areas and lymphocytic stromal infiltrate [19,44]. As for patterns of recurrence, the metastasis tend to be more aggressive and visceral (mainly lung, central nervous system and lymph nodes), resulting in a relatively high mortality rate [44,45]. All these characteristics make basal-like BC a very aggressive cancer for which there is no targeted therapy available, since these tumors do not respond to hormone nor HER2-targeted therapy. As a result, standard care for patients with basal-like BC includes surgery followed by post-operative (adjuvant) radiotherapy and anthracycline- and taxane-based chemotherapy. Although basal-like cancers show higher response rates to chemotherapy than luminals, the risk of relapse is higher during the first 3 years [42].

The IHC profile of these cancers is defined as ER-/PR-/HER2-negative and therefore, in clinical terms is referred as 'triple negative breast cancer' (TNBC) [28]. Although most TNBC fall into the basal-like subtype, it is important to emphasize that the terms *basal-like* and *triple negative* are not completely synonyms and there is approximately 30% discordance across studies (**Figure 10**). Hence, they should be regarded as different but overlapping categories [46,47]. The term of *triple-negative* is based on the IHC classification referring to tumors lacking ER, PR and HER2 protein expression, whereas the *basal-like* is described by gene expression microarray analysis [25,43].

Of note, an additional intrinsic subtype of BC, known as claudin-low, was identified years later in human and mouse tumors [48] and in BC cell lines [49], showing several common features with basal-like tumors and reflecting the diversity of tumors with a low luminal

differentiation status. Importantly, basal-like and claudin-low tumors form the majority of TNBC. A hallmark of the claudin-low subtype is the low expression of genes involved in tight junctions and cell-cell adhesions, including claudins 3, 4, and 7, occludin, and E-cadherin, as well as showing high expression of epithelial-mesenchymal transition (EMT) genes, immune response genes and cancer stem cell-like features, but are in many other aspects remarkably heterogeneous. Clinically, the majority of claudin-low tumors are poor prognosis triple negative IDC with a high frequency of metaplastic and medullary differentiation [28,49]. Moreover, patients with claudin-low tumors had a worse overall survival when compared to patients with luminal A type BC [50]. However, the pioneer work conducted by Fougner, Sørli *et al.* have recently reported that claudin-low is not simply a subtype analogous to the intrinsic subtypes as previously portrayed, but is a complex additional phenotype which may permeate breast tumors of various intrinsic subtypes [51]. Therefore, these findings not only elucidate the heterogeneity in claudin-low breast tumors, but also substantiate a re-definition of claudin-low as a cancer phenotype.

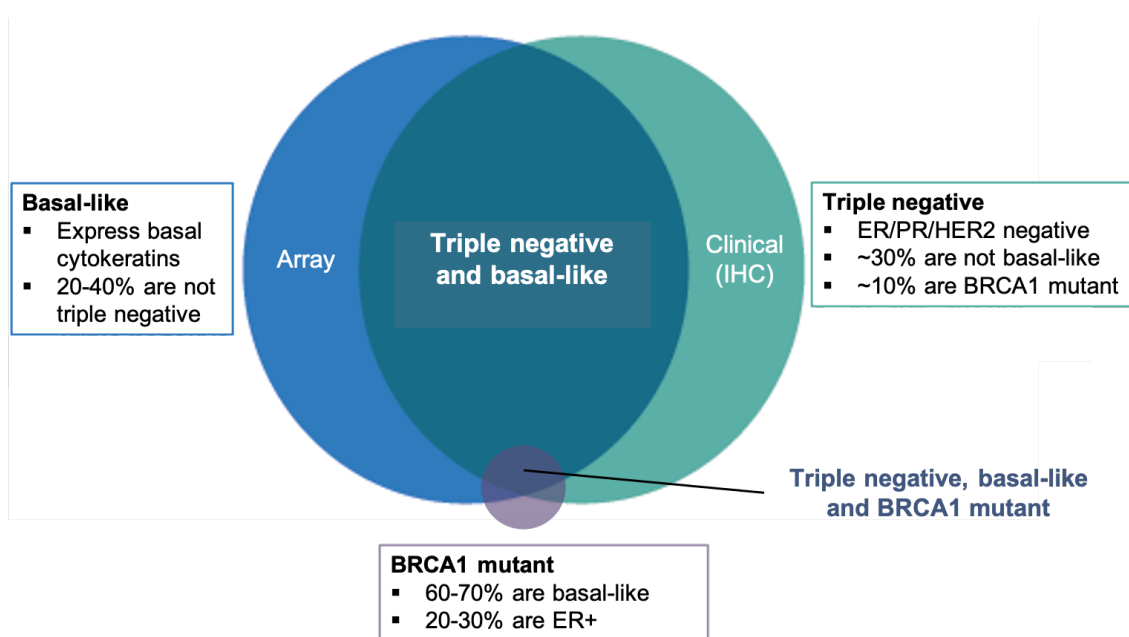


Figure 10. Overlap among basal-like, triple-negative and BRCA1-mutant BC. Most TNBC are basal-like and vice versa. While most BRCA1-mutant BC are both TNBC and basal-like, only a small proportion of total TNBC or basal-like are BRCA1-mutant. Triple-negative term is based on IHC classification referring to tumors lacking ER, PR and HER2 expression, whereas the basal-like is described by gene-expression microarray analysis.

1.1.4.2.4. Normal-like

The normal-like subtype accounts for about 5-10% of all breast carcinomas. Sørli *et al.* revealed that this BC subgroup expresses gene characteristics of adipose and other non-epithelial cell types. These tumors also showed strong expression of basal epithelial genes and low expression of luminal epithelial genes, presenting an intermediate prognosis between luminal and basal-like cancers and usually do not respond to neoadjuvant chemotherapy. According to this gene expression data, this subtype resembles the normal breast tissue profiling [26]. Normal-like tumors lack the expression of ER, PR, and HER2, and low levels of Ki-67 (**Table 1** and **Figure 8**). Although these tumors lack the expression of all three markers, are not considered basal-like cancers, as they are also negative for CK5 and EGFR [25]. However, there are few studies on this subtype and their clinical significance remains to be determined. Indeed, the existence of these tumors has been questioned and some researchers believe they could in fact be a technical artifact from high contamination with normal tissue during the microarrays [52,53]. Therefore, future larger studies should be necessary to address the existence of this breast tumor subtype.

1.2. Triple negative breast cancer

The definition of TNBC applies to all tumors that lack the expression of ER, PR and HER2, and represents 15 to 20% of newly diagnosed BC cases (**Figure 8**) [54]. Within TNBC disease, all the intrinsic molecular subtypes can be identified, although the vast majority fall into the basal-like subtype (**Figure 10**). TNBC is characterized by an increased proliferation rate (Ki-67 index > 30%), an earlier age of presentation and a significant association with BRCA1 germline mutations. Furthermore, the tumor suppressor gene TP53 and several DNA repair genes, particularly the BRCA genes, are either mutated or abnormally expressed in TNBC [26]. Patients with TNBC usually have a relatively poorer outcome compared with those with other BC subtypes owing to an inherently aggressive clinical behavior, higher rates of relapse and risk of metastasis and a lack of recognized molecular targets for therapy [54,55].

1.2.1. Triple negative breast cancer classification

As a result of the improvement in the molecular and expression profiling technologies, much progress has been made over the last years in understanding the molecular complexity of this disease. Nowadays, TNBC is considered a heterogeneous group of tumors with regard to its histological features, biomarker expression profile, clinical course and prognosis. Different molecular studies have divided TNBC into different subtypes opening the door to potential new-targeted treatment options [56].

The majority of TNBC cases (95%) are classified histologically as IDC-NST and lack distinctive histological characteristics. However, there are other less frequent histologic variants, as metaplastic, medullary and apocrine carcinomas [57].

In the last years, many gene expression profiling studies have been focused on better understanding of the heterogeneity of this particularly aggressive form of BC. Lehmann *et al.* clustered TNBC into six additional subtypes on the basis of gene-expression profiles: basal-like 1 (BL1), basal-like 2 (BL2), an immune modulator (IM), a mesenchymal (M), mesenchymal stem-like (MSL) and luminal androgen receptor (LAR). Each subtype display unique ontologies and differential response to standard-of-care chemotherapy (**Figure 11**) [58]. Later, the same authors re-classified these TNBC molecular subtypes from six into four tumor-specific subtypes, the BL1, BL2, M and LAR, and demonstrated differences in diagnosis age, grade, local and distant disease progression and histopathology [59]. Subsequent gene expression studies demonstrate an overlap between this molecular TNBC subtype classification and the intrinsic

classification of BC defined by Perou *et al.* [60]. Gene expression analysis by PAM50 revealed that four of six TNBC subtypes were classified within intrinsic basal-like tumors (BL1 (99%), BL2 (95%), IM (84%) and M (97%)), with the exception of MSL and LAR subtypes. For MSL TNBC, about 50% were classified as basal-like, 28% as normal-like and 14% as luminal B tumors, whereas tumors within the LAR subtype were mainly classified as HER2-enriched (74%) or luminal B (14%). During the last decade, numerous studies have developed exclusive molecular classifications for TNBC, defining distinct molecular subgroups, as the claudin-low and interferon-rich subtypes [49,61].

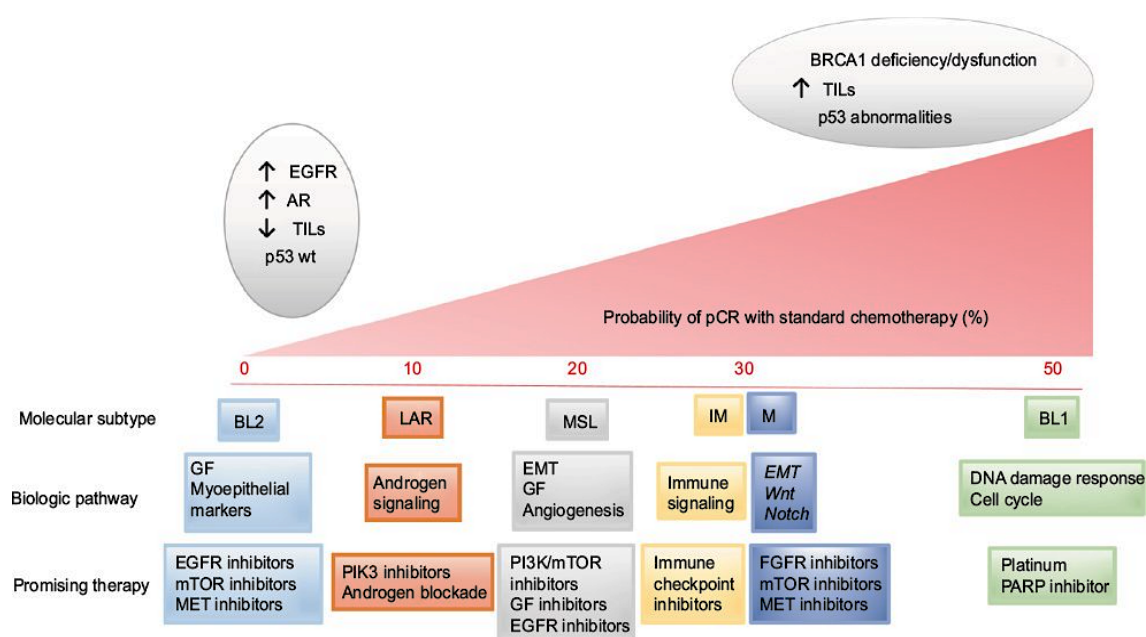


Figure 11. Triple negative breast cancer molecular subtypes, main involved pathways and promising therapies. Each of these subclasses show varying pathological complete response (pCR) rates following standard neoadjuvant chemotherapy. Promising therapies for every molecular subtype have been suggested, based on the main signaling pathways involved in each subtype. Taken from [62].

While these insights have yet to translate into clinical utility, they have provided valuable information to unveil the biological complexity and molecular basis for heterogeneity of this particular BC subtype. All the progress that has been made over the last decade on TNBC molecular stratification, based on unique cellular signatures and global RNA expression profiles, may provide therapeutic insights for each specific subset of TNBC patients. Therefore, using the molecular-based TNBC classifications, new subtype-specific tumor vulnerabilities and actionable drug targets may be identified to further increase the efficacy of current and novel therapies to treat chemo-resistant, late-stage, and metastatic TNBC tumors, and ultimately, to improve outcomes for TNBC patients.

All these relevant findings on TNBC molecular subtyping have resulted in critical necessities of developing useful TNBC cell models to better identify molecular-based therapies. As a result, gene expression signatures derived from the TNBC subtypes were used to identify representative TNBC cell lines to serve as models for each subtype [58,60]. Going a step further, Lehmann *et al.* using the panel of cell lines, they pharmacologically targeted prominent signaling pathways revealed by gene-expression signatures, showing that the cell lines representing the various subtypes had different sensitivities to targeted therapies currently under laboratory and clinical investigation [58]. These findings not only gave a great insight into the heterogeneity of this disease, but also provided useful preclinical platforms for the development of effective treatment. Some of the TNBC cell lines most commonly used in preclinical research are shown in **Table 2**. In this study, the cell lines BT-20, BT-549, HCC-1806, MDA-MB-231 and MDA-MB-468 were used as TNBC models.

Table 2. Assignment of TNBC cell lines to subtypes by gene expression analysis.

Adapted from [58].

Cell line	TNBC subtype	Histology	Mutations
BT-20	Unclassified	IDC	CDKN2A; PIK3CA; TP53
BT-549	M	IDC	PTEN; RB1; TP53
HCC-1187	IM	DC	TP53; CTNNA1; DDX18; HUWE1; NKFBIA
HCC-1806	BL2	ASCC	CDKN2A; TP53; UTX
Hs578T	MSL	CS	CDKN2A; HRAS; TP53
MDA-MB-231	MSL	IDC	BRAF; KRAS; CDKN2A; NF2; PDGFRA; TP53
MDA-MB-436	MSL	IDC	BRCA1; TP53
MDA-MB-453	LAR	AC	PI3KCA; CDH1; PTEN
MDA-MB-468	BL1	DC	PTEN; RB1; SMAD4; TP53

AC, adenocarcinoma; ASCC, acantholytic squamous cell carcinoma; CS, carcinosarcoma; DC, ductal carcinoma; IDC, invasive ductal carcinoma; BL1, basal-like 1; BL2, basal-like 2, IM, immune modulator; LAR, luminal androgen receptor; M, mesenchymal; MSL, mesenchymal stem-like.

1.3. Models of tumor heterogeneity and cancer propagation

It is undeniable that a high degree of phenotypic and genetic intra-tumor heterogeneity exists in BC, and specially in TNBC tumors. During the last years, accumulating evidences of intra-tumor genetic heterogeneity have been well documented, resulting in a paradigm shift in regards to our understanding of this disease. Advancing knowledge in this concept has provided some answers to clinical questions, having a direct impact on both diagnosis and disease management [63].

The intrinsic subtypes of BC represent fundamentally distinct disease processes with very different origins and patterns of evolution. Accordingly, it has been proposed that each of the five molecular BC subtypes (normal breast-like, luminal A and B, basal-like, and HER2-enriched), together with the claudin-low group, might initiate in different types of stem or progenitor cells. These cell types of origin would not only be of distinct cell lineages, but also of different stages of mammary epithelial cell differentiation (**Figure 12**). Therefore, luminal A/B and basal-like tumors likely arise as a result of transformation of a luminal progenitor cell of origin.

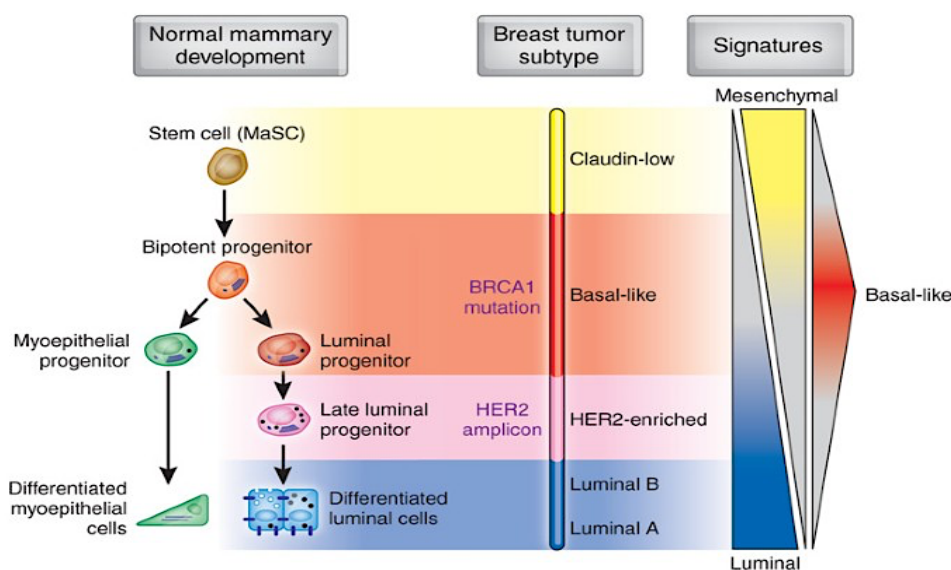


Figure 12. Model of the human mammary epithelial hierarchy linked to cancer subtype. The various breast tumor subtypes molecularly compared to subpopulations from normal breast tissue and their defined expression patterns, which may be best represented as gradients of expression, as opposed to a discrete 'on' or 'off' state of expression. Taken from [64].

Alternatively, rare metaplastic/claudin-low breast tumors may have a different origin, either from a long-lived mammary tissue stem cell or from a unipotent myoepithelial stem cell (**Figure 12**). Besides, as most of basal-like cancers do not show either a loss of

BRCA1 expression or a BRCA1 mutation, it has been suggested that a different genetic driver may allow the luminal progenitor cell of origin to transdifferentiate or adopt basal-like features during tumor development [65]. Other studies using the lineage tracing approach have provided more evidence that oncogenic events in different cell types lead to distinct tumor types and that these differences correlate with clinical outcomes [66,67].

Two models have emerged to explain the heterogeneity of breast tumors, the clonal evolution model [68] and the cancer stem cell (CSC) model [69] (**Figure 13**). Both models propose that tumors originate from single cells that have acquired multiple molecular alterations and developed indefinite proliferative potential under optimal microenvironment to form a cancer [63,70]. Accordingly, the 'cells of origin' and the nature of those genetic mutations during neoplastic progression, are both determinant of the tumor phenotype and hence, may also have a critical impact on the behavior and progression of the resulting tumor [65]. Therefore, the identification of these crucial target cell populations may allow earlier detection of malignancies, a better prediction of tumor behavior and patient outcome, besides leading to preventive therapies for individuals at high risk of cancer development and targeted therapies. Finally, the gene signature of the cell of origin may elucidate key molecular pathways and driver mutations that could lead to new therapeutic approaches to prevent or target early-stage disease [71].

According to clonal evolution (stochastic) model, all the cells in the tumor have a similar tumorigenic potential and tumor heterogeneity arises as a result of the generation of intra-tumoral clones through the sequential mutations [68]. The clonal evolution is promoted by the elevated rate of mutation in tumor cells, known as genomic instability. The accumulation of these genomic changes give rise to a complex mixture of cell populations each one with specific genomic changes and phenotypic features, which contribute both to the intra-tumor heterogeneity and diversity, and to differential response to treatment with outgrowth of resistant and aggressive subclones (**Figure 13**) [63,70].

On the other hand, the CSC model states that cancers originate from the malignant transformation of a stem or progenitor cell through the deregulation of self-renewal program [69]. According to this model, cancer is organized in a cellular hierarchy with differences in the cellular differentiation status, in which at the apex of the hierarchy are the CSCs. Breast CSCs are defined as a particular population of tumor cells that exhibits stem cell-like properties, including self-renewal ability, unlimited proliferation potential, tumorigenicity and the capacity of differentiation giving rise to all cell tumor types, thereby contributing to tumor cellular heterogeneity and being the responsible for tumor progression and inherently therapy-resistant (**Figure 13**) [63,70]. This CSC hypothesis

further suggests that the type of genetic event and the cell of origin, which could be either breast stem cells or their progenies, would be the underlying causes for the morphological and molecular heterogeneity found in breast cancers [19,71].

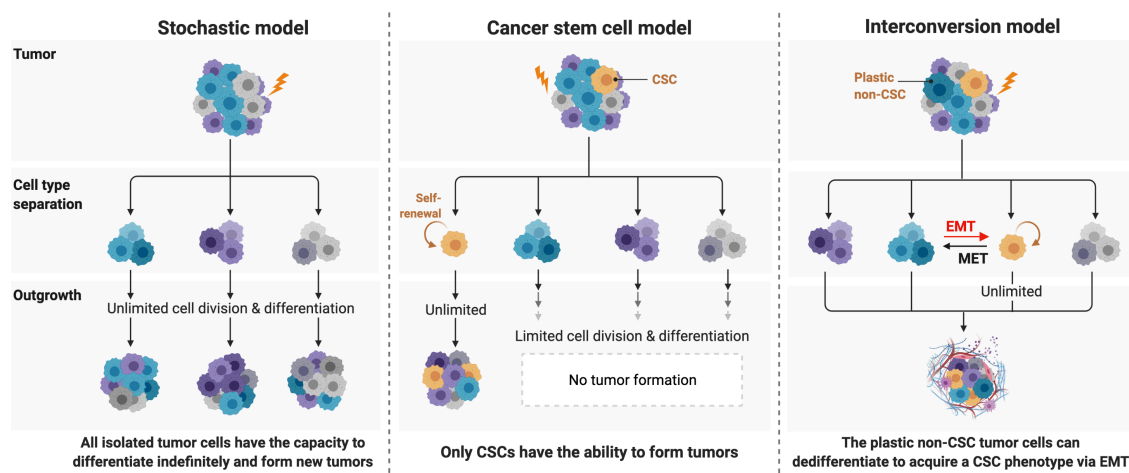


Figure 13. Models of tumor heterogeneity and cancer propagation. The clonal evolution theory proposes that distinct cancer cell populations evolve progressively by multistep acquisition of mutation finally generating heterogeneous tumor with clonal expansion of dominant subclones. According to this model, all tumor cells have similar characteristics and equal tumorigenic potential. A second model is described by the classical CSC theory, which proposes that tumor heterogeneity arises when cancer cells within a given tumor reside in different states of stemness or differentiation. According to this model, only CSCs can self-renew, have long-term propagating capacity and can generate tumor. Critical to this model is the notion that CSC to non-CSC conversion is a unidirectional process. In the 'interconversion model', cancer cells are able to rapidly switch back and forth between a stem and a non-stem state in response to the changing microenvironment. According to model, plastic non-cancer cells can undergo reprogramming into a CSC via epithelial-mesenchymal transition (EMT) activation, and at the same time, CSCs can also differentiate to bulk cancer cells via mesenchymal-epithelial transition (MET). Created with BioRender.com.

In recent years, it has been introduced the concept of CSC plasticity and bidirectional conversion between CSC and differentiated cells, which has a profound impact in tumor heterogeneity [72,73]. This third model, so-called 'the interconversion model' addresses the ability of tumorigenic cancer cells to dynamically interconvert between less and more actively malignant/proliferative states, enabling cells the ability of shifting from a CSC state to a non-CSC state and vice versa (**Figure 13** and **14**) [72,74]. In addition, it has been proposed that CSC plasticity may be modulated by particular microenvironmental tumor factors and cellular interactions coming from the tumor niche [75].

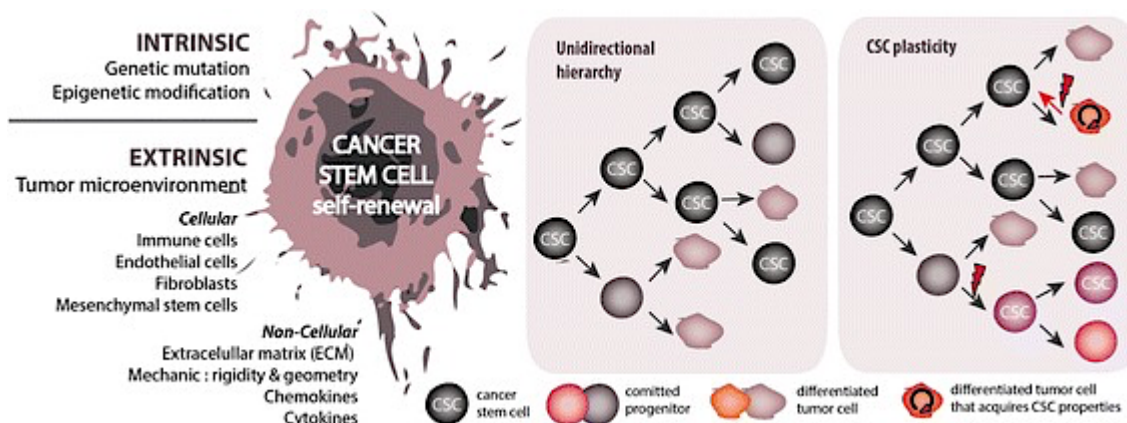


Figure 14. Interconversion model explaining tumor heterogeneity. The original CSC model assumes that only CSCs are able to generate the bulk of tumor via symmetric or asymmetric division based on strictly unidirectional hierarchy. While the interconversion model is based on CSC plasticity. This model states that tumor cells display the dynamic ability of bidirectional conversion from a non-CSC state to a CSC state and vice versa, which may be influenced by diverse intrinsic and extrinsic factors. Taken from [76].

These models might be complementary rather than mutually exclusive as initially thought, and contribute to tumor heterogeneity in varying degrees depending on tumor types. Indeed, malignant transformation may occur in both normal multipotent stem cells as well as more differentiated progenitors through clonal evolution, which then results in the existence of multiple cell lineages [63,77]. At the same time, CSC population may also interconvert between more and less actively malignant states. Although CSCs may play a key role during tumorigenesis and the CSC hierarchical model may contribute to the intratumor heterogeneity of many cancers, tumor progression appears to result from the evolution of a large population of genetically and epigenetically distinct cells [73]. Finally, recent studies have demonstrated the enormous genetic complexity that underlies intra-tumor heterogeneity, indicating that evolutionary selection pressures act upon multiple tumor cell populations, perhaps generated by distinct tumor-initiating cell populations. In addition, extrinsic mechanisms may also contribute to tumor heterogeneity, as interactions between tumor cells and the stromal microenvironment are a crucial determinant of malignant growth [78,79]. The tumor microenvironment (TME) includes not only cancer cells but also immune cells, inflammatory cells, lymphatic cells, vascular cells, fibroblasts and fibrous tissue, all of which have an impact in the response of cancer to therapy [78]. Accordingly, combinatorial approaches targeting distinct tumor cell populations and the tumor microenvironment will be necessary for successful cancer treatment [71].

1.4. Breast cancer stem cells

The first direct evidence for the existence of CSCs came from the work of John Dick *et al.*, who first identified the presence of CSCs in acute myeloid leukemia in 1994 [80]. Even though, it was not until the year 2003 that CSCs were identified for the first time in human solid tumors of BC by Al-Hajj *et al.* [81]. To date, CSCs have been discovered in a broad spectrum of solid tumors, including lung cancer, colon cancer, prostate cancer, ovarian cancer, brain cancer and melanoma, among others [82]. CSCs exhibit multiple unique features, including strong self-renewal and proliferation properties, which make them the driving force behind BC tumor initiation, progression, metastasis, drug resistance, and recurrence (**Figure 15**) [83,84].

1.4.1. Breast cancer stem cells properties

CSCs represent a small subset of tumor cells of the overall cell population within breast tumors, that have the ability to undergo symmetrical **self-renewing** cell division, resulting in two identical pluripotent descendant tumor cells that retain the same stemness features and maintain the pool, or an asymmetrical self-renewing cell division producing a more differentiated tumor progenitor cell and an identical daughter CSC. This self-promoting mechanism results in an increased number of CSCs as the tumor grows as well as an expansion of the overall tumor in size. Therefore, CSCs have the unlimited potential capacity to generate phenotypically different neoplastic cells which contribute to tumor bulk by the process of differentiation [85,86].

Importantly, CSCs are substantially insensitive to most conventional anticancer therapies, including chemotherapy and radiation. Such **treatment resistance** is a consequence of their high expression of **antiapoptotic agents**, increased capacity for **DNA repairing** and higher stability in **hypoxic conditions** (**Figure 15**) [85,87]. CSCs exhibit a unique metabolic and energetic phenotype compared to most differentiated bulk tumor cells. Increasing evidence indicates that CSCs can rely either on glycolysis or on oxidative phosphorylation (OXPHOS), mainly depending on the niches localization, tumor type and TME stimuli that trigger cell plasticity and metabolic reprogramming, allowing them to survive under adverse conditions such as hypoxia, acidosis or starvation [88,89]. CSCs rely more on glycolysis for energy production even in the presence of oxygen, so-called the Warburg effect or aerobic glycolysis. This metabolic adaptation of CSCs results in an increased glycolysis activity, which is essential for the maintenance and acquisition of their stem cell-like properties, such as highly proliferative status, increased survival, therapy resistance and metastatic ability [90,91]. This

metabolic reprogramming results in an increased glucose (Glu) uptake to sustain adenosine triphosphate (ATP) production and is mediated by the overexpression of glucose transporter membrane proteins (GLUT), primarily GLUT1, which in turn its expression has been significantly associated with the TNBC subtype and its poor prognosis and increased metastasis rate [92–94].

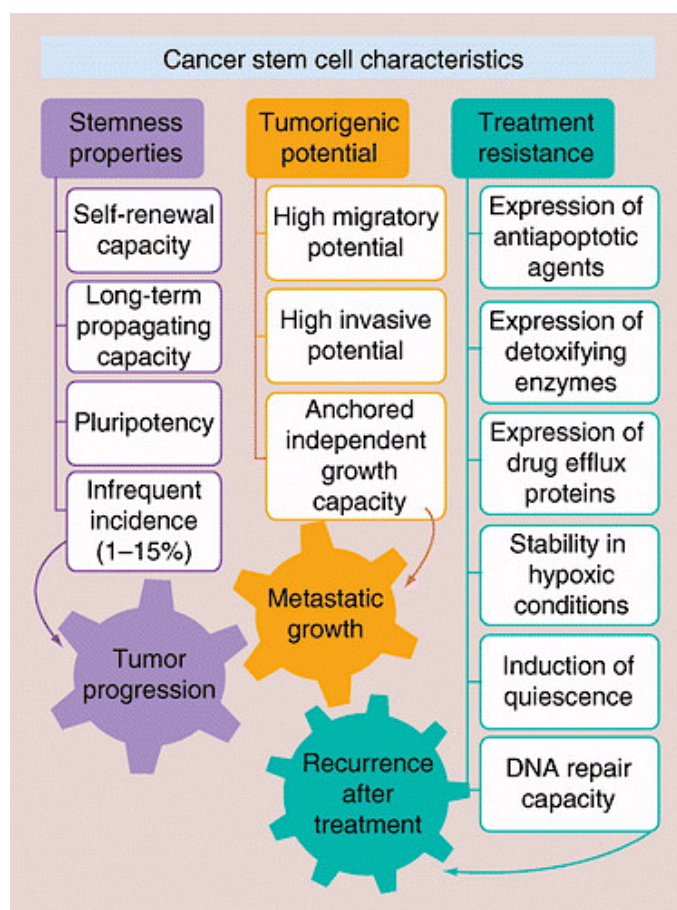


Figure 15. Schematic presentation of essential stemness CSC characteristics and functions. CSCs exhibit essential stemness properties, like self-renewal, pluripotency, tumor initiation capacity and long-term repopulation potential. CSCs have increased migration and invasion capacity and survive in non-attachment conditions, essential features for generating distant metastasis at specific sites. Besides, CSCs are substantially insensitive to most conventional anticancer therapies, antimitotic agents and/or radiation. Taken from [95].

Moreover, CSCs show overexpression of **drug-efflux proteins**, including the P-glycoprotein (P-gp), the ATP-binding cassette super-family G member 2 (ABCG2) and multidrug resistance (MDR)-associated proteins, at the cell membrane which pump-out chemotherapeutic agents from the intracellular space, thereby decreasing intracellular drug accumulation [85,96]. Besides, increased expression of **detoxifying enzymes** like aldehyde dehydrogenase (ALDH) and bleomycin hydrolase provide CSCs with further

protection against chemotherapy. In addition, CSCs usually display a slow rate of division and are capable of activating **quiescence induction** mechanisms under stress conditions. All these features provide CSCs a potent protection against anticancer therapies resulting in an increase in the percentage of CSC population within tumor following treatment [83,85]. The survival of drug-resistant CSCs often leads to cancer recurrence and relapse of patients, as well as to the metastatic growth, since only few CSCs are necessary and sufficient for tumor regeneration *in vivo* [85,87]. For all these reasons, if cancer has to be eradicated, new therapies should specifically target the CSC population.

CSCs have increased **migratory and invasive potential** to invade the surrounding stroma and intravasate the bloodstream generating distant metastasis at specific sites [85,97]. Moreover, CSCs are capable to survive in **anchorage independent conditions** showing capacity to grow as tridimensional tumorspheres and initiate tumor growth *in vivo*.

1.4.2. Cancer stem cell markers

Al-Hajj *et al.* made the initial discovery of breast CSCs using a set of cell surface markers, which consisted in a strong expression of the adhesion molecule CD44, in combination with a decreased or absent expression of CD24 and lack of mammary epithelial lineage markers, so-called as the $CD44^+/CD24^{-low}/lineage^-$ stem cell phenotype. The authors found that only this small subset of breast tumor cells had the potential to generate and maintain tumors in immunodeficient NOD/SCID mice through serial transplantations. The $CD44^+/CD24^{-low}/lineage^-$ phenotype was also associated with specific CSC features, such as long-term self-renewal and high tumorigenic potential [81]. CD44 is a transmembrane glycoprotein that mediates cell-cell and cell-extracellular matrix interactions through binding to hyaluronic acid, and hence, playing a prominent role in cell signaling, adhesion, migration and invasive proliferation. Moreover, high levels of CD44 mRNA and protein expression levels have been linked to significantly worse overall survival in BC [85,98]. While CD24 is an adhesion glycoprotein expressed on the surface of many cell types, especially, in those highly differentiated tumor cells. The absence of CD24 has been shown to increase tumor growth and promote metastasis. The $CD44^+/CD24^{-low}$ signature have been established as minimum biomarkers for breast CSCs and the upregulation of CD44 has been associated with tumor formation and enhanced invasion and metastasis [85]. Moreover, this phenotype seemed to be enriched in those basal-like BC subgroups and absent in those HER2-enriched. Besides,

CD44⁺/CD24^{-/low} phenotype has been also associated with BRCA1 mutational status, which in turns is correlated with the basal-like subtype. Whereas the presence of this phenotype has been correlated with several poor prognostic features and with the basal-like BC subtype, it has not a distinct prognostic value [99]. Due to the great cellular heterogeneity of the CD44⁺/CD24^{-/low}/lineage⁻ population, additional CSC markers have been defined, as the aldehyde dehydrogenase 1 (ALDH1) and CD133 expression. ALDH1 is a detoxifying enzyme responsible for the oxidation of intracellular aldehydes and retinol, which activity can be assessed by the ALDEFLUOR assay. ALDH1 is another functional marker widely used to characterize stemness as an increased ALDH1 activity has been found in normal and malignant stem/progenitor breast cells serving as an indicator for poor prognosis [98,100]. In particular, ALDH1A1 and ALDH3A1 isoforms have been found to be overexpressed in breast CSC population, both involved in self-protection and differentiation mechanisms, as well as in radiation and chemotherapy resistance acquisition [101]. Although CD44⁺/CD24^{-/low} and ALDH1 have been found expressed differently in different BC subtypes, its expression is conserved during tumor development and metastasis [100]. CD133 (Prominin 1) is a transmembrane glycoprotein that has been used in combination with the CD44⁺/CD24^{-/low} phenotype for the detection of breast CSC [102]. CD133 has a significant predictive value as an indicator of increased tumor cell malignancy by regulating the expression of proteins involved in metastasis and drug resistance [103]. Moreover, numerous other breast CSC markers have been identified, including expression of the epithelial cell adhesion molecule (EpCAM), the integrins CD49f and CD29, CD61, CXCR4, CD47, ABCG2, Sca-1, transmembrane glycoprotein mucin 1 (MUC1), stage-specific embryonic antigen-3 (SSEA-3) and Thy-1 cell surface antigen, among others, which expression has been correlated with stem cell activity in BC [85,101]. Furthermore, stemness markers related with the stem-cell expression signature of breast CSCs have also been identified, such as POU class 5 homeobox 1 (POU5F1/OCT4), SOX2, ALOX5, KLF4, chemerin chemokine-like receptor 1 (CMKLR1), NANOG, Notch2/4, AKT2, Hedgehog, Wnt and Nestin [104,105]. A summary of these breast CSC markers is shown in **Table 3**.

Table 3. Summary of breast CSC markers.

Breast CSC markers	Other names	Putative role of the molecule
CD24 ^{low} / -	Heat stable antigen	Adhesion molecule expressed in the majority of lymphocytes and differentiating neuroblasts
CD44 ⁺	---	Cell-surface glycoprotein involved in cell-cell interaction, cell adhesion and migration. Usually presented in progenitor cells
ALDH1 ^{high}	---	Aldehyde dehydrogenase 1, a detoxifying enzyme involved in the metabolism of aldehydes and retinol
CD133 ⁺	Prominin-1	A transmembrane glycoprotein that functions in maintaining stem cell properties by suppressing differentiation
EpCAM ⁺	Epithelial-specific antigen (ESA)	Transmembrane glycoprotein involved in Ca ²⁺ dependent cell-cell interactions associated to cell signaling, migration, proliferation and differentiation
CD49 ⁺	Alfa6-integrin	Expressed in normal mammary stem cells
CD29 ⁺	1-integrin	
CD61 ⁺	Beta3-integrin	Beta3-integrin expressed in luminal progenitor cells, a prognostic factor in BC
CXCR4 ⁺	---	Chemokine receptor and its ligand CXCL12, play a pivotal role in immunological processes. Defined as critical in the metastatic spread of the disease. Present on the surface of mesenchymal stem cells
CD47 ⁺	Integrin-associated protein	A transmembrane protein involved in the regulation of various cellular functions, as T-cell activation and cell migration
ABCG2 ⁺	BC resistance protein (BCRP)	A transmembrane transporter, ATP-binding cassette subfamily G member 2, expressed in normal and CSCs
Sca-1 ⁺	Ly6a	Stem cell antigen expressed in mammary gland progenitors
SSEA-3 ⁺	---	Stage-specific embryonic antigen-3, the globo-series glycan
MUC1 ⁺	CA153	A transmembrane protein, mucin-1, a well-known tumor antigen of BC
Thy-1 ⁺	CD90	A cell-surface antigen that mediates the cell adhesion, and communication of CSCs
OCT4	Oct3/4 or POU5F1	A transcriptional factor involved in stem cell self-renew and pluripotency maintenance
SOX2	---	SRY-related HMG box-containing transcription factor-2 involved in pluripotency maintenance. Is highly expressed in embryonic tissues
ALOX5	---	Arachidonate 5-lipoxygenase involved in oxidative stress response, inflammation, cancer development and with CSC malignancy
KLF4	---	Kruppel-like factor 4 associated with cell proliferation, apoptosis, metastasis, CSC regulation and prognostic and predictive value for BC patients
CMKLR1	---	The chemokine-like receptor 1 and its ligand chemerin are known to be involved in inflammation, immune response, adipogenesis and glucose metabolism
NANOG	---	Transcriptional factor exclusively expressed in early embryonic stages and in germline stem cells maintaining the self-renewal and pluripotency of these cells
NOTCH2/4	---	Transmembrane protein receptors and their ligands regulate proliferation, cell fate decisions, embryonic development, and renewal and maintenance of adult tissue. Are known to be crucial in endocrine therapy resistance and EMT
AKT2	Protein kinase B (PKB)	Serine/Threonine Kinase 2 involved in many biological processes and pathologies, such as metabolism regulation, cell growth, survival, proliferation, cancer, and neurodegenerative disorder
Hedgehog	---	Hedgehog family consists of Sonic hedgehog (SHH), Indian hedgehog (IHH), and Desert hedgehog (DHH) and is crucial for embryonic development and stem cell programs
WNT	---	WNT proteins are a family of glycosylated peptides which function in diverse processes such as embryonic induction, generation of cell polarity, and cell fate specification. Its de-regulation contributes to tumor formation and metastasis
Nestin	---	Intermediate filament protein expressed in the basal/myoepithelial cells of the mammary gland. Is involved in the mechanisms underlying BC progression, including tumor proliferation, angiogenesis and self-renewal.

However, despite all the advances that contributed to a better understating of CSC surface and molecular markers, there is still no standardized criteria for breast CSC identification in human breast carcinomas. In fact, it became unfeasible to obtain a universal combination of markers that could specifically identify breast CSCs in all cases of BC. All these findings revealed the high heterogeneity within CSC populations in BC. The complexity of the evolutionary mechanisms, microenvironmental signals and the intrinsic genomic instability might contribute to the diversity of CSCs, resulting in tumors that harbor heterogeneous and biologically distinct populations of CSCs. Moreover, the variety of CSC markers observed in different studies as well as the reported differences in the phenotype of CSC between individual patient tumors of the same subtype, may be attributed to distinct levels of BC hierarchy and thus, to distinct differentiation status in CSC within tumors [83]. In addition, the bidirectional interconversion process and dynamic phenotype of breast CSC population could also play a role [97]. Therefore, it is crucial to define which breast CSC phenotypes display high tumorigenic potential as well as an increased intrinsic resistance to conventional anticancer agents [106].

1.4.3. Cancer stem cell identification and isolation

The stemness of CSCs, non-CSC reversion to CSCs, and EMT processes are regulated by similar signaling pathways, therefore, it is crucial to identify good markers and appropriate models.

Different methodologies are used to identify and isolate CSCs, that depend either on the high expression of cell surface markers or on the intrinsic functional properties of CSCs (**Figure 16A** and **Table 4**).

The most widely used method of CSC isolation is based on the expression of **specific cell surface biomarkers**, allowing to isolate CSCs from heterogeneous tumor cell populations by fluorescence-activated cell sorting (FACS) or magnetic cell sorting (MACS) [107,108]. Both methods allow to label CSCs with specific antibodies and then sorted for their isolation and enrichment. The most common surface markers used for CSC isolation in BC are CD44⁺/CD24^{-low}. However, other surface markers as CD133, EpCAM, CD49f, CD90 and CD61 have also proved suitable for CSC identification in vivo and in vitro [109]. This method is more specific in comparison with other isolation methods explained below. However, there are some limitations to this method. Cell sorting approach based on cell surface expression does not consider the diversity existing between CSC derived from different subclones [110]. Besides, these cell surface markers are not expressed by CSCs exclusively, their expression is shared with many

normal stem cells and even some normal tissues, and generally, its expression is highly affected by the microenvironment and cell culture conditions [111]. Therefore, detection of surface markers is normally associated with other functional assays to provide persuasive evidence for the existence of CSCs, such as the side population assay, detection of enzymatic activity of ALDH1, sphere-forming assay in serum-free media or soft agar culture and measurement of the expression of specific CSC genes, explained in detail below.

The **side population (SP) assay** is based on the identification of CSCs by their distinctly low Hoechst 33342 dye staining pattern using FACS techniques. CSCs have the capacity to efflux the fluorescent dye by their increased overexpression of ABC transporters and MDR proteins [108,111]. Among the different members of ABC family transporters, ABCG2 is considered the molecular determinant of the SP phenotype, which has been found overexpressed in breast CSC population [112].

Another commonly used method for breast CSC isolation is the **ALDEFLUOR assay**, which is based on the detection of high levels of ALDH1A1 enzymatic activity. Cells with high levels of ALDH become brightly fluorescent and can be identified by flow cytometry or enriched by cell sorting for more purification [107]. However, this staining is transient and depends on the presence of the enzymatic substrate, which makes the system suitable only for CSC segregation in a limited timeframe.

Taking advantage of the capacity of CSCs to survive in anchorage independent conditions, one straightforward method to isolate and test the self-renewal ability in vitro of CSCs consists in culture cells at low density under ultra-low attachment conditions with serum-free and growth factors-rich media. In these culture conditions, only CSCs are able to survive and grow in suspension leading to the formation of spherical colonies, also called mammospheres. A mammosphere is a collection of breast tumor cells that arise from a single CSC [113,114]. Accordingly, **mammosphere assay** has been accepted as a suitable method for the enrichment and propagation of CSC allowing this way a useful system for the study of underlying mechanisms of growth under anchorage-independent conditions and to discover key molecular pathways implicated in CSCs survival (**Figure 16B**). Moreover, this assay also enables to study self-renewal ability of a specific cell population by evaluating the ability of single cells, isolated from mammospheres previously formed, in generating second and later generation mammospheres [86,115].

CSCs have been described to display an increased migratory and invasive potential, which allow them to invade the surrounding stroma and intravasate the bloodstream generating distant metastasis at specific sites [85,97]. Accordingly, several in vitro assays can be used to study this feature, such as **colony formation** in soft agar, **invasion** and **migration assays** [86,116]. Another in vitro assay widely used to identify stem cells is the **label-retention assay**, which takes advantage of the relatively quiescent nature of CSCs. Therefore, this method is able to effectively discriminate dormant CSCs or slow-cycling label-retaining stem cell populations from fast-cycling cells, based on their varying proliferative abilities [86].

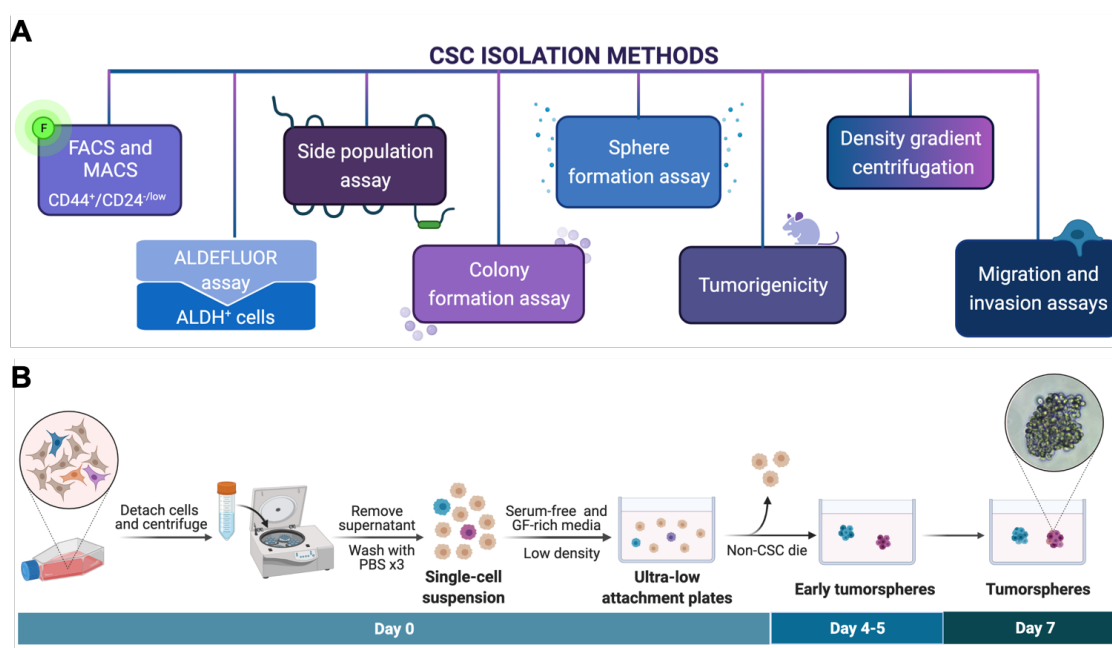


Figure 16. Current approaches in identification and isolation of cancer stem cells. A) Summary of the most commonly methodologies used for the identification and isolation of CSC population. **B)** Schematic diagram of the CSC sphere formation protocol for the generation of first generation of mammospheres in vitro. Created with BioRender.com.

Despite that these in vitro methods are widely accepted methods for CSC isolation and identification, they should be used in combination rather than individually to demonstrate that the cells detect are CSCs, since normal stem cells or progenitors may have the same characteristics [117]. Moreover, another important limitation of using these in vitro isolation methods is that cannot show tumor propagation and tumor heterogeneity is generally not considered. Besides, the specific culture conditions used, like in sphere forming assays, can exert a selection pressure in tumor cell populations, leading to the selection of only those cells able to survive and proliferate under such specific conditions

[117]. A detailed summary of the main advantages and disadvantages of each CSC in vitro method for isolation and characterization of CSCs can be found at **Table 4**.

In this context, in vivo assays are regarded as the gold standard for CSC identification, such as the serial transplantation in animal models, which can complement and enhance the ability of in vitro assays to identify CSCs. The serial transplantation method allows the evaluation of both CSC hallmarks, the self-renewal potential and tumor propagation of CSCs, by isolating cells from the tumors and grafted into a second recipient animal [86]. Another useful method for the assessment of tumorigenic capacity and stemness nature of CSCs in vivo, consists in injecting orthotopically enriched CSCs into the mammary fat pad of immunodeficient mice to further monitor tumor incidence, tumor formation and tumor growth over time.

Table 4. Advantages and disadvantages of CSC isolation methods in vitro.

Methods	Advantages	Disadvantages
<i>CSC isolation by surface markers</i>		
Magnetic-activated cell sorting (MACS)	High specificity Fast and easy	No universal marker for determination of different CSCs Mono-parameter separation
Fluorescence-activated cell sorting (FACS)	High specificity Multi-parameter separation	No universal marker for determination of different CSCs Require large number of cells Complicated, time consuming and expensive processing
<i>CSC isolation by functional assays</i>		
Spheroid formation assay	No need for complicated laboratory equipment	Discrimination between cell aggregation and spheroid formation No presence of quiescent CSCs in spheroid formation Heterogeneity and presence of difference cells
Colony formation assay	No need for complicated laboratory equipment	Toxicity of agar Need proper cell dilution to certify each colony results from a single cell
Aldehyde dehydrogenase activity	High stability in comparison with surface markers	Not proper CSC marker for all tumor types, especially in liver and pancreas Low specificity because of the existence in normal or CSC
Side population assay	No requirement of any cell specific marker	Low purity Low specificity Toxicity
<i>CSC isolation by using physical CSCs properties</i>		
Density gradient centrifugation	Fast and easy	Heterogeneity of isolated cells

There are some recently developed approaches for isolating CSCs. The use of reporter genes under the transcriptional control of gene promoters, which are particularly active in CSC, has demonstrated the feasibility of generating in vitro models [118,119]. In BC, most of the CSC reporter systems developed have been based on the use of green fluorescent protein (GFP) reporters driven by promoters for pluripotent stem cell transcription factors, such as OCT4, SOX2 and NANOG, or high ALDH1A1 activity [119–126]. However, several limitations of using this technology have also been identified, such as the blockage of CSC differentiation, hence preventing asymmetric division and non-CSC regeneration. In this regard, reporter vectors should be designed to selectively signal only under CSC status, in order to avoid unwanted interferences in the balance levels of CSC and non-CSC found in human tumors and cell lines.

Based on this strategy, we have already identified and traced CSC from the highly aggressive TNBC cell line, MDA-MB-231 [127], as well as from MCF-7 BC cell line and HCT116 colon cancer cell line [119]. In these models, the expression of the red fluorescent protein tdTomato is under the control of the specific human breast CSC promoter ALDH1A1 (**Figure 17**), which as previously mentioned, is a marker found overexpressed in CSC subpopulation, and thus, its fluorescence is detected exclusively in the CSC subpopulation, while differentiated cells do not express the fluorescent marker. This approach enables a permanently CSC tagging and has proved successful to partly mimic the complexity of phenotypic dynamism in laboratory conditions [119,127]. Therefore, the use of ALDH1A1/tdTomato reporter vectors enables the identification and isolation of CSCs from heterogeneous populations, as well as to monitor CSC sensitivity in situ of potential anti-CSC targeted therapies. Accordingly, tdTomato⁺ and tdTomato⁻ cells correspond to breast CSC and non-CSC subpopulations, respectively.

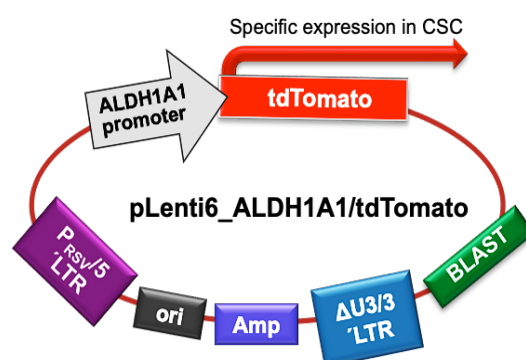


Figure 17. Schematic diagram of pLenti6_ALDH1A1/tdTomato-based plasmid. The plasmid was made by inserting the ALDH1A1 and tdTomato cDNA into the pLenti6/V5-TOPO vector.

1.4.4. Signaling pathways regulating breast cancer stem cells

Over the last decades, dysregulation of several signaling pathways have been identified to contribute for the stem cell maintenance, self-renewal, tumorigenic potential, metastasis and differentiation ability of CSCs. Besides, compared to other subtypes of BC TNBC tumors are enriched in several stemness pathways, including Notch, Wnt/ β -catenin, Hedgehog, janus kinase/signal transducer and activator of transcription (JAK/STAT) and phosphoinositide 3-kinase (PI3K)/Akt/mTOR (mammalian target of rapamycin), that are also relevant in the maintenance of CSCs [128,129] (**Figure 18**). Crosstalk among Notch, Wnt/ β -catenin or Hedgehog signaling, together with other signaling, including PI3K/Akt/mTOR and JAK/STAT, contribute to CSC enrichment and maintenance. Although dysregulation of an individual pathway may result in BC, the fact is that these pathways hardly ever operate in isolation. Therefore, the interplay between these signaling pathways plays a prominent role to the maintenance of CSC phenotype in the presence of external stimuli.

Notch signaling pathway plays a critical role in stem cell fate determination by maintaining a balance of cell cycle progression, cell differentiation and apoptosis, as well as in angiogenesis [104,129]. Notch signaling is predominantly involved in cell-cell communication between adjacent cells through transmembrane receptors (Notch1-4) and ligands, such as jagged proteins (JAG1 and JAG2) and delta-like ligands (DLL1, DLL3 and DLL4), and its dysregulation activates downstream genes contributing to cell proliferation and inhibition of apoptosis in cancer cells, providing this way a survival advantage for tumors (**Figure 18**) [104,129]. Several studies have demonstrated that BC cells with increased Notch activity (Notch⁺ cells) correspond to ESA⁺/CD44⁺/CD24^{-low} cell population and exhibited CSC features, such as an increased sphere formation, higher tumor initiation capacity and higher expression of stemness markers, including NANOG, SOX2, ALDH and krüppel-like factor 4 (KLF4) [83,87]. In certain tumor types, including BC, the activation of Notch signaling plays a crucial role in the control tumor immunity and in the maintenance of CSC phenotype within tumors, increasing the rate of EMT and acquiring chemoresistance [85,129]. Indeed, increased Notch activity is usually found in breast CD44⁺/CD24^{-low} CSC, contributing to the brain metastases of BC. Numerous studies have shown that inhibition of Notch signaling, whether through Notch inhibitors or knocking-down Notch, results in a reduction of CD44⁺/CD24^{-low} CSC population by sensitizing CSCs to anticancer therapies, as well as inhibited tumor initiation and decreased the formation of brain metastases from BC [83,130]. Altogether, these studies highlight how Notch signaling is intricately regulated in TNBC to promote stemness and invasiveness.

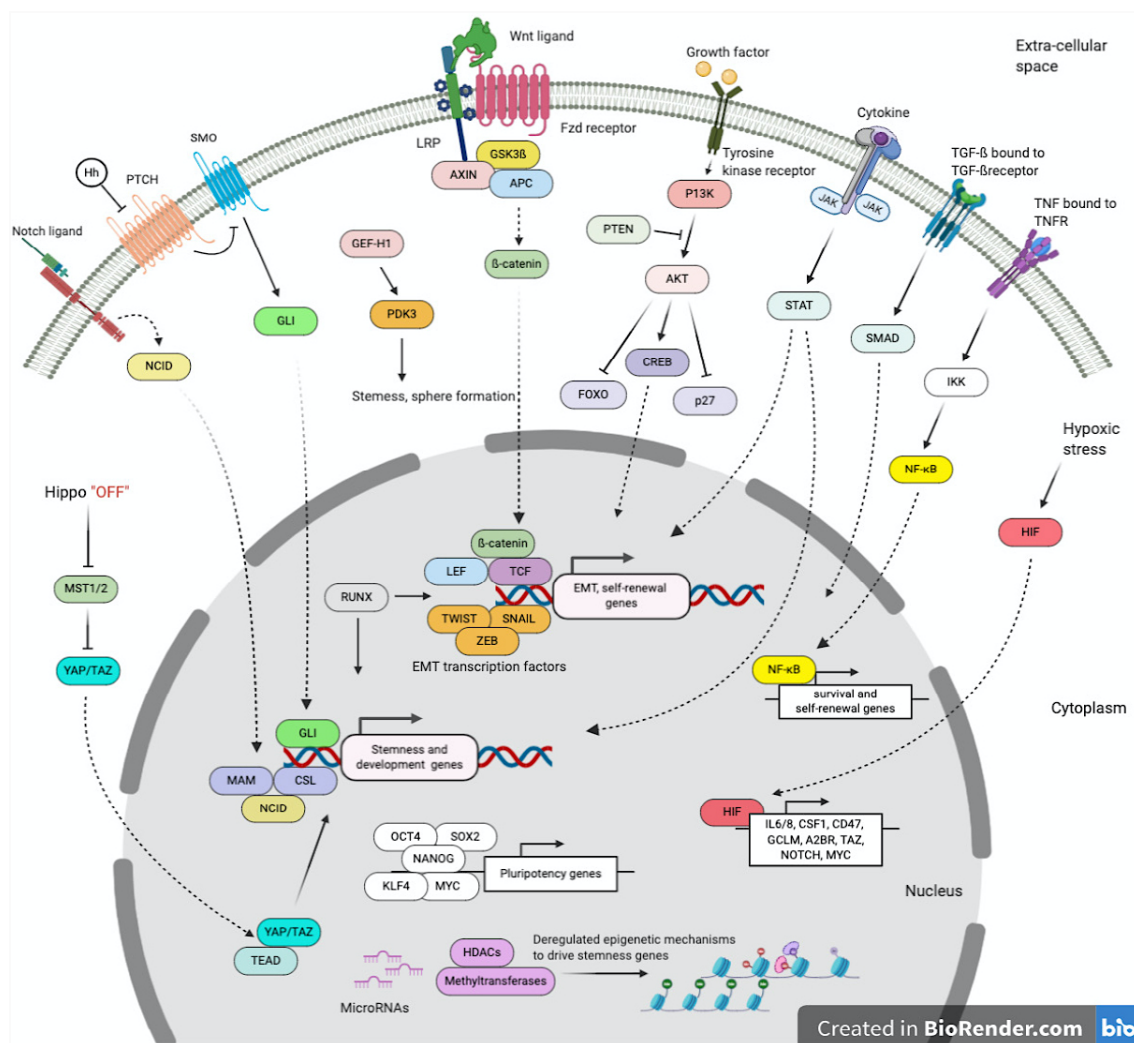


Figure 18. Signaling pathways and epigenetic and transcriptional mechanisms relevant for CSCs in TNBC. Dysregulation of several signaling pathways have been identified to contribute for the stem cell maintenance, self-renewal, tumorigenic potential, metastasis and differentiation ability of CSCs, which include Notch, Wnt/ β -catenin, Hedgehog, JAK/STAT, PI3K/Akt/mTOR, MAPK (mitogen-activated protein kinase) and NF- κ B signaling pathways, and their crosstalk. Regulators of EMT, including SNAIL, and TWIST transcription factors, are also vital to CSC stemness maintenance. Overexpression of transcriptional factors, including OCT4, SOX2, NANOG, KLF4, and MYC contribute to promote pluripotency and self-renewal of CSCs. Taken from [131].

The **Wnt/ β -catenin** pathway modulates stem cell differentiation and pluripotency of normal breast cells as well as abnormal tumorigenesis [104]. Therefore, the Wnt/ β -catenin signaling has a prominent role in self-renewal and differentiation of CSCs by maintaining and preserving their undifferentiated stem state. Wnt is a glycoprotein that serves as a ligand for the transmembrane heterodimer receptor (frizzled domain (FZD) and low-density-lipoprotein (LRP)), its binding results in the nuclear translocation of cytosolic non-phosphorylated β -catenin, where it acts as a transcriptional coactivator in

combination with T-cell factor (TCF) and lymphoid enhancer-binding factor (LEF) (**Figure 18**) [83,87]. Dysregulation of the Wnt pathway has been strongly associated with breast carcinogenesis, leading to breast tumor formation in transgenic mice [83,85]. Indeed, aberrant activation of the Wnt pathway is usually found in breast CSC ALDH⁺ population, resulting in higher level of therapeutic resistance compared to non-CSC bulk tumor cells [83]. Highly active Wnt signaling has been reported in various subtypes of BC, particularly in TNBC. In fact, TNBC patients that showed an increased activation of the Wnt signaling had a higher chance of developing lung and brain metastasis [128]. A recent study showed that the use of a specific Wnt pathway inhibitor reduces both CD44⁺/CD24^{-low} and ALDH⁺ breast CSCs, and inhibits the self-renewal and metastasis of this cell population [132]. Additionally, Wnt signaling was also shown to contribute to dedifferentiation of BC cells into pluripotent CSCs [131]. Overall, these studies suggest a vital role for Wnt signaling in CSCs and TNBC recurrence.

The **Hedgehog (Hh)** signaling pathway plays an important role in various cellular processes during vertebrate embryonic development and tissue homeostasis. This signaling pathway controls self-renewal, stem cell fate maintenance, cell differentiation and proliferation, as well as tissue polarity and EMT [85,129]. The Hh pathway is essential for the proper development of mammary epithelium and its disruption has been linked to tumorigenesis in a wide variety of tissues, including human breast [129]. The Hh signaling consists of Hh ligands, such as Sonic (Shh), Indian (Ihh) and Desert (Dhh), which bind to transmembrane receptor protein patched homolog 1 (PTCH) regulating transmembrane protein smoothed (SMO), which in turns induces downstream activation or repression of transcription via glioma-associated oncogene (GLI) proteins (GLI 1-3). Activated GLI undergo nuclear translocation to regulate downstream target genes that are involved in survival, proliferation, apoptosis inhibition and angiogenesis (**Figure 18**) [104,129]. Hh signaling has been widely implicated in breast CSC self-renewal and cell fate determination [104]. Indeed, increased activation of the Hh pathway is usually found in breast CD44⁺/CD24^{-low} and ALDH⁺ CSC population, contributing to retain their stemness potential [87]. In addition, aberrant activation of GLI and other signaling components such as Shh and PTCH, have been linked to angiogenesis, node-positive metastasis, higher tumor grade and poor disease-free survival, as well as to increased tumor formation and development of BC [85,133]. Moreover, recent studies have evidenced that CSCs are able to produce endogenous Hh ligand Shh regulating cancer-associated fibroblasts (CAFs) via paracrine activation of Hh signaling. CAFs subsequently provide essential growth factors and cytokines thereby promoting

enrichment, expansion and self-renewal of CSCs, as well as helping to maintain suitable microenvironment conditions for CSC existence, survival and proliferation [134].

The **JAK/STAT** signaling pathway is involved in cytokine-mediated immune responses and in many biological processes such as proliferation, apoptosis, and migration, as well as in stem cell maintenance and self-renewal [104]. Cancer cells commonly show frequent dysregulation of the JAK/STAT signaling, which in turn is usually associated with aberrant regulation of the PI3K/Akt and the mTOR signaling pathways (**Figure 18**). The interplay between JAK/STAT and PI3K/Akt/mTOR signaling contributes to CSC enrichment and maintenance [87]. The PI3K/Akt/mTOR signaling cascade is crucial to stem cell proliferation, metabolism and differentiation, and one of the major regulators of survival during cellular stress. The role of this pathway is crucial in cancer, since tumors exist in an intrinsically stressful environment, mainly with limited nutrients access, hypoxic conditions and low pH. Therefore, it is not surprising that this pathway is improperly regulated in most human cancers, including in the TNBC subtype [135].

Receptor tyrosine kinases (RTKs) constitute a class of receptors that play important role in BC progression, tumor relapse and drug resistance [136]. In recent years, several members of RTKs have been identified, among which EGFR, platelet-derived growth factor receptor (PDGFR), vascular endothelial growth factor (VEGFR) and AXL have been defined as key elements in BC progression and stemness, as all regulate various downstream signaling cascades, including MAPK, PI3K/Akt and JAK/STAT, all involved in the regulation of cancer stemness, angiogenesis and metastasis [87,136]. PI3K are lipid kinases activated by a wide range of RTKs. PI3K activation leads to the generation of the secondary messenger phosphatidylinositol-3,4,5-trisphosphate (PIP₃), which couples PI3K to downstream effectors associated to key stemness signal transduction pathways involved in apoptosis suppression, tumor growth and proliferation (**Figure 18**) [137]. In particular, the EGFR has been reported to be overexpressed in TNBC. In addition, the overexpression of AXL has been correlated with tumor stage in BC. Indeed, increased AXL signaling activity has been associated with the activation of several signal transduction pathways, such as MAPK, NF- κ B, STAT and PI3K/Akt. Constitutive activation of AXL is usually found in breast CSC population, inducing the expression of CSC associated EMT markers, such as SNAIL, SLUG, TWIST and N-cadherin [87].

Much effort has been made over the last decades to better understanding the dysregulation of these signaling pathways and their role in driving tumorigenesis, CSC proliferation and stemness maintenance. Accordingly, novel approaches targeting these stemness pathways have been proposed as CSC-related therapeutic options to improve

treatment efficacy in BC. These promising therapeutic targeting strategies against CSCs are discussed in more detail in following sections.

1.4.5. Implications of the EMT and the dynamic CSC/non-CSC conversion

EMT program activation during carcinogenesis leads to the transformation of epithelial cancer cells into a more aggressive mesenchymal phenotype. In particular, during EMT cancer cells lose their cell-cell adhesion and apical-basal polarity and gain the ability to individually migrate and invade basement membrane and blood vessels, and hence, promoting local invasion and dissemination at distant organs (**Figure 19**) [138]. Several studies have evidenced strong parallelisms between EMT activation and CSC formation, since has been identified an increase in CSC signature during EMT processes in different human carcinomas, including BC [139,140]. Accordingly, both cell types are believed to function in a complementary manner to achieve therapeutic resistance against common anticancer treatments, ensure disease progression, contribute to tumor recurrence and cause metastatic growth [141,142].

Importantly, cancer cells are able to switch between epithelial and mesenchymal phenotypes by activating the EMT programs via SMAD/TGF- β (transforming growth factor β), Wnt/ β -catenin and NF- κ β pathways, tyrosine-kinase and the extracellular matrix (ECM) integrin signaling cascade (**Figure 18**). The activation of these pathways converges leading to the upregulation of EMT-related transcription factors, such as SNAIL, SLUG, ZEB, and TWIST, which further control the cellular conversion process by inducing EMT through the inhibition of E-cadherin and direct alteration of the expression of genes involved in cell adhesion, differentiation and motility (**Figure 19**) [141,143]. As a consequence of this dynamic reversion process, cell lines and tumors harbor epithelial and mesenchymal states as well as intermediate states that occur during transition. Hence, it is no wonder that the different molecular subtypes of BC are characterized by different frequencies of mesenchymal and epithelial CSC types as well as differentiation states of bulk cell populations. Tumors from patients with recurrent resistant BC show higher numbers of CSCs and cells with EMT phenotype, leading to poorer survival and worse outcome [144,145]. Indeed, various studies have evidenced that TNBC subtype harbor the highest proportion of CSCs along with a subcomponent of mesenchymal bulk tumor cells compared with other BC subtypes, contributing to the poor prognosis associated with this BC subtype [97,146].

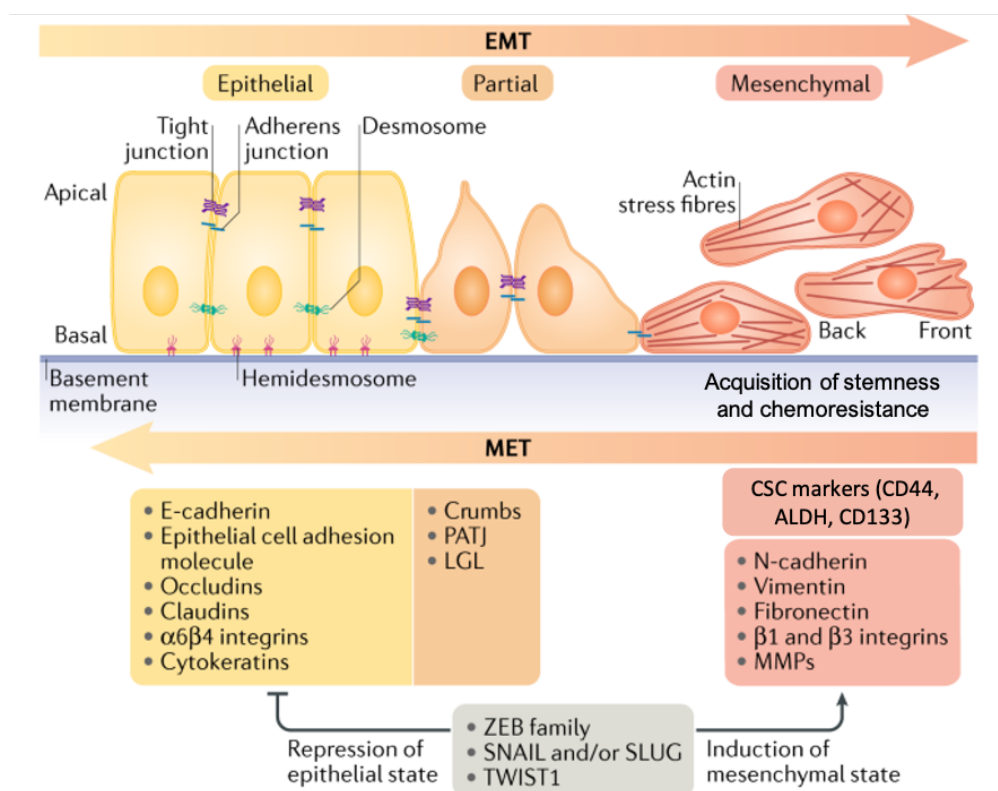


Figure 19. Epithelial-to-mesenchymal transition (EMT) and the reverse mesenchymal-to-epithelial transition (MET) process in cells. Epithelial cells exhibit apical–basal polarity and they are attached tightly via tight junctions and adherence junctions, and desmosomes are attached to the basement membrane via hemidesmosomes. These cells express molecules that are associated with the epithelial state and help maintain cell polarity (listed in the yellow and light orange boxes, respectively). Induction of EMT leads to the expression of the EMT-inducing transcription factors ZEB, SNAIL, SLUG and TWIST. These factors suppress epithelial genes (yellow box) and activate mesenchymal genes (dark orange box). These changes in gene expression result in cellular changes, such as disassembly of epithelial cell–cell junctions and loss of apical–basal cell polarity (color of the cell indicates EMT progression). This loss of the epithelial phenotype results in the gain of a mesenchymal phenotype, where cells become motile and acquire invasive capacities. EMT is a reversible process, and mesenchymal cells can revert to the epithelial state by undergoing mesenchymal–epithelial transition. Both EMT and MET processes occur during normal development and cancer progression. Cells that have shifted toward a mesenchymal state through the upregulation of these markers often acquire stem-like features and chemoresistance. Adapted from [147].

While EMT activation plays a key role in promoting metastatic cascade by conferring migratory and invasive capabilities to cancer cells, once cells have extravasate and spread to secondary sites, metastatic cells need to revert to an epithelial phenotype for adhesion, colonization and effective growth in distant organs (**Figure 20**) [143,148]. This reversal of EMT, so-called mesenchymal–epithelial transition (MET), could be the

explanation to coexpression of epithelial and mesenchymal markers as well as stem cell markers found in circulating tumor cells (CTC). CTC that display a semi-mesenchymal phenotype show higher proliferative and invasive abilities than cells with complete EMT phenotype, and have the capacity to generate distant metastasis [149,150]. Moreover, coexpression of epithelial and mesenchymal genes promotes mammosphere formation and expression of stemness genes, as well as drives tumor growth in vivo [140,151]. These findings supported that cancer-associated EMT may not result in a complete interconversion of epithelial and mesenchymal phenotypes, but rather in highly plastic and reversible stem-like states, which lead to cells with partial EMT phenotype, exhibiting both epithelial and mesenchymal features [152].

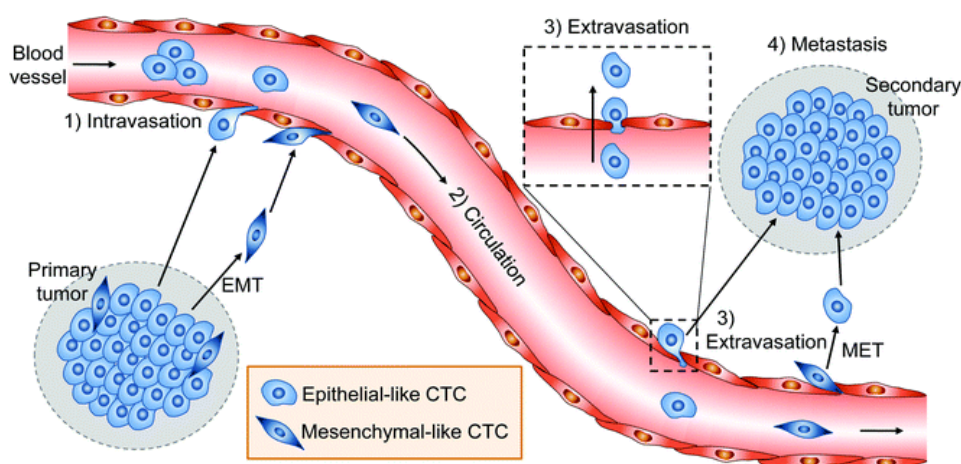


Figure 20. Schematic representation of the participation of CTC in multiple stages of metastasis. 1) The sequential metastasis process initiates with a loss of adhesion of tumor cells in the primary site and their migration out of the primary tumor. Next, the tumor cells attach to the blood vessels and invade the blood or lymphatic circulation, which is called intravasation. 2) The invasive tumor cells circulate through the bloodstream. 3) Once at a distant site, CTC adhere to blood vessel walls, extravasate and undergo MET. 4) Some of the metastatic tumor cells may remain in dormancy, while others grow locally to develop into secondary tumors. Taken from [153].

According to the interconversion model, CSCs and non-CSC bulk tumor cells are subjected to a dynamic phenotype within tumors, been able to interconvert each other influenced by external stimuli, whether due to factors coming from the microenvironment, paracrine communications or in response to treatment, maintaining a controlled equilibrium between both populations within the tumor [154,155]. Hypoxia, for instance, activates CSC reversion and EMT by inducing the overexpression of hypoxia-inducible factors (HIFs). BC patients with increased HIF expression levels, especially HIF-1 α overexpression, have been correlated with distant recurrence, poor outcomes and increase risk of metastasis [156,157]. In BC, HIF-1 α factor overexpression results in

regulation of SNAIL expression, which induces EMT program and Notch activation, promoting stemness, increased migration and CSC aggressiveness and survival. Accordingly, cancer cells might survive to stress conditions by entering dedifferentiation as survival mechanism, guaranteeing tumor cell repopulation [143,157,158].

Therefore, the dynamic phenotype of CSCs and the EMT activation represent an important challenge for targeted cancer therapies, as tumor cell populations are continuously evolving. Thus, therapeutic strategies to prevent and achieve tumor remission should consider not only eradicating potential aggressive CSCs and EMT cell populations within the tumor, but also targeting those key factors involved in the dynamic phenotype interconversion process and EMT program to prevent tumor repopulation.

1.5. Treatment of triple negative breast cancer

Compared to other BC subtypes, TNBC has limited treatment options. Its lack of expression of ER, PR, and HER2, makes the existing specific endocrine treatments and targeted therapies ineffective. Consequently, treatment of TNBC is based on the combination of cytotoxic chemotherapy, radiation therapy and surgery [159].

1.5.1. Chemotherapy

Cytotoxic chemotherapy remains the mainstay of treatment for TNBC. Despite the lack of known targetable biomarkers and an overall poor prognosis, patients with TNBC show higher response to chemotherapy and higher pathologic complete response (pCR) than patients with other BC types. The higher proliferation rate that TNBC tumors often present in comparison with hormone receptor-positive BC subtypes, make them generally more sensitive to chemotherapy [160]. However, patients with TNBC show decreased 3-year progression-free survival rates and 3-year overall survival rates. Although no agent is specifically approved for TNBC, chemotherapeutics that are approved for metastatic BC are also used in the setting of TNBC, among which the preferred ones are summarized in **Figure 21**. Several studies have consistently reported the clinical benefits of using neoadjuvant chemotherapy regimens in the treatment of TNBC in comparison with the other BC subtypes, including higher response rates and an improved prognosis of TNBC patients [161,162].

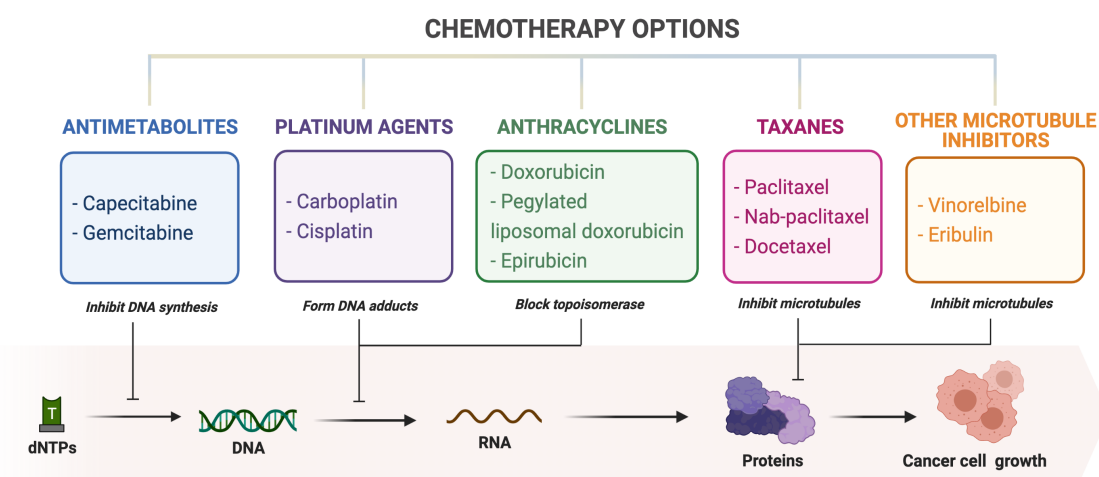


Figure 21. Chemotherapy treatments for TNBC and their mechanism of action. Chemotherapeutics can be divided into different groups on the basis of their mechanism of action, the most common include antimetabolites, platinum agents, anthracyclines, taxanes and microtubule inhibitors. The figure collects the main first-line agents recommended by NCCN and ESMO guidelines for the treatment of TNBC. Created with BioRender.com.

1.5.1.1. Guidelines for the treatment of triple negative breast cancers

The recommended standard-of-care for newly diagnosed early-stage TNBC consists of neoadjuvant chemotherapy followed by surgery, while for metastatic TNBC is recommended the use of sequential single-agent chemotherapy. However, less than 30% of patients with metastatic tumors survive 5 years after diagnosis, despite adjuvant chemotherapy [163]. For those patients with relapsed TNBC, there is no current standard chemotherapy regimen established, as response to treatment is just temporary and generally followed by rapid relapse and onset metastasis [164].

The National Comprehensive Cancer Network (NCCN) and the European Society for Medical Oncology (ESMO) recommend either anthracyclines or taxanes as preferred first-line treatment options for patients who have not previously received these agents as neoadjuvant or adjuvant treatment (**Figure 22**). Although the current guideline-recommended approach is single-agent chemotherapy, combination regimens based on taxanes, anthracyclines, antimetabolites and platinum agents may be appropriate for specific patients, including those with extensive disease or frequent visceral involvement, aggressive course, and risk of rapid patient deterioration (**Figure 22**) [165]. In this regard, an appropriate selection of chemotherapeutic agents together with an optimization of the combination chemotherapy regimens are critical. The use of multiple drugs with differing mechanisms of action allows for additive or synergistic effects on the tumor with minimum toxicity and tends to minimize the emergence of drug resistance by effectively attacking heterogeneous populations of tumor cells [166].

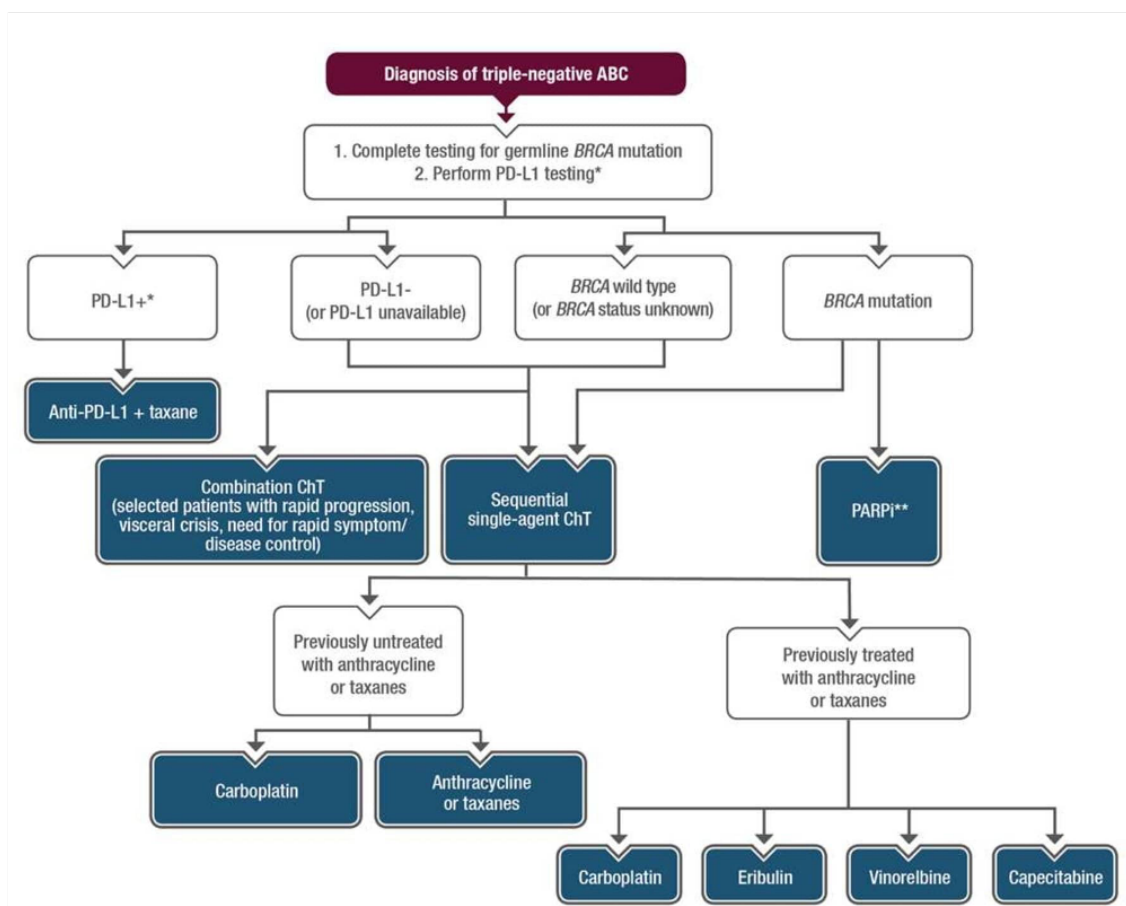


Figure 22. ESMO guidelines-recommended treatment regimens for newly diagnosed early-stage and refractory TNBC. The ESMO Guidelines states that cytotoxic chemotherapy is the standard of care for the treatment of TNBC and that the choice of the regimen should be made after consideration of disease-related factors, including germline BRCA status, programmed-death ligand 1 (PD-L1) levels (immunotherapy options), previous therapies and response, tumor burden, and need for rapid disease/symptom control. Combination chemotherapy is more often required because of frequent visceral involvement, aggressive course, and risk of rapid patient deterioration. Finally, there is no a standard approach for chemotherapy after first line. *Refer to relevant guidelines for PD-L1 testing. **If PARP inhibitors (PARPi) unavailable, preference should be given to a platinum agent. Taken from [167].

Chemotherapy agents can be classified into cell cycle-specific and cycle-nonspecific drugs, depending on whether their major cytotoxic effects are exerted on cells in a specific phase or at any phase within the cell cycle (including G₀). Most traditional chemotherapy agents have their primary effect on either macromolecular synthesis or function of tumor cells by interfering in DNA and RNA synthesis as the **anthracyclines** doxorubicin and epirubicin [168], or the **antibiotics** bleomycin and daunomycin (**Figure 23**). More precisely, anthracyclines work by inhibiting the DNA topoisomerases I and II and intercalating and destabilizing DNA, leading to deregulation of DNA damage

response and stopping the process of DNA transcription and replication. As a result, the cell cycle is blocked during S phase and mitosis. While cycle-nonspecific **platinum** agents (cisplatin and carboplatin) inhibit DNA synthesis, by inducing DNA crosslink strand breaks that result in apoptosis. Importantly, preclinical and clinical studies of platinum-based chemotherapy have consistently reported an enhanced sensitivity to DNA-damaging agents in TNBC compared with other subtypes, as a result of the intrinsic genomic instability and defects in DNA repair of this subtype [168]. Mutations in BRCA 1/2 lead to impaired DNA repair, transcriptional misregulation of genes and genomic instability, making BRCA-mutated cancers highly vulnerable and sensitive to DNA cross-linking agents, such as platinum drugs [169]. Besides, the use of **antimetabolites** as capecitabine or gemcitabine, have demonstrated to affect various cellular pathways required for DNA, RNA synthesis. They are structural analogs or they inhibit several enzymes, and S-phase specific (**Figure 23**). The chemotherapeutic agents as **taxanes**, including paclitaxel (PTX) or docetaxel, are anti-microtubule agents which antitumor effect is caused by the inhibition of microtubule depolymerization forcing cells to stop during mitosis, which leads to an inhibition of proliferation (**Figure 23**) [168].

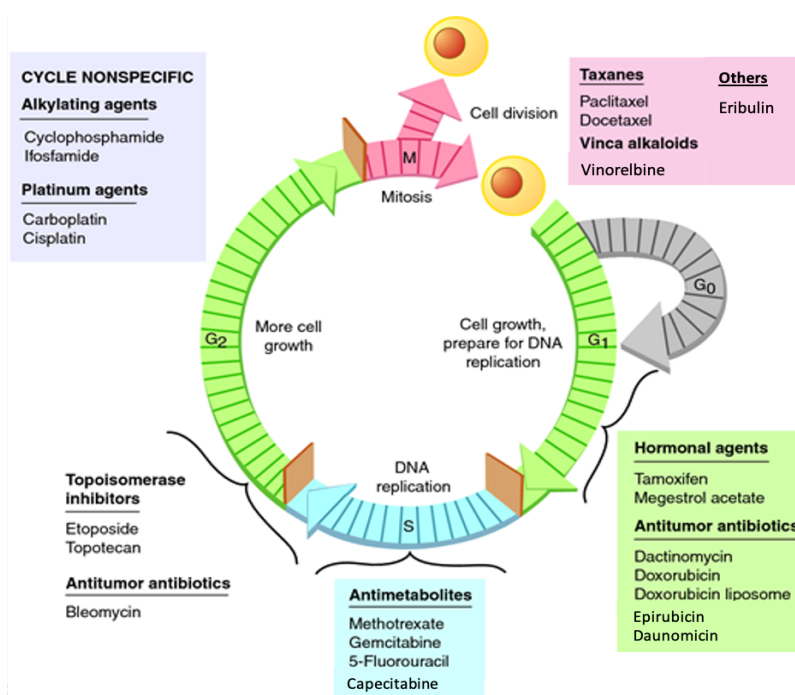


Figure 23. Main antineoplastic agents according to the cell cycle stage in which they are most effective.

Standard adjuvant and neoadjuvant therapies usually combine sequential taxane and anthracycline-based regimens, combination that leads to a pCR in 30-40% of women with TNBC, which in turns translates into an improved long-term outcome [161,162].

Additional combined regimens include PTX combined with other agents, such as gemcitabine or carboplatin, as well as combinations of docetaxel with gemcitabine, among others. Likewise, in those patients pretreated with adjuvant taxanes and anthracyclines, vinorelbine and capecitabine are the preferred choices as second line of treatment options. Additional regimens include an alternative taxane (standard or nab-paclitaxel, nab-PTX), rechallenge with anthracyclines (liposomal formulation) or platinum agents, such as carboplatin [167].

1.5.2. Targeted therapies in triple negative breast cancer

Despite great advances in the stratification of BC subtypes and in the management of TNBC after adjuvant and neoadjuvant chemotherapy, the current situation is, unfortunately, that 60-70% of patients do not achieve a complete response after chemotherapy and end up suffering tumor relapse over time [164]. Considering the heterogeneity of TNBC, personalized treatment strategies targeting molecular tumor-specific alterations would be the most appropriate to effectively treat these patients. The advancement in genome sequencing has provided breakthrough molecular data for launching a new generation of clinical trials using innovative therapies for the identification of potential targets for the different subsets of TNBC, with the aim to circumvent intrinsic chemoresistance. They include Poly(ADP-ribose)polymerase (PARP) inhibition, immuno-directed therapy with checkpoint inhibitors, antibody-drug conjugates against specific surface receptors and molecular targeting for signaling transduction pathways (i.e. AKT signaling pathway), among others (**Figure 24** and **Table 5**) [170,171]. Thus far, 3 newly targeted therapies have been approved by the FDA for TNBC, the PARP inhibitors olaparib and talazoparib for germline BRCA mutation associated BC and most recently, the checkpoint inhibitor atezolizumab in combination with nab-PTX for programmed death-ligand 1 (PD-L1+) advanced TNBC [171–173].

PARP inhibitors (PARPi) are showing considerable promise for the treatment of BRCA mutation-associated BC. This approach exploits a synthetic lethal strategy to target the specific DNA repair pathway in cancers that harbor mutations in the BRCA1 or BRCA2 genes [174,175]. There are currently several PARPi in clinical development, including olaparib, veliparib, niraparib, rucaparib and talazoparib, which have shown promising activity in preclinical and clinical trials. Results from the phase III OlympiAD (NCT0000622) [176,177] and EMBRACA (NCT01945775) [178] studies demonstrated superior efficacy and outcome of both olaparib and talazoparib PARPi, respectively, showing significantly improved response rates and prolonged progression-free survival

of patients over chemotherapy. Many studies are evaluating the potential benefit of combining PARPi with other therapies, including neoadjuvant chemotherapy and immunotherapy, some of which are detailed in **Table 5**.

Immune checkpoints are protective molecules in the immune system that prevent normal tissue damage caused by over-activation of T cells. In the treatment of BC, the most widely studied immune checkpoint receptors include programmed death 1 (PD-1), and its ligand PD-L1, both associated with tumor immune resistance. PD-L1 expression is prevalent among high-grade, hormone receptor-negative breast cancers, especially in the TNBC subtype. Therefore, the use of immune checkpoint inhibitors (ICIs) should be considered as feasible and potential therapeutic agents for TNBC. Different trials are ongoing to establish the role of ICIs, either alone or in combination in TNBC, including pembrolizumab, nivolumab and atezolizumab. Most significantly, atezolizumab has been the first checkpoint inhibitor to be approved for use in treating metastatic TNBC. Results from the IMpassion130 study (NCT02425891) showed a benefit to the addition of atezolizumab in combination with nab-PTX for PD-L1+ TNBC as first line therapy [179]. The combination of atezolizumab + PTX as first line therapy in TNBC is currently being evaluated (NCT03125902).

Another promising strategy that is generating much excitement is the use of antibody-drug conjugates (ADCs). This novel approach is based on targeted delivery of a potent cytotoxic 'payload' to cancer cells through the specific binding of an antibody to a selective cancer cell surface molecule, and hence, providing a second chance to prior discarded cytotoxics due to their high toxicity. A number of ADCs are being investigated in TNBC, among which the ADCs sacituzumab govitecan [180] and ladiratumumab vedotin [181] have shown encouraging results in phase I studies. Further evaluation of both ADCs either as monotherapy or in combination with checkpoint inhibitor in TNBC is ongoing (NCT02574455).

Given that hyperactivation of the PIK3/AKT/mTOR pathway is a relatively frequent event in TNBC, targeting the AKT pathway is an attractive option in TNBC [182]. Several studies have investigated the benefit of combining PTX with AKT inhibitors as first-line treatment in advanced and/or metastatic TNBC, such as ipatasertib [183,184] or capiwasertib [185]. Besides, other promising therapeutic opportunities for TNBC are currently being investigated, including androgen receptors (AR) inhibitors, cyclin-dependent kinase (CDK) inhibitors, MEK inhibitors and EGFR inhibitors [186]. A representative summary of current trials, including potential targeted therapy and emerging combination strategies, is listed in **Table 5**.

Table 5. Targets of TNBC under active clinical evaluation. Part I.

Class	Agent	Drug specification	Combination therapy	Clinical application	Phase	Identifier
PARP inhibitor	Olaparib	Orally active selective inhibitor of PARP1/2	Paclitaxel, carboplatin	TNBC and/or germline BRCA mutated BC	II/III	NCT03150576
			Carboplatin, gemcitabine, pembrolizumab	Locally recurrent inoperable or metastatic TNBC	II/III	NCT04191135
	Veliparib	Orally active selective inhibitor of PARP1/2	Cisplatin	Metastatic TNBC and/or germline BRCA mutated BC	II	NCT02595905
	Talazaloparib	Orally active selective inhibitor of PARP1/2	None	Advance TNBC HR deficient or HER(-) BC	II	NCT02401347
	Niraparib	Orally active selective inhibitor of PARP1/2	None	HER2(-) BRCA-mutated or TNBC with molecular disease (ZEST)	III	NCT04915755
			Pembrolizumab	Advanced or metastatic TNBC	I/II	NCT02657889
Immune checkpoint inhibitor	Atezolizumab	IgG1 PD-L1 monoclonal antibody drug	Paclitaxel	Previously untreated locally advanced or metastatic TNBC	III	NCT03125902
			Nab-paclitaxel	Previously untreated locally advanced or metastatic TNBC	III	NCT02425891
			Paclitaxel, dose-dense doxorubicin or epirubicin, and cyclophosphamide	Stage II-III TNBC	III	NCT03498716
			Carboplatin/paclitaxel, doxorubicin or epirubicin, and cyclophosphamide	No metastatic disease	III	NCT03281954
			Nab-paclitaxel, doxorubicin and cyclophosphamide	Early-stage TNBC	III	NCT03197935
	Avelumab	IgG1 PD-L1 monoclonal antibody drug	None	High-risk TNBC	III	NCT02926196
	Toripalimab	IgG4K PD-1 monoclonal antibody drug	Nab-paclitaxel	First/second-line treatment of metastatic or recurrent TNBC	III	NCT04085276
	Nivolumab	IgG4 PD-1 monoclonal antibody drug	Carboplatin	First-line Metastatic TNBC	II	NCT03414684
	Pembrolizumab	IgG4 PD-1 monoclonal antibody drug	Nab-paclitaxel or paclitaxel or gemcitabine/carboplatin	Previously untreated locally recurrent inoperable or metastatic TNBC	III	NCT02819518
			carboplatin and gemcitabine	Metastatic TNBC	II	NCT02755272
Paclitaxel/carboplatin, followed by doxorubicin or epirubicin			Locally advanced TNBC	III	NCT03036488	

Table 5. Targets of TNBC under active clinical evaluation. Part II.

Class	Agent	Drug specification	Combination therapy	Clinical application	Phase	Identifier
AKT inhibitor	Ipatasertib	Orally Akt kinase inhibitor	Paclitaxel, atezolizumab	Locally advanced unresectable or metastatic TNBC	III	NCT04177108
			Paclitaxel	PIK3CA/AKT1/PTEN-altered, locally advanced or metastatic TNBC	III	NCT03337724
	Capivasertib	Orally Akt kinase inhibitor	Paclitaxel	Locally advanced (inoperable) or metastatic TNBC	III	NCT03997123
PI3K inhibitor	Alpelisib	Orally selective PI3K α inhibitor	Nab-paclitaxel	Advanced TNBC, with either PIK3CA mutation or PTEN loss	III	NCT04251533
AR inhibitor	Bicalutamide	Orally active androgen antagonist	Palbociclib (CDK4/6 inhibitor)	Advanced AR(+) TNBC	I/II	NCT02605486
			Taselisib (PI3KCA inhibitor)	Metastatic AR(+) TNBC	I/II	NCT02457910
	Enzalutamide	Nonsteroidal androgen antagonist	Paclitaxel	Stage I-III AR(+) TNBC	II	NCT02689427
			None	Early-stage AR(+) TNBC	II	NCT02750358
EGFR inhibitor	Afatinib	Pan-HER TKI	Paclitaxel	TNBC	II	NCT02511847
	Desanitinib	Pan-Src TKI	None	Stage I-III nuclear EGFR(+) TNBC	II	NCT02720185
VEGFR inhibitor	Apatinib	Oral VEGFR-2 inhibitor	Carelizumab (PD-1 monoclonal antibody drug), nab-paclitaxel	Unresectable locally advanced or metastatic TNBC	III	NCT04335006
			Capecitabine	Advanced TNBC	II	NCT03775928
			Vinorelbine	Recurrent or metastatic TNBC	II	NCT03932526
	Bevacizumab	Humanized anti-VEGF monoclonal antibody	Atezolizumab, paclitaxel	Advanced or metastatic TNBC	II	NCT04408118
FGFR inhibitor	Lucitanib	FGFR1/2/3, VEGFR1/2/3 and CSF-1 oral inhibitor	Rucaparib (PARP inhibitor), sacituzumab govitecan	TNBC	I/II	NCT03992131
MEK inhibitor	Selumetinib	Orally MEK1/2 inhibitor	AZD6244 (MEK1/2 inhibitor)	TNBC	I/II	NCT02583542
Antibody-drug conjugates	Sacituzumab govitecan	Topoisomerase I inhibitor (SN-38)	Pembrolizumab	Metastatic TNBC	II	NCT04468061
			Pembrolizumab	Localized TNBC	II	NCT04230109
		Anti-trophoblast cell-surface antigen 2 (Trop-2)	Capecitabine or carboplatin/cisplatin	HER2(-) BC or TNBC	III	NCT04595565
	Ladiratumzumab vedotin	Anti-LIV-1	Pembrolizumab	First-line treatment for unresectable locally-advanced or metastatic TNBC	I/II	NCT03310957

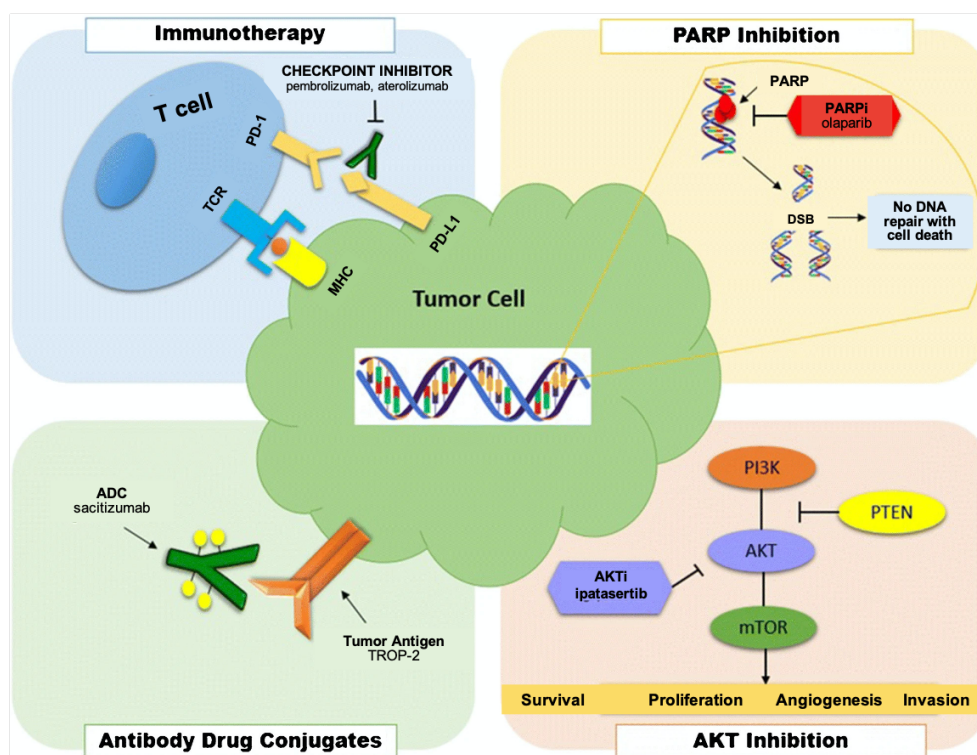


Figure 24. Emerging therapeutic targets in TNBC. To date, 3 new targeted therapies for TNBC have recently been approved, including the PARP inhibitors (PARPi) olaparib and talazoparib for germline BRCA mutation associated BC (gBRCAm-BC) and most recently the checkpoint inhibitor, atezolizumab in combination with nab-PTX for programmed death-ligand 1 (PD-L1+) advanced TNBC. Other novel approaches include antibody-drug conjugates against specific surface receptors and molecular targeting for signaling transduction pathways (i.e. AKT signaling pathway), among others. Taken from [171].

Accumulating evidence suggests that CSCs which have tumor-initiating potential and possess self-renewal capacity, may be responsible for the poor outcome of TNBC subtype by promoting therapy resistance, tumor recurrence and metastasis. CSCs have been consistently reported as one of the determining factors contributing to tumor heterogeneity [187]. In this regard, targeting CSCs has emerged as a promising, novel strategy for the treatment of TNBC. In recent decades, different CSC-targeting strategies have been proposed, some of which have shown therapeutic effects on TNBC in multiple preclinical studies and are currently being evaluated in clinical trials. The characteristics of breast CSCs, including their molecular markers, phenotypic plasticity, regulatory key signaling pathways and complex microenvironment, as well as their therapeutic implications and current advances in CSC-targeted approaches, are discussed in detail below.

Taken together, the above-mentioned highlights the importance of testing valid for precise and individualized treatment of TNBC, such as the need for dose escalation and the incorporation of new antitumor agents into the standard regimen. Determining the optimal use of these inhibitors within drug combinations has been challenging, and new biomarkers may be needed to identify appropriate populations who may benefit most from these novel approaches. Besides, many questions remain unanswered and several goals still to be achieved in order to identify effective therapeutic strategies in the setting of neoadjuvant, adjuvant and metastatic therapies for each TNBC subtype.

1.6. Therapeutic targeting strategies against cancer stem cells

Despite all the progress achieved in conventional BC treatments in the last decades, there is an urgent need for new specific targeted therapies for TNBC treatment in order to improve clinical outcome, prevent tumor recurrence and avoid treatment resistance and undesirable side effects. The better knowledge of the relationship among CSCs, EMT and the TME, as well as their implication in tumor angiogenesis, metastasis and drug resistance in BC and, in particular, in TNBC subtype, has opened the door to new strategies for developing more effective anticancer treatments.

Because many studied CSC-related pathways are also involved in EMT, and the ones studied as potential EMT targets are usually representative of CSC stemness, new treatments should eliminate CSC while reverting the EMT phenotype and vice versa. Accordingly, multiple strategies have been designed to therapeutically target CSCs and EMT activated cells by affecting different functional and molecular aspects. These include targeting specific stem cell markers, signaling pathways linked to CSC stemness properties like self-renewal and pluripotency (including Notch pathway, Wnt pathway, and Hh signaling), TME, CSC-driven drug resistance, cell survival and proliferation pathways (such as PI3K-AKT, JAK/STAT, and NF- κ B signaling), CSC metabolism, inhibition of drug-efflux pumps, induction of CSCs' apoptosis and differentiation [128]. A summary of these therapeutic strategies is presented in the **Figure 25**. On the other hand, to target EMT several therapeutic strategies have been reported, based mainly on targeting adhesion-related proteins (such as E-cadherin), microenvironment factors (such as SPARC) cell membrane molecules (including integrins and TGF- β), intracellular transcription factors (including ZEB, SNAIL, SLUG, TWIST, and E47) and microRNAs (such as miRNA200, miRNA29), among others [188].

Therapeutic targeting of breast cancer stem cell markers: CD44 and CD133 are the most common CSC markers and both have phenotypic and functional significance in the maintenance of stemness in breast CSCs. Therefore, therapeutically targeting these markers can be an important approach for breast CSCs eradication. Immunotherapy based on the use of anti-CD44 antibodies has been effective at inducing terminal differentiation of CSCs, resulting in reduced tumor growth and a significant decrease in tumor metastasis. Moreover, differentiation therapy by knocking down CD44 has also shown to induce differentiation of the CSCs, resulting in a loss of stemness and an increase in susceptibility to chemotherapy and radiation, including the antitumor drug doxorubicin [189,190]. Besides, the generation of an immunotoxin against CD133 has

also shown promising results as a therapeutic agent for TNBC treatment through targeting CD133+ CSC population [191]. Moreover, targeting ALDH1 can also be considered a useful strategy to eradicate CSCs, as its activity has been positively correlated to the maintenance of stemness in CSCs. Downregulating ALDH1 through diethylaminobenzaldehyde (DEAB) or all-trans retinoic acid (ATRA) treatments, resulted in significant sensitization of CD44⁺/ALDH^{high} cells to chemo- and radiotherapy [192]. Likewise, the use of withaferin A has been reported to efficiently target ALDH1 resulting in a loss of stemness and self-renewal ability of breast CSCs [193].

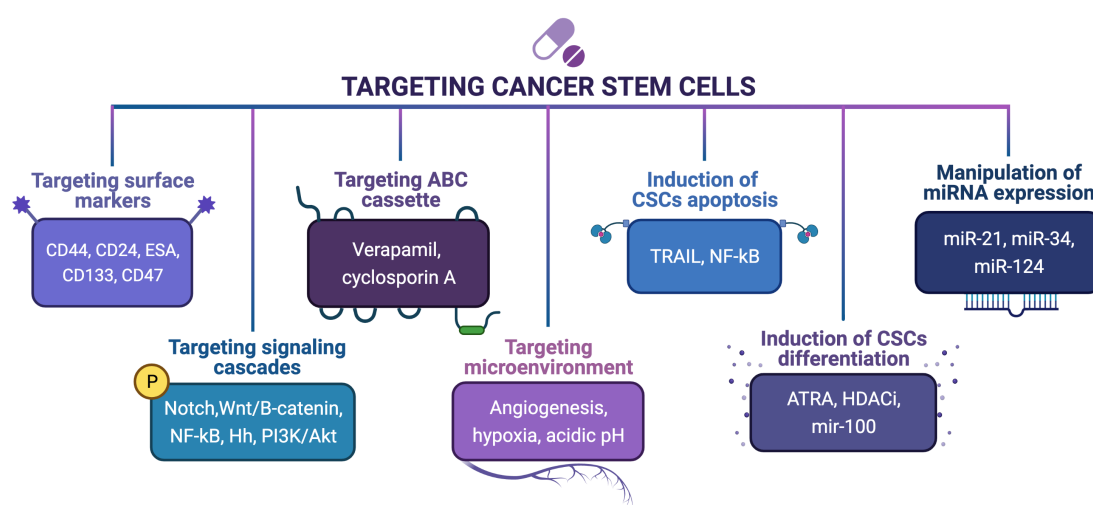


Figure 25. Therapeutics strategies used to target CSCs. Created with BioRender.com.

Targeting self-renewal pathways: Targeting CSC signaling pathways that play critical roles in self-renewal and pluripotency maintenance, including Notch pathway, Wnt pathway, and Hh signaling, has been an area of increasing research and clinical trials for BC treatment. Inhibitors that address dysregulation of these signaling pathways are considered attractive targets for CSCs eradication. Of all the different approaches, one of the most clinically promising candidates are γ -secretase inhibitors. The γ -secretase is a proteolytic enzyme essential for Notch signaling activation, which cleaves Notch receptors releasing the intracellular domain, which in turn acts as a transcription factor regulating important oncogenic gene functions. Numerous studies have shown that inhibition of Notch signaling using γ -secretase inhibitors, like MK-0752 and PF-03084014, sensitized breast CSCs to chemotherapeutic agents (such as docetaxel) as and to radiation therapy making them more responsive [194,195]. Moreover, vitamin D compounds, like BXL0124, have been shown to effectively inhibit breast CSCs and induce differentiation in TNBC by specially down-regulating the expression of essential

Notch signaling molecules, including Notch1-3, JAG1, JAG2 and NF- κ B, which are involved in breast CSC maintenance [196].

There are several strategies to target Wnt/ β -catenin pathway for controlling breast CSC population. The use of Wnt/Frizzled/ β -catenin inhibitors including non-steroidal anti-inflammatory drugs (such as celecoxib), cyclooxygenase-2 (COX-2) inhibitors and anti-diabetic drugs (such as pioglitazone), which have all shown promising preclinically results as therapeutic agents capable of eradicating and reducing the ability of CSCs to self-renew via down-regulation of Wnt pathway activity [85,197]. Additionally, anti-FZD receptor monoclonal antibodies, such as OMP-18R5 (vantictumab), have proven effective in inhibiting tumor growth and regressing CSC populations, as well as exhibiting synergistic activity with standard-of-care chemotherapeutic agents [198]. Moreover, small-molecule inhibitors have also been developed to block Wnt ligand secretion, such as the LGK-974 drug. Currently, a phase I study of LGK-974 monotherapy is recruiting patients with multiple solid cancer types, including the TNBC subtype (NCT01351103) [187]. Moreover, the Wnt inhibitor pyrvinium pamoate has shown to successfully reduce both CD44⁺/CD24^{-low} and ALDH⁺ CSCs and to inhibit the EMT, CSC self-renewal ability and metastasis by decreasing β -catenin expression in breast CSCs when combined with docetaxel [132,199].

Another pathway regulating breast CSC subpopulation and stemness maintenance is the Hh signaling pathway. The Hh pathway can be potentially inhibited through several strategies such as antibodies to Hh ligands, inhibition of SMO and inhibition of GLI [200]. Cyclopamine, a well-known Hh antagonist and its improved derivatives, have shown to deplete CSC populations via inhibition of CSC proliferation, as well as to reduce tumor size in multiple cancers, including BC [201,202]. Early phase clinical trials evaluating the combination of chemotherapy with SMO inhibitors (like vismodegib and sonidegib) in TNBC are underway. Indeed, combination therapy with the SMO inhibitor sonidegib and docetaxel chemotherapy showed clinical benefit in some patients with metastatic TNBC [203]. In addition, the GLI1 inhibitor GANT61 was shown to preclinically attenuate CD44⁺/CD24⁻ stem cell phenotype, increased apoptosis and reduced sphere forming capacity in several TNBC cell lines. While in mouse xenograft BC model, it showed to inhibit tumor growth, EMT and distant metastasis [204].

This line of research represents a promising strategy, due to most cancers share dysregulation of the same signaling pathways and, also, because these signaling are closely linked. Accordingly, the use of combination therapies targeting at the same time more than one signaling pathway together with conventional chemotherapeutic agents

has been evidenced as a promising strategy to improve antitumor efficacy and survival of cancer patients [205].

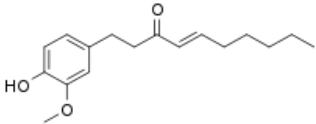
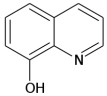
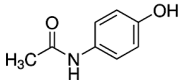
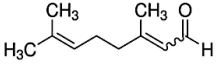
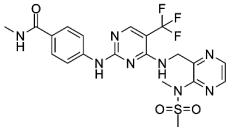
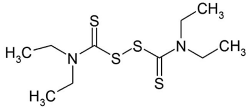
Since the oncogenic signaling pathways TGF- β , TNF- α /NF- κ B, PI3K/AKT/mTOR and RTK play a critical role in stem cell renewal, survival, differentiation and chemoresistance of breast CSCs, several selective inhibitors of these pathways are currently being evaluated [83,128].

Targeting ATP-binding cassette (ABC) transporters: Aberrant expression of ABC transporters plays a crucial role in breast CSCs MDR, including several chemotherapeutic agents in clinical use, such as anthracyclines and taxanes. Drug resistance in CSCs can be potentially overcome through different approaches, including development of competitive or allosteric inhibitors (like XR9576, LY335979, and flupentixol), antibodies (such as UIC2 and MRK16), targeting transcriptional regulation of ABC transporters (like trabectedin) or using anticancer drugs that are poor substrates of P-gp, as the drug ixabepilone [206,207].

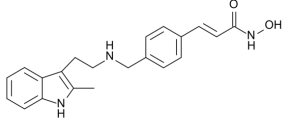
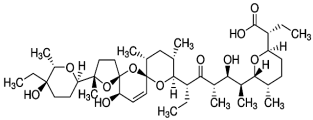
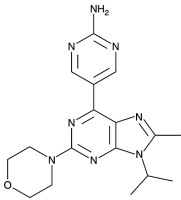
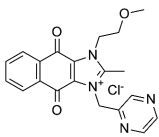
In addition to targeting CSC surface markers, transporters and signaling pathways, many studies have demonstrated a decrease in tumor growth together with an increase sensitivity to chemotherapy by targeting the TME in BC. Antibodies against the chemokine receptor 1 (CXCR1, IL-8 receptor) and reparaxin (small molecule CXCR1/CXCR2 inhibitor) have shown promising effects by targeting CSCs, retarding tumor growth and reducing metastasis in both tumor xenografts models and phase I trials (NCT02001974), [208,209]. Indeed, combination therapy with reparaxin and docetaxel drastically reduced tumor volume, metastatic lesions and secondary tumor formation by CXCR1 blockade, resulting in an increased sensitivity of breast CSC subpopulation to chemotherapeutics. Moreover, the use of differentiating agents (like ATRA and histone deacetylase (HDAC) inhibitors) could also represent a promising strategy to induce breast CSC differentiation, resulting in an attenuation of the stem cell phenotype [210]. Since cellular metabolism in TNBC has been demonstrated to be highly dependent on glycolysis, the use of metabolic inhibitors (such as IACS-010759, etomoxir and perhexiline) could efficiently target and eradicate CSCs [187]. Lastly, as the apoptosis mechanism is normally damaged in CSCs during BC development and progression, approaches to selectively trigger apoptosis of CSC could be of potential benefit for BC therapy. To date, a variety of selectively CSC-targeting agents have been developed, including synthetic chemicals (as PF-03084014), antibodies or recombinant proteins (like bevacizumab) and oligonucleotides (including miRNAs) [211].

Most of these strategies are still in evaluation by preclinical and clinical trials. Approaches involving more specific targeted therapeutics have shown clinical benefit and improved patients' outcomes, particularly when they are administered in combination with conventional anticancer therapies. For this reason, the combination of these potential strategies may allow a new way of targeting breast CSCs from different fronts at the same time, and together with conventional anticancer therapies may provide real improvements in tumor remission and tumor recurrence by targeting both, CSCs and bulk tumor cells. However, no targeted anti-CSC therapies have been already approved for TNBC treatment. Therefore, the identification of novel therapeutic anti-CSC agents is essential for developing effective therapeutics for this subtype. In this thesis, we focused on the identification and validation of potential anti-CSC drugs that could drive CSC proliferation inhibition as well as downregulation of essential signaling pathways related with CSC properties maintenance. For this purpose, a battery of 17 compounds was initially identified, being all clinically-approved drugs with already described anti-CSC activity, thus being promising candidates for drug repurposing in TNBC. Most of these drugs target CSCs by modulating the above-mentioned specific stem signaling pathways (such as 8-quinolinol (8Q), niclosamide (NCS) and metformin (MET) compounds), while others act by inducing CSC differentiation (like the HDAC inhibitor Panobinostat (PNB)) or target specific stem markers (as the ALDH1A3 inhibitor citral (CIT)). The therapeutic anti-CSC mechanisms of drug candidates are summarized in **Table 6**. Of note, some of these drugs have been already tested in early-stage clinical trials or are currently underway for BC treatment applications, including the TNBC. Most of these clinical trials have studied their potential in combination with chemotherapeutic agents, including taxanes and anthracyclines. Indeed, phase I/II studies have already assessed the tolerability and safety of PNB when is combined with other therapeutic agents, including capecitabin and lapatinib, (NCT00632489), trastuzumab and PTX (NCT00788931) and letrozole (NCT01105312) in patients with metastatic or locally recurrent BC. An ongoing multi-centric phase III study is evaluating MET on recurrence and survival in early-stage BC (NCT01101438). While others have evaluated the combination of MET and erlotinib in a phase 1 study of patients with metastatic TNBC (NCT01650506). Other drugs have been studied in early-stage clinical trials but for other oncologic clinical applications, as the phase I/II studies of the anthelmintic drug NCS in prostate (NCT02532114) and colorectal cancer (NCT02687009). While in the case of other drugs, such as CIT, its therapeutic potential evaluation is still at preclinical phase.

Table 6. Repurposed drugs selected as potential candidates for anti-CSC selective targeting in TNBC.

Chemical structure	Drug and CAS number	Drug class	Therapeutic targeting mechanism	Functional mechanism of BCSC eradication	Ref.
	6-shogaol (6-SHO) 555-66-8	Bioactive constituent of ginger	Hedgehog/Akt/GSK3- β	Selectively eradication of CSC with CD44+/CD24- phenotype and inhibition of mammosphere formation Increased the sensitivity of isolated BCSCs to chemotherapeutic drugs	[212,213]
	8-quinolinol (8Q) 148-24-3	Chelating agent	NF- κ B HDAC inhibitor	Preferential targeting against CSCs-like sphere cells Inducing cell apoptosis and differentiation with antiproliferative activity	[214,215]
	Acetaminophen (ACE) 03-90-2	Non-steroidal anti-inflammatory and analgesic drug	Wnt/ β -catenin canonical	Inducing differentiation of CSC in MDA-MB-231 cell line	[216,217]
	Citral (CIT) 5392-40-5	Lemongrass oil component	ALDH1A3 inhibitor	Antitumor effect in targeting ALDH ⁺ cells reducing tumor recurrence, BC growth and metastasis	[218,219]
	Defactinib (DFT) 1073154-85-4	Chemical compound	FAK inhibitor	Preferential targeting CSC resulting in a reduced proportion of CSCs within tumors and tumor-initiating capability	[220,221]
	Disulfiram (DSF) 97-77-8	Anti-alcoholism drug	ALDH1 inhibitor STAT3 signaling	Inhibiting proliferation of BCSC and increase sensitivity of CSCs to conventional anticancer drugs Suppression of CD44+/CD24- and of CD49f+/CD44+ cells and impairment of mammosphere formation	[222–224]

	Everolimus (EVE) 159351-69-6	mTOR inhibitor	PI3K/Akt/mTOR	Favorable activity against basal-like subtypes of TNBCs	[225,226]
	Flubendazole (FLU) 31430-15-6	Anti-helminthic drug	Tubulin polymerization	Reduction of CD44 ^{high} /CD24 ^{low} cells and mammosphere formation ability Induces cell differentiation, inhibits migration and enhances response to conventional therapeutic drugs	[227–229]
	Glabridin (GLA) 59870-68-7	Polyphenolic flavonoid of the licorice root	miR-148a/TGF-β/ SMAD2	Attenuates tumor growth, mesenchymal characteristics, and CSCs-like properties in vitro and in vivo	[230,231]
	Isoliquiritigenin (ISO) 961-29-5	Licorice antioxidant	PI3K/Akt/MAPK	Inhibition of triple-negative MDA-MB-231 breast cancer cell growth through autophagy-mediated apoptosis Anti-cancer effect on migration and invasion	[232,233]
	Metformin hydrochloride (MET) 1115-70-4	Diabetes mellitus drug	mTOR Anti-hyperglycemic	Inhibiting mammosphere formation of CSCs in different BC cell lines in a dose-dependent manner Inhibition of proliferation and suppression of self-renewal in BCSC in HER2+ BC	[234,235]
	Niclosamide (NCS) 50-65-7	Anti-helminthic drug	Wnt/β-catenin canonical	Induces stem-like specific toxicity and apoptosis in breast CSCs by downregulating stem pathways	[236,237]
	Nitidine chloride (NIT) 13063-04-2	Natural polyphenolic compound	Hedgehog c-Src/FAK	Suppressed breast cancer EMT and CSCs-like properties, including cell invasion and migration	[238,239]

	Panobinostat (PNB) 404950-80-7	Organic compound	HDAC inhibitor	Inhibited proliferation and survival, and mammosphere formation and growth of TNBC ALDH1 ⁺ cells Decrease <i>in vivo</i> tumorigenesis and reversion EMT	[240,241]
	Salinomycin (SAL) 53003-10-4	Antibiotic and cationic ionophore	Hedgehog STAT3 downregulation	Targeting selectively CD44 ^{high} /CD24 ^{low} BCSCs inducing CSC-specific toxicity and inhibiting tumor proliferation Induced mitochondrial dysfunction, DNA damage, autophagy, cell cycle arrest, increase ROS production	[241–243]
	VS-5584 (VS) 1246560-33-7	Purine analog	Dual inhibitor of mTORC1/2 and class I PI 3-kinases	Targeting CSC by inhibiting proliferation and survival	[244,245]
	YM-155 hydrochloride (YM) 355406-09-6	Small molecule	Survivin inhibitor Autophagy-NF-kB	Preferentially induces cell death apoptosis in BC cells and targets cancer cell with stem-like phenotype	[246,247]

1.6.1. Combination therapy against cancer stem cells

The discovery of new insights into the current knowledge of the properties and regulatory mechanisms of stemness of CSCs, non-CSC reversion to CSCs and EMT processes, together with the heterogeneity of CSC themselves, has opened the door to new concepts and development of novel and more effective therapeutic strategies to target CSCs and EMT cells with the aim to add drug sensitivity and prevent tumor remission in BC. The ultimate goal for the cancer treatment field is to find the way to reach and eliminate all cancer cell types within the tumor, the aggressive ones displaying stem cell like properties together with bulk tumor cells, since these cells have interconversion capacity and could originate new clones of CSCs or mesenchymal cells via the EMT process. Therefore, the switch between CSCs and non-CSCs implies the necessity of combination of CSC-targeted therapy with standard anticancer therapy together. In this scenario, combination therapy has shown to be a promising strategy for cancer treatment, since combination of drugs may help to achieve a high synergistic therapeutic efficacy at lower drug doses, while decreasing toxicity and reducing or delaying development of drug resistance [248,249]. Nowadays, different therapeutic multimodal approaches have been proposed in adjuvant therapy of BC implying combination of various novel therapeutic agents with chemotherapy, gene therapy or immunotherapy, some of which have been discussed in detail in the previous section 1.5. Besides, given the tumor heterogeneity and complexity in BC, and in particular in TNBC, personalized multi-drug therapies individually tailored to meet the specific needs of each patient may improve outcomes in those patients with refractory malignancies [250].

At present, as previously indicated, clinically used of combination regimens in BC comprise only chemotherapeutic agents or combinations of chemotherapeutic agents with hormonal therapy or immunotherapy. Indeed, chemotherapeutic combination regimens have now become the conventionally applied strategies in clinical practice. For instance, the combination of cyclophosphamide with antimetabolites, like 5-fluorouracil (5-FU) and methotrexate, showed a significant reduction in the risk of recurrence and improved clinical outcomes of BC patients when compared to single treatment. Likewise, combination of PTX with other cytotoxic agents, like doxorubicin, has been evaluated in different clinical trials for metastatic BC (NCT00096291). Moreover, combination of PTX with other agents such as cyclophosphamide, 5-FU and cisplatin at different dose combinations, have also been assessed in the treatment of advanced and metastatic BC, some of which, also included the TNBC subtype [249]. Besides, as was already mentioned, the use of trastuzumab and PTX has been approved as first-line treatment

of HER2-enriched metastatic BC, since this combination has showed to produce higher response rates and longer survival duration than single treatment [251]. However, despite the growing investigation and promising findings using this approach, there are still many barriers for clinical application, such as unacceptable side toxicities and the challenge to determine the optimum combination regimen for each case.

1.7. Nanotechnology-based drug delivery system

Despite the promise of new targeted and biologic agents, cytotoxic chemotherapy remains the mainstay of treatment for TNBC. As stated earlier, exist different chemotherapeutic agents that work through a number of different mechanisms, however, all them include indiscriminately killing growing cells, being unable of differentiating between tumor cells and normal cells, which cause serious side effects, such as bone marrow suppression and hair loss. Besides, acquired drug resistance generated after chemotherapeutic treatment is responsible for most of tumor relapses and consequently, one of the major causes of cancer death [252].

1.7.1. Targeted drug delivery systems in cancer therapy

Over the last decades, nanotechnology has been increasingly used in medicine, including applications for diagnosis, treatment, and tumor targeting in a safer and more effective manner [253]. The use of nanotechnology-based drug delivery systems (DDS) in cancer treatment offers the possibility to circumvent some limitations of conventional anticancer drugs, including the lack of specificity to target tumor cells and their systemic biodistribution after administration, as well as to improve the therapeutic outcomes and safety of anticancer drugs [254,255]. Besides, DDS are able to incorporate drugs or gene products with active antitumoral or anti-CSC activity but poor solubility, low bioavailability or inadequate toxicological profile [256]. In this context DDS offer a platform to deliver the poor soluble drugs into circulation, preventing the use of solubilizing agents and/or organic solvents, and at the same time, allowing the administration of higher tolerated doses [254,255]. In **Table 7** are summarized the main challenges of drug cancer therapy and how nanomedicine has emerged as a potent strategy to circumvent at least some of these limitations.

Moreover, the capability of nanoparticles to bear multiple therapeutic agents allows the possibility to combine different treatment compounds or strategies within the same platform, which helps overcome mechanisms of drug resistance, including efflux transporter overexpression, defective apoptotic pathway, and hypoxia tumor microenvironment [254,257].

Table 7. A summary of the key limitations to BC drug therapy and the ways nanomedicine can be used to overcome these challenges. Adapted from [258].

Challenges of BC drug therapy	The role of nanomedicine in cancer therapy
1. Insufficient specificity for breast cancer	Enhanced and specific drug delivery by passive/active targeting, while preventing the accumulation in healthy tissues and reducing undesired side-effects
2. Inefficient access of drugs to metastatic sites such as brain and bone	Many nanomedicine formulations inherently may improve brain and bone penetration
3. Undesirable pharmacokinetics such as quick clearance and short half-life	Use of strategies such as PEGylation to extend the circulation time and enable sustained or stimulus-triggered drug release
4. Dose-limiting toxicity of the anticancer drugs or the excipients (surfactants and organic-solvents)	Improvement of the drug therapeutic index by increasing efficacy and/or reducing toxicities; controlled drug release; solvent-, surfactant-free nanoformulation
5. Drug resistance at cellular level, for example, increased drug efflux transport	Passive and active targeting may enhance endocytosis; some nanoformulations may inhibit drug efflux mechanisms; co-delivery of drugs that target drug resistance mechanisms
6. Drug resistance at tumor microenvironment level, (lower pH, hypoxia, TME and crosstalk)	Targeting tumor microenvironment; use of stimulus-responsive nanoformulations (i.e. pH-responsive devices); inherent therapeutic properties of some nanomaterials upon stimulation
7. Difficulty in eradicating cancer stem cells	Targeted delivery of drugs to cancer stem cells
8. Undesirable pharmaceutical properties of the drugs, as low aqueous solubility and poor stability	Enhancement of pharmaceutical properties (i.e. stability, solubility, circulating half-life and tumor accumulation) of therapeutic molecules; solubilization and protection of unstable drugs
9. Suboptimal dosing schedule and sequence, especially when multiple drugs combinations	Co-delivery of multiple drugs at controlled synergistic ratios to improve therapeutic efficacy, without having to increase the frequency of administration and overcome drug resistance

Cancer nanomedicines passively accumulate inside tumors due to an enhanced permeability of the intratumoral vasculature and a defective lymphatic drainage system, so-called the enhanced permeability retention (EPR) effect [254,255]. Indeed, most of the clinically available cancer nanomedicines are passively targeted nanocarriers, as Doxil[®] and Abraxane[®] [259,260]. However, this interpretation of EPR is somewhat oversimplified, as multiple factors severally impact on the efficiency of drugs delivered by passive targeting based on the EPR effect, such as interactions with serum proteins, blood circulation, tumor heterogeneity and TME, resulting in a reduced transport and penetration of drugs into the tumor as well as limiting the control and prevention of non-specific delivery of cytotoxic drugs to normal tissue [257,261]. Besides, nanoformulations

properties, including size, surface features, composition and targeting moieties, can also influence the EPR effect [254]. However, there are some limitations with regards to passive targeting, including non-specific drug distribution, non-universal existence of the EPR effect and different permeability of blood vessels across various tumors [262]. On the other hand, active targeting has emerged as a potent strategy of improving drug efficiency. This is achieved through the decoration of the nanocarrier surface with ligands (targeting moiety) binding to receptors overexpressed in the surface of cancer cells. This strategy improves the affinity of the nanocarriers for the surface of cancer cells and hence, enhance drug penetration as well as allows them to distinguish targeted cells from healthy cells. These ligands specifically bind to receptors on targeted cells promoting the receptor-mediated endocytosis, which results in the internalization and successful release of the therapeutic drug inside the targeted tumor cell [262].

1.7.2. Currently used nanomedicine in breast cancer treatment and novel nanoformulations targeting CSC

During the last decades, several nanotherapeutic platforms have been formulated and approved by The Food and Drug Administration (FDA) for BC disease, of which highlight liposomes, polymeric nanoparticles (NPs), protein-based NPs and immunoconjugates (**Table 8**) [261,263]. All these nanoformulations display a clinically-demonstrated ability to reduce toxicity and improve efficacy compared to treatment with the drug free form.

Liposomal nanoformulations have been employed to deliver critical chemotherapeutic drugs, including doxorubicin (Doxil[®], Lipodox[®] and Myocet[®]), PTX (Lipusu[®]) or daunorubicin (DaunoXome[®]). Additional approaches include **protein nanoparticles**, such as Abraxane[®], and **polymeric micelles**, as Genexol-PM[®] or Nanoxel[®], which are all nanoformulations of the chemotherapeutic drug PTX. An **antibody-drug conjugate** (Kadcyla[®]) of trastuzumab and emtansine (DM1), has also been formulated. A summary of these FDA-approved anticancer nanomedicines is shown in **Table 8**.

Doxil[®] is a PEGylated liposomal formulation clinically used as second-line treatment for metastatic BC. Doxil[®] treatment has demonstrated to enhance tumor growth suppression and increase overall survival [264]. Despite the clear benefits obtained using Doxil[®], this liposomal nanoformulation also induces severe side effects (such as oral mucositis and skin toxicity) [258]. Alternatively, the nanoparticle albumin-bound (nab) technology has emerged as a potential strategy in the clinical setting to enhance drug solubility, bioavailability, stability and biodistribution. Nab-technology approach relies on taking advantage of proteins found in the blood serum, like albumin, to facilitate transport and

dilution of poor water-soluble drugs during circulation [257,260]. Abraxane[®] is a formulation of PTX complexed with albumin in a reversible non-covalent manner (nab-PTX) that was approved by the FDA in 2005 to treat metastatic BC [265]. Abraxane[®] allows a safer clinical administration of higher doses of PTX, yielding greater efficacy. The increased tolerance and reduction of toxicity of Abraxane[®] relied on the non-use of Cremophor EL[®] and ethanol for drug dissolution and administration [260,266]. Abraxane[®] formulation has demonstrated superiority over free PTX treatment, via increasing tumor accumulation of PTX and improving overall response rate in patients with advanced BC. Moreover, gemcitabine, the standard first-line chemotherapy for treating pancreatic cancer, has been also successfully loaded in human serum albumin NPs and showed strong inhibitory effect on tumor growth against resistant pancreatic cell lines both in vitro and in vivo [267]. The antibody-drug conjugate Kadcyra[®] is a molecular targeted therapy that was FDA-approved in 2013 to treat HER2+ metastatic BC patients [268] and further in 2019 as an adjuvant treatment for HER2+ BC with residual disease. Kadcyra[®] treatment demonstrated a superior efficacy in reducing the risk of invasive BC relapse compared with free trastuzumab [269].

Table 8. FDA-approved nanomedicines in routine clinical use for breast cancer treatment.

Adapted from [258].

Name	Nanocarrier	Drug/Compound	Approval date	BC indication
Doxil [®]	PEGylated liposome	Doxorubicin	1995	Metastatic
Lipodox [®]	PEGylated liposome	Doxorubicin	2013	Metastatic
Myocet [®]	Non-PEGylated liposome	Doxorubicin	2000	Metastatic
Lipusu [®]	Liposome	Paclitaxel	2006	Non-metastatic
Abraxane [®]	Albumin-bound	Paclitaxel	2005	Metastatic
Genexol-PM [®]	mPEG-PDLLA	Paclitaxel	2007	Non-metastatic
Nanoxel [®]	NIPAM-VP	Paclitaxel	2006	Metastatic
Kadcyla [®]	Antibody	Trastuzumab/ emtansine	2013	Metastatic HER2+
			2019	Early HER2+, residual

PEG, Poly(ethylene glycol); mPEG-PDLLA, Poly(ethylene glycol)-poly(lactide acid); NIPAM, N-isopropyl acrylamide; VP, Vinylpyrrolidone.

Among the different polymeric approaches, micelles have gained much attention and are considered a promising tool for their application in nanomedicine therapeutics and drug delivery. **Polymeric micelles (PM)** are composed of amphiphilic block copolymers that self-assemble in an aqueous environment, resulting in the formation of nanosized, spherical, supramolecular colloidal particles with a hydrophobic core and a hydrophilic

corona. The hydrophobic segment of the polymer forms the internal core of the micelles, that is suitable for encapsulating poorly water-soluble drug molecules, thus improving their solubility and stability. While the hydrophilic segment forms the corona of the micelles, a shell that interfaces the biological media and inhibits rapid drug biodegradation, hence improving their bioavailability and providing a longer half-life in bloodstream of the encapsulated drugs [270,271]. During the last years, PM have received growing attention as multifunctional nanocarriers in comparison with other drug delivery systems, due mainly to their customize potential for a slow and controlled drug delivery and release, a feature that is associated to the chemical versatility allowed by their core/corona micellar structure [272]. Consequently, PM can achieve different particle size (between 10 and 100 nm), shape, surface chemistry, drug loading and release characteristics depending on their composition [271,272]. Moreover, PM can increase the passive targeting of drugs to solid tumor sites by the EPR effect, improving drugs pharmacokinetics and reducing off-target cytotoxicity. These reasons explain the successful clinical translation of PM-based systems, like the well-known PTX-loaded polymeric micellar formulation, Genexol-PM[®] [254,273]. This micellar nanoparticle encapsulating PTX has been used in the treatment of several cancers, including BC. Genexol-PM[®] has demonstrated a prolonged circulation time and an improved overall response rate with fewer secondary effects compared to free PTX treatment.

Even though long circulation times favor that nanomedicines extravasate at the tumor site, the active targeting against tumor cells would result in a more efficient drug delivery improving their therapeutic efficacy. In this regard, the hydrophilic surface of NPs, and in particular, in PM formulations, enables cell- or tissue-specific delivery through functionalization with active-targeting moieties, such as actively targeting CSCs [270,273]. In recent years, several potential nanomedicine approaches have been explored to eliminate therapeutically-resistant CSCs by targeting CSC metabolism (Glu uptake), inhibiting ABC transporters, blocking essential signaling pathways involved in self-renewal and survival of CSCs, targeting CSCs surface markers and destroying the TME. However, the clinical translation of these nanoformulations is tough, as many challenges still remain unaddressed. In **Table 9** are listed few examples of the different nanocarriers that have been developed against breast CSCs.

Despite the potential and promising use of drug carrier systems, we should not forget the limitations and considerations of using these approaches, the most common are immunogenicity, highly sophisticated technology requirements, limited large scale production, difficulty to maintain stability of dosage forms, limited carrying capacity, rapid clearance via RES, premature drug release and poor metabolic stability [254,257].

Table 9. Nanomedicine for breast CSC therapy.

Delivery systems	Therapeutic agent (s)	Targeting moieties	Mechanism of action
PEG-b-PLA nanoparticles	All-trans-retinoic acid/doxorubicin	---	Co-delivery of drugs inducing breast CSCs to differentiate into non-CSCs and inhibiting tumor cells
	Decitabine/doxorubicin	---	Combination of drugs for sensitizing breast CSCs to chemotherapy
	Chloroquine/doxorubicin/docetaxel	---	Co-delivery of drugs for sensitizing breast CSCs to chemotherapy
PLGA nanoparticles	Salinomycin/paclitaxel	Hyaluronic acid	Co-delivery of drugs targeted toward breast CSCs and bulk breast cancer cells
	Paclitaxel	Anti-CD133 mAb	Selective inhibition of breast CSCs
	Wedelolactone	---	Sensitize breast CSCs by downregulating SOX2 and ABCG2
	Doxorubicin/cyclopamine	Hyaluronic acid	Inhibition of breast CSCs and bulk tumor cells by inhibiting Hedgehog signaling pathway
Chitosan decorated Pluronic® F127 nanoparticles	Doxorubicin	Chitosan	Improved eradication of breast CD44 ⁺ CSCs with low systemic toxicity
PLGA-co-PEG micelles	Paclitaxel	Anti-CD44 Ab	Improved sensitivity of CSCs to paclitaxel
	Zileuton	---	Selective inhibition of breast CSCs and CTCs in the bloodstream and metastatic spread
MSN-PEI-Glu nanoparticles	γ -secretase inhibitor	Glucose/Glucose transporter I	Selective inhibition of breast CSCs by inhibiting Notch signaling pathway
Stabilized phospholipid micelles	Curcumin	---	Inhibition of breast CSCs and bulk tumor cells by downregulating stem signaling pathways
Pluronic® F127-based micelles associated with PEI	siRNA	AKT2	Strong suppressive effects on breast CSCs invasion and mammosphere formation ability
Mixed micelle system	shRNA	---	Selective inhibition of breast CSCs by downregulating the NF- κ B signaling
Lipid-polymer hybrid nanoparticles	Paclitaxel, verteporfin, and combretastatin	---	Simultaneously inhibiting bulk cancer cells, CSCs, and angiogenesis by inhibiting Hippo signaling pathway

HYPOTHESIS & OBJECTIVES

HYPOTHESIS AND OBJECTIVES

TNBC is the most devastating form of BC because of its aggressive and heterogeneous nature. To date, not a single targeted therapy has been approved for the treatment of TNBC, and cytotoxic chemotherapy remains the standard systemic treatment. However, conventional chemotherapeutic agents lead to serious side effects and often derive in the acquisition of drug resistances and the development of early, aggressive metastatic relapses, thereby reducing the number of treatment options for metastatic disease. Recent studies suggest that CSCs play an important role in tumorigenesis and tumor biology of TNBC. Evidences of enriched breast CSC population in TNBC may explain the propensity of this BC subtype for chemotherapy resistance and tumor metastasis.

In this regard, new therapies against TNBC should compile two requirements: (i) reduce the toxicity seen in cytotoxic therapies and most importantly, (ii) target efficiently CSC population. Despite the availability of an increasing number of anti-CSC agents, their clinical translations are hindered by many issues, such as instability, low bioavailability, and off-target effects. Drug delivery systems have shown significant promise because of their potential to overcome these drawbacks.

Considering the complexity and diversity of TNBC, together with the heterogeneity and plasticity of the CSC population, eradicating all cancer cells populations using only one strategy is a challenging task. Hence, multi-drug cancer therapy has emerged as a successful treatment alternative to increase therapy efficacy and to prevent the development of drug resistance. However, functional validation of potential anti-CSC candidates and combination therapies might become a difficult task unless CSC are easily distinguishable from bulk tumor non-CSC. In this context, generation of optimal in vitro CSC models is a needed requirement for preclinical validation of anticancer treatments.

GENERAL OBJECTIVE

The main goal of this thesis is to explore the use of CSC-targeting agents and nanotechnology-based drug delivery systems as a way to improve the treatment of TNBC with conventional chemotherapeutic drugs.

SPECIFIC OBJECTIVES:

Objective 1. To generate valuable in vitro fluorescent CSC models of TNBC cell lines for preclinical validation of anti-CSC drugs. Validation of the stemness nature of labeled CSCs, while ensuring that the phenotypic interconversion process between tumor cells is not restrained.

Objective 2. To select anti-CSC drugs with high therapeutic anti-CSC potential for the treatment of TNBC. In vitro screening analysis to identify the best/s anti-CSC candidate/s.

Objective 3. To explore the synergistic effect of selected anti-CSC drugs with conventional chemotherapeutic agents in TNBC cell lines. Combination in vitro analysis to provide cell line-specific drug ratios.

Objective 4. To explore nanotechnology-based drug delivery systems containing chemotherapeutic drugs and/or selected anti-CSC agents for the treatment of TNBC. Evaluation of the efficacy and/or safety of antitumor drug co-delivery systems in TNBC cellular and mouse models.

MATERIALS & METHODS

MATERIALS AND METHODS

3.1. Materials

3.1.1. Reagents and compounds

D-(+)-Glucose, 8-quinolinol (8-Hydroxyquinoline), acetaminophen (4-Acetaminophenol), citral, disulfiram, everolimus, flubendazole, metformin, niclosamide, panobinostat, salinomycin, YM-155, dimethyl sulfoxide (DMSO), 3-(4,5-dimethylthiazol-2-yl)-2,5-diphenyltetrazolium bromide (MTT), heparin, bovine serum albumin (BSA), epidermal growth factor (EGF), fibroblast growth factor-2 (FGF2), putrescin, apo-transferrin, insulin, selenium, progesterone, crystal violet, ethylenediaminetetraacetic acid (EDTA), Tween[®] 20, collagenase type I, HEPES, β -mercaptoethanol and Cremophor[®] EL were purchased from Sigma-Aldrich (Madrid, Spain). VS-5584, SN-38 and defactinib were obtained from Selleckchem (Houston, TX, USA). Everolimus and paclitaxel were acquired from Novartis and Teva, respectively. DMEM/F-12 medium, DMEM high glucose medium, RPMI 1640 medium, Opti-MEM I reduced serum medium, Basal Medium Eagle, phosphate buffered saline (PBS), fetal bovine serum (FBS), antibiotic-antimycotic 100X (10,000 U/mL penicillin, 10,000 μ g/mL streptomycin and 25 μ g/mL antimycotic Fungizone[®]), L-glutamine, sodium pyruvate, MEM non-essential amino acids 100X, 10 mg/mL blasticidin S HCl, 50 mg/mL geneticin, 10 mg/mL puromycin, 0.25% Trypsin-EDTA and 0.4% Trypan blue solution were purchased from Gibco (Thermofisher Scientific, Madrid, Spain). Lipofectamine 2000[®], 4',6-Diamidino-2-phenylindole dihydrochloride (DAPI) and D-luciferin were acquired from Life Technologies (Thermofisher Scientific, Madrid, Spain). The PrestoBlue[™] cell viability reagent (invitrogen[™]) and the M-PER mammalian protein extraction buffer were purchased from Thermofisher Scientific (Madrid, Spain).

3.1.2. Cell lines and culture conditions

Human TNBC cell lines MDA-MB-231, MCF-7, BT-549, BT-20, MDA-MB-468 and HCC-1806 were obtained from American Type Culture Collection (ATCC, LGC Standards, Barcelona, Spain) (see **Table 2**). MDA-MB-231 and MCF-7 cell lines were cultured in DMEM/F-12 medium, BT-549, BT-20 and HCC-1806 cells in RPMI 1640 medium and MDA-MB-468 in DMEM high glucose medium. All media was supplemented with 10% heat-inactivated FBS, 1% of antibiotic-antimycotic 100X, 2 mM L-glutamine, 1% MEM

non-essential amino acids and 1 mM of sodium pyruvate, unless they have already been pre-supplemented. MDA-MB-231-ALDH1A1-tdTomato cells, previously developed in our laboratory [127] were cultured in DMEM/F-12 medium supplemented with 1 µg/mL blasticidin and 10 µg/mL geneticin. MDA-MB-468.Fluc.ALDH1A1-tdTomato and HCC-1806-RedFluc.ALDH1A1:tdTomato fluorescent CSC models, both generated in this thesis, were cultured in complete RPMI medium supplemented with 1 µg/mL blasticidin and 1 µg/mL puromycin.

All cell lines were incubated in a humidified incubator at 37°C containing 5% CO₂. Culture media was renewed every two to three days and cells were subcultured when 80-90% confluent. To harvest cells for subculture or experimental assays, cells were washed twice with PBS 1X and incubated with 0.25% trypsin-EDTA at 37° for 5-10 min or until the cells detached. Afterwards, cells were resuspended in complete medium. Seeding density was determined using an automated cell counter (Invitrogen™ Countess™ II) and 0.4% trypan blue. BC cell lines were tested for mycoplasma contamination periodically and were amplified and stored at -80 °C or in liquid nitrogen.

TNBC cells were cultured as mammospheres in serum-free RPMI medium supplemented with 60 mg/mL glucose, 10 µL/mL L-glutamine, 10 µL/mL antibiotic-antimycotic mixture, 4 µg/mL heparin, 2 mg/mL BSA, 0.02 µg/mL EGF, 0.01 µg/mL FGFb, 10 µg/mL putrescin, 0.1 mg/mL apo-transferrin, 25 µg/mL insulin, 30 µM selenium and 20 µM progesterone.

3.2. Methods

3.2.1. Generation of cell line models with fluorescently labelled CSC

In this project, fluorescent CSC models were generated on TNBC MDA-MB-468 and HCC-1806 cell lines using specific promoter elements that drive the expression of both sensitive luciferase and tdTomato fluorescent protein. In these models, the fluorescent tdTomato reporter gene is driven by the human CSC specific promoter ALDH1A1, and its fluorescence is detected exclusively in the CSC subpopulation (tdTomato+ cells), while differentiated bulk tumor cells do not express the tdTomato fluorescent marker (tdTomato- cell subpopulation).

3.2.1.1. Lentiviral transduction

Pre-made lentiviral expression particles for luciferase were purchased from Amsbio (LVP434) and Perkin Elmer (CLS960002). For the lentiviral transduction in MDA-MB-468 cell line, lentiviral particles from Amsbio were used. These particles express firefly luciferase II gene under EF1 α promoter. RediFect™ Red-Fluc lentiviral particles from Perkin Elmer were used for lentiviral transduction of HCC-1806 cells. These particles carry red-shifted *Luciola Italica* luciferase transgene under control of the stable UbC promoter. Both promoters are constitutive, and therefore, a high and constant luciferase gene expression is expected. For viral infection of both TNBC cell lines, 20,000-50,000 cells were plated in complete medium into a 24-well plate and incubated for 24 h. Then, cells were incubated with the lentiviral particles (50 μ L) for 24 h. Since both lentiviral particles also encode for a puromycin resistance gene for transduction selection, cells were then washed and grown in culture media containing 10 μ g/mL puromycin dihydrochloride for an additional 72 h. Transduced cells were allowed to recover and to proliferate in order to expand puromycin resistant cells to generate a stable cell line. Transduction efficiency and, therefore, luciferase expression intensity, was checked by bioluminescence imaging (BLI, ph/s/cell) (explained in detail in section 3.2.2). The resulting transduced TNBC cell lines were named MDA-MB-468.Fluc and HCC-1806.RedFluc, according to the lentiviral particle used.

3.2.1.2. DNA plasmid transfection

DNA transfection is a commonly used method to introduce and overexpress a gene of interest in a specific cell line, in this case, the expression of the red fluorescent protein tdTomato. To obtain an efficient gene transfer by transfection, the DNA plasmid, which contains the gene tdTomato of interest, was complexed with the lipid reagent lipofectamine to mediate efficient delivery into the nucleus of cells. This process is essential for subsequent protein expression of the gene of interest. CSC fluorescent models were generated using previous transduced TNBC cell lines, MDA-MB-468.Fluc and HCC-1806.RedFluc cells. The ALDH1A1-tdTomato reporter vector previously used to generate the MCF-7-ALDH1A1-tdTomato and MDA-MB-231-ALDH1A1-tdTomato CSC models was the same used in these experiments [119,127]. The protocol used for cell transfection was adapted from manufacturer's recommendations. Briefly, MDA-MB-468.Fluc and HCC-1806.RedFluc cells were seeded in a 6-well plate at a density of 150,000 cells/well and incubated for 2-3 days. Then, complexes for cell transfection were prepared. In order to optimize the transfection procedure, different transfection mixtures of DNA plasmid:Lipofectamine 2000[®] were prepared (1:1, 1:2 and 1:4 tested ratios). Therefore, Lipofectamine 2000[®] and DNA were diluted, separately, in Opti-MEM I reduced serum medium and incubated for 5 min at room temperature (RT). After incubation time, the diluted DNA (1 µg of DNA diluted in OptiMEM I/each well) was mixed with the different diluted lipofectamine preparations and incubated for 20 min at RT. Culture medium was removed from 6-well plates and 1.5 mL of fresh media without antibiotics (which may interfere in cellular transfection) was added together with 500 µL/well of the proper transfection complexes. Cells were incubated overnight at 37°C. Next day, the medium was changed to incorporate 10 µg/mL blasticidin as a selection antibiotic.

3.2.1.3. CSC line validation

Positive and negative tdTomato cells (tdTomato⁺ and tdTomato⁻) generated were expanded, sorted by FACS (see section 3.2.4.1) and reseeded with the aim of reproducing the mother cell line in which tumoral non-CSC show no expression of tdTomato. For this, enriched tdTomato⁺ cells were cultured and the percentage of tdTomato⁺ within the cell line was monitored after each passage by flow cytometry (explained in 3.2.4.2 section) until it was obtained a tdTomato⁺ stabilized cell subpopulation (1-3%). The % of CSC within a tumor cell line seems to be characteristic for each cell line and varies among cancer cell lines. Overexpression of known stemness markers (ALDH1A1, ABCG2, ALOX5, CMKLR1, NOTCH4, OCT4 and NANOG) was

confirmed in tdTomato+ cells by quantitative reverse transcription polymerase reaction (RT-PCR) (section 3.2.10). In addition, tdTomato+ cells were tested for their capacity to form tumorspheres when growing in non-attachment conditions (see 3.2.5 section) and further tested for in vivo tumorigenic capacity, tumor growth incidence and metastasis potential by repopulation assay using orthotopic cancer mice models (detailed information in 3.2.12.1 section).

3.2.2. In vitro bioluminescence assay for luciferase reporter proteins

Bioluminescent light emitted from transduced TNBC cell lines was quantified in vitro. A two-fold serial cell dilution was performed in a black 96-well plate in 50 μ L and then, 50 μ L of bioluminescent substrate D-luciferin (D-luc, 300 μ g/mL) was added to each well. Immediately after the addition of the substrate, plate was imaged continuously for 30 min using the IVIS Spectrum instrument (PerkinElmer). Average emission of bioluminescence in photons per second (ph/s) was analyzed and quantified using the Living Image 3.2 software (PerkinElmer). Negative controls (no cells and cells without substrate) were included. Finally, results were adjusted to show photons per second per cell (ph/s/cell) and plotted using Prism 6 Software (GraphPad Software, Inc., CA, USA).

3.2.3. Anti-CSC drugs selection

The compounds used in this thesis were selected based on their reported activity against CSC, their presence in clinical trials and their commercial availability. First, a literature screening was carried out in Pubmed using the terms 'breast cancer stem cells' 'targeting' 'triple negative breast cancer'. The objective was to find FDA-approved compounds with specific activity against CSC to further demonstrate their activity in our CSC models. Seventeen compounds were finally selected: 6-shogaol, 8-quinolinol, acetaminophen, citral, defactinib, disulfiram, everolimus, flubendazol, glabridin, isoliquiritigenin, metformin hydrochloride, niclosamide, nitidine chloride, panobinostat, salinomycin, VS-5584 and YM-155 hydrochloride. Stock solutions were prepared, aliquoted in the freezer (at -20 or -80°C) or stored at room temperature, always according to medical reconstitution directions (using either DMSO or water as solvent) and drug storage recommendations. All drugs were diluted to the final concentration in fresh culture medium on the day of experiments. Summary of selected compounds including their chemical structure and targeting activity is provided in **Table 6**.

3.2.3.1. Cell viability assays by MTT in standard cultures

This assay is based on the ability of viable cells to convert the water-soluble MTT compound into insoluble purple formazan crystals by mitochondrial dehydrogenase enzymes. Therefore, the color obtained is directly proportional to the number of viable cells. Briefly, cells were seeded on 96-well plates at a density of 8,000-10,000 cells per well and left to attach for 24 h. For MTT assays in CSC and non-CSC, tdTomato+ and tdTomato- enriched cell subpopulations were used (explained in section 3.2.4.1), always verifying its purity (above 95%) before seeding by flow cytometry. Then, cells were incubated with increasing concentrations of the selected compounds for 72 h. Complete medium was used as negative control and 10% DMSO as positive control of toxicity. Subsequently, 5 mg/mL of MTT (diluted in PBS) were added to each well and cells were incubated for 2 to 4 h in order to allow formazan crystals to form. Formazan precipitates were resuspended in DMSO and plate absorbance was measured at 590 nm (ELx800, BioTek, Germany). Cell viability was calculated and normalized to negative controls (100% viability) and positive controls (0% viability). Dose-response curves were plotted and half inhibitory concentrations (IC_{50}) were determined using Prism 6 Software (GraphPad Software, Inc., CA, USA). All experiments were run in triplicate to determine an accurate IC_{50} and standard error of the mean (SEM).

3.2.3.2. Drug combination analysis

Drug combination studies were performed to evaluate the pharmacological interactions of 8Q and NCS with the antineoplastic reference drug Paclitaxel. For this purpose, the effect of combined treatments on cell viability was investigated using the MTT assay. Briefly, cells were treated simultaneously with increasing concentrations of one of the drugs together with the IC_{50} concentration of the other drug for 72 h, and vice versa, evaluating this way multiple drug combinations at multiple dose levels. Cell viability results obtained were then analyzed using the classical isobole method of Chou *et al.* [274]. According to this method, synergism, additivity or antagonism in different combinations is calculated on the basis of the multiple drug effect equation and quantitated by the combination index (CI). The CI was calculated using the CompuSyn software (ComboSyn Inc., NJ), where $CI=1$ indicates that the two drugs have additive effects, $CI<1$ indicates that the two drugs are synergistic and $CI>1$ indicates antagonistic activity. Single drug treatments were also included. All experiments were run in triplicate to determine an accurate CI and SEM.

3.2.4. Cell sorting and flow cytometry assays

3.2.4.1. Fluorescence-activated cell sorting (FACS)

FACS assay was performed to select, enrich and expand separately CSC-tdTomato⁺ and non-CSC-tdTomato⁻ subpopulations for CSC model validation and treatment evaluation by cell viability assays. Briefly, TNBC cells stably transfected with ALDH1A1-tdTomato plasmid were harvested, centrifuged (1,000 rpm for 5 min) and resuspended in 'Cytometry Buffer' (10% hi-FBS, 2% antibiotic-antimycotic and 10 µg/mL DAPI) at a final concentration of $5 \cdot 10^6$ viable cells/mL. Cell suspensions were filtered using 30 µm sterile filters (CellTrics[®], Sysmex Europe GmbH, Germany) before subjecting to cell sorter with the Flow Cytometer FACSAria[™] (High Speed FACSAria Digital Cell Sorter, Becton Dickinson Bioscience, USA). The yellow-green laser of 561 nm was used for the tdTomato detection and the violet laser of 405 nm for DAPI detection. Thereafter, enriched cells were seeded for the correct expansion of both cell subpopulations. The selection antibiotics puromycin and blasticidin were added once cells were completely attached to the culture plates.

3.2.4.2. Flow cytometry assays for tdTomato⁺ and tdTomato⁻ evaluation

Flow cytometry assays were performed to evaluate the percentage of CSC-tdTomato⁺ and non-CSC-tdTomato⁻ within cell culture of fluorescent CSC models generated, either to monitor the decrease of tdTomato⁺ cells after each passage or to verify the percentage of tdTomato⁺ and tdTomato⁻ cells before using them in in vitro assays. For this, cells were harvested, centrifuged (1,000 rpm for 5 min) and resuspended in 'Cytometry Buffer', at a final concentration of $1 \cdot 10^6$ viable cells/mL. Cell suspensions were examined through BD LSRFortessa[™] Cytometer (Becton Dickinson, Bioscience, San Jose, USA). At least three replicates were analyzed for each sample.

3.2.4.3. Flow cytometry assays for treatment evaluation in CSC

Flow cytometry assays of fluorescent CSC models were performed to evaluate if selected treatments (alone or in combination) led to an increase or reduction of CSC-tdTomato⁺ subpopulation. The tdTomato⁺ and tdTomato⁻ cell subpopulations were cultured at 50%-50% conditions, seeding cells on 6-well plates at a density of 200,000 cells per well. After 24 h, cells were incubated with the selected treatments (individual therapy and in combination) for 72 h. To mimic chemotherapeutic cycles, medium was then removed and cultures were reseeded with complete medium to allow cellular recovery

in the absence of drug/s for 48 h. The non-treated cells were also included as a negative control. Protocol followed for sample preparation was exactly the same as explained in previous section. Changes in the % of tdTomato+ were evaluated by the BD LSRFortessa™ Cytometer (Becton Dickinson, Bioscience, San Jose, USA) and subsequently analyzed using FCS express 7 Flow cytometry software (De novo, USA) to calculate the increase or decrease in the tdTomato+ ratio according to the % of tdTomato+ of non-treated cells. All experiments were performed in triplicate.

3.2.5. Mammosphere assay

Sphere assays were performed in order to study the ability of selected drugs in affecting both mammosphere-forming efficiency (MSF) and mammosphere viability (MSV), and thus, in inhibiting CSC proliferation in vitro. Cells were seeded in ultra-low attachment 96-well plates (Corning, NY, USA) at low density (1,000 viable cells/well) in serum-free RPMI 1640 Medium (media supplements specified in section 3.1.2). For MSF assays, 24 h after seeding, cells were treated with drugs for 7 days, while for MSV assays cells were cultured for one week to allow tumorspheres to form before adding drugs. The formed spheres were observed by the optical microscope (Olympus IMT-2 model) and quantified by MTT to further calculate IC₅₀ as previously described.

3.2.6. Colony formation assay (anchorage-independent growth)

Colony formation assay in soft agar is an excellent in vitro approach to study the effect of novel therapeutic cancer drugs in neoplastic transformation, specifically, in affecting anchorage-independent growth ability, which is considered one of the distinctive features that transformed malignant cells display. Anchorage-independent growth was assessed using CytoSelect™ Cell Transformation Assay Kit (Cell Biolabs, Inc., San Diego, USA). A semisolid agar media was prepared in a 96-well plate according to manufacturer's instructions. Cell suspension (10,000 cells/well) and selected drugs were added to plates and subsequently incubated for 6-8 days at 37°C in a 5% CO₂ incubator. Following treatment, colonies formed were observed under optical microscope and viable transformed cells were quantified by MTT. All experiments were performed in triplicate.

3.2.7. Wound healing assay

The wound-healing (or scratch) assay is a standard *in vitro* technique for studying collective cell migration, which has been related with many pathological processes, such as cancer invasion and metastasis. Therefore, this method is suitable to assess malignant cell migration over time under treatment conditions. Of note, the study was limited to 24 h to minimize the contribution of cell proliferation to gap filling. Moreover, to avoid interferences of undefined growth factors, 24 h hi-FBS starvation was also applied. Briefly, a scratch was made in confluent monolayers of MDA-MB-231 cells by using a sterile 2-20 μL pipette tip. After washing away suspended cells, cultures were reseeded with medium in the presence of selected treatments. Non-treated cells were used as negative control. Wound closure space was measured at 0, 8 and 24 h after wounding using an inverted microscope (FSX100 microscope, Olympus Life Science) and the ImageJ software. Wound closure was determined as the difference between wound width at 0 h and 8 h. All treatment conditions were tested in triplicate.

3.2.8. Matrigel cell invasion assay

Cell invasion assays were performed in order to assess the effect of drugs in invasive cell behavior, a property closely related with tumor dissemination and cancer metastasis. Invasion experiments were conducted using a conventional 24-well plate with cell culture inserts (membrane pore size of 8 μm ; FalconTM, Fisher Scientific, USA). Briefly, the coating buffer (0.01 M Tris pH 8.0 and 0.7% NaCl) was prepared and then mixed with Matrigel (1 mg/mL) to prepare the coating solution. Subsequently, cell culture inserts were coated with 100 μL of the coating solution and plate was incubated at 37°C for 2 h. After Matrigel solidification, MDA-MB-231 cells (10,000 cells/300 μL , previous 24 h hi-FBS starvation) were added into the upper chamber of each insert together with the selected treatments. Non-treated cells were used as negative control. The chemo-attractant (complete medium with 10% hi-FBS) was placed in the lower chamber of each well. After 24 h incubation, the upper surface of the filter was wiped with a cotton-tipped applicator to remove non-invading cells. Cells that had invaded through the filter pores and attached to the under surface of the filter were fixed with Methanol 100% and stained with 0.4% crystal violet (Sigma) solution for 15 min. The membranes were mounted on glass slides, and cells from 10 random microscopic fields (20x magnifications) were counted using ImageJ software. Cell invasion rate was calculated referred to control values. This experiment was repeated in triplicate.

3.2.9. CSC reversion assay

Cell reversion experiments were performed to study the dynamic interconversion process from which CSC can differentiate to non-CSC, which in turn are able to de-differentiate into cells with stem cell-like properties. This dynamic plasticity between non-CSC and CSC populations confer to non-CSC tumor initiation capacity and therapy resistance. Briefly, enriched tdTomato⁺ and tdTomato⁻ subpopulations by FACS (see 3.2.4.1 section) were used. After cell sorting (day 0), overexpression and underexpression of several stemness markers was confirmed by quantitative RT-PCR (see following section) in sorted tdTomato⁺ and tdTomato⁻ cells, respectively. Next, both populations were cultured for subsequent cell passages. Percentage of tdTomato⁺ cells within the culture was monitored at cell passage number 1 and 5 by flow cytometry. Meanwhile, cell samples were also collected and changes in the stemness gene signature were studied by quantitative RT-PCR. Results were calculated and referred to the initial values from both populations at day 0.

3.2.10. Stemness gene expression-based analysis

The overexpression of several stemness markers involved in the maintenance of CSC pluripotent properties has been described in poorly differentiated BC subtypes, specifically, in the TNBC subtype. In this context, we analyzed a panel of genes responsible for CSC reprogramming and behavior in both tdTomato⁺ and tdTomato⁻ populations in the fluorescent models developed. CSC phenotype is defined by special transcription factors such as ALDH1A1, ABCG2, ALOX5, CMKLR1, NOTCH4, NANOG, SOX2, and OCT4. The present genomic study aimed to determine changes in gene expression of the above markers in correlation with the treatments tested as well as to validate the stemness nature of tdTomato⁺ cells of fluorescent CSC models generated.

3.2.10.1. Total RNA purification and quantification

For treatment evaluation experiments, cells were seeded in 6-well plates at a density of 200,000 cells per well and left to attach for 24 h. Then, cells were incubated with the selected compounds (either single or combined therapy) for 72 h. While for validation studies, cells were just cultured until they reached a confluence of 80-90%. From this point on, the protocol followed was the same for all the samples. Total RNA was extracted using the RNeasy Mini Kit (Qiagen, Hilden, Germany) following the manufacturer's protocol. Quantification and quality evaluation of purified RNA samples were assessed by NanoDrop 2000 spectrophotometer (NDS, Thermo Scientific™)

following the software's instructions. Purified eluted RNA samples were stored at -80°C to avoid RNA degradation.

3.2.10.2. Retrotranscriptase polymerase chain reaction (RT-PCR)

The reverse transcription for synthesizing cDNA from total RNA was performed using the High-Capacity cDNA Reverse Transcription Kit (ThermoFisher scientific, CA, USA) according to manufacturer's instructions. This kit uses the random primer scheme for initiating cDNA synthesis from total RNA (3 μg of RNA of each sample), ensuring this way that the first strand synthesis occurs efficiently. For reverse transcription reaction, it was used the thermal cycler (MJ Research PTC-100 Thermal Cycler, Marshall Scientific) under the thermal cycling conditions specified in the kit guideline. The resulting cDNA was stored at -20°C until use.

3.2.10.3. Quantitative real time PCR (qRT-PCR)

Quantitative real time PCR is a valuable tool for measuring gene expression in biological cell samples. In this thesis, the cDNA reverse transcription products were amplified with specific primers by qRT-PCR using the SYBR Green method (ThermoFisher Scientific, CA, USA). The primer design was performed according to the target sequences of interest, which were the selected pluripotential genes ALDH1A1, ABCG2, ALOX5, CMKLR1, NOTCH4, NANOG, SOX2 and OCT4. Glyceraldehyde 3-phosphate dehydrogenase (GAPDH) and β -Actin genes were also included as endogenous controls. The qRT-PCR reactions were performed using 12.5 $\text{ng}/\mu\text{L}$ cDNA, 2x SYBR Green PCR Master mix (#4309155, ThermoFisher Scientific, CA, USA) and 0.5 μM of primers (primer sequences are provided in **Table 10**). All the qRT-PCR reactions were performed in triplicate on a 7500 Real time PCR system (ThermoFisher Scientific, CA, USA) using the following cycle conditions, an initial denaturing 95°C for 10 minutes, a denaturing process for 15 seconds at 95°C and the annealing process for one minute at 60°C , these last two steps were repeated during 40 cycles. Gene expression was normalized against GAPDH and β -Actin housekeeping genes. The relative fold-change quantification of gene expression was calculated using the comparative Ct method ($2^{-\Delta\Delta\text{CT}}$) [275].

Table 10. Primer sequences used in qRT-PCR assays.

Target gene	Primer sequence (5'-3')
ALDH1A1	Forward CGCAAGACAGGCTTTTCAG Reverse TGTATAATAGTCGCCCCCTCTC
ALOX5	Forward AGAACCTGGCCAACAAGATTGT Reverse TCTGGTGGACGTGGAAGTCA
ABCG2	Forward AGCTCAGATCATTGTCACAGTCGT Reverse GAACCCAGCTCTGTTCTGG
OCT-4	Forward CCTGCACCGTCACCCCT Reverse GGCTGAATACCTTCCCAAATAGAAC
CMKLR1	Forward GGAGCCTGTGATTGGCAGAA Reverse CAGCCAATCAGTCCCTGTACAC
SOX2	Forward GGGAAATGGGAGGGGTGCAAAGAGG Reverse TTGCGTGAGTGTGGATGGGGATTGGTG
Notch4	Forward GCCCCTCTGGTTTCACAGG Reverse AGTTGGCCTTGCTTTCTGGTC
Nanog	Forward AGATGCCTCACACGGAGACTG Reverse TTGACCGGGACCTTGTCTTC
GAPDH	Forward ACCCACTCCTCCACCTTTGAC Reverse CATACCAGGAAATGAGCTTGACAA
β-Actin	Forward CATCCACGAAACTACCTTCAACTCC Reverse GAGCCGCCGATCCACAC

3.2.11. Western blot

Western blot technique was used to study changes in target protein expression of specific signaling pathways -reported to be essential for the CSC stem cell-like phenotype- in correlation with the treatments tested (individual and combined therapy).

3.2.11.1. Protein extraction from cell cultures

Cells were seeded in 100 mm culture dishes and cultured until they reached a confluence of 60-70%. Then, cells were incubated with different concentrations of selected drugs for 24 h. For control samples, non-treated cells were cultured until they reached a confluence of 80-90%. Following treatment, culture dishes were placed on ice and cells were washed, harvested, and lysed in M-PER mammalian protein extraction buffer (ThermoFisher Scientific, CA, USA) supplemented with 1X phosphatase and 1X EDTA-free protease inhibitor cocktails (#539134 and #524625; Merck Millipore, MA, USA) using a cold plastic 25 cm cell scraper (Sarstedt®). Cell lysis was done on ice for 60 min and

vortexed every 15 min for 30 s. Lysates were cleared by centrifugation (Refrigerated microcentrifuge 5415R, Eppendorf, Germany) at 13,000 rpm for 20 min at 4°C. Protein samples were stored at -20°C until further use.

3.2.11.2. Determination of protein concentration and sample preparation

Protein concentration was determined using the Pierce™ BCA Protein Assay kit (ThermoFisher Scientific, CA, USA) following manufacturer's instructions. Thirty µg of protein were prepared in 1X loading buffer (10% SDS, 0.5 M Tris buffer pH 6.8, Glycerol, bromophenol blue 0.2% and DTT 1 M) and further reduced and denatured by heating the samples at 95°C for 5 min.

3.2.11.3. Protein separation by SDS-PAGE and protein wet transfer

Samples were run in 8-10% SDS-polyacrylamide gels in running buffer 1X (1% SDS, 0.25 M Tris and 1.9 M Glycine) for 1-2 h at 100 V at room temperature (RT). After electrophoresis, proteins were transferred to methanol-activated nitrocellulose membranes (Bio-Rad Laboratories, CA, USA) through wet transfer method by placing the membrane sandwich in a transfer bank and run for 90 min at 0.3 A.

After protein transfer, membranes were incubated with blocking solution (Tris-buffered saline with 0.1% Tween 20 (TBS-T) and 5% BSA) at RT for 1 h. Next, membranes were incubated overnight in constantly rocking at 4°C with the indicated antibodies (see **Table 11**), properly diluted using the same blocking solution. After three washings with TBS-T of 5 min at RT, membranes were incubated with the corresponding horseradish peroxidase (HRP)-conjugated secondary antibody (see **Table 11**) at RT for 1 h, properly diluted in blocking solution. Anti-β-Actin-HRP was used as loading control.

For signal detection, membranes were washed 3 times with TBS-T of 5 min each. Then, reagent for signal chemiluminescence development was added following the kit manufacturer's recommendations. For abundant protein targets was used the Clarity Western ECL Substrate (#1705061; Bio-Rad Laboratories, CA, USA), while for low abundance proteins was used the Amersham ECL Prime Western Blotting Detection Reagent (GE Healthcare, UK). In both cases, images were acquired with a chemiluminescent imaging system (LAS-3000 Imager, Fuji film) and protein band intensity was quantified using the ImageJ software and further normalized to the loading control (β-actin protein expression).

Table 11. List of antibodies used for protein detection in western blot assays.

Primary and secondary antibodies used in WB					
Antigen	Molecular weight (kDa)	Specie	Antibody conditions	Company	Reference number
β -Actin-HRP [AC-15]	42	Mouse	1:20,000 in TBS-T + 5% BSA	Abcam	ab49900
Phospho-NF- κ B p65 (Ser536)	65	Rabbit	1:1,000 in TBS-T + 5% BSA	Cell Signaling Technology	#3033
Phospho- β -Catenin (Ser33/37/Thr41)	92	Rabbit	1:1,000 in TBS-T + 5% BSA	Cell Signaling Technology	#9561
NF- κ B p65 (D14E12)	65	Rabbit	1:1,000 in TBS-T + 5% BSA	Cell Signaling Technology	#8242
Phospho-GSK-3 β (Ser9) (D85E12)	46	Rabbit	1:1,000 in TBS-T + 5% BSA	Cell Signaling Technology	#5558
GSK-3 β (3D10)	46	Mouse	1:1,000 in TBS-T + 5% BSA	Cell Signaling Technology	#9832
Anti-rabbit HRP-Linked	---	Donkey	1:10,000 in in TBS-T + 5% BSA	Cytiva	NA934
Anti-mouse HRP conjugate	---	Goat	1:10,000 in TBS-T + 5% BSA	Agilent Technologies	P0447

3.2.12. In vivo studies

Six-week-old female NOD/SCID mice (NOD.CB-17-Prkdc^{scid}/Rj) were obtained from Janvier Laboratories (Le Genest-Saint-Isle, France), housed under specific pathogen-free conditions and provided with food and water ad libitum.

Animal care was handled in accordance with the Guide for the Care and Use of Laboratory Animals of the Vall d'Hebron University Hospital Animal Facility. Experimental procedures were approved by the Animal Experimentation Ethical Committee at the institution (approval number CEA-OH/9467/2). All the in vivo studies were performed by the Unique Scientific and Technical Infrastructures (ICTS) "NANBIOSIS", more specifically at the Bioengineering, Biomaterials and Nanomedicine Research Center in vivo Experimental Platform of the Functional Validation and Preclinical Research area (<https://www.nanbiosis.es/portfolio/u20-in-vivo-experimental-platform>, Barcelona, Spain)

3.2.12.1. In vivo tumorigenic and metastatic capacity assay

In vivo validation of fluorescent CSC models generated on TNBC MDA-MB-468 and HCC-1806 cell lines was performed using tdTomato⁺ and tdTomato⁻ subpopulations previously enriched and sorted by FACS (see 3.2.4.1 section). After cell sorting, overexpression and underexpression of stemness markers was confirmed by qRT-PCR in tdTomato⁺ and tdTomato⁻ cells, respectively (section 3.2.10).

For both cell lines validation, three different cell densities (100,000, 10,000 and 1,000 cells per mouse) of tdTomato⁺ and tdTomato⁻ subpopulations were inoculated orthotopically into the right mammary fat pad (i.m.f.p.) of mice (5 animals/each group, total n=30). For cell inoculation, enriched tdTomato⁺ and tdTomato⁻ cells were harvested, counted and centrifuged. Then, cells were suspended in a 1:1 mixture of PBS and Matrigel (BD Bioscience, Bedford, MA, USA). Tumor growth was monitored twice a week by conventional caliper measurements ($D \times d^2/2$, where D is the major diameter and d the minor diameter). Once primary tumors reached a tumor volume range between 250–450 mm³, tumors were excised, weighted, and divided into several fragments for cytometry analyses (detailed protocol in section 3.2.13). Whole blood samples were drawn from each animal by cardiac puncture and transferred directly into commercial EDTA containing tubes and processed immediately to isolate and analyze circulating tumor cells content by flow cytometry (see section below). Afterwards, tissues (lungs, kidney, spleen and liver) were harvested and weighted. Immediately after necropsy, lung tissues were placed individually into separate wells containing 300 µg/mL of D-luciferin, and imaged and quantified using Living Image[®] 4.5.2 software to assess lung metastasis potential of cells inoculated. All tumor and tissue samples collected were formalin-fixed, and paraffin-embedded for hematoxylin and immunohistochemical staining.

3.2.12.2. Stem cell isolation and detection from mice blood samples

Metastasis starts with the dissemination of cancer cells from the primary site to the bloodstream and ends with tumor formation in distant organs. Cancer cells that intravasate entering the bloodstream are called circulating tumor cells (CTC). Therefore, isolation and quantification of CTC is a valuable tool for validating metastatic potential of CSC-tdTomato⁺ cells as well as for assessing therapeutic efficacy of drugs.

Blood samples were drawn from each animal by cardiac puncture and further processed to isolate CTC using the following protocol. First, collected samples were subjected to several cycles of erythrocytes lysis using a lysis buffer, which consisted in a mixture of 90% of 0.16 M NH₄Cl and 10% of 0.17 M Tris (pH 7.65). A total of 5 mL of lysis buffer was added to each tube and samples were incubated for 5 min at 37°C. Following incubation, samples were then centrifuged (500G for 10 min at 4°C). These steps were repeated until a white cell pellet was obtained, thus indicating a proper lysis of RBC. Subsequently, pelleted cells were resuspended in cytometry buffer and examined by flow cytometry. Data was analyzed using the FCS Express 7 software. Of note, in those in vivo studies where the inoculated cells did not express any fluorescent marker, a detection method was previously optimized to differentiate CTC from blood components.

This method consisted in adding a known number of tumor cells in blood samples and processing them following the same hemolysis protocol in order to establish the optimal flow cytometry settings and parameters for CTC detection.

3.2.12.3. In vivo therapeutic efficacy assay

To study the anti-tumor and anti-CSC potential of PTX in combination with NCS (either free or encapsulated in PM), single and combined treatments were tested using an orthotopic mice model in order to evaluate their therapeutic efficacy in reducing tumor growth and progression, and metastasis generation (**Figure 26**). With this aim, $1 \cdot 10^6$ MDA-MB-231 cells were suspended in a 1:1 mixture of culture medium and Matrigel and injected i.m.f.p. in NOD-SCID mice. When tumor volumes reached 70-80 mm³, mice were randomized into four groups according to administration of vehicles (n=6), PTX (n=9), combination treatment with PTX and NCS (n=9) or PTX and PM-NCS combination (n=10). The vehicle group was intravenously and intraperitoneally administered with saline solution (two times a week) and with Cremophor:DMSO 50:50 (five times a week), respectively. PTX (10 mg/kg) and PM-NCS (4 mg/kg) were intravenously administered 3 times a week during the first week and then 2 times a week the next 2 weeks, and finally, NCS (10 mg/kg) was intraperitoneally administered 5 times a week. All treatments were administered over a period of 24 days, in order to assess treatments' efficacy on tumor regression, number of CTC and lung metastasis generation (**Figure 26**). Tumor growth was monitored twice a week by conventional caliper measurements. Upon reaching the endpoint, mice were treated with their corresponding last treatment and 1 h after administration were euthanized and blood was immediately collected by cardiac puncture for the analysis of CTC content by flow cytometry (explained in previous section 3.2.12.2). To measure the extent of lung metastasis ex vivo, BLI was also performed using the IVIS Spectrum after administering 150 mg/kg of D-luciferin to mice. Afterwards, tumors and tissues (lungs, kidney, spleen and liver) were harvested and weighted. Immediately after necropsy, lung tissues were placed individually into separate wells containing 300 µg/mL of D-luciferin, and imaged and quantified using Living Image[®] 4.5.2 software. All tumor and tissue samples collected were formalin-fixed, and paraffin-embedded for hematoxylin and immunohistochemical staining.

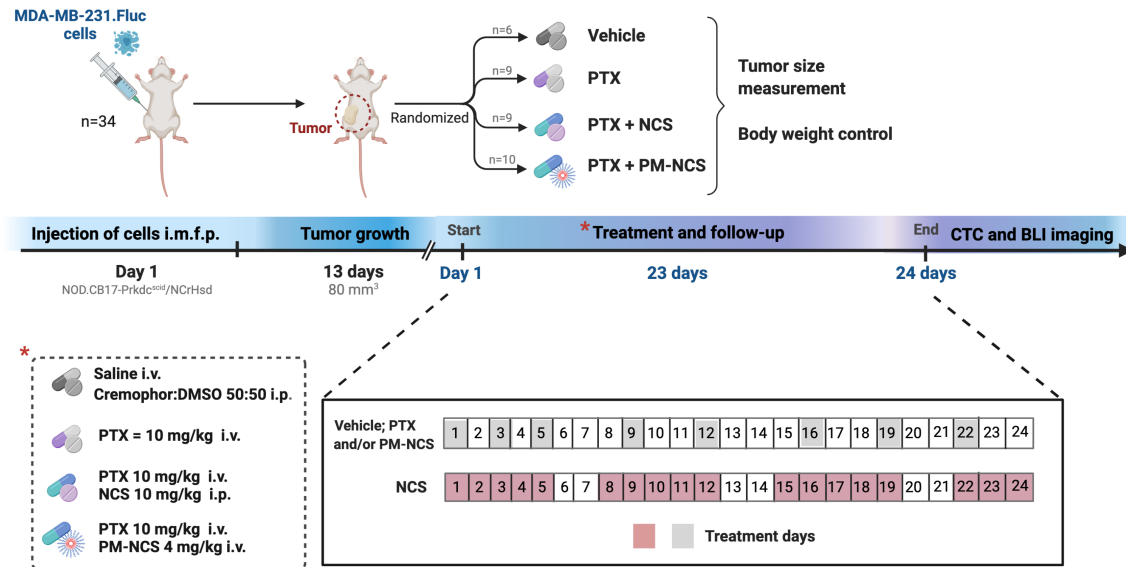


Figure 26. Experimental protocol schedule for the in vivo therapeutic efficacy assay in mice. MDA-MB-231 cells were injected i.m.f.p. of NOD/SCID mice. When tumors reached volumes of 70-80 mm³, mice were randomized into four experimental groups: vehicle (n=6), PTX (n=9), combination treatment with PTX and NCS (n=9), or PTX and PM-NCS combination (n=10). The vehicle group was administered with saline solution (2 times/week; i.v.) and with Cremophor:DMSO 50:50 (5 times/week; i.p.). PTX (10 mg/kg i.v.) and PM-NCS (4 mg/kg i.v.) were administered 3 times/week during the first week and then 2 times/week the next 2 weeks. NCS (10 mg/kg i.p.) was administered 5 times/week. All treatments were administered over a period of 24 days. After treatment, CTC content was evaluated by flow cytometry and BLI imaging in vivo and ex vivo was performed to measure the extent of metastasis.

3.2.13. Analysis of tdTomato expression in solid tumors

Ex vivo analysis of tdTomato expression from excised tumors was performed with the aim of fully validating the TNBC CSC models generated as well as to elucidate the dynamic interconversion process by which non-CSC can dedifferentiate to CSC. Accordingly, following surgical tumor resection, tumors were immediately placed in ice-cold PBS, followed by mechanical tissue disaggregation using a 24-scalpel blade in 1-2 mL of Basal medium eagle (BME) supplemented with 10 mM HEPES. Next, tissue fragments were collected in tubes containing 'enzyme medium', which consisted in BME-HEPES supplemented with DNase I (1500 Kunitz units) and Collagenase type I (200 U/mL) and then incubated for enzyme digestion for 30 min at 37°C in continuous stirring. Single cell suspensions were prepared by passing the digested tissue through 40 µm nylon cell strainers (BD Biosciences). Subsequently, cell suspensions were centrifuged for 5 min at 1,200 rpm, resuspended in 'cytometry buffer' and further examined by flow cytometry (BD LSR Fortessa™ Cytometer, Becton Dickinson Bioscience, USA). Since

cells of interest ranged between 0.5-2% of the total, cytometer parameters were carefully defined to analyze the cell population of interest. For each sample, at least 10,000 individual cells (number of events) were collected. Data was analyzed using the FCS Express 7 software.

3.2.14. Immunohistochemistry analysis

Tumors were removed, fixed in 10% neutral-buffered formalin, and embedded in paraffin. Tissue sections of 4 mm thickness were mounted on positively charged glass slides and de-paraffinized with xylene and subsequently dehydrated through a graded alcohol series to water. For antigen retrieval, sections were boiled in a pressure cooker or microwave heating in citric acid buffer (pH 6). Tissue sections with primary antibodies in antibody-diluent were incubated overnight at 4°C, and then reacted with corresponding secondary antibodies (summarized in **Table 12**). DAB (3,3'-diaminobenzidine) was used as a chromogen, and sections were counterstained with hematoxylin.

Table 12. List of antibodies used for immunohistochemistry (IHC) assays.

Primary and secondary antibodies used in IHC					
Antigen	Specie	Dilution	Antigen retrieval conditions	Company	Reference number
tdTomato	Mouse	1:100	Autoclave, CB pH 6	Origene – Quimigen SL	TA180009
ALDH1A1 (B-5)	Mouse	1:500	Pressure cooker, CB pH 6	Santa Cruz Biotechnology	sc-374149
CD133/1 (AC133)	Mouse	1:50	Microwave oven, CB pH 6	Miltenyi Biotec	130-108-062
ABCG2 (B-1)	Mouse	1:50	Microwave oven, CB pH 6	Santa Cruz Biotechnology	sc-377176
Ep-CAM (C-10)	Mouse	1:100	Pressure cooker, CB pH 6	Santa Cruz Biotechnology	sc-25308
Anti-mouse HRP labeled polymer	Goat	Ready to use	---	Agilent Technologies (Dako)	K4000

CB: Citric acid buffer

3.2.15. Statistical analysis

All experimental procedures were repeated at least three times, each involving 2 to 6 technical replicates. All data plotted as dose-response curves and bar graphs were expressed as the mean value \pm SEM (standard error of the mean), expressed as error bars. One-way ANOVA analysis, unpaired two-tailed student's t-test or equivalent non-parametric tests were used to investigate the differences between tested compounds and controls. Differences were considered statistically significant when p-value was equal or below 0.05 (*), 0.01 (**), 0.001 (***) and 0.0001 (****).

RESULTS

RESULTS

4.1. Generation of TNBC reporter cell lines with constitutive expression of luciferase and fluorescently labelled cancer stem cells

In order to study the efficacy of drug candidates and nanoparticles in marginal population of highly aggressive CSCs, two novel in vitro TNBC fluorescent CSC models were generated. In these models, the reporter genes of both bioluminescent luciferase and fluorescent tdTomato proteins were used.

4.1.1. Luciferase reporter expression in HCC-1806 and MDA-MB-468 TNBC cells

Luciferase reporter is a widely used method for image-based cell tracking in vivo, including in vivo monitoring of tumor growth and metastasis [276–278]. Thus, we generated bioluminescent tumor cell lines from HCC-1806 and MDA-MB-468 cells by viral transduction with luciferase constructs. The resulting transduced cell lines were then selected for antibiotic resistance and subcloned for stable performance. The luciferase expression intensity was evaluated to assess the level of reporter expression and the relationship between bioluminescence (BLI) signal and viable number of cells. As shown in **Figure 27A** and **B**, the BLI intensity in both cell lines increased proportionally with cell number. A strong correlation between number of cells and light emission was obtained ($R^2_{\text{HCC-1806.Red-Fluc}} = 0.999$ and $R^2_{\text{MDA-MB-468.Fluc}} = 0.998$). Further, BLI intensity *per cell* was calculated as an indicator of luciferase activity for both cell lines. As shown in **Figure 27C**, the photon output of HCC-1806.Red-Fluc clones ranged from 2,600 to 3,600 ph/s/cell (mean value 3,200 ph/s/cell), nearly three times higher than MDA-MB-468.Fluc cells, whose BLI signal was around 1,300 ph/s/cell. Such differences in luciferase activity may be attributed to the different luciferase viral constructs used. Red-Fluc (red-shifted firefly luciferase) has been described to be brighter than other firefly luciferases, emitting higher signal intensity and longer wavelength light. Besides, the red-shifted signal emission allows more sensitive tumor and metastasis detection as well as an improved tumor growth monitoring in deep tissues in mice [279].

Both transduced cell lines showed good performance in vitro, showing similar BLI intensity values than previous generated luciferase-expressing cell lines in our laboratory (i.e., 1,200 ph/s/cell for HCT-116.Fluc2 and 3,500 for MCF-7.Luc2) and other research groups [119,280–282]. Therefore, the signal intensity obtained from both transduced cell lines was strong enough for image-based cell tracking in vivo.

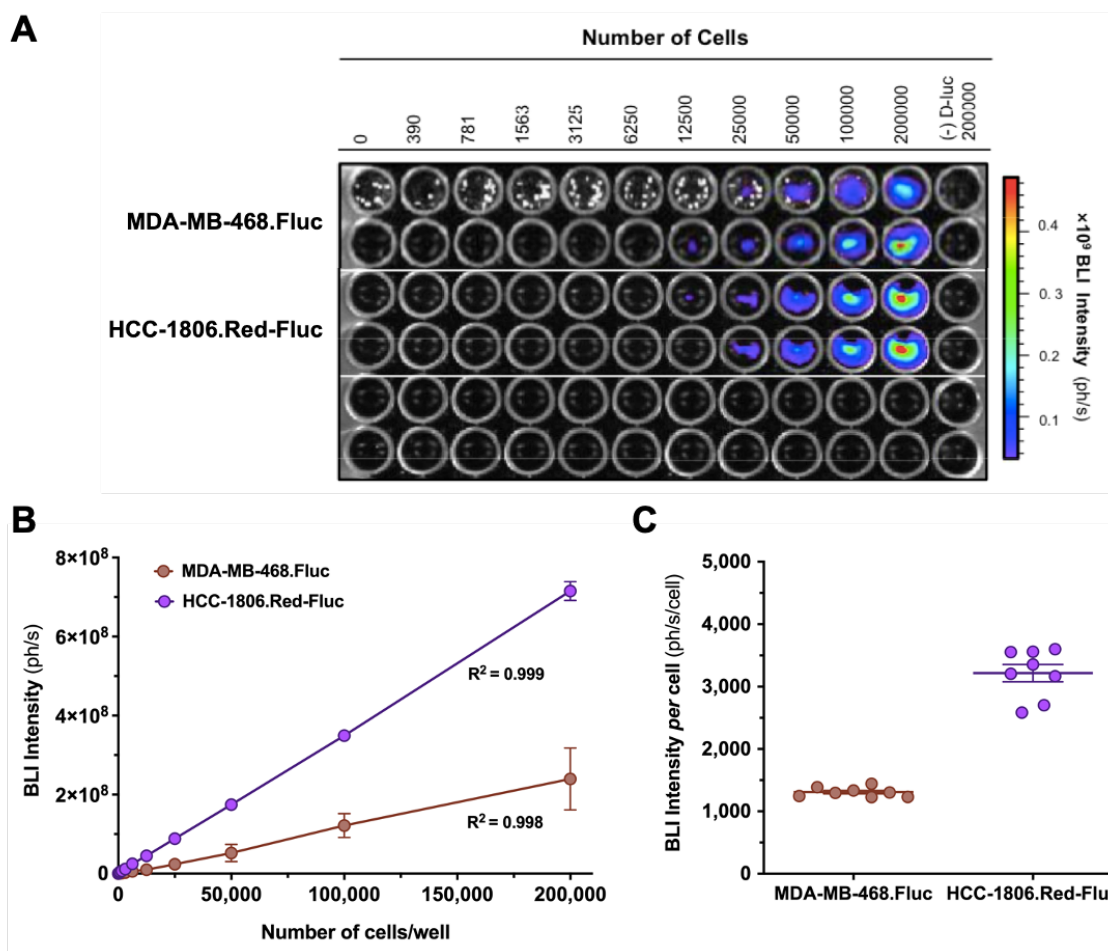


Figure 27. Bioluminescence characterization of luciferase-transduced TNBC cell lines. **A)** Representative IVIS image of black 96-well plate with bioluminescent MDA-MB-468.Fluc and HCC-1806.Red-Fluc transduced cells 15 min after D-luciferin substrate addition. **B-C)** Bioluminescence detection and quantification using IVIS SpectrumCT system. **B)** In vitro linear regression plots generated from both cell lines. Each point corresponds to bioluminescence signal represented by the total mean flux recorded (ph/s) from well duplicates. In both cell lines, linear regression analysis showed a very strong positive correlation between bioluminescence signal and cell number, since the correlation square coefficients (R^2) for both cell lines were above 0.99. **C)** Bioluminescent light production *per cell* (ph/s/cell).

4.1.2. In vitro characterization of ALDH1A1-tdTomato expressing HCC-1806 and MDA-MB-468 TNBC cells

In order to obtain permanently tagged CSCs, TNBC cell lines already expressing luciferase reporter were stably transfected with the ALDH1A1/tdTomato reporter vector (**Figure 28**). Since the majority of BC tumors express ALDH1A1 in the CSC subpopulation, reporter constructs based on ALDH1A1 promoter are considered a good approach to identify and trace this cell subpopulation in cancer cell lines [121]. The same strategy has proved successful for the highly aggressive MDA-MB-231 TNBC cell line, MCF-7 BC cell line and HCT-116 colon cancer cell line [119,127]. In these models, fluorescence was detected exclusively in the CSC subpopulation (tdTomato+ cells), while differentiated bulk tumor cells did not express the tdTomato fluorescent marker (tdTomato- cell subpopulation).

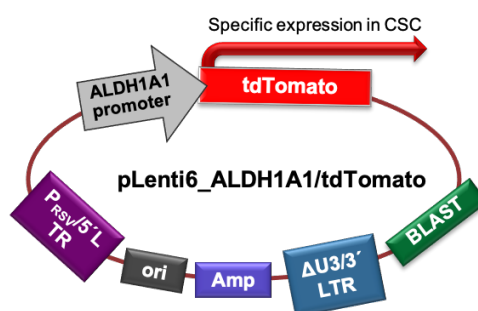


Figure 28. Schematic diagram of pLenti6_ALDH1A1/tdTomato-based plasmid. The tdTomato reporter cDNA was cloned under the minimal ALDH1A1 promoter (forward TTCTGATTCGGCTCCTGG; reverse TTGCTCTGAGTTTGTTTCATCC) in the pLenti6/V5-TOPO vector. The result is a plasmid in which the expression of the tdTomato fluorescent protein is under the control of the CSC specific promoter ALDH1A1.

Transfected cells were sorted by fluorescence-activated cell sorting (FACS) based on tdTomato fluorescence and reseeded in normal attachment conditions to reproduce the parent cell line, and so to figure out the baseline percentage of CSCs, which seems to be specific of each tumor cell line. Adherent culture media of CSCs causes their differentiation to non-CSCs, resulting in their loss of tdTomato expression (**Figure 29A**). As shown in **Figure 29B** and **29D**, subsequent cell passages of the initial enriched tdTomato-expressing cells (99.99%) led to a progressive decline and then stabilization of the tdTomato+ subpopulation in a very low percentage in both cell lines. In the HCC-1806.Red-Fluc.ALDH1A1-tdTomato cell line, hereinafter referred to as 'HCC-1806-tdTomato', the stabilization of the tdTomato+ subpopulation was reached at cell passage number 30, which accounted for 1.41% ± 0.14% of tdTomato+ cells (**Figure 29C**), while

in the MDA-MB-468.Fluc.ALDH1A1-tdTomato cell line, hereinafter referred to as 'MDA-MB-468-tdTomato', the amount of tdTomato+ cells stabilized after 18 passages at $1.42\% \pm 0.18\%$ (Figure 29E).

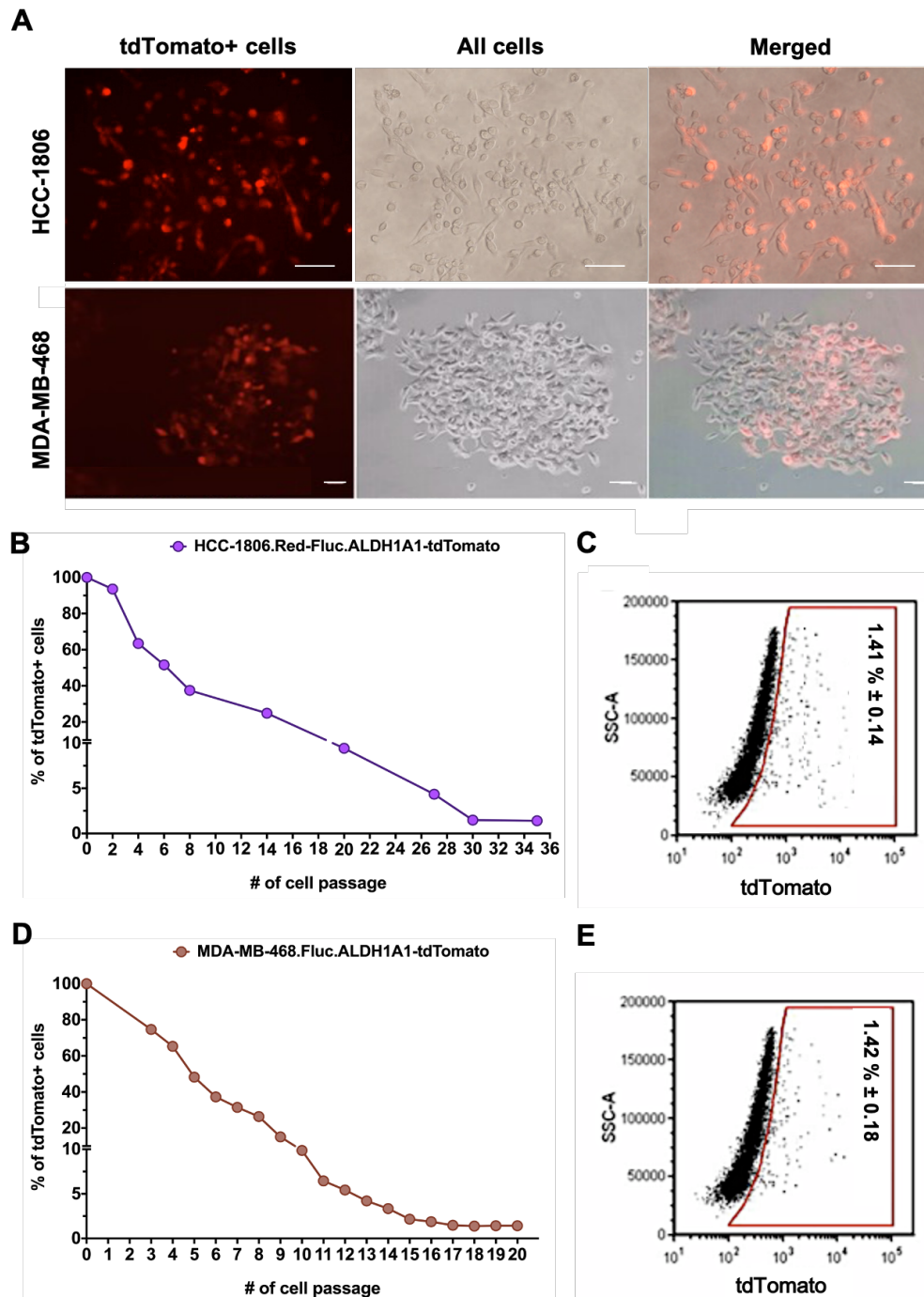


Figure 29. HCC-1806- and MDA-MB-468-tdTomato models. **A)** After transfection with the reporter ALDH1A1/tdTomato, CSC-like cells express the fluorescent reporter tdTomato under the CSC specific promoter (ALDH1A1). Scale bar represents 20 μm . **B,D)** Sorted tdTomato+ cell population dropped and stabilized over passages in both cell lines. **C,E)** HCC-1806- and MDA-MB-468-tdTomato+ cells were sorted by FACS and quantified as 1.41% and 1.42% of total cell population, respectively.

The stemness nature of tdTomato-expressing cells was studied by analyzing mRNA expression of stem cells markers, such as ALOX5, OCT4, ABCG2, NOTCH4 and NANOG by qPCR (**Figure 30**). As expected, the tdTomato⁺ population showed a significant increase of ALDH1A1 mRNA levels in both HCC-1806- and MDA-MB-468-tdTomato cell lines (1.79 ± 0.13 , $p = 0.026$ and 2.64 ± 0.08 , $p = 0.0021$ respectively). Furthermore, in the HCC-1806-tdTomato cell line, other CSC markers such ALOX5, OCT4, ABCG2, NOTCH4 and NANOG were also found to be overexpressed in tdTomato⁺ cells (2.32 ± 0.03 , $p = 0.0005$; 2.28 ± 0.09 , $p = 0.0056$; 1.45 ± 0.08 , $p = 0.028$; 5.13 ± 0.21 , $p = 0.0024$; 2.58 ± 0.14 , $p = 0.0073$ respectively) (**Figure 30A**).

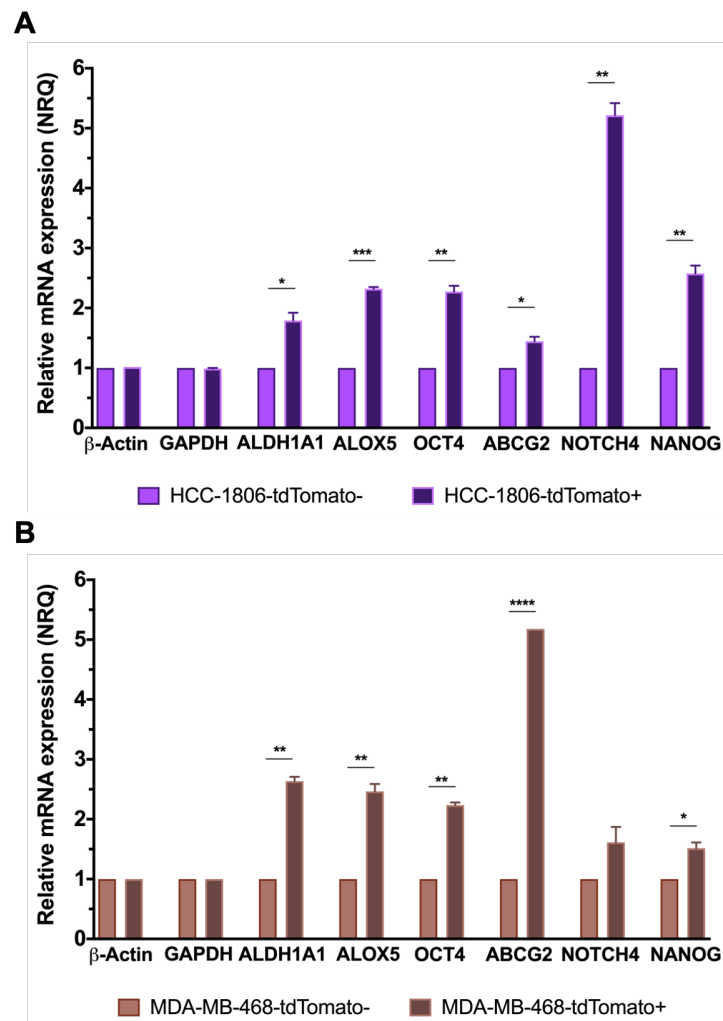


Figure 30. Stem cell-like gene expression profile of enriched CSC and non-CSC subpopulations from TNBC fluorescent models measured by qRT-PCR. The stem cell phenotype of tdTomato⁺ cells from HC-1806 (**A**) and MDA-MB-468 (**B**) fluorescent models was confirmed by a significant overexpression of almost all the stem cell markers analyzed. Results are expressed as NRQ (normalized relative quantities) mean \pm SEM ($n \geq 3$); * $p < 0.05$; ** $p < 0.01$, *** $p < 0.001$, **** $p < 0.0001$.

In the MDA-MB-468-tdTomato cell line, the CSC markers ALOX5, OCT4, ABCG2 and NANOG were also overexpressed in tdTomato⁺ cells (2.47 ± 0.13 , $p = 0.0073$; 2.24 ± 0.05 , $p = 0.0014$; 5.19 ± 0.01 , $p < 0.0001$; 1.52 ± 0.09 , $p = 0.0331$, respectively) (**Figure 30B**). Despite NOTCH4 mRNA levels were higher in MDA-MB-468-tdTomato⁺ cells compared to tdTomato⁻, the differences were not significant (1.62 ± 0.26 , $p = 0.1392$).

CSCs are identified by their ability to survive under very harsh cell culture conditions, i.e. serum free media and suspension cultures. In BC, when tumor cells are grown in such conditions, only CSCs are able to survive and proliferate, leading to the formation of three dimensional spheres, known as mammospheres [107]. In order to evaluate if tdTomato-expressing cells were CSCs, both tdTomato⁺ and tdTomato⁻ cells were seeded under these conditions. As expected, tdTomato⁺ cells from both cell lines were able to grow as mammospheres when cultured in serum free media in low attachment plates (**Figure 31**). HCC-1806-tdTomato⁻ cells were also able to grow in these conditions but formed fewer number and smaller size of mammospheres compared to tdTomato⁺ cells (**Figure 31A**). Of note, MDA-MB-468-tdTomato⁻ cells did not survive in mammosphere culture conditions. Further, the enrichment of tdTomato⁺ cells within mammospheres was confirmed by visualizing them under the fluorescent microscope (**Figure 31B**).

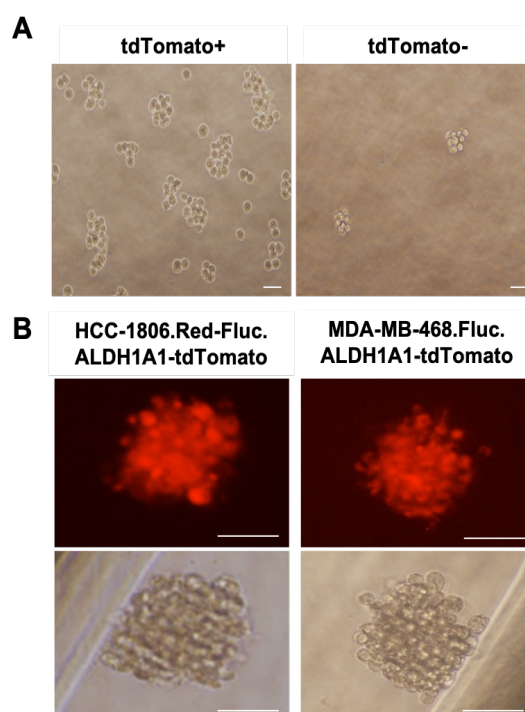


Figure 31. Mammosphere culture of tdTomato⁺ and tdTomato⁻ cells. A) Enriched HCC-1806 tdTomato⁺ cells when seeded in low attachment plates in serum free media were able to form larger number and bigger mammospheres than non-CSC tdTomato⁻ cells. **B)** Observation of red fluorescence in the mammospheres from both cell lines (100 μm scale bar in both images).

These results suggested that tdTomato-expressing cells correspond to a subpopulation with higher stemness functionalities than the tdTomato-. In addition to mammosphere formation-based CSC identification method, other *in vitro* approaches based on functional aspects of CSCs are currently used to further establish evidence for their presence in tumor cell lines, such as colony formation in soft agar, invasion and migration assays [107]. Therefore, to improve future CSC validation studies it would be interesting to include any of these assays.

4.1.3. *In vivo* characterization of TNBC ALDH1A1-tdTomato cell models

Tumor initiation or repopulation assay is considered as gold standard method for the evaluation of active CSCs frequency and for the examination of their tumorigenic capacity. This approach consists in injecting a gradient number of tumor cells into mice to further evaluate their tumorigenic potential based on their capacity to form tumors [107]. In order to confirm the stemness nature of tdTomato-expressing cells of both cell lines, tdTomato+ and tdTomato- cell populations were tested for their tumorigenic capacity using an orthotopic mouse model.

4.1.3.1. HCC-1806-Red-Fluc.ALDH1A1-tdTomato model *in vivo*

Starting from a cell culture with approximately 30% of tdTomato+ cells, the expansion and subsequent enrichment by FACS based on their expression of tdTomato was performed. The resulting sorted tdTomato+ and tdTomato- cell subpopulations were reanalyzed to determine their sorting purity, which accounted for 99.5% of purity in tdTomato+ cells and for 99.9% in tdTomato- cells. Immediately after cell sorting, both collected cell subpopulations were prepared for animal inoculation.

Tumor initiation capacity of HCC-1806-tdTomato+ cells was proved by injecting 1,000, 10,000 and 100,000 HCC-1806 tdTomato+ and tdTomato- cells (5 animals each) orthotopically into the mammary fat pad (i.m.f.p.) of NOD.CB-17-Prkdc^{scid}/NCrHsd mice (from Envigo).

CSCs are known to have the ability to form new tumors when inoculated at very low quantities [283]. In the case of HCC-1806 tdTomato+ cells, 5 out of 5 animals inoculated with 1,000 cells developed tumors, whereas only 1 out of 5 mice inoculated with the same amount of tdTomato- cells developed tumors (**Figure 32A**). Moreover, even though no differences were obtained in tumor incidence for the groups of 10,000 and 100,000 between tdTomato- and tdTomato+ cells, when tumor volumes of the groups

inoculated with 1,000 and 10,000 were compared, differences between tdTomato+ and tdTomato- became significant (**Figure 32B,C**). More specifically, in the group inoculated with 10,000 tdTomato+ cells, the tumor volumes were about 4 times higher than those obtained in the group inoculated with the same number of tdTomato- cells ($207.0 \pm 26.15 \text{ mm}^3$ and $52.70 \pm 13.27 \text{ mm}^3$, respectively; $p = 0.0019$) (**Figure 32B,C**). In the group inoculated with 1,000 sorted tdTomato+ cells, tumor volumes were $146.20 \pm 16.99 \text{ mm}^3$, while in the group inoculated with 1,000 tdTomato- cells the only tumor detected had a volume of 17.6 mm^3 . As might be expected, no differences in tumor volume were observed in animals inoculated with 100,000 cells ($249.2 \pm 39.93 \text{ mm}^3$ for tdTomato+ cells and $277.8 \pm 49.15 \text{ mm}^3$ for tdTomato- cells, $p = 0.6633$) (**Figure 32B,C**). Of note, no metastasis in lungs were detected in either experimental group.

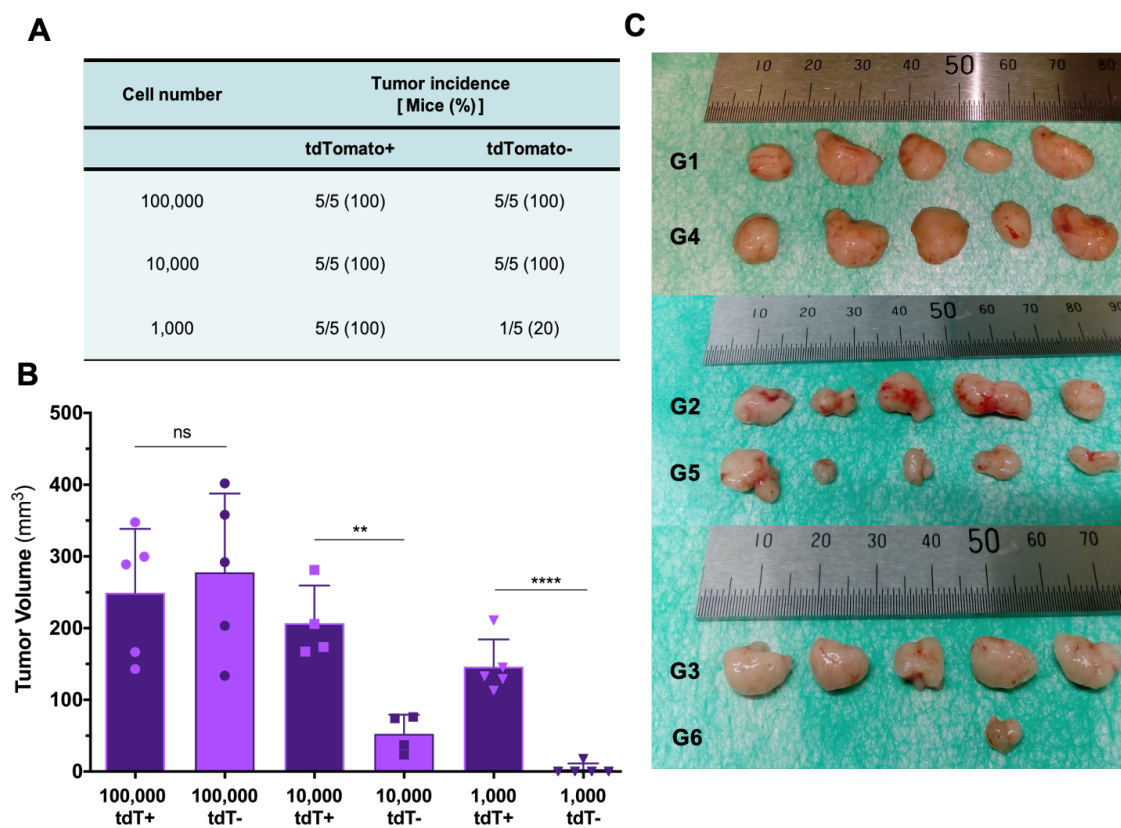


Figure 32. Tumor initiation capacity of tdTomato+ and tdTomato- in HCC-1806.RedFluc.ALDH1A1-tdTomato model. **A)** Mice were inoculated i.m.f.p. with 100,000, 10,000 and 1,000 of tdTomato+ or of tdTomato- cells and tumor incidence was evaluated 28 days post-inoculation. **B)** Ex vivo tumor volumes at 28 days post-inoculation. Differences were regarded as statistically significant (non-parametric Kruskal–Wallis test and unpaired student's *t*-test) when *p*-value was smaller than 0.01. Data is represented as mean \pm SEM ($n \geq 4$). ** $p < 0.01$, **** $p < 0.0001$.

Furthermore, excised tumors were disaggregated and the percentage of tdTomato⁺ cells within tumors of different groups was analyzed by flow cytometry. As expected, the percentage of tdTomato⁺ was significantly higher in tumors from animals inoculated with tdTomato⁺ cells ($9.59 \pm 0.57\%$, $11.71 \pm 1.09\%$ and $8.72 \pm 0.87\%$ for groups inoculated with 100,000, 10,000 and 1,000 tdTomato⁺ cells, respectively). Interestingly, tdTomato⁺ cells were also detected in tumors of mice inoculated with 100,000 and 10,000 tdTomato⁻ cells, but in significant smaller percentage ($2.97 \pm 0.53\%$ and $0.61 \pm 0.18\%$, respectively) (**Figure 33**). Indeed, there was a strong correlation between the tumoral volume and the percentage of tdTomato⁺ cells detected in these tumors ($R^2 = 0.940$). These results suggested that tdTomato⁻ cells were able to revert to a CSC-like phenotype, which induced tdTomato expression. The level of reversion appeared to be directly related with the tumoral volume. Therefore, the more tumor cells there are and the bigger tumors get, the more likely that growing bulk tumor cells enter into reversion process.

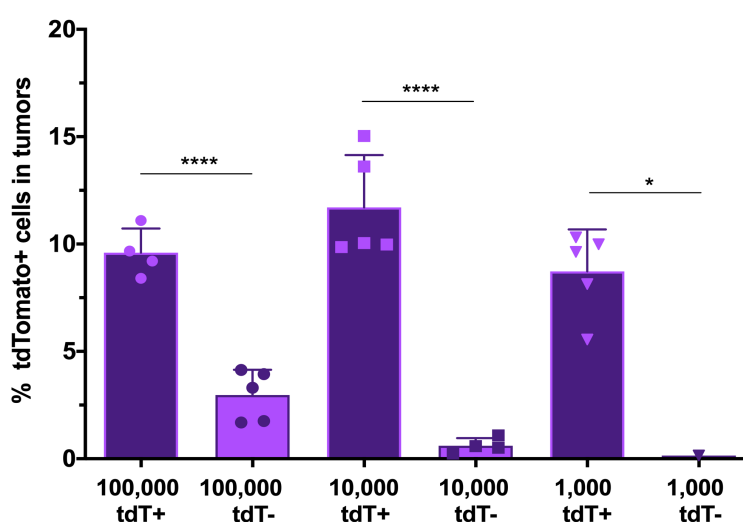


Figure 33. Presence of tdTomato⁺ cells in HCC-1806.Red-Fluc.ALDH1A1-tdTomato tumors. Ex vivo analysis of tdTomato expression in excised tumors determined by flow cytometry. Results are represented as the percentage of tdTomato⁺ cells within tumors of different groups. Differences were regarded as statistically significant (non-parametric Kruskal–Wallis test and unpaired student's *t*-test) when *p*-value was smaller than 0.05. Data is represented as mean \pm SEM ($n \geq 4$), except for the group inoculated with 1,000 tdTomato⁻ cells, as only one mouse eventually developed tumor. **p* < 0.05, *****p* < 0.0001.

Collectively, these results suggested that HCC-1806.Red-Fluc.ALDH1A1-tdTomato cell line generated by using fluorescent reporter vectors is a valid model for visualizing and monitoring CSC biological performance in heterogeneous cancer cell population.

4.1.3.2.MDA-MB-468-Fluc.ALDH1A1-tdTomato in vivo

In order to validate in vivo the CSC nature of tdTomato-expressing cells from MDA-MB-468.Fluc.ALDH1A1-tdTomato fluorescent model, the tumor initiation capacity of tdTomato+ and tdTomato- cells were also evaluated.

Starting from a cell culture with 20-25% of tdTomato+ cells, the expansion and subsequent enrichment by FACS based on their expression of tdTomato was performed. The resulting sorted tdTomato+ and tdTomato- cell subpopulations were reanalyzed to determine their sorting purity, which accounted for 98.6% of purity in tdTomato+ cells and for 99.2% in tdTomato- cells. Immediately after cell sorting, both collected cell subpopulations were prepared for animal inoculation.

Tumor initiation capacity of MDA-MB.468-tdTomato+ cells was proved following the same procedure as mentioned for the HCC-1806-tdTomato cell line. Likewise, right after the cell sorting, increasing densities of tdTomato+ and tdTomato- cells (1,000, 10,000 and 100,000 cells) were inoculated orthotopically i.m.f.p. of NOD.CB-17-Prkdc^{scid}/NCrHsd mice (5 animals each).

In the case of MDA-MB-468 tdTomato+ cells, 4 out of 5 animals inoculated with 10,000 and 100,000 cells developed tumors, whereas 5 out of 5 mice inoculated with the same amount of tdTomato- cells developed tumors (**Figure 34A**). Besides, the same tumor incidence was obtained in the groups inoculated with 1,000 cells, being 5 out of 5 animals for both positive and negative tdTomato cells. Moreover, no significant differences were observed in tumor volumes between groups inoculated with the same number of tdTomato cells (**Figure 34B**). Unlike expected, there appeared to be no correlation between the number of inoculated cells and tumor volumes developed. For instance, the tumor volumes of the group inoculated with 100,000 tdTomato+ cells were about 3 times smaller than those of the group inoculated with 10,000 of tdTomato+ cells ($96.77 \pm 25.72 \text{ mm}^3$ and $284.60 \pm 106.10 \text{ mm}^3$, respectively) (**Figure 34B**). Therefore, no differences were detected in tumorigenic capacity between tdTomato+ and tdTomato-subpopulations.

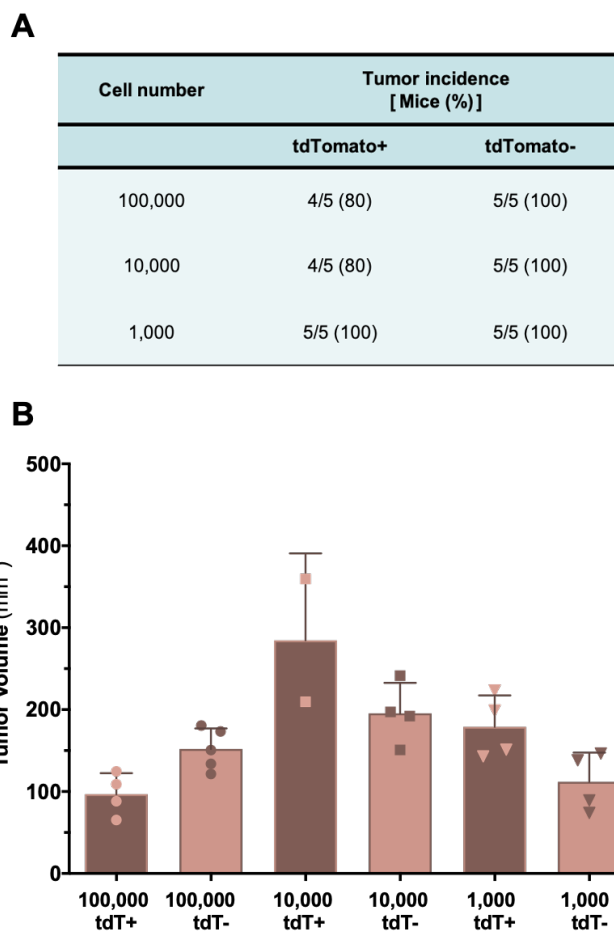


Figure 34. Tumor initiation capacity of tdTomato+ and tdTomato- in MDA-MB-468.Fluc.ALDH1A1-tdTomato model. A) Mice were inoculated i.m.f.p. with 100,000, 10,000 and 1,000 tdTomato+ and tdTomato- cells and tumor incidence was evaluated 70 days post-inoculation. **B)** Ex vivo tumor volumes at 70 days post-inoculation. No statistically significant differences were detected between tumor volumes.

Breast CSCs are able to spread to distant sites, generally to lung, where they proliferate promoting cell lung colonization and metastasis development [83,284]. In this regard, to evaluate the metastatic potential of tdTomato+ cells from the MDA-MB-468.Fluc.ALDH1A1-tdTomato model, mice were evaluated for metastatic lung lesions in vivo (at day 53 post-inoculation) by bioluminescence imaging.

In vivo imaging detected bioluminescence in the thoracic region of 4 out of 5 animals of all three groups inoculated with tdTomato+ cells. Besides, same metastasis incidence was observed for the tdTomato- groups, since bioluminescence signal was detected in the thoracic region of 4 out of 5 animals inoculated with tdTomato- cells. In addition, there were no substantial differences in BLI signal intensity (ph/s) between the experimental groups (**Figure 35A**).

Since lung metastasis were detected in most of the animals, we decided to analyze the tdTomato-expression in circulating tumor cells (CTC) present in the blood stream, which are considered an intermediate stage of metastasis and their study provides significant insight into the metastatic process. To this end, mice blood samples were collected and immediately processed for flow cytometry analysis. As there were no significant differences between groups inoculated with different cell densities, flow cytometry data was analyzed and compared based only on tdTomato expression, without regard to the number of cells inoculated. Interestingly, tdTomato-expressing cells were detected in the CTC population from both MDA-MB-468-tdTomato+ and tdTomato- groups. In fact, a higher percentage of CTC expressing tdTomato was obtained in the tdTomato- group ($5.61 \pm 2.59\%$) in comparison to the tdTomato+ group ($2.84 \pm 1.74\%$) (**Figure 35B**).

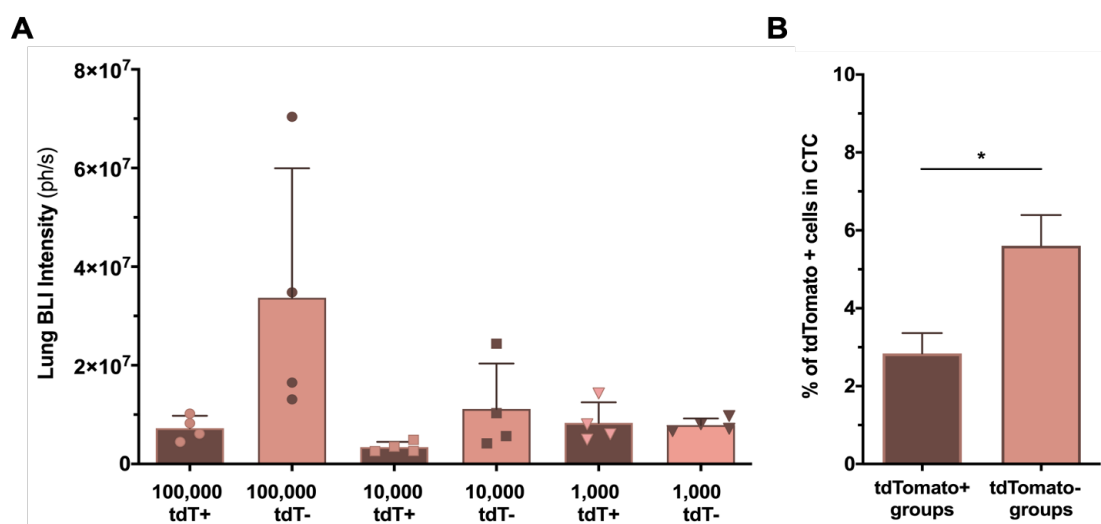


Figure 35. Evaluation of lung metastasis in MDA-MB-468.Fluc.ALDH1A1-tdTomato model. **A)** Bioluminescence (BLI) lung signal at day 53 post-inoculation. Results are expressed as BLI intensity (ph/s) mean \pm SEM. **B)** Quantification of tdTomato+ expressing cells in circulating tumor cell (CTC) population isolated from the blood of tumor bearing mice and analyzed by flow cytometry. Results are plotted as the percentage of tdTomato+ detected in the total CTC population from mice blood samples per gram of tumor (mean \pm SD). The gating strategy used in flow cytometry was specially designed for the selective identification of CTC population, ensuring the exclusion of both doublets and cells from the immune system. A positive control of tdTomato+ cells from conventional culture was included. Statistical analysis t-test was performed, * $p < 0.05$.

Altogether, the observation of similar tumor incidence and tumor volumes derived from sorted tdTomato- and tdTomato+ cells, together with a similar capacity in lung metastasis development, made us wonder whether it was due to a wrong cell line generation or the result of a strong phenotypic dynamism between both cell subpopulations. Considering the findings in the CTC population, we believed it was necessary to go more deeply in

research for a better understanding of these results. For this purpose, the tdTomato expression in excised MDA-MB-468.Fluc.ALDH1A1-tdTomato tumors was analyzed by flow cytometry, following the same procedure as mentioned for the HCC-1806.Fluc.ALDH1A1-tdTomato cell line. As expected, all tumors derived from tdTomato+ cells showed a high expression of tdTomato ($52.21 \pm 12.72\%$) (**Figure 36A**). Interestingly, when tumors derived from tdTomato- cells were analyzed, presence of tdTomato+ cells was detected in all tumors, even though in a lower percentage than tdTomato+ CSC-like cells ($8.50 \pm 5.32\%$), thus indicating that initial non-CSC fraction was able to revert to a CSC-like phenotype, which implied tdTomato expression (**Figure 36A**). A similar behavior of tdTomato- cells was previously observed in the MDA-MB-231 TNBC cell model [127], increasing the robustness of our results.

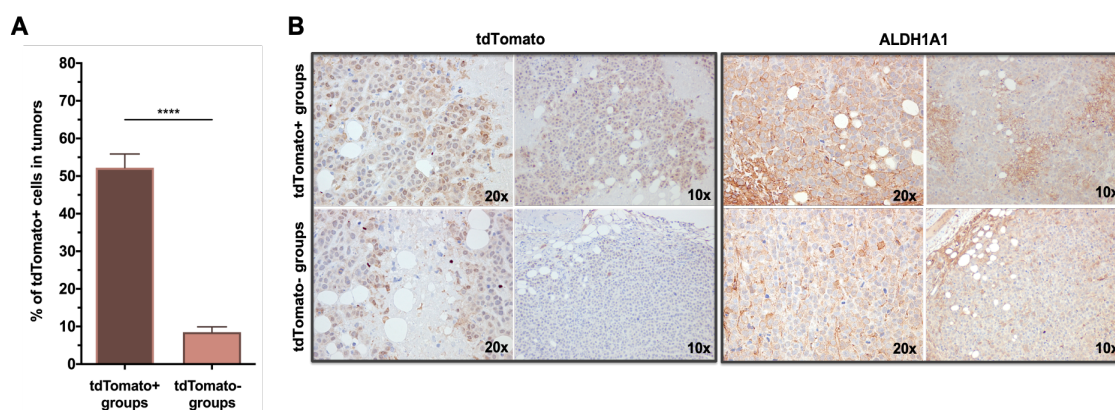


Figure 36. Presence of tdTomato+ cells in MDA-MB-468.Fluc.ALDH1A1-tdTomato tumors.

A) Quantification of tdTomato+ cells in MDA-MB-468 tumors at 70 days post-inoculation by flow cytometry. As no significant differences were detected between groups inoculated with different cell densities, data was processed by joining the results (G1-G3 and G4-G6) to compare tdTomato+ vs tdTomato-, respectively ($****p < 0.0001$). **B)** Immunohistochemistry analysis of tdTomato and ALDH1A1 expression in excised tumors. Examples of immunohistochemistry (hematoxylin/tdTomato and hematoxylin/ALDH1A1) in representative tumors of animals inoculated with 10,000 sorted tdTomato+ and tdTomato- cells (both positive for tdTomato and ALDH1A1). Image acquisition was done at 20x objective magnifications.

To confirm this data and validated our hypothesis, the expression of tdTomato and ALDH1A1 in same excised tumors derived from both tdTomato+ and tdTomato- cells was then evaluated by immunohistochemistry. The ex vivo analysis showed expression of both tdTomato and ALDH1A1 in all tumors of the tdTomato+ group (**Figure 36B**). Accordingly, when tumor samples derived from inoculated tdTomato- cells were evaluated, the analysis revealed the presence of tdTomato- and ALDH1A1-expressing cells, confirming previous results in flow cytometry analysis (**Figure 36B**). Nevertheless,

the expression of both markers was lower in comparison with tdTomato+ samples. Taken together, these findings supported our theory of the existence of a dynamic phenotypic interconversion process between CSC and non-CSC populations.

4.1.4. MDA-MB-468-Fluc-ALDH1A1-tdTomato in vitro reversion

Having shown that tdTomato- cells from the MDA-MB-468 fluorescent model originated a tumor containing tdTomato-expressing cells, we then examine whether the dedifferentiation of non-CSCs to CSC also occur in vitro. For this purpose, enriched tdTomato+ and tdTomato- subpopulations were seeded and monitored over passages by fluorescent microscopy, gene expression analysis and flow cytometry (**Figure 37**). As expected, continuous culture of enriched tdTomato+ cells resulted in a progressively reduction of tdTomato-expressing cells within culture, specifically, from the initial 98.6% of tdTomato+ cells (post-sorting) to 81.9% at cell passage number 5 (P5) (**Figure 38A**). In agreement with ex vivo data, flow cytometry analysis revealed a significant increase in the percentage of tdTomato+ cells within the sorted tdTomato- after 5 passages, more specifically, from $0.001 \pm 0.0001\%$ of tdTomato+ cells to $3.5 \pm 0.51\%$ (**Figure 38C**).

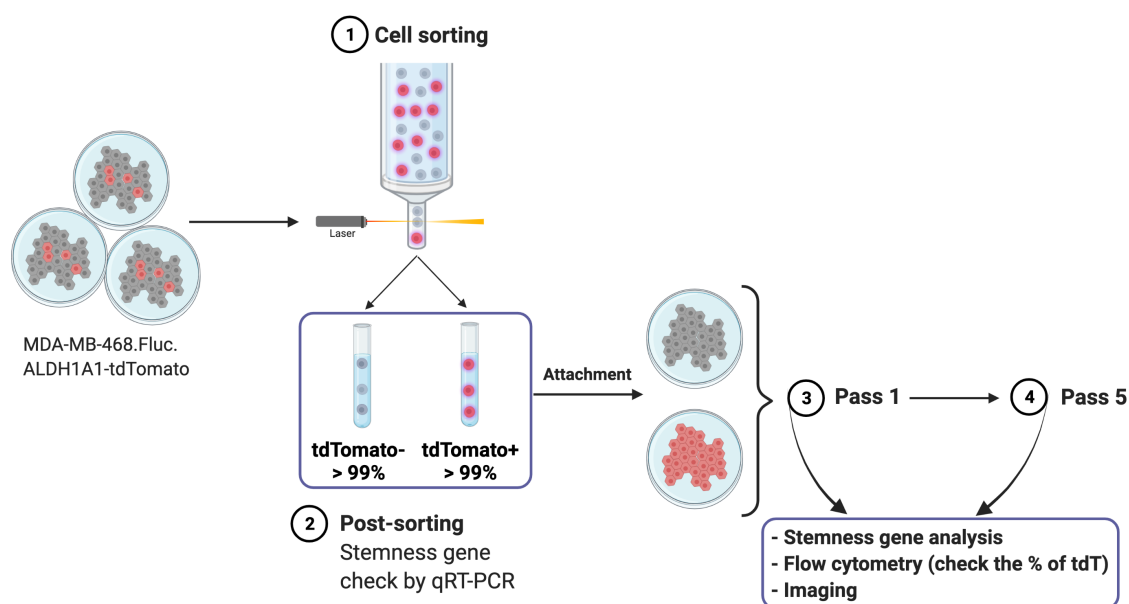


Figure 37. Schematic representation of in vitro cell reversion experiments performed in MDA-MB-468.Fluc.ALDH1A1-tdTomato fluorescent CSC model. Briefly, tdTomato+ and tdTomato- cells were sorted and enriched by FACS. A gene expression analysis by qPCR was done to check the stemness nature of tdTomato+ enriched cells. Then, cells were plate into adherent plates in complete medium and were allowed to grow. Cells were monitored over the time, at passage number 1 and number 5, by fluorescent microscopy and flow cytometry, and changes in the CSC phenotype by qPCR were also evaluated.

In addition, we analyzed the stem cell gene expression profile in both subpopulations after cell sorting and at passage number 5. Not surprisingly, we found a significant relative decrease of OCT4, ABCG2, ALOX5 and NANOG mRNA in tdTomato⁺ after 5 passages in comparison with the mRNA levels from the initial sorted tdTomato⁺ cells (5.37 ± 0.12 , $p = 0.00087$; 3.20 ± 0.17 , $p = 0.00078$; 1.55 ± 0.06 , $p = 0.0065$; 2.48 ± 0.11 , $p = 0.0054$; respectively) (**Figure 38B**). However, no significant differences in ALDH1A1 mRNA levels were obtained (when comparing results between cell passage 0 and 5). Next, we assessed the mRNA levels for tdTomato⁻ subpopulation. Gene expression analysis revealed a significant relative increase of mRNA of all CSC markers in tdTomato⁻ cells at passage number 5 when compared to mRNA levels after sorting (ALDH1A1 2.35 ± 0.11 , $p = 0.07$; OCT4 3.38 ± 0.08 , $p = 0.0005$; ABCG2 8.14 ± 0.11 , $p < 0.0001$; ALOX5 2.78 ± 0.07 , $p = 0.00041$; NANOG 3.13 ± 0.13 , $p = 0.00032$; respectively) (**Figure 38D**). These results were further confirmed when both subpopulations were monitored and observed by fluorescent microscopy (**Figure 39**).

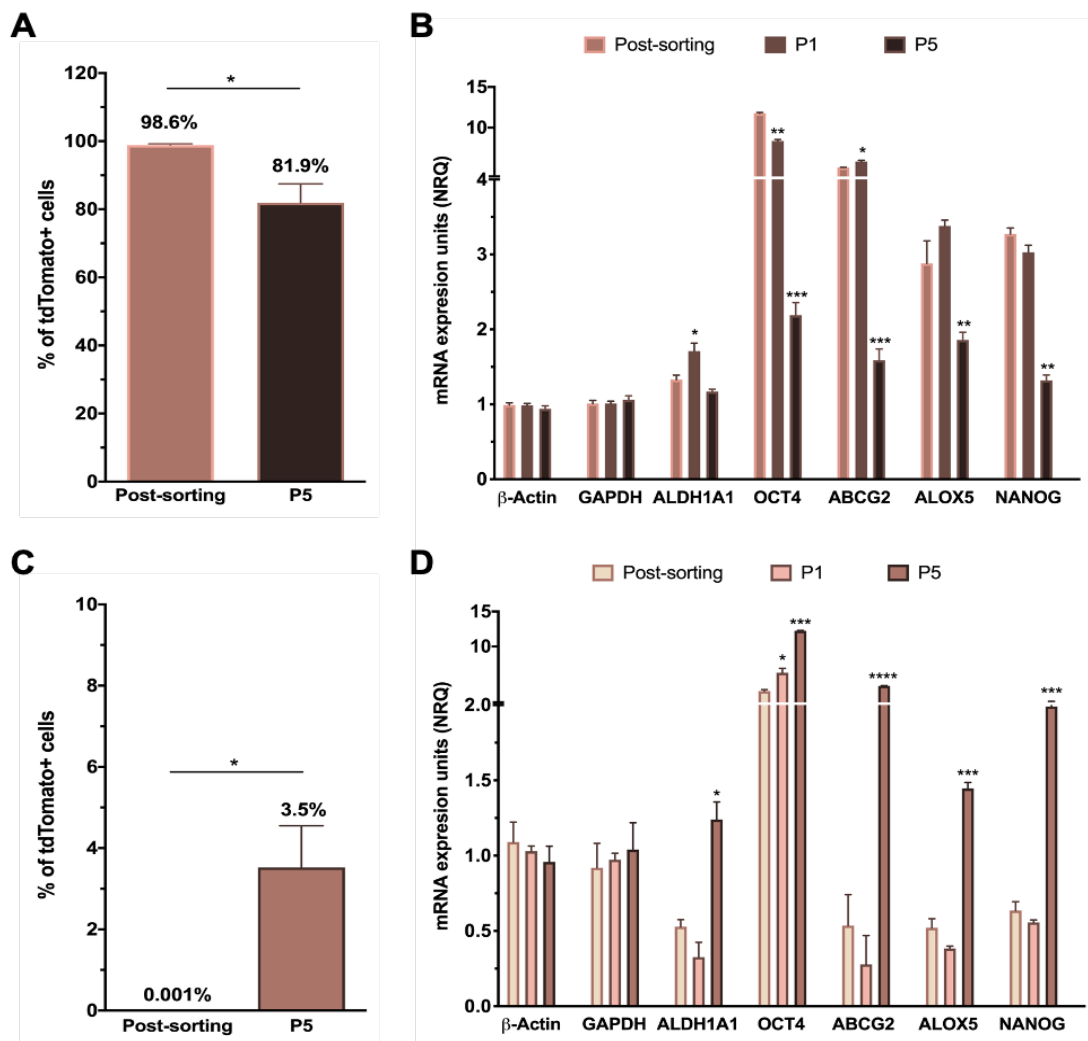


Figure 38. Monitoring of CSC reversion in the MDA-MB-468.ALDH1A1.Fluc-tdTomato fluorescent model. A-B) Characterization of tdTomato+ derived cells and **C-D)** of tdTomato-derived cells. The increase or decrease of tdTomato+ cells within culture was monitored post-sorting (cell passage 0) and at cell passage number 5 (P5). Stem cell gene expression analysis measured by qRT-PCR of tdTomato+ and tdTomato- cells cultured in attachment post- cell sorting enrichment by FACS. Changes in the stem cell gene expression profile were monitored over cell passages, specifically, after cell sorting (post-sorting), at cell passage number 1 (P1) and 5 (P5). Results are expressed as NRQ (normalized relative quantities) mean \pm SEM ($n \geq 3$); * $p < 0.05$; ** $p < 0.01$, *** $p < 0.001$, **** $p < 0.0001$.

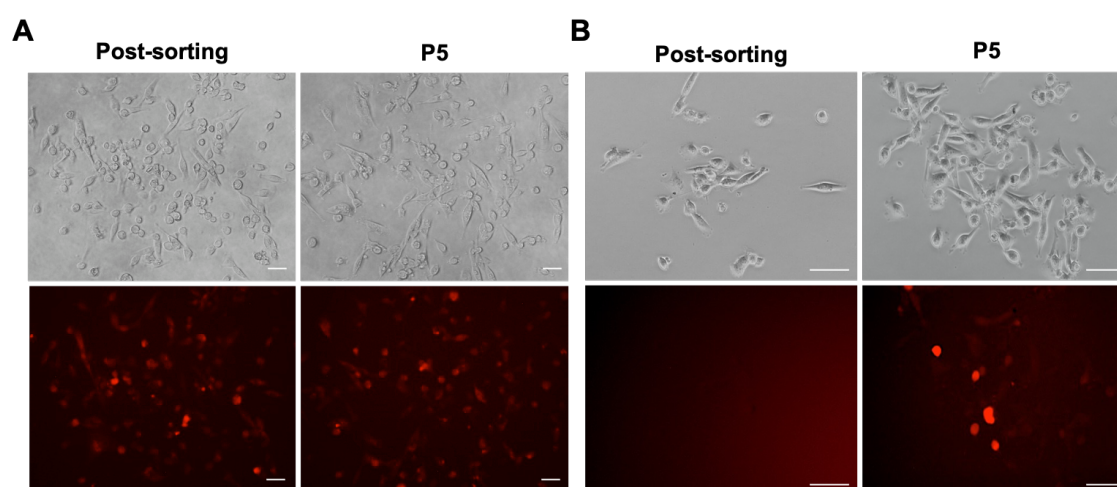


Figure 39. Detection of CSC reversion by tdTomato- cells of the MDA-MB-468 fluorescent model. After the enrichment of both cell subpopulations by FACS, cells were cultured in attachment and grown for subsequent passages. **A)** Similar expression of tdTomato+ cells were detected after 5 cell passages in comparison with the initial enriched tdTomato+ subpopulation. **B)** After 5 cell passages, tdTomato-expressing cells were detected in the initial enriched tdTomato- subpopulation. Scale bar represents 20 μ m.

Taken together, our data provided strong evidence of the dynamic interconversion process between CSC and non-CSC, where CSC can differentiate to non-CSC and non-CSC can change their phenotype to CSC-like phenotype.

4.2. Identification of compounds with potential anti-CSC activity

4.2.1. Identification of compounds with described anti-CSC preferential activity by compound library screening

In order to explore potential anti-CSC candidates that may lead to a selective eradication of this therapeutically resistant cell population, we performed an exhaustive literature screening to identify FDA-approved drugs with already described anti-CSC activity.

Repurposing of approved drugs is an effective strategy in discovering or developing drug molecules with new pharmacological and/or therapeutic indications, thus bypassing the time-consuming stages of drug development [285]. Thereby, 17 compounds were identified as positive hits from the screen: 6-shogaol (6-SHO), 8-quinolinol (8Q), acetaminophen (ACE), niclosamide (NCS), citral (CIT), disulfiram (DSF), flubendazole (FLU), defactinib (DFT), everolimus (EVE), glabridin (GLA), nitidine chloride (NTC), panobinostat (PNB), metformin hydrochloride (MET), salinomycin (SAL), YM-155 hydrochloride (YM), VS-5584 (VS) and isoliquiritigenin (ISO), and were grouped according to their chemical composition (**Figure 40** and **41**). All are considered small drugs that interfere with essential signaling pathways related with CSC properties maintenance. For further details regarding the therapeutic effect and mechanism of action of each drug refer to the introduction section 1.6, **Table 6**, where publications consulted are also specified.

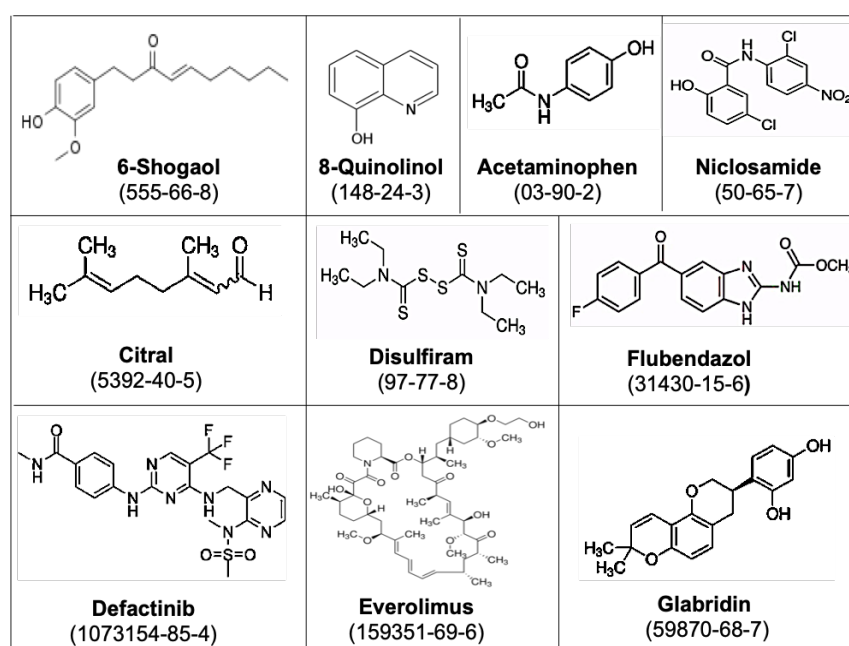


Figure 40. Selected anti-CSC drugs (Part I). Representation of the chemical structures and CAS numbers of the anti-CSC drugs selected in this thesis.

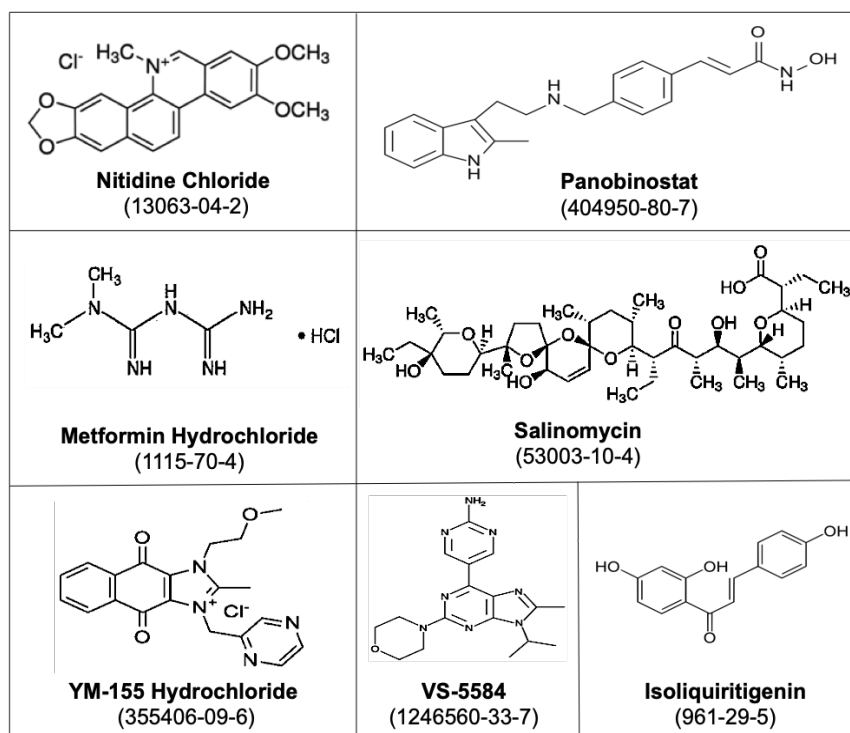


Figure 41. Selected anti-CSC drugs (Part II). Representation of the chemical structures and the corresponding CAS numbers of the anti-CSC drugs selected in this thesis.

4.2.2. Identification of potential candidates with a high anti-proliferation activity against human breast cancer cell lines

We first evaluated the in vitro cytotoxicity of test compounds by MTT in the basal-like MDA-MB-231 and the luminal A MCF-7 cell lines and compared it to paclitaxel (taxol, PTX), an anti-neoplastic drug used as a first line treatment in TNBC. In this regard, we tested increasing concentrations of all drugs for 72 h (drug dilution factors and range of concentrations tested are summarized in **Table 13**). Then, cell viability was determined for each concentration to obtain a dose response curve to further calculated the half maximal inhibitory concentration (IC_{50}) for all the compounds. A summary of the IC_{50} values obtained can be found in **Table 14**.

Table 13. Summary of the concentrations tested in cell viability assays of all compounds in MDA-MB-231 and MCF-7 cell lines. Range of concentrations and serial dilutions tested for all compounds in MTT assays using the MDA-MB-231 and MCF-7 cell lines.

Drug	Concentration range (μM)	Serial dilutions	Drug	Concentration range (μM)	Serial dilutions
PTX	10 – 0.0001	1/5	GLA	100 – 5.853	1/1.5
6-SHO	100 – 5.853	1/1.5	ISO	150 – 8.779	1/1.5
8Q	250 – 0.003	1/5	MET	10,000 – 78.13	1/2
ACE	9,000 – 70.31	1/2	NCS	60 – 0.004	1/4
CIT	200 – 1.563	1/2	NTC	65 – 0.100	1/2.5
DFT	100 – 0.006	1/4	PNB	5 – 0.0003	1/4
DSF	100 – 0.001	1/5	SAL	50 – 0.0006	1/5
EVE	100 – 0.006	1/4	VS	200 – 0.00002	1/10
FLU	100 – 0.045	1/3	YM	0.25 – 0.0001	1/3

Drug abbreviations stand for: PTX, paclitaxel; YM, YM-155 hydrochloride; PNB, panobinostat; VS, VS-5584; NCS, niclosamide; FLU, flubendazole; NTC, nitidine chloride; DSF, disulfiram; 8Q, 8-quinolinol; EVE, everolimus; GLA, glabridin; ISO, isoliquiritigenin; 6-SHO, 6-shogaol; MET, metformin hydrochloride; ACE, acetaminophen; CIT, citral

Out of the total of screened compounds, six displayed high cytotoxic potency with IC_{50} values below 10 μM in MDA-MB-231 and MCF-7 cell lines, namely YM, PNB, VS, NCS, NTC and SAL, close to the values obtained for the reference drug PTX (**Figure 42** and **Table 14**).

As expected, MCF-7 cells were more sensitive (lower IC_{50} values) to the tested compounds than MDA-MB-231 cells, known to be highly chemo-resistant and aggressive [286]. In the case of the reference drug PTX, an increased sensitivity of MCF-7 cells was obtained, since its IC_{50} value was 122.75-fold lower for the luminal cells (**Table 14**) than for the basal-like cells. For some tested drugs, differences between both cell lines appeared to be more pronounced. More specifically, VS, FLU and 8Q drugs showed an IC_{50} value 48.52, 22.71 and 5.75-fold lower in MCF-7 cell line in comparison to that obtained in MDA-MB-231 cells, respectively. Conversely, no differences were obtained for PNB, NTC, EVE, GLA, 6-SHO, MET and ACE drugs between both cell lines (**Figure 42** and **Table 14**).

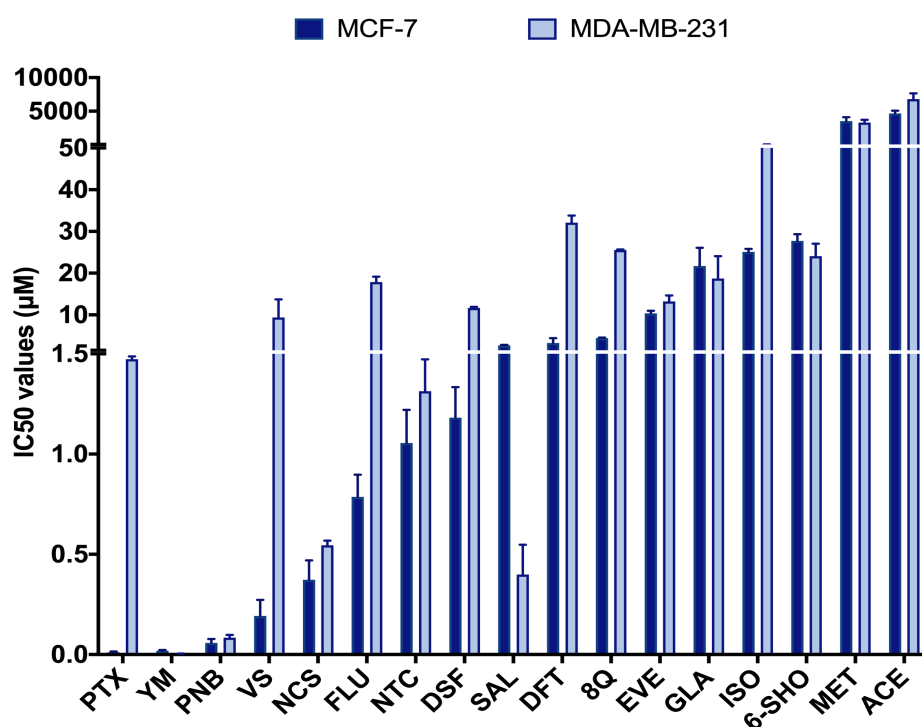


Figure 42. Differential responses of MCF-7 and MDA-MB-231 cell lines to tested compounds. Both cell lines were treated with increasing concentrations of selected drugs for 72 h. Afterwards, IC₅₀ values for each compound in both cell lines were calculated. IC₅₀ values are represented as the mean ± SEM of three independent experiments.

Interestingly, YM and SAL were the only compounds that showed greater cytotoxicity in the basal-like cell line compared to the luminal A, as IC₅₀ values obtained were 4.75 and 6.77-fold lower for the MDA-MB-231 cells, respectively. On the other hand, we found that IC₅₀ values for MET and ACE drugs were both above mM, thus reflecting that for both compounds the concentration required to obtain a successful cytotoxic anti-tumor effect must be extremely high (**Figure 42** and **Table 14**). Therefore, these two drugs along with CIT, 6-SHO, ISO, GLA and EVE, which also showed relatively low efficacy (IC₅₀ above 10 µM) in both cell lines (no differential treatment sensitivity), were discarded for further experiments. In fact, the IC₅₀ value for CIT drug could not be calculated, as the maximum concentration tested (200 µM) clearly failed to reach the eradication of 50% of cells.

Table 14. Cytotoxic efficacy of selected compounds assessed by MTT assays. IC₅₀ values of the assessed compounds in Luminal A cell line MCF-7 and in TNBC cell lines (mean ±SEM).

Drugs	IC ₅₀ values (mean ±SEM)					
	MCF-7	MDA-MB-231	HCC-1806	MDA-MB-468	BT-549	BT-20
PTX	0.012 ±0.003	1.473 ±0.014	0.008 ±0.002	0.004 ±0.001	0.015 ±0.007	0.012 ±0.004
YM	0.019 ±0.004	0.004 ±0.001	0.018 ±0.002	0.002 ±0.001	0.025 ±0.001	0.001 ±0.001
PNB	0.058 ±0.022	0.084 ±0.014	0.016 ±0.004	0.002 ±0.001	0.144 ±0.007	0.084 ±0.032
VS	0.193 ±0.078	9.365 ±4.329	---	---	---	---
NCS	0.373 ±0.097	0.545 ±0.024	3.106 ±0.101	1.878 ±0.458	0.960 ±0.034	1.547 ±0.062
FLU	0.787 ±0.110	17.87 ±1.300	0.402 ±0.130	0.001 ±0.001	0.504 ±0.049	0.041 ±0.003
NTC	1.055 ±0.166	1.314 ±0.159	---	---	---	---
DSF	1.182 ±0.152	11.65 ±0.253	---	---	---	---
SAL	2.702 ±0.107	0.399 ±0.149	---	---	---	---
DFT	3.242 ±1.180	32.10 ±1.720	---	---	---	---
8Q	4.442 ±0.137	25.55 ±0.151	25.19 ±1.08	3.295 ±0.111	79.74 ±2.890	16.15 ±0.67
EVE	10.38 ±0.591	13.21 ±1.449	---	---	---	---
GLA	21.71 ±4.367	18.72 ±5.362	---	---	---	---
ISO	25.11 ±0.724	53.33 ±5.275	---	---	---	---
6-SHO	27.73 ±1.597	24.08 ±2.995	---	---	---	---
MET	3523 ±601	3315 ±396	---	---	---	---
ACE	4670 ±417	6806 ±842	---	---	---	---
CIT	> 200	> 200	---	---	---	---

Drug abbreviations stand for: PTX, paclitaxel; YM, YM-155 hydrochloride; PNB, panobinostat; VS, VS-5584; NCS, niclosamide; FLU, flubendazole; NTC, nitidine chloride; DSF, disulfiram; SAL, salinomycin; DFT, defactinib; 8Q, 8-quinolinol; EVE, everolimus; GLA, glabridin; ISO, isoliquirigenin; 6-SHO, 6-shogaol; MET, metformin hydrochloride; ACE, acetaminophen; CIT, citral.

Furthermore, we thought it was interesting to evaluate whether the anti-proliferative activity of drugs obtained was similar in other TNBC cell lines. To this end, of all drugs with a good anti-proliferative profile, five were randomly selected (YM, PNB, NCS, FLU and 8Q) and further tested in additional MTT assays in extended battery of breast cancer cell lines, including the HCC-1806, MDA-MB-468, BT-549 and BT-20 cell lines, to subsequently calculate the IC₅₀ values (Table 14). As expected, when IC₅₀ values from the different TNBC cell lines were compared, the drug cytotoxic efficiency differed substantially depending on the tested cell line (Table 14). In fact, for YM, PNB and NCS compounds, the differences obtained when IC₅₀ values were compared were an order of magnitude greater or lower depending on the cell line.

4.2.3. Identification of potential candidates with selective anti-CSC activity

To narrow down which significant candidates could be of potential therapeutic relevance, we next subjected our drug set (except for compounds already discarded) to proliferation assays in CSC and non-CSC subpopulations sorted from the MDA-MB-231-ALDH1A1:tdTomato reporter cell line [127]. In this model, as in both fluorescent models explained in previous section, the expression of tdTomato is under the control of the CSC specific promoter ALDH1A1, allowing the identification and isolation of CSC and non-CSC subpopulations. Accordingly, both subpopulations were enriched by FACS prior the cell viability was determined and IC_{50} values were calculated. Importantly, stem-like phenotype of sorted tdTomato+ cells was confirmed before performing the experiments by increased expression of stemness markers compared to tdTomato- cells (Figure 43).

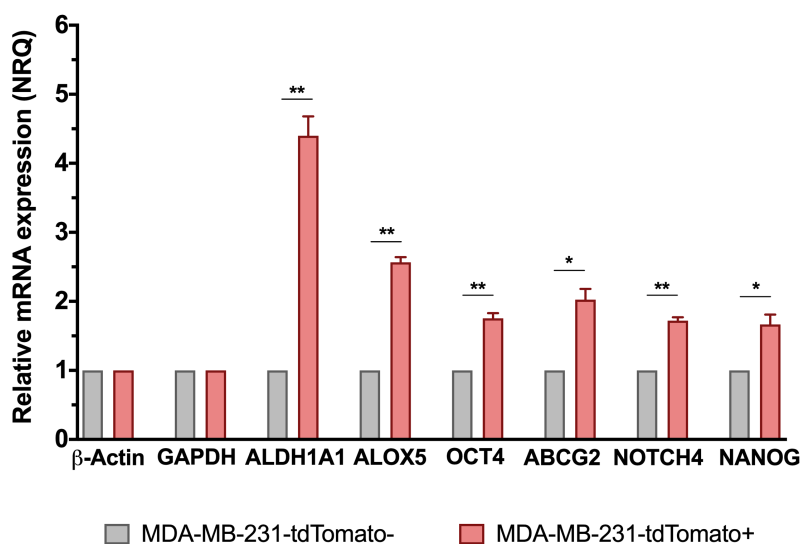


Figure 43. Stem cell-like gene expression profile of enriched CSCs and non-CSCs from MDA-MB-231 fluorescent model measured by qRT-PCR. The stem cell phenotype of tdTomato+ cells was confirmed by a significative overexpression of all the stem cell markers analysed. Results are expressed as NRQ (normalized relative quantities) mean \pm SEM ($n \geq 3$); * $p < 0.05$; ** $p < 0.01$.

No significant differences in treatment sensitivity were observed between CSCs and non-CSCs when were treated with the reference drug PTX, thereby confirming that the chemotherapeutic agent does not show a selective cytotoxic effect against CSCs (Figure 44). These results were consistent with those reported in the literature, thus underlining the robustness of our work [287,288]. Moreover, 8Q and NCS were the only two compounds that exhibit a significant higher sensitivity in CSC compared to non-CSC.

Indeed, IC₅₀ values for 8Q and NCS compounds were 1.33 and 3.66-fold lower ($p < 0.05$) in the CSC in comparison with the non-CSC subpopulation, respectively (**Figure 44**). Results for SAL also moved in the same direction, but differences among IC₅₀ values of CSC and non-CSC were not statistically significant. Conversely, NTC, VS, DSF, FLU and DFT drugs showed no differences in cell viability between CSC and non-CSC and were discarded.

Notwithstanding the lack of specificity obtained against CSC, YM and PNB were considered interesting candidates, as both showed the lowest IC₅₀ values of the set of drugs tested in both cell subpopulations, including also the reference drugs. Based on these results, YM had been followed up and a novel research line with this drug has been initiated in the laboratory, carried out by Dr. Simó Schwartz's group (Laboratory of Drug Delivery and Targeting, CIBBIM Nanomedicine, Vall d'Hebron Institut de Recerca (VHIR), Barcelona, Spain).

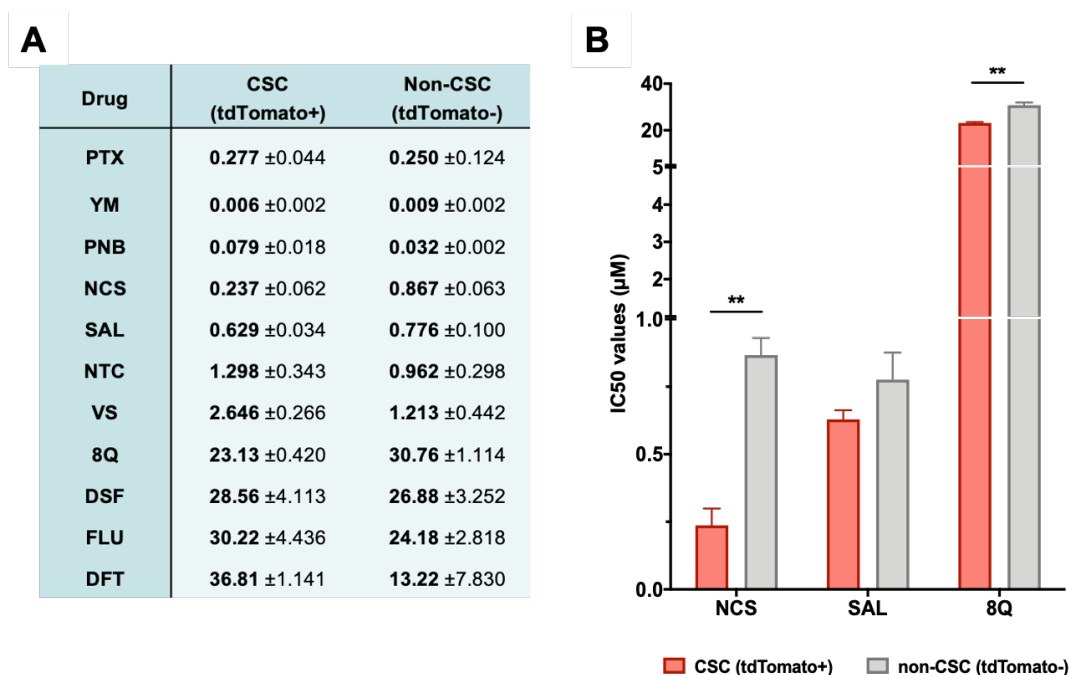


Figure 44. Selective anti-CSC activity of screened drugs in CSC and non-CSC MDA-MB-231 cells grown in attachment conditions. A) IC₅₀ values for each compound in both subpopulations after 72 h incubation. **B)** Representation of IC₅₀ of those compounds that showed a greater cytotoxic effect against CSCs compared to non-CSCs. Differences were statistically significant when comparing IC₅₀ values of 8Q and NCS between both cell subpopulations, but not in the case of SAL. Data is represented as the mean ±SEM of three independent experiments. Statistically significant results were only obtained when comparing IC₅₀ values of 8Q and NCS in both cell subpopulations (** $p \leq 0.05$).

The effect of 8Q, NCS and SAL on CSCs was further studied in low attachment conditions, where the mammosphere formation (MSF) is promoted. To this end, MDA-MB-231 cells were grown in suspension using serum-free medium and further treated with the selected drugs for one week. In these culture conditions, only the CSCs are able to survive and grow giving rise to the formation of tumor colonies, known as mammospheres. The drug doses tested were chosen according to the IC_{50} values obtained in the preliminary cell viability assays performed.

As shown in **Figure 45A**, the inhibition of mammosphere-forming efficiency increased in a dose-dependent manner in all-three anti-CSC drugs, being higher in the case of 8Q and NCS (**Figure 45A**), which prevented MSF in a $27.4\% \pm 6.7\%$ and $13.8\% \pm 7.5\%$, respectively, when the highest concentration was tested (**Figure 45B**). Accordingly, these were the compounds that showed the lowest IC_{50} values, $2.71 \mu\text{M} \pm 0.14$ for 8Q and $1.65 \mu\text{M} \pm 0.79$ for NCS.

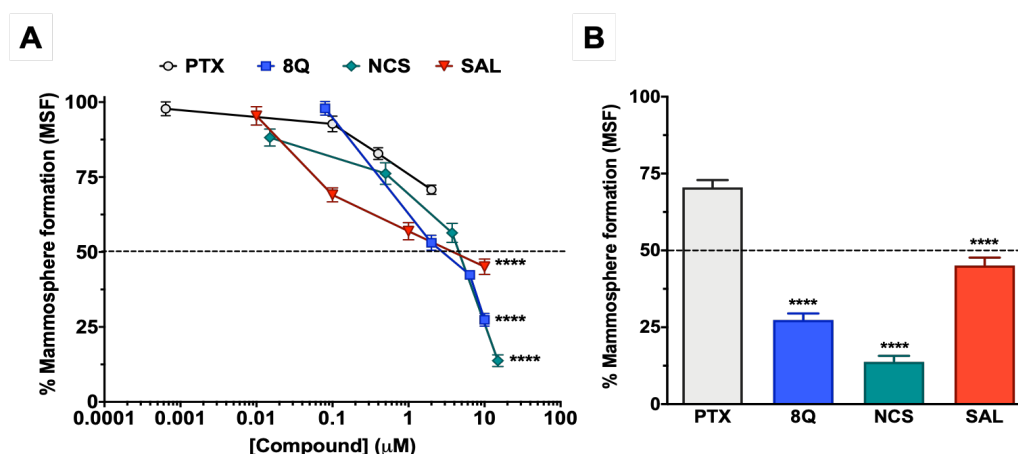


Figure 45. Anti-CSC activity of selected compounds in the MDA-MB-231 CSC population cultured under low attachment conditions. A) Dose-response curves of CSC mammosphere-forming efficiency (MSF) of MDA-MB-231 cells after drug treatments. **B)** Percentage of mammosphere after 7-day incubation with 1 μM PTX, 10 μM SAL and 8Q, and 15 μM NCS. Statistically significant results were obtained for all tested compounds when compared to PTX. Data is represented as the mean \pm SEM of three independent experiments. **** $p \leq 0.0001$.

Furthermore, the effect on MSF was remarkably lower for SAL (IC_{50} of $4.95 \mu\text{M} \pm 0.83$) in comparison with 8Q and NCS, but significantly higher ($p < 0.0001$) than the produced by the anti-neoplastic reference drug PTX (**Figure 45A, B**). Indeed, MSF was considered not affected when treated with PTX, since none of drug doses tested succeeded in reducing a 50% mammosphere growth. These results pointed out that PTX was not as effective in selectively eradicating CSC population as 8Q, NCS or SAL, in accordance

with our previous results. These findings were consistent with those described in the literature, in which PTX drug has been shown to mainly inhibit bulk growing tumor cells, but have no or little effect on CSC [287,288]. Moreover, given that 8Q and NCS showed the highest efficacy in inhibiting the MSF, these two drugs were chosen to continue with functional assays.

To validate and reinforced the results in low attachment, we further analyzed the anti-CSC activity of all-three drugs 8Q, NCS and SAL using other TNBC cell lines, specifically, BT-549, MDA-MB-468, BT-20, and HCC-1806. Of note, PNB was also included in order to evaluate its performance when tested in other TNBC cell lines. The experimental procedure followed was the same as the used for the MDA-MB-231 cell line. The results obtained indicated that all tested compounds were effective in reducing the number of cells growing as mammospheres (**Figure 46**). However, effectiveness obtained differed much between cell lines, since IC_{50} values of 8Q and SAL in BT-20 and HCC-1806 cell lines were almost 10 times higher in comparison with those obtained in BT-549 and MDA-MB-468 cells (**Figure 46** and **Table 15**). Unlike the results obtained in the MDA-MB-231 cell line, in this case PNB was the compound that showed the highest efficacy in preventing MSF of CSC, as IC_{50} values were the lowest compared to the other drugs ($IC_{50} < 0.2 \mu M$) in all-four alternative TNBC cell lines (**Table 15**). Moreover, 8Q, NCS and SAL also showed efficacy in inhibiting MSF, but to a lesser extent than PNB, since IC_{50} values were in some cases 100-fold higher in comparison with those of PNB (**Figure 46** and **Table 15**).

In light of these positive results in attachment and in low attachment conditions, 8Q and NCS could be both considered as promising candidates for selectively eradicating CSC population in TNBC, and thus, were selected for additional studies explained below. It is worth stressing that PNB compound also showed a strong tumor growth inhibition potential and thus, was not discarded and taken into account for future research experiments.

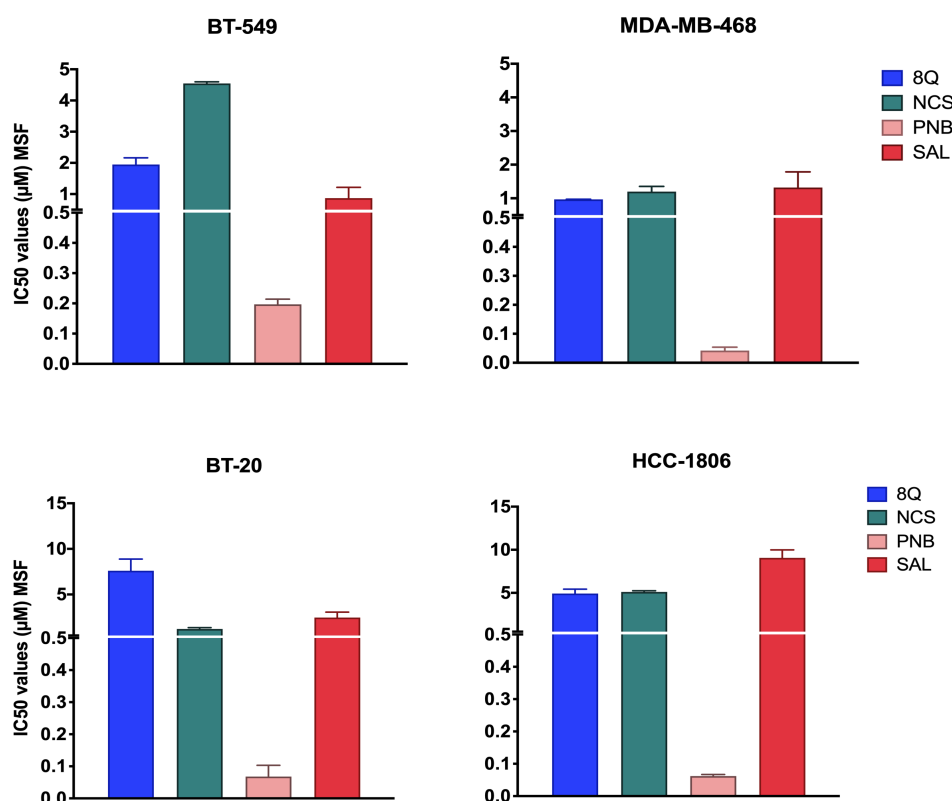


Figure 46. Effect of drugs in mammosphere formation ability (MSF) in other TNBC cell lines. BT-549, MDA-MB-468, BT-20 and HCC-1806 parental cells were seeded under low attachment conditions in serum free media and further treated with increasing concentrations of selected drugs for one week. Afterwards, IC₅₀ values for each compound in all cell lines were calculated and plotted using the GraphPad software. Data is represented as the mean \pm SEM of three independent experiments.

Table 15. Mammosphere formation inhibition of selected drugs in CSC. Summary of IC₅₀ values obtained from tested compounds in TNBC cell lines (mean \pm SEM).

Drugs	MDA-MB-231	HCC-1806	MDA-MB-468	BT-549	BT-20
PTX	> 2	---	---	---	---
SN-38	> 10	---	---	---	---
8Q	2.709 \pm 0.137	4.922 \pm 0.509	0.969 \pm 0.001	1.946 \pm 0.217	7.600 \pm 1.285
NCS	1.648 \pm 0.792	5.107 \pm 0.135	1.199 \pm 0.154	4.548 \pm 0.050	1.218 \pm 0.150
PNB	3.119 \pm 0.763	0.062 \pm 0.005	0.042 \pm 0.012	0.197 \pm 0.017	0.068 \pm 0.035
SAL	4.949 \pm 0.828	9.062 \pm 0.934	1.319 \pm 0.465	0.871 \pm 0.344	2.471 \pm 0.597

4.2.4. 8-Quinololinol and Niclosamide affect specific stem cell-like features of breast CSC subpopulation

Given the promising results obtained showing that 8Q and NCS drugs selectively inhibit the growth of CSC subpopulation, we decided to go a step further and evaluate the ability of both drugs in affecting other distinctive features and hallmarks of CSC. Therefore, we next examined whether 8Q and NCS impacted on other distinctive features of CSCs, including migration, anchorage independent growth (neoplastic transformation) and cell invasion ability, using the MDA-MB-231 cell line (**Figure 47**).

Regarding migration, a significant lower wound closure was observed in cells treated with anti-CSC drugs compared to controls (**Figure 47A,B**). At 24 h, the open wound detected for control samples was almost minimal ($4.45\% \pm 1.12\%$), while in cells treated with 8Q and NCS was $33.9 \pm 1.8\%$ and $24.9 \pm 1.7\%$, respectively (**Figure 47A**). Of note, treatment with PTX also showed a high inhibitory effect in cell migration ($37.16\% \pm 1.94\%$ of open wound) (**Figure 47A,B**).

Having shown that treatment with anti-CSC drugs resulted in a decrease in cell migration, we then examined whether same treatments would also exhibit an inhibitory effect on the neoplastic transformation of MDA-MB-231 cells. In this context, we evaluated the efficacy of drugs in reducing the anchorage-independent growth, considered one of the distinctive features that only transformed malignant cells display. Interestingly, anchorage independent growth of MDA-MB-231 cells in soft agar was significantly inhibited by treatments with 8Q and NCS (**Figure 47C**). At the highest tested concentration of 8Q ($50 \mu\text{M}$) and NCS ($15 \mu\text{M}$), the capacity of malignant cells to form colonies was significantly reduced to $5.40 \pm 1.23\%$ and $11.48 \pm 1.11\%$ of the growth observed in non-treated cells, respectively. Conversely, PTX treatment was not able to reduce the anchorage independent growth below 50%, thereby demonstrating 8Q and NCS had a superior anti-CSC activity (**Figure 47C**).

Furthermore, we explored the effect of 8Q and NCS on the invasiveness of stem cell-like cells. Invasiveness is considered one of the most relevant hallmarks of malignant tumor cells because plays an essential role in tumor dissemination and metastasis by enabling tumor cells to reach and invade normal surrounding tissues. Results showed that 8Q significantly reduced the ability of cells to cross the Matrigel-covered $8\text{-}\mu\text{m}$ filter, leading to almost complete inhibition of cell invasion ability (**Figure 47D**). In the case of NCS, no inhibitory effect was observed in cell-invasion assays. PTX also showed some efficacy in reducing cell invasion, but significantly lower than that obtained with 8Q (**Figure 47D**).

Altogether, results demonstrated that 8Q and NCS had a strong anti-CSC activity in MDA-MB-231 cells by inhibiting crucial stemness hallmarks of CSCs.

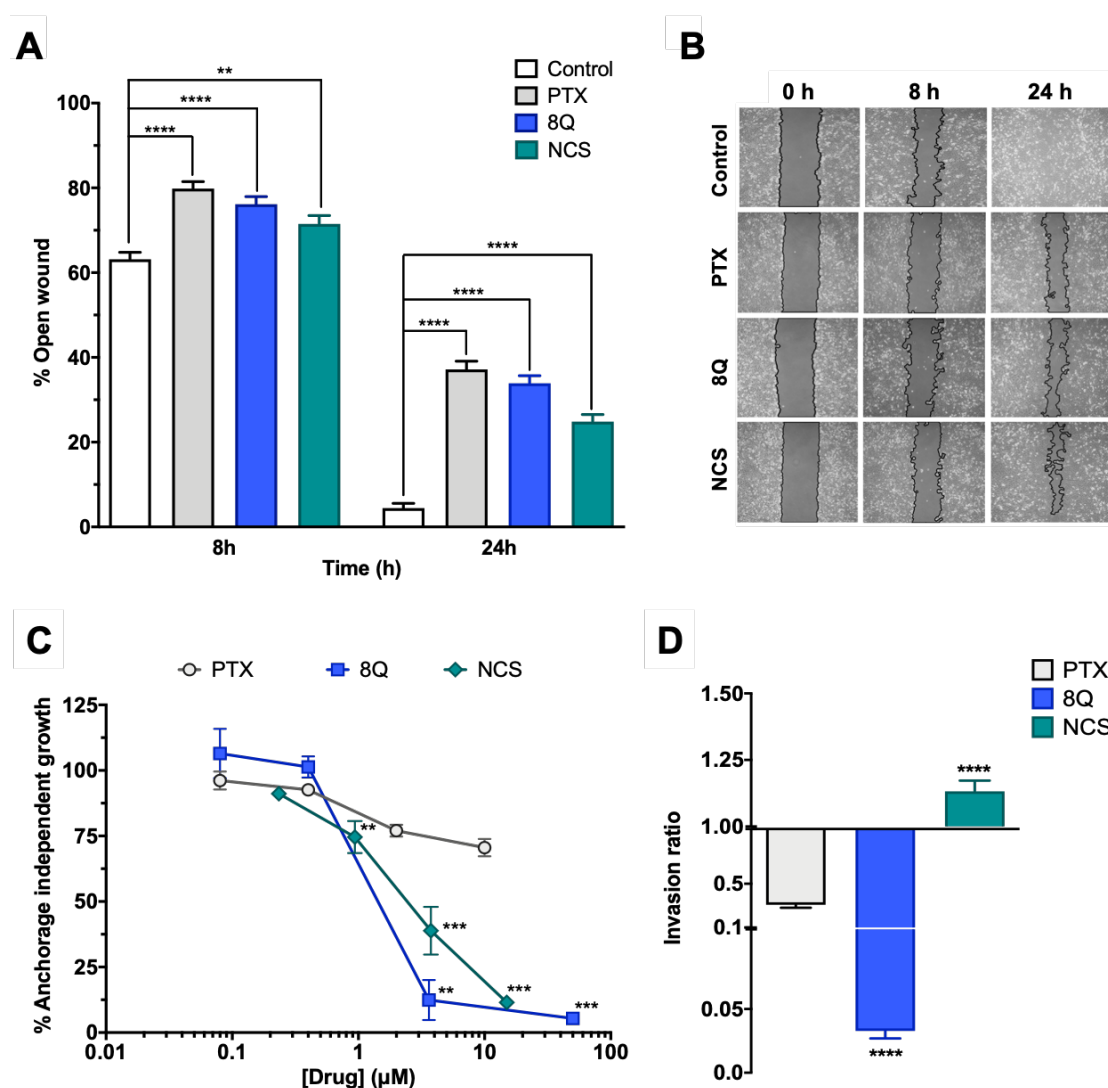


Figure 47. Efficacy of 8Q and NCS inhibiting migration, tumorigenicity and invasion in MDA-MB-231 cell line. A) Wound healing assay showing the percentage of open wound after 8 and 24 h of treatment with 1 µM PTX, 25 µM 8Q and 0.5 µM NCS. **B)** Representative images of the wound closing over time. The wound area has been outlined in black and pseudo-colored in grey. **C)** Cell growth in soft agar (anchorage independent growth) upon treatment with different concentrations of PTX, 8Q and NCS. **D)** Rate of cell invasion in Matrigel after 24 h treatment of 1 µM PTX, 25 µM 8Q and 0.5 µM NCS. All Graphs show the mean ± SEM of at least three independent experiments. All statistical analyses were performed compared to the control non-treated cells. ** $p < 0.05$, *** $p < 0.005$, **** $p < 0.0001$.

4.3. Combined therapy of anti-CSC drugs with chemotherapy as a novel strategy to enhance their anti-cancer efficacy for TNBC treatment

4.3.1. 8Q and NCS display a synergistic effect when combined with PTX at specific ratios in different TNBC cell lines

Since anti-CSC drugs are not meant to be used solely in cancer treatment, but rather as combination therapy with current anticancer reference agents, we hypothesized that the use of anti-CSC drugs in combination with chemotherapeutic agents could be a powerful tool to achieve a high synergistic therapeutic efficacy at lower drug doses. In this regard, the combination of 8Q and NCS in combination with PTX was evaluated on MDA-MB-231, HCC-1806 and MDA-MB-468 cell lines by MTT assays.

Depending on the drug doses, combination can yield a synergistic, additive or antagonistic effect, thus the combination index (CI) for each drug interaction was estimated for different drug ratios. To better determine the potential synergism of the drugs, assays were conducted fixing each of the drugs at its IC_{50} value and varying the other one. This way, we can evaluate multiple drug combinations at multiple dose levels. Afterwards, CI values were calculated to analyze whether there is a synergistic effect between the combinations tested.

The results obtained of the combination assays in the MDA-MB-231 cell line are shown as dose-response curves in **Figure 48**. In the case of PTX-8Q treatment, dose-response curves analysis showed much lower cell viabilities at almost all combinations tested, as evidenced by the shift of the curve downward relative to the single drug concentration-response curves, thereby indicating a strong potential for combination treatment (**Figure 48A,B**). Similar results were obtained for PTX-NCS combination, in which cell viability values were much lower when both drugs were used in combination rather than individually, thus reflecting that combination of drugs enhanced their cytotoxic effect (**Figure 48A,B**). Interestingly, when cells were treated simultaneously with PTX fixed at its IC_{50} together with increasing concentrations of both anti-CSC drugs, more especially from 25 to 100 μ M for 8Q and from 1 to 10 μ M for NCS, the cytotoxicity enhancement was greater than the opposite conditions (**Figure 48A,B**).

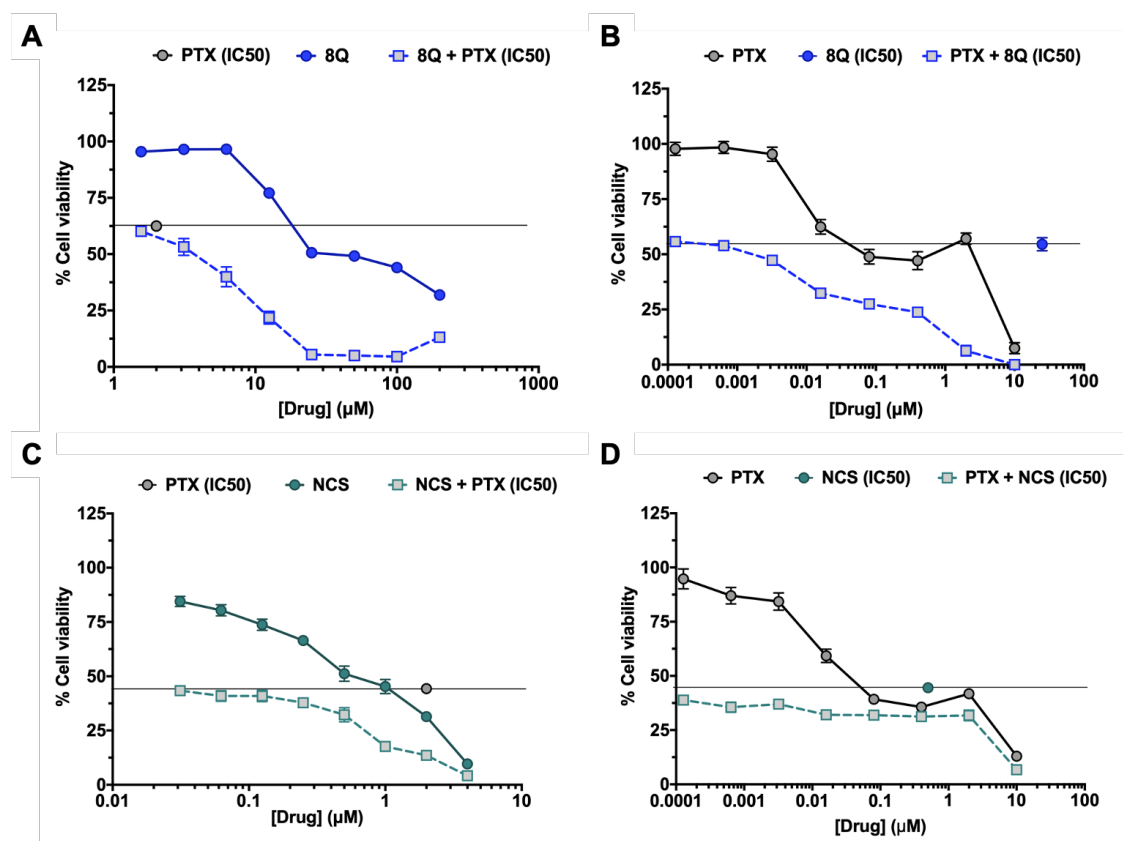


Figure 48. Analysis of the combined therapy of PTX with 8Q and NCS anti-CSC drugs in MDA-MB-231 cells. Effect on cell viability when tested simultaneously PTX at its IC_{50} (2 μ M) in combination with 8Q (A) or NCS (C) at different concentrations. Effect on cell viability when tested simultaneously 8Q (B) or NCS (D) fixed at its IC_{50} (25 and 1 μ M, respectively) in combination with PTX at different concentrations. Results are represented as dose-response curves and show the mean \pm SEM of three independent assays. In all experiments they were also tested in parallel the individual treatments (both fixed IC_{50} value and the variable concentrations), of which results obtained are also included in graphs.

In order to qualitatively evaluate whether the combination of 8Q and NCS with PTX could generate synergistic anti-proliferative effects in the MDA-MB-231 cell line, the CI was calculated based on the previous results of MTT tests using the Compusyn software. The CI values for combined studies of PTX with 8Q and PTX with NCS along with their corresponding ratios tested are shown as heat map tables in **Figure 49A** and **49C**, in which red, white and blue colors indicate synergism ($CI < 1$), additivity ($CI = 1$) or antagonism ($CI > 1$), respectively. Synergism was observed when MDA-MB-231 cells were treated with high concentrations of anti-CSC drugs with PTX fixed at its IC_{50} (red color), while additivity to antagonism was observed at lower concentrations of anti-CSC drugs (**Figure 49A,C**).

For the PTX-8Q combination, an enhanced cytotoxic effect was observed at multiple PTX:8Q ratios, of which the 1:12.5 was the one that resulted in the highest synergistic effect with the lowest CI value (CI=0.06) (**Figure 49A,B**). For the PTX-NCS combination, the greatest drug synergy was observed at 1:2 ratio of PTX:NCS with a CI value close to 0, thus indicating a strong positive synergism between both drugs (**Figure 49C,D**). Accordingly, these ratios were used in later studies in MDA-MB-231 cells.

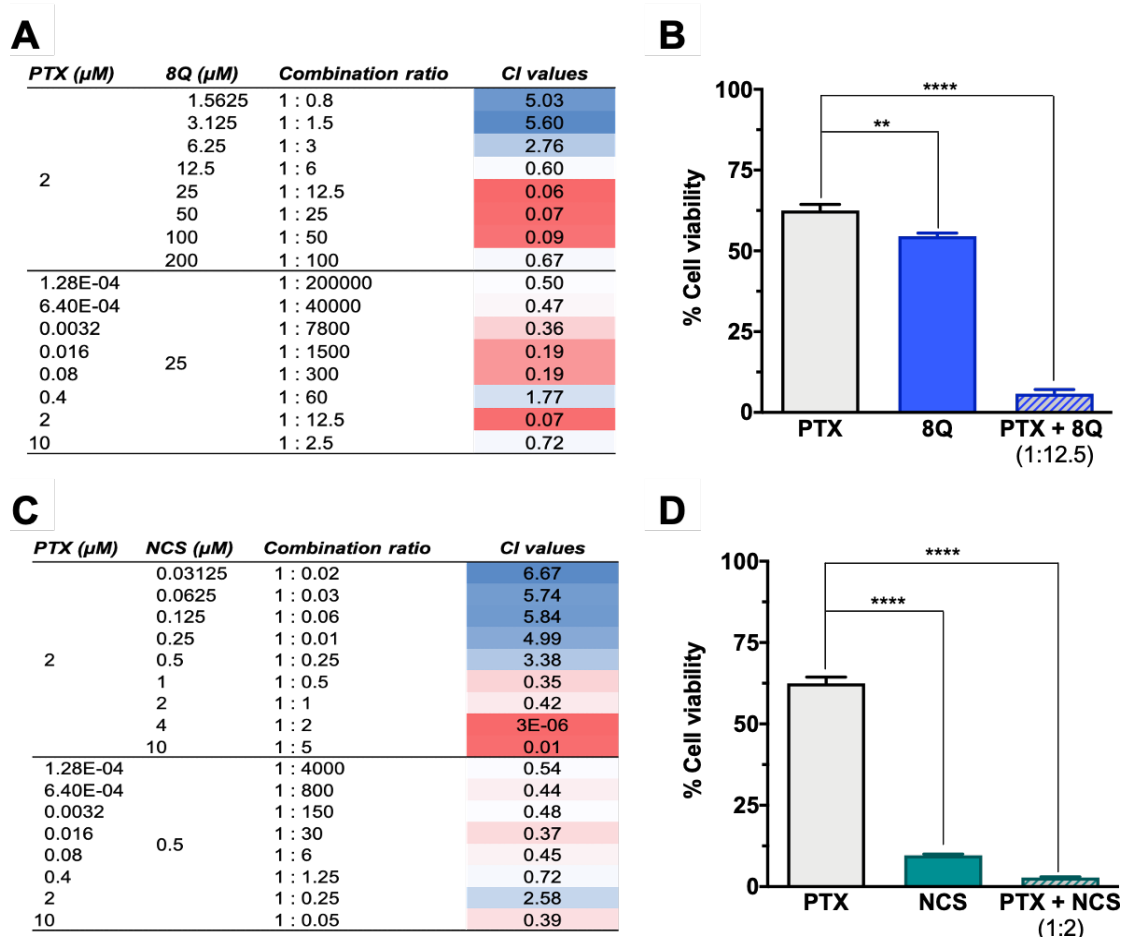


Figure 49. Effect of the combination of 8Q and NCS with PTX in the cell viability of MDA-MB-231 cells. **A**) Combination index (CI) of different PTX to 8Q drug ratios, shown as heat maps (CI>1 indicating antagonism in blue, CI<1 showing synergism in red). Studies were done fixing PTX concentration first at its IC₅₀ value (2 μM) and changing the 8Q concentration (top values), and fixing 8Q concentration at its IC₅₀ value (25 μM) and varying then PTX concentration (bottom values). **B**) Viability of MDA-MB-231 cells treated with PTX, 8Q or the 1:12.5 PTX:8Q ratio. **C**) CI of different PTX to NCS ratios, again fixing first the PTX at its IC₅₀ value (2 μM) and changing the NCS concentration (IC₅₀ value 0.5 μM) and vice versa (lower part of the table). **D**) Viability of MDA-MB-231 cells treated with PTX, NCS or the 1:2 PTX:NCS ratio. Data is represented as the mean \pm SEM of three independent experiments. ** p < 0.05, **** p < 0.0001.

Once established the optimal dose ratios between drugs, we found interesting to assess whether the synergistic effect would be altered when varying the concentration range of drugs. For this purpose, MDA-MB-231 cells were treated with increasing drug concentrations, while maintaining the previous established drug proportions (1:12.5 for PTX-8Q and 1:2 for PTX-NCS). In both combined treatments, dose-response curves analysis and CI values calculated showed that the synergistic effect between both anti-CSC drugs with PTX was partially maintained along with the concentration range, specifically, when 8Q and NCS were tested at a concentration equal or above their IC_{50} . Indeed, the cytotoxicity and synergistic effect obtained of both combined therapies was greater as drug concentrations increased, indicating that synergism was concentration-dependent. Accordingly, the inhibitory effect on cell viability decreased as drug concentrations were reduced, while the CI values increased and so on until it was reached a point where the synergistic effect was lost and became additive or even antagonistic. As an example, in **Figure 50** are shown the results for the PTX-NCS combination at 1:2 ratio. This figure clearly showed the importance of drug concentration for synergism evaluation and drug ratio determination. In this case, starting from 0.25 μ M of PTX and 0.5 μ M of NCS concentrations (equivalent to their IC_{50}) we went from having an additive to a synergistic effect, which improved (lower CI values) as drug concentrations increased (**Figure 50B**).

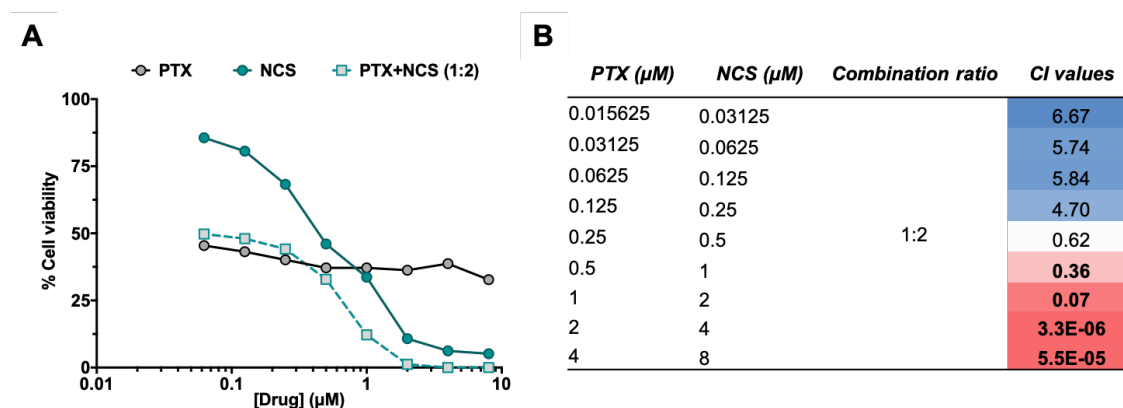


Figure 50. Synergism of 1:2 PTX-NCS ratio is concentration-dependent in MDA-MB-231 cells. MDA-MB-231 cells were treated with increasing concentrations of both drugs maintaining at all times the established 1:2 ratio. **A)** Effect on cell viability of PTX-NCS combined treatment at micromolar ratio 1:2. In all experiments were also tested in parallel the corresponding individual treatments, which results obtained are also included in graph. Data is represented as the mean \pm SEM of three independent experiments. **B)** Heat map of drug combination studies of the PTX-NCS treatment (1:2).

To further explore the synergistic effects of 8Q and NCS with PTX, combination studies were also performed in HCC-1806 and MDA-MB-468 cell lines. Combination assays also showed an improved cytotoxicity when combined at specific ratios in HCC-1806 and MDA-MB-468 cell lines (**Figure 51** and **52**, respectively).

In HCC-1806 cells, the greatest synergy was obtained at 1:5 (with a CI close to 0) and 1:0.4 (CI=0.17) ratios for PTX-8Q and PTX-NCS treatments, respectively (**Figure 51**). In MDA-MB-468 cells, it was obtained at 1:1,250 (CI=0.02) and 1:1,000 (CI=0.12) drug ratios (**Figure 52**). **Figures 51B** and **52B** show the effects on cell viability when HCC-1806 and MDA-MB-468 were treated with 8Q and PTX, both individually and in combination with the established synergistic ratios, respectively. While, **Figures 51D** and **52D** show the improvement in cytotoxic efficacy when cells were co-treated with NCS and PTX drugs in comparison with the individual treatments. Accordingly, these ratios were the ones used for subsequent studies in both cell lines.

Interestingly, the analysis of compusyn results from the HCC-1806 cell line showed that most of micromolar ratios tested of both combined treatments resulted in additive or synergistic effect, since practically all CI values were between 0-1 (**Figure 51A,C**). By contrast in MDA-MB-468 cell line, the results indicated that synergism between drugs was only obtained at specific ratios. More specifically, synergism was obtained when high doses of the anti-CSC drugs (concentration above their IC₅₀ value) were combined with low doses of PTX (equal to or below its IC₅₀). By contrast, other drug combination ratios resulted in a strong undesired antagonistic effect (**Figure 52A,C**). The differences in the established optimal ratios between these cell lines are likely a reflection of differential molecular and intracellular signaling changes as well as differential drug sensitivity to treatments tested, demonstrating the cell-type specific response to combined therapy.

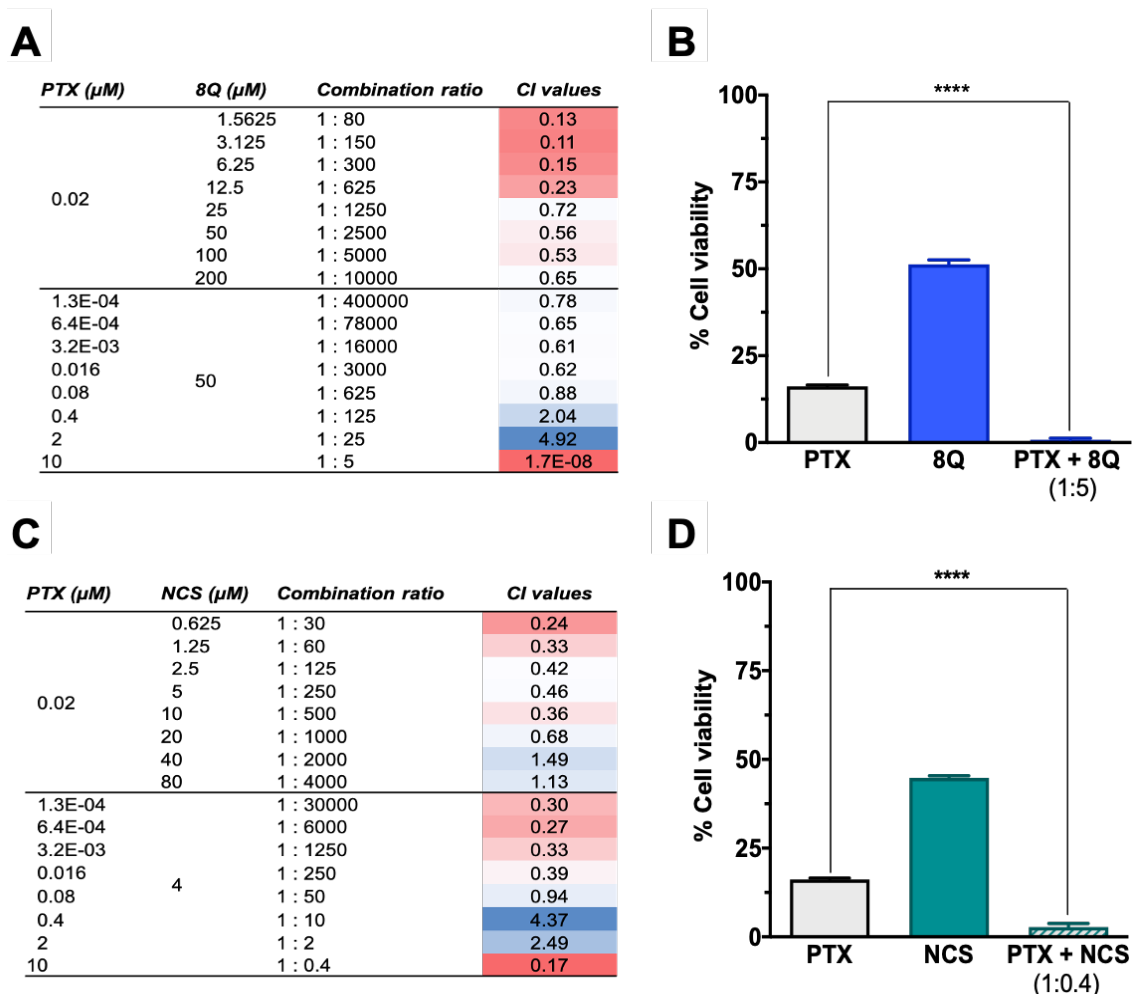


Figure 51. The anti-CSC drugs 8Q and NCS displayed a synergistic inhibition of cell viability when combined with the chemotherapeutic drug PTX in HCC-1806 cell line. Heat maps of (A) PTX with 8Q and (C) PTX with NCS combined treatments. Graphs show representative results of cell viability (%) when cells were treated with (B) PTX and 8Q or (D) PTX and NCS, as individual therapy and in combination at 1:5 or 1:0.4 ratios, respectively. Data is represented as the mean \pm SEM of three independent experiments. **** $p < 0.0001$.

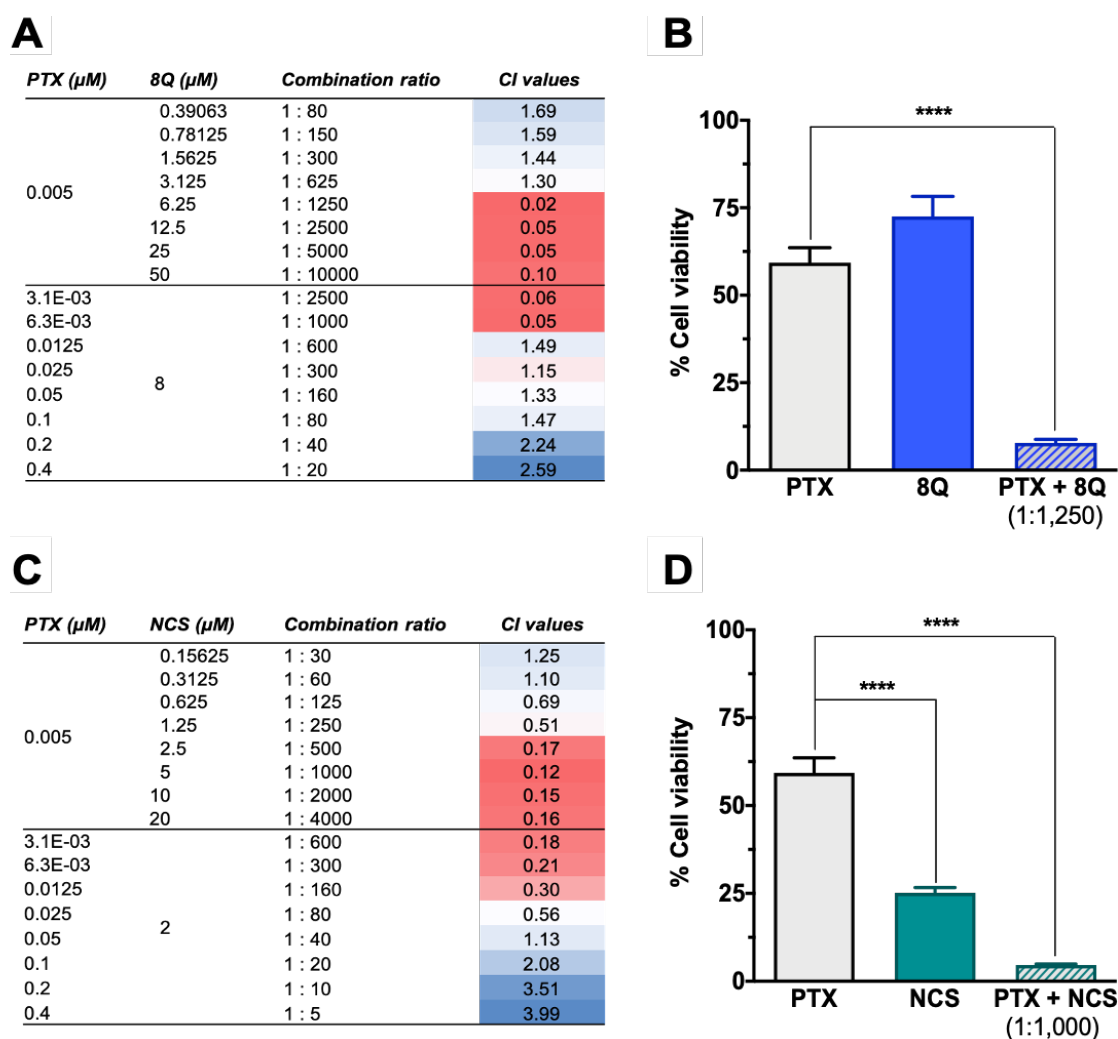


Figure 52. Combination of 8Q or NCS anti-CSC drugs with PTX enhances their synergistic cytotoxic effect in MDA-MB-468 cells. Heat maps of (A) PTX with 8Q and (C) PTX with NCS combined studies. (B, D) Synergism of the combination of anti-CSC drugs with PTX at selected ratios in MDA-MB-468 cells, represented as the % of cell viability obtained when cells are treated with (B) PTX and 8Q or (D) PTX and NCS, alone and in combination at 1:1,250 or 1:1,000 ratios, respectively. Data is represented as the mean \pm SEM of three independent experiments. **** $p < 0.0001$.

4.3.2. Combination of 8Q or NCS with PTX increases the anti-CSC efficacy of the drugs

Once the synergistic activity of 8Q and NCS with the reference drug PTX was confirmed and the combination ratios in all three-cell lines were established, we moved towards our aim of finding efficient therapeutic options to target CSC subpopulation. To evaluate whether combination therapy of PTX-8Q and PTX-NCS could offer therapeutic advantages, drug ratios with best CI values were evaluated in the fluorescent tdTomato CSC models. Changes on CSC subpopulation were monitored by flow cytometry and

stem cell gene expression analysis (Figure 28 for MDA-MB-231 cell line and Figures 29 for MDA-MB-468 and HCC-1806). For these assays, cells were seeded at 50% of CSC-tdTomato⁺ and 50% of non-CSC-tdTomato⁻ conditions. In order to mimic chemotherapeutic cycles in a similar way than used as standard-of-care in clinics, cells were treated with their corresponding treatments for 72 h and then left to recover for additional 48 h in complete medium. Of note, individual treatments were also included.

As expected, following PTX exposure the relative abundance of CSCs (tdTomato⁺ cells) significantly increased ($p < 0.0001$) in a dose-dependent manner in MDA-MB-231 cells (**Figure 53A**). Conversely, upon incubation with 8Q and NCS anti-CSC drugs, the relative amount of MDA-MB-231-tdTomato⁺ cells remarkably decreased ($p < 0.0001$ for both drugs) when compared to PTX treatment (**Figure 53A**). Of note, low doses of 8Q achieved a significant reduction on MDA-MB-231 CSC subpopulation, while at higher doses the effect on CSCs was only preventive.

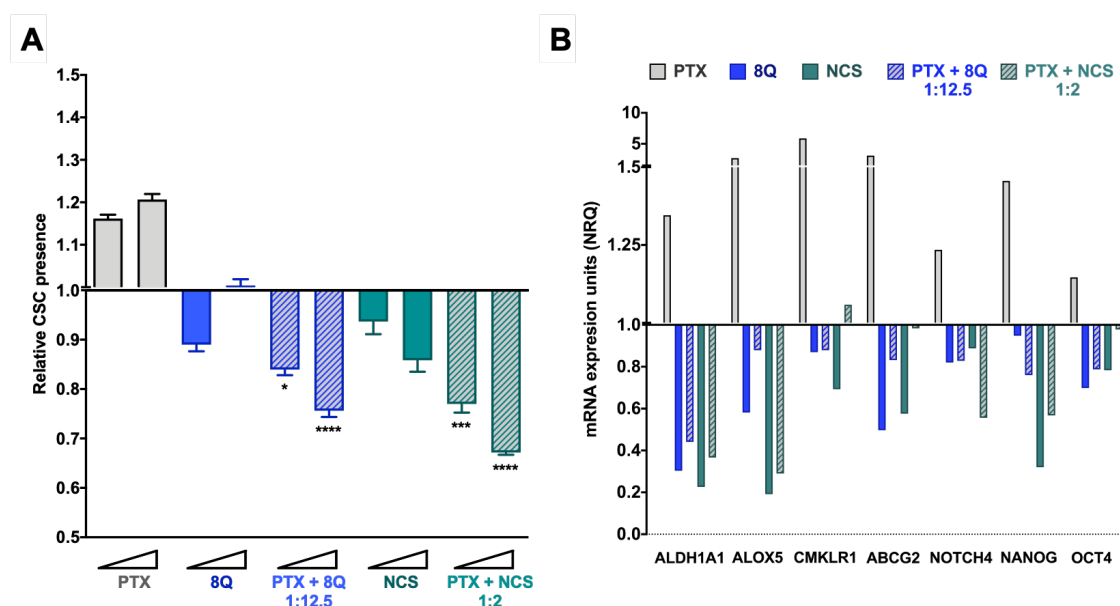


Figure 53. Anti-CSC activity of 8Q and NCS in combination with PTX in MDA-MB-231 fluorescent CSC model. **A)** Relative CSC-tdTomato⁺ presence determined by flow cytometry and referred to control condition. Values below than, equal to or above 1 indicate reduction, maintenance or increase of CSC-tdTomato⁺ cells within population, respectively. Data is represented as the mean \pm SEM of three independent experiments. Statistic t-test analysis were performed comparing drug combinations with single anti-CSC drug treatments at the corresponding equivalent drug dose. **B)** Changes in the stem cell gene expression profile determined by quantitative RT-PCR. Results are expressed as normalized relative quantities (NRQ) and referred to control condition. Concentrations tested for drugs were 0.5 and 1 μ M for PTX, 6.25 and 12.5 μ M for 8Q, 1 and 2 μ M for NCS and the corresponding combined ratios. * $p < 0.01$, *** $p < 0.005$, **** $p < 0.0001$.

In the case of NCS treatment, such decrease in CSC-tdTomato+ was dose dependent. Interestingly, combined treatments of 8Q and NCS with PTX significantly abrogated the relative increase of MDA-MB-231-tdTomato+ cells induced by PTX (**Figure 53A**), as well as significantly enhanced the anti-CSC effect of 8Q and NCS individual treatments ($p = 0.0201$ and $p = 0.003$ for lower doses of PTX-8Q and PTX-NCS, respectively, while for higher doses was $p < 0.0001$ for both combinations; compared to individual anti-CSC therapy).

These results were further confirmed in MDA-MB-468 and HCC-1806 cell lines. Consistent with previous data in MDA-MB-231 cells, PTX treatment also led to a significant increase of CSCs in a dose-dependent manner in both TNBC cell lines (**Figure 54A,C**), being more evident in the MDA-MB-468. Moreover, upon incubation of TNBC cell lines with 8Q and NCS anti-CSC drugs, the relative presence of tdTomato+ cells was significantly reduced ($p < 0.0001$; for both drugs in both cell lines) when compared to PTX treatment. In the case of NCS treatment, such decrease was more evident and dose dependent in HCC-1806 and MDA-MB-468 cell lines than in MDA-MB-231 (**Figure 54A,C**). Furthermore, the anti-CSC effect of 8Q and NCS was significantly enhanced when drugs were administered in combination with PTX rather than as individual therapy. Interestingly, combined treatments in MDA-MB-468 and HCC-1806 cells achieved a greater anti-CSC effect than in MDA-MB-231.

These results were further confirmed by the gene expression analysis in all three TNBC cell lines. In MDA-MB-231 cells, we found a remarkable relative increase in the expression of all stem cell genes analyzed, including ALDH1A1, ALOX5, CMKLR1, ABCG2, NOTCH4, Nanog and OCT4 after PTX individual treatment (**Figure 53B**). While 8Q and NCS treatments, either alone or in combination with PTX, substantially downregulated the stem cell gene expression. In particular, 8Q single treatment led to a strong decrease of ALDH1A1, ALOX5 and ABCG2 mRNA levels, while for the other genes, the effect obtained was slighter. In the case of NCS treatment, such decrease was greater in ALDH1A1, ALOX5 and Nanog mRNA, and indeed, was stronger than when treated with 8Q. Combination of both drugs with PTX remarkably downregulated the expression of almost all stem-cell like markers analyzed, such as ALDH1A1, ALOX5, NOTCH4 and Nanog, thus indicating preferential and efficient effect against CSCs when 8Q and NCS were used in combination with PTX (**Figure 53B**). These results were further confirmed in HCC-1806 and MDA-MB-468 cell lines (**Figure 54B,D**). Importantly, in both cell lines a prominent increase of stem cell gene expression was also obtained after PTX treatment. Such increase was stronger in NOTCH4 and OCT4 mRNA than in the MDA-MB-231 cell line. Moreover, 8Q and NCS, either alone or in combination with PTX,

remarkably down-regulated the stem cell gene expression in both cell lines, overcoming, and in some cases only matching, the effect of individual treatments in almost all genes analyzed.

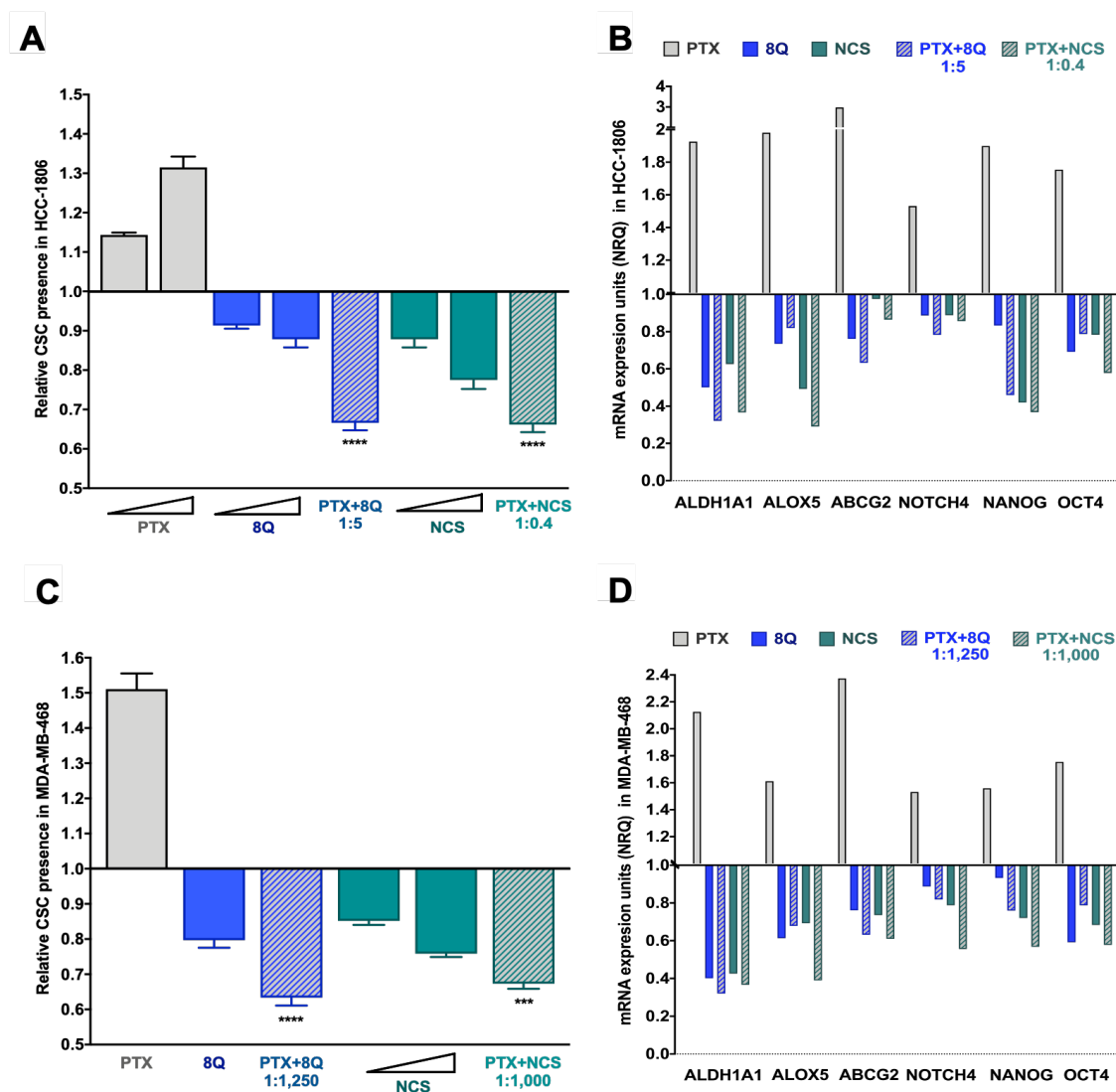


Figure 54. Anti-CSC activity of 8Q and NCS in combination with PTX in TNBC fluorescent CSC models. Relative CSC-tdTomato⁺ presence in (A) HCC-1806 and (C) MDA-MB-468 fluorescent models, determined by flow cytometry and referred to control condition. Values below, equal or above 1 indicate reduction, maintenance or increase of CSC-tdTomato⁺, respectively. Data is represented as the mean \pm SEM of three independent experiments. Statistic t-test analysis were performed comparing combination treatments with individual anti-CSC drugs at the corresponding equivalent drug dose. Changes in the stem cell gene expression profile of (B) HCC-1806 and (D) MDA-MB-468 models determined by quantitative RT-PCR. Results are expressed as normalized relative quantities (NRQ) and referred to control condition. Concentrations tested for drugs in the HCC-1806 cell line were 0.0025 and 5 μ M for PTX, 25 and 50 μ M for 8Q, 2 and 5 μ M for NCS, while for MDA-MB-468 were 0.005 for PTX, 6.25 μ M for 8Q, 2.5 and 5 μ M for NCS, and the corresponding combined ratios. **** $p < 0.0001$.

Of note, gene expression values changed along with the treatments, cell lines and markers evaluated, which rendered accurate and more deeply comparisons difficult. Despite this, gene expression analyses corroborated the synergy between 8Q and NCS and PTX, indicating that combined therapy prevented the CSC enrichment induced by PTX and thus leading to an enhanced anti-CSC effect.

The effect of the combination of 8Q and NCS with PTX on the CSC subpopulation was further confirmed by analyzing their effect on the mammosphere viability (MSV) and the ability to form new ones (mammosphere-forming efficiency, MSF) in all three TNBC cell lines (**Figure 55** and **56**). For this, cells were cultured in suspension in serum free media and treated with both anti-CSC drugs, alone and in combination with PTX, and mammosphere viability and formation ability were evaluated.

Consistent with previous results, the ability of MDA-MB-231 stem-like cells to grow as mammospheres was significantly reduced when treated with 8Q and NCS ($p < 0.0001$ in both cases). Such reduction was significantly greater when drugs were used in combination ($p = 0.0014$ and $p = 0.0101$ for combinations of PTX with 8Q and NCS, respectively) than as single treatments (**Figure 55A**). The anti-neoplastic drug PTX showed a limited impact on mammosphere growth, since PTX dose did not succeed in reducing to 50% the MSF ($75.9\% \pm 4.7\%$) (**Figure 55A**). Similar results were obtained when MSV was analyzed in MDA-MB-231 (**Figure 55B**) where the effect of PTX was limited ($85.5\% \pm 4.7\%$), but the use of 8Q and NCS induced relevant loss of mammosphere viability, especially when combined with PTX ($p = 0.0005$ and $p = 0.0186$ for combinations with 8Q and NCS, respectively).

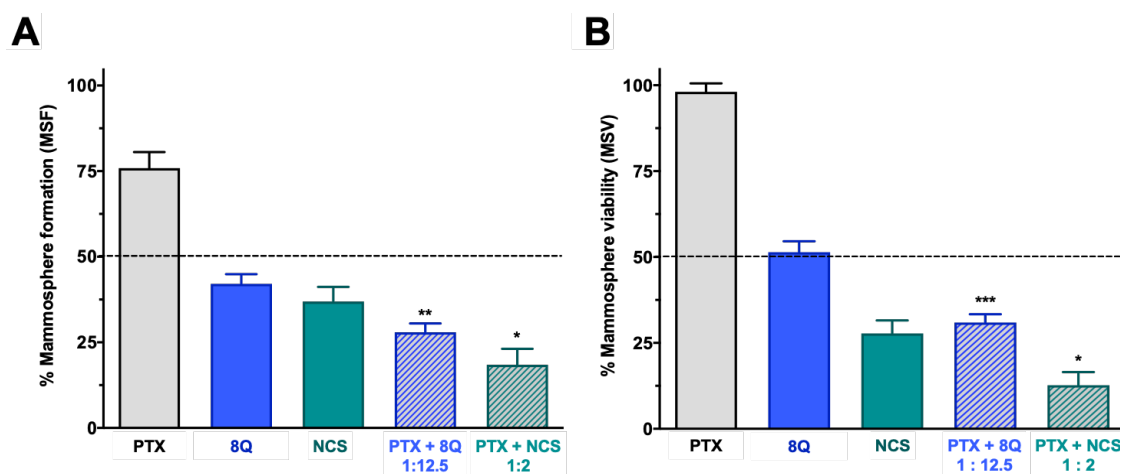


Figure 55. Effect of the combination of 8Q or NCS with PTX in MDA-MB-231 mammospheres. A) Mammosphere-forming (MSF) efficiency of PTX, 8Q, NCS and their combination (2 μ M, 25 μ M and 4 μ M, respectively). **B)** Mammosphere viability (MSV) of PTX, 8Q, NCS and their combination (4 μ M, 50 μ M and 8 μ M, respectively). Results are represented as the mean \pm SEM of three independent experiments and referred to non-treated control condition. Statistic t-test analysis were performed comparing combination therapy with single anti-CSC treatments at the corresponding equivalent drug dose. * $p < 0.01$, ** $P < 0.05$, *** $p < 0.005$.

Described results were confirmed in HCC-1806 and MDA-MB-468 TNBC cell lines (**Figure 56**). In these cells, PTX showed no impact in MSF or MSV (65.9% \pm 4.3% and 83.3% \pm 2.6% in MSF for HCC-1806 and MDA-MB-468 cells, respectively; while in MSV was 92.4% \pm 3.9% and 86.7% \pm 5.1%, respectively). On the contrary, the ability of stem-like tumor cells to grow as mammospheres from both TNBC cell lines was significantly reduced when treated with 8Q and NCS ($p < 0.0001$ for both drugs). Such reduction was significantly greater when drugs were used in combination ($p < 0.0001$ and $p = 0.0031$ for combinations of PTX with 8Q and NCS in HCC-1806 cells, respectively; $p < 0.0001$ and $p = 0.0043$ for MDA-MB-468 cells, respectively) than as single treatments (**Figure 56A,C**). Similar findings were observed when MSV was analyzed (**Figure 56B,D**). The use of 8Q and NCS induced relevant loss of mammosphere viability, especially when combined with PTX ($p = 0.0069$ and $p = 0.0014$ for combinations with 8Q and NCS in HCC-1806, respectively; $p = 0.004$ and $p = 0.0046$ for MDA-MB-468 cells, respectively). Altogether, NCS showed a superior effect in comparison to 8Q treatment, either alone or in combination with PTX regarding mammosphere formation and growth.

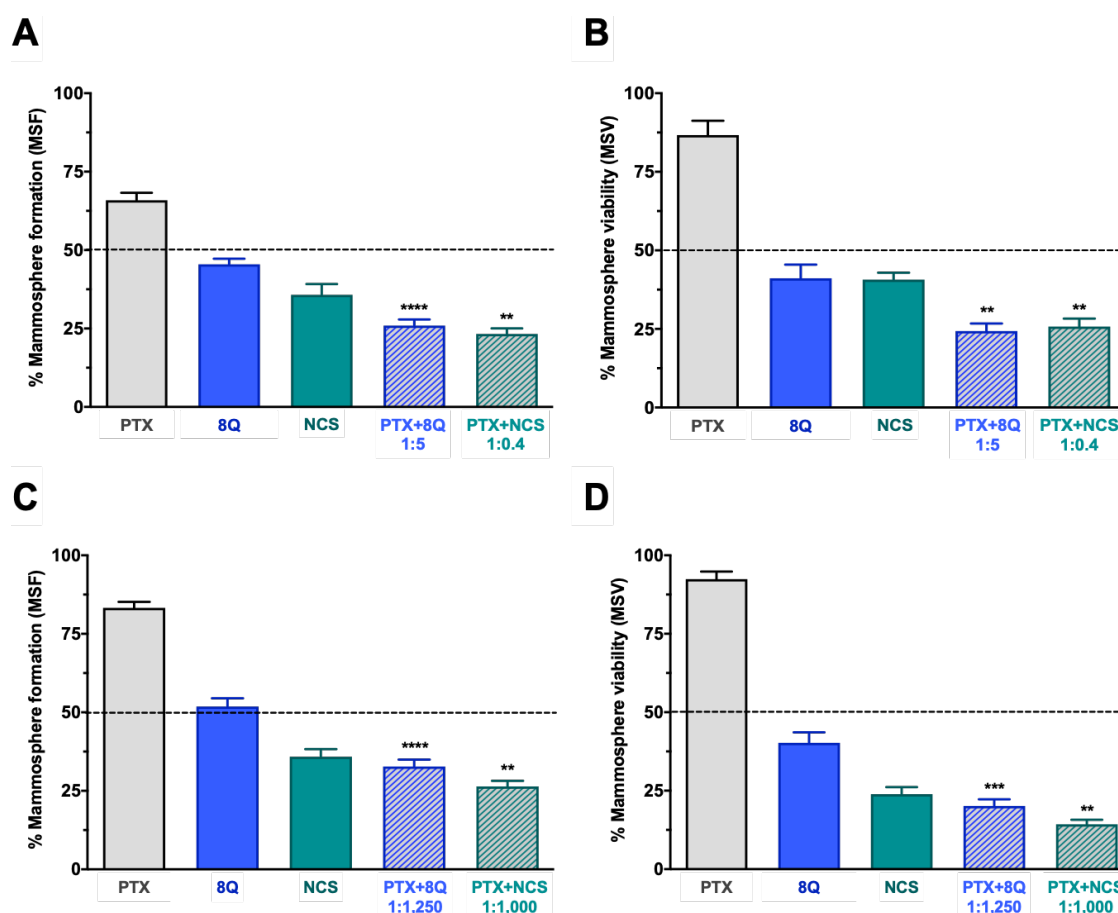


Figure 56. Combination of 8Q or NCS anti-CSC drugs with PTX enhances their synergistic anti-CSC activity in low attachment conditions in other TNBC cell lines. Efficacy of 8Q and NCS, alone and in combination in reducing mammosphere-forming efficiency (MSF) in both **A**) HCC-1806 and **C**) MDA-MB-468 cells, and in affecting mammosphere viability (MSV) in **B**) HCC-1806 and in **D**) MDA-MB-468 cell lines. Data is represented as the mean \pm SEM of three independent experiments and referred to non-treated control condition. Drug concentrations used PTX 10 μ M, 8Q 50 μ M and NCS 4 μ M in HCC-1806 cells, while for MDA-MB-468 cells were 0.005 μ M, 6.25 μ M and 5 μ M, respectively. Statistical analysis of combined therapy in comparison with individual anti-CSC treatments are shown in black asterisks. ** $p < 0.05$, *** $p < 0.005$, **** $p < 0.0001$.

4.3.3. The combination of 8Q and NCS inhibits NF- κ B and Wnt/ β -catenin signaling pathways

8Q and NCS have been described as inhibitors of nuclear factor- κ B (NF- κ B) and Wnt/ β -catenin signaling pathways, respectively. Both pathways are known to be crucial in the maintenance of the stem phenotype [214,289]. In order to elucidate whether the synergism observed on cell viability between 8Q and NCS and the PTX was sustained by alterations in these two pathways, MDA-MB-231 cells were treated with 8Q, NCS and PTX for 24 h, and signaling protein levels were assessed by Western blot. Results

pointed out that a significant reduction of phospho-NF- κ B (p-NF- κ B) subunit p65 was observed for 8Q concentrations as low as 12.5 μ M, while the total expression of NF- κ B subunit p65 was not changed, thus confirming the role of 8Q drug as a selective inhibitor of the NF- κ B signaling pathway (**Figure 57A,C**). As expected, PTX treatment showed no efficacy in inhibiting the NF- κ B signaling pathway. Moreover, a marked reduction of p-NF- κ B p65 subunit was also observed in cells treated with the combination compared to non-treated (control) or PTX-treated ones, and the inhibition of NF- κ B p65 phosphorylation with the PTX+8Q combination was as efficient as with the 8Q alone (**Figure 58**).

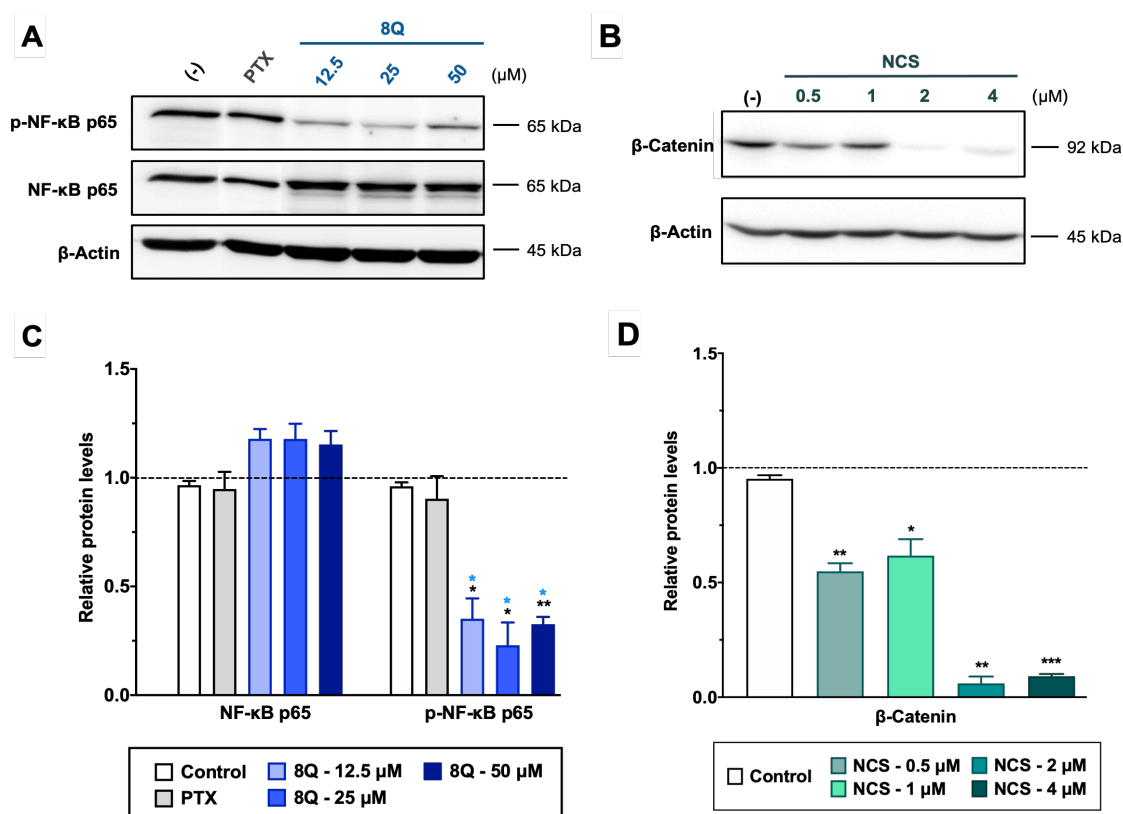


Figure 57. Effect of the combination of 8Q or NCS with PTX in NF- κ B and Wnt/ β -catenin signaling pathways in MDA-MB-231 cells. A) Representative Western blots of total and phosphorylated NF- κ B (p-NF- κ B) p65 protein levels upon treatment with different concentrations of 8Q. **B)** Representative Western blots of β -catenin levels after treatment with increasing concentrations of NCS. The β -actin protein expression level was used as loading control. **C-D)** Graphs represent the quantification band intensity signal referred to β -actin expression, represented as mean \pm SEM of three independent experiments. Statistical t-test analysis of anti-CSC drug therapy was performed in comparison with control non-treated cells (black) as well as with PTX treatment (blue).

As for the NCS, MDA-MB-231 cells treated with the drug showed a significant dose-dependent reduction of β -catenin protein level as well as an increase of phosphorylated GSK3- β (p-GSK3- β) protein (while total expression of GSK3- β was not changed) (**Figure 57B,D**). Conversely, PTX treatment showed no efficacy in inhibiting the Wnt signaling. Importantly, Western blot analyses confirmed a significant increase of p-GSK3- β and reduction of β -catenin proteins in TNBC cells when treated with combined therapy (**Figure 59**).

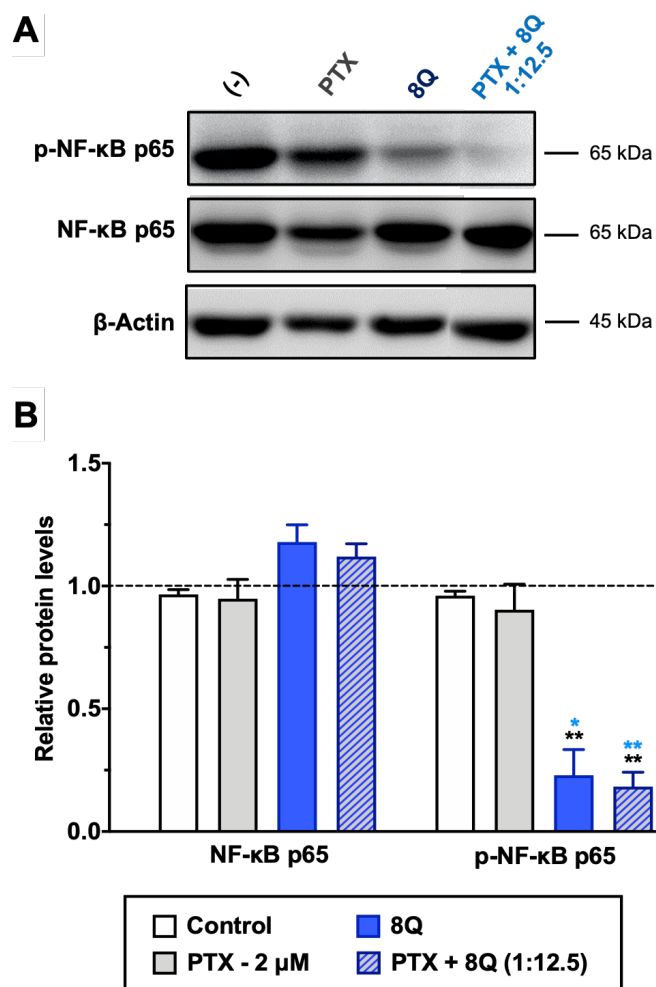


Figure 58. Effect of 8Q and PTX treatments in the NF- κ B signaling pathway in MDA-MB-231 cells. **A**) Representative Western blots of total and phosphorylated NF- κ B p65 protein levels upon treatment with PTX, 8Q or their combination (2 μ M and 25 μ M, respectively). The β -actin protein expression level was used as loading control. **B**) Quantification of band intensity in Western blots. Results are expressed as normalized protein levels referred to β -actin expression, represented as mean \pm SEM of three independent experiments. Statistic t-test analysis of 8Q and combined therapy were done in comparison with control non-treated cells (black) as well as with PTX treatment (blue).

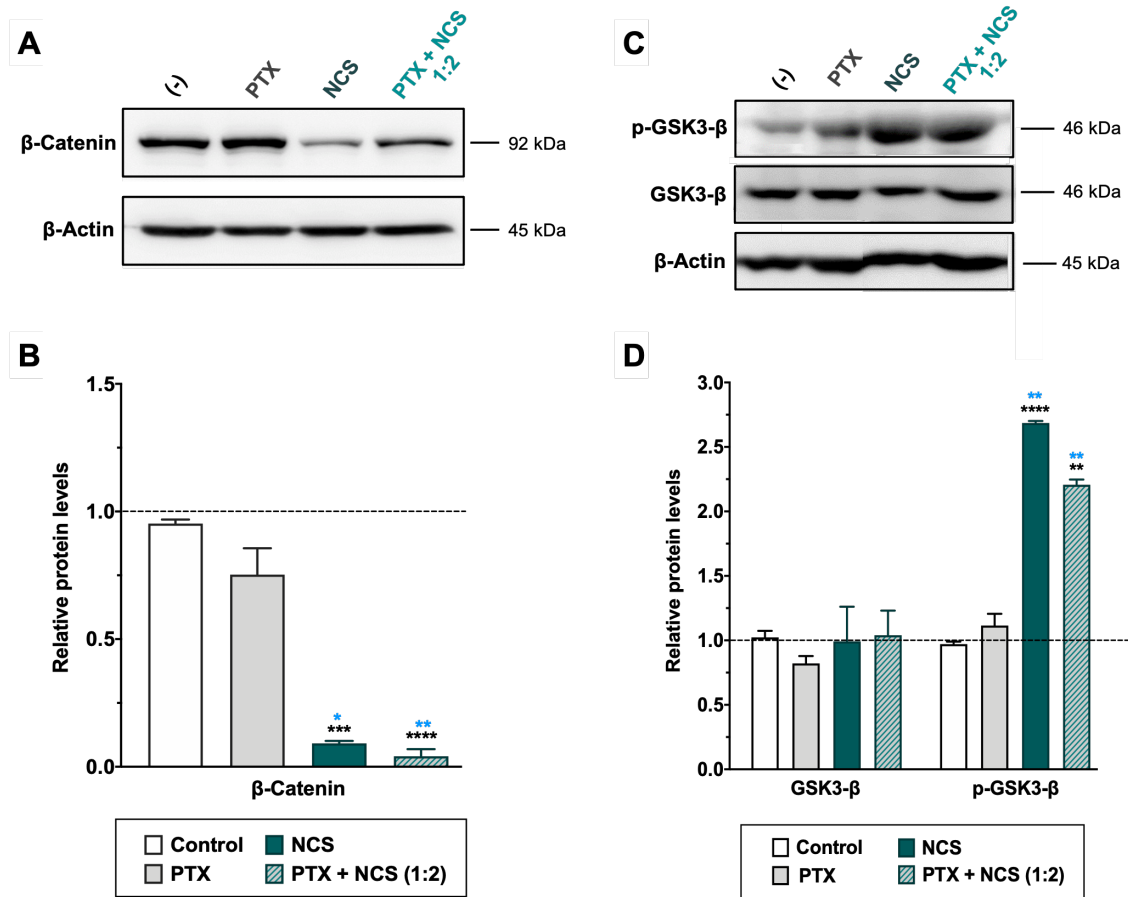


Figure 59. Effect of NCS and PTX treatments in the Wnt/ β -Catenin signaling pathway in MDA-MB-231 cells. β -Catenin, total- and phosphorylated-GSK3- β protein levels expression levels after PTX and NCS treatment, both alone and in combination (1:2 ratio). **A,C**) Representative β -catenin and GSK3- β protein levels after drug treatments. The β -actin protein expression level was used as loading control. **B,D**) Graphs represent the quantification band intensity signal referred to β -actin expression, represented as mean \pm SEM of three independent experiments. Statistic t-test analysis of NCS and combined therapy were performed in comparison with control non-treated cells (black) as well as with PTX treatment (blue).

4.4. New designed polymeric micellar systems for anti-cancer drug delivery

To circumvent some limitations of conventional formulations and to improve the therapeutic outcomes of anticancer drugs, nanotechnology-based drug delivery systems, like polymeric micelles (PM), have been successfully used in the clinical setting to enhance their solubility, bioavailability, stability and biodistribution [271,290]. In this context, polymeric micelle-based drug delivery systems for encapsulation of chemotherapeutics and/or anti-CSCs drugs have been reported as an effective strategy to improve the intracellular delivery of treatments into both bulk tumor cells and CSCs [271,291]. In this thesis, we have developed and validated two novel micellar systems using two different polymeric composition: i) Soluplus-based micellar systems encapsulating the chemotherapeutic drug PTX and ii) Pluronic® F127-based micellar systems encapsulating the anti-CSC drugs 8Q and NCS alone and co-loaded with PTX at defined ratios.

4.4.1. PTX-loaded Glu-decorated polymeric micelles for PTX delivery in vitro

Among the emerging nanocarrier systems, mixed PM are one of the most promising approaches that have improved the solubility and stability of hydrophobic drugs due to the possibility of combining advantages of different types of single polymeric micelles [292]. In this regard, in a collaborative project with Dr. Diego Chiappetta group (Universidad de Buenos Aires, Facultad de Farmacia y Bioquímica, Cátedra de Tecnología Farmacéutica I, Buenos Aires, Argentina) a novel polymeric micellar formulation was developed based on two biocompatible copolymers, the polyvinyl caprolactam–polyvinyl acetate–polyethylene glycol (Soluplus®) and the D- α -tocopheryl polyethylene-glycol 1000 succinate (TPGS), to improve the aqueous solubility and the in vitro anti-tumor activity of the chemotherapeutic drug PTX.

Soluplus® is a polymer with amphiphilic and solubilizing properties for poorly water-soluble drug substances [293,294]. TPGS has also been used as solubilizer and absorption enhancer in some drug delivery formulations. Besides, it has been shown that TPGS can inhibit the P-glycoprotein, an efflux pump that plays a key role in multidrug resistance in tumor cells [295–297]. Moreover, to further expand the PM potential, we decided to incorporate glucose (Glu) moieties as targeting units into the hydrophilic micellar corona, since one of the main characteristics of cancer cells and specially, CSCs, is their increased Glu uptake mediated by the overexpression of glucose transporters (GLUTs) [88,90]. Previous published results by Dr. Chiappetta group

evidenced that surface decoration of PM with Glu moieties significantly improved the in vitro antitumoral activity as well as the PTX intracellular levels (in comparison with Genexol) in MCF-7 and MDA-MB-231 cancer cell lines [298]. Therefore, this micellar nanoformulation represents an attractive strategy for the development of a novel PTX delivery system for optimizing the aqueous solubility and the in vitro anti-tumor activity of this chemotherapeutic, hence preventing from side effects associated with the use of Cremophor EL[®].

In this collaboration, it was incorporated hydroxypropyl- β -cyclodextrines (β -OH-CDs) in the structure of these PTX-loaded Glu-decorated micelles, since the large number of hydroxyl groups offered multiple reactive sites that could form hydrogen bonding with water to increase the water solubility and provided a hydrophobic cavity. Therefore, two different nanoformulations were developed, Soluplus(Glu):TPGS:CD (5:1:5), which corresponded to the blank, and Soluplus(Glu):TPGS:CD (5:1:5) loaded with PTX (4 mg/mL). Hereinafter referred as empty and PTX-loaded glycosylated micelles, respectively.

4.4.1.1. Physicochemical characterization of PTX-loaded glycosylated micelles

The physicochemical characteristics of resulting empty (eGM) and PTX-loaded (PTX-GM) glycosylated micelles, such as particle size, size distribution and morphology were investigated.

Both nanoformulations were characterized by dynamic light scattering (DLS) to determine their sizes and distributions (**Table 16**). Size and size distribution assays showed that both nanoformulations had a similar size pattern, since mean size value for eGM was 122.6 ± 40.8 nm and after PTX encapsulation was 126.8 ± 45.4 nm. Moreover, a narrow size distribution was observed both before and after PTX encapsulation (**Table 16**). Collectively, these results suggested that the incorporation of PTX did not directly affect micellar size and size distribution of the nanomicellar system developed.

Table 16. Micellar size and size distribution (Pdl, polydispersity index) of glycosylated micelles in the absence (eGM) and presence (PTX-GM) of PTX. Table shows the mean \pm SD of three independent experiments.

Name	Composition	Size (nm) Mean \pm SD	Pdl (nm) Mean \pm SD
eGM	SOLUPLUS(GLU):TPGS:CD (5:1:5)	122.6 \pm 40.8	0.153 \pm 0.01
PTX-GM	SOLUPLUS(GLU):TPGS:CD (5:1:5) – PTX 4 mg/mL	126.8 \pm 45.4	0.137 \pm 0.01

Finally, the morphological characterization of the PTX-GM demonstrated rod-shaped micelles with a unimodal size distribution (**Figure 60A**). This non-spherical morphology obtained was due to the Soluplus[®] chemical composition. These findings were consistent with those obtained in previous studies [299]. In addition, it should be noted that the PTX-loaded GM developed could be lyophilized without the need of using lyoprotectants, thereby, samples could be easily redispersed in distilled water by vortexing obtaining a translucent colloidal dispersion (**Figure 60B**).

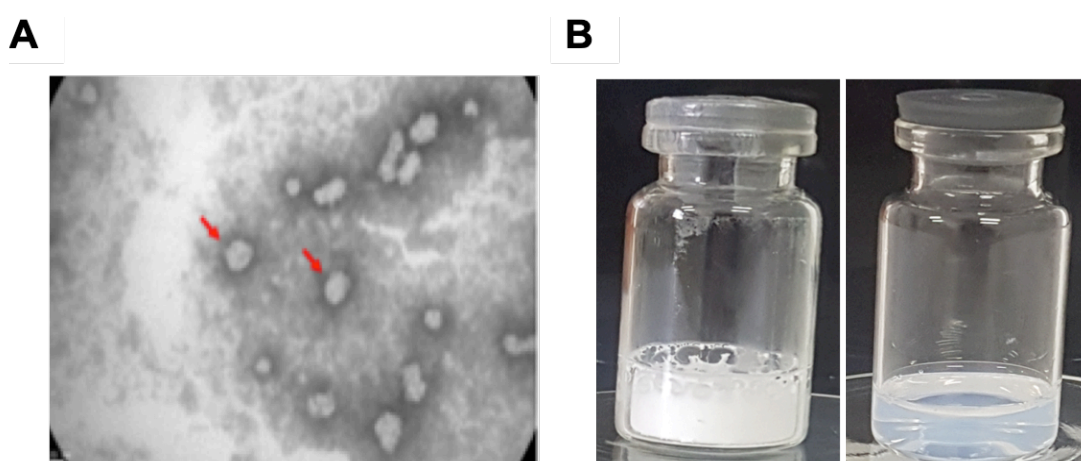


Figure 60. Morphological characterization and macroscopic appearance of PTX-loaded glycosylated micelles. **A)** TEM (transmission electron microscopy) micrograph of PTX-loaded GM at 4 mg/mL (few individual micelles are pointed by red arrows). The scale bar represents 20 nm. **B)** Representative images of vials showing the macroscopic appearance of PTX-GM, when lyophilized (left) and redispersed in water (right).

4.4.1.2. PTX-loaded micelles enhance chemotherapeutic antitumor activity in vitro

To explore the in vitro anticancer performance of the PTX-GM, MDA-MB-231 human BC cells were exposed to loaded micelles and to free PTX solution for 6 h at increasing concentrations. Then, cells were washed with PBS and left for 72 h before reading the absorbance at 590 nm. Empty micelles (eGM) were also included in order to evaluate the polymer toxicity of the micellar system.

The analysis of cytotoxic assays demonstrated that PTX-based micellar formulation showed a significant ($p < 0.0001$) improvement in its cytotoxic profile in comparison with free PTX when the highest concentration (10 $\mu\text{g/mL}$) was tested (**Figure 61A,B**). Indeed, cell viability was reduced up to $33.57 \pm 2.24\%$ when MDA-MB-231 cells were treated

with PTX-GM, while when free PTX was used, the effect on cell viability was significantly lower, $47.18 \pm 2.31\%$ (**Figure 61B**). Conversely, no differences were obtained between loaded micelles and free PTX when were tested at lower concentrations than $10 \mu\text{g/mL}$ (**Figure 61A**). Moreover, eGM showed no cytotoxic effect at any of the concentrations tested, since cell viability results obtained were all above 95%, thereby confirming that the improvement in the anti-proliferative effect was due to the PTX encapsulation and not associated with the micellar composition.

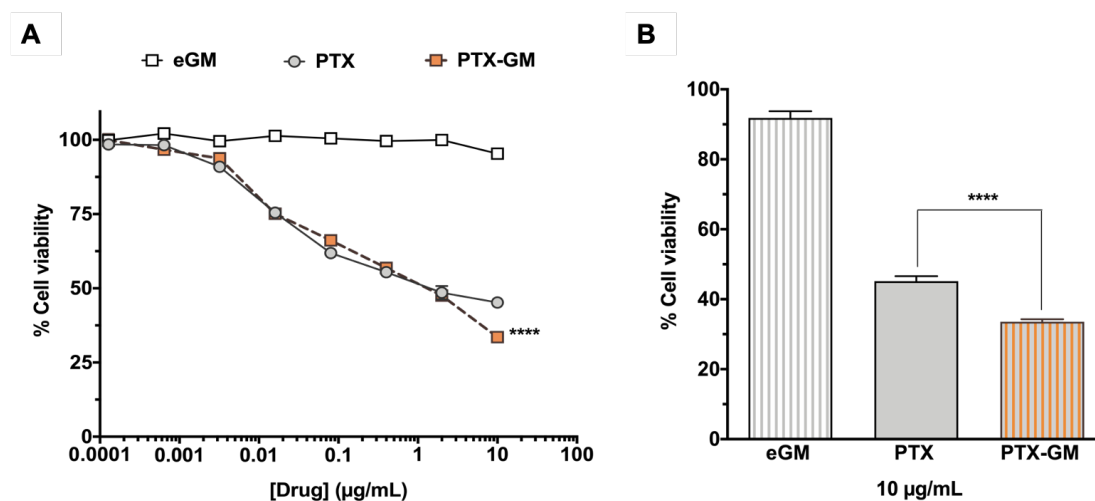


Figure 61. Evaluation of the anti-proliferation activity of eGM and PTX-GM using MDA-MB-231 cells. A) Cell viability curves of tumor cells treated with PTX-loaded and empty GM, and free PTX. **B)** Graph shows the percentage of cell viability obtained at drug concentration of $10 \mu\text{g/mL}$. Data is represented as mean \pm SEM of three independent experiments. Statistic t-test analysis of PTX-GM was performed in comparison with the free PTX treatment, **** $p < 0.0001$.

It is worth remembering that TNBC tumors always required chemotherapy, since they do not respond to conventional hormonal therapy. Hence, the improvement of the cytotoxic effect in the estrogen-independent MDA-MB-231 BC cell line due to PTX encapsulation within the glycosylated system is clinically relevant to enhance chemotherapy in TNBC.

4.4.1.3. The encapsulation of PTX within glycosylated micelles improves its anti-CSC effect in vitro

Having shown that treatment of MDA-MB-231 cells with $10 \mu\text{g/mL}$ of PTX-loaded glycosylated micelles resulted in a significant decrease in cell proliferation, we then tested their efficacy in targeting CSC subpopulation by assessing the effect in both MSF and MSV, using the same TNBC cell line. Moreover, corresponding treatments of both free PTX solution and free loaded GM (the empty ones) were also included. Surprisingly,

the ability of CSCs to form mammospheres (MSF) was completely inhibited when treated with PTX-loaded GM (values obtained were around zero), but not after PTX exposure ($60.86 \pm 15.6\%$) (**Figure 62A**). Free loaded GM showed no effect at the concentration tested, since values obtained were around 95%. Similar results were obtained when MSV was analysed. MSV was remarkably decreased after PTX-loaded GM treatment ($17.30 \pm 4.47\%$) but not when treated with free PTX alone ($60.63 \pm 6.52\%$) (**Figure 62B**). Besides, in this case, eGM showed a slight effect in mammosphere viability (values obtained were around 85%), being this result probably related with the presence of TPGS in the micellar system.

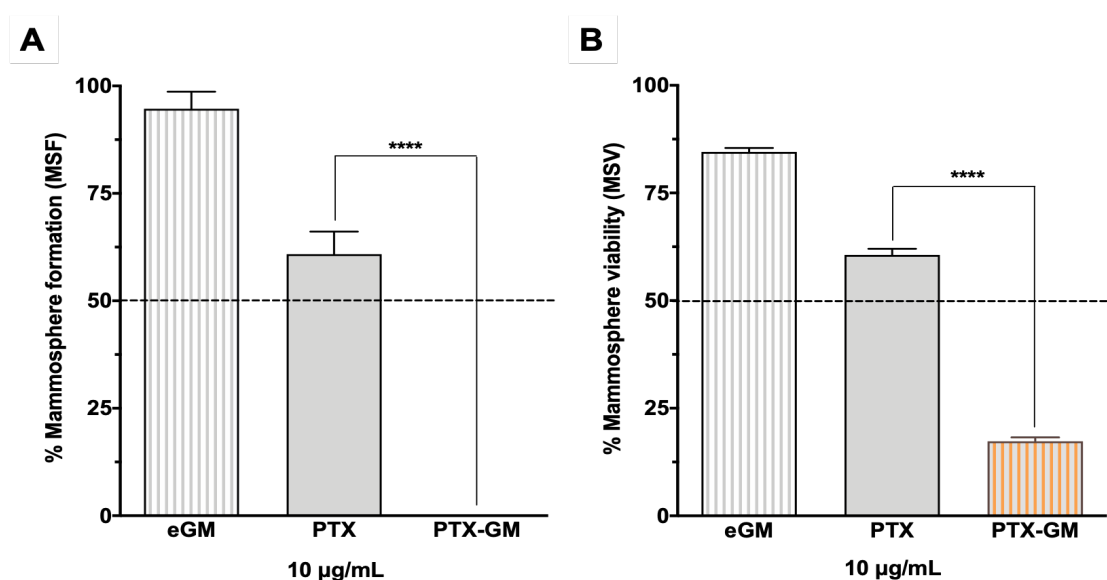


Figure 62. The encapsulation of PTX within glycosylated micelles remarkably enhanced its anti-CSC activity in low attachment conditions in MDA-MB-231 cells. Cells were seeded in suspension in serum free media and treated with the PTX-loaded GM and MSF ability and MSV were evaluated. The corresponding free PTX solution and blank micelles (eGM) were also included. Effect of treatments in CSC (**A**) mammosphere forming (MSF) ability and (**B**) viability of mammospheres already formed (MSV). Data is represented as the mean \pm SEM of three independent experiments. Statistic t-test analysis of PTX-loaded GM were performed in comparison with the free PTX treatment. **** $p < 0.0001$.

Altogether, these findings indicated that the in vitro anti-CSC efficacy of PTX was significantly improved when encapsulated within micelles in comparison with free PTX solution, in the MDA-MB-231 cancer cell line.

4.4.1.4. Evaluation of glycosylated micelles internalization in CSCs

To explore if the glycosylation of micelles with sugar residues (Glu moieties) could result in an increased internalization in CSCs, the glycosylated micellar system was labelled with the 5-DTAF fluorochrome following the protocol previously described [300,301]. The labelled micelles, hereinafter referred to as 5-DTAF-GM, were used to assess the *in vitro* internalization in attachment and non-attachment cell culture conditions.

For the internalization studies in normal adherent plates, the fluorescent MDA-MB-231 breast cancer cell model was used, in which CSC tdTomato⁺ and non-CSC tdTomato⁻ subpopulations were cultured at 40% and 60% conditions, respectively. Briefly, cells were incubated with 5-DTAF-GM at different time points (15, 30, 60 and 180 min) at a polymer concentration of 10 mg/mL. The fluorescence intensity of cells internalizing 5-DTAF-GM was quantified by flow cytometry. Cytometry results indicated that fluorescence intensity increased in a time-dependent manner in both cell subpopulations (**Figure 63A**). However, tdTomato⁻ cells showed a significant higher uptake rate of 5-DTAF-GM in comparison with tdTomato⁺ cells after 60 min of incubation ($p < 0.0001$ at 60 min and $p = 0.041$ at 180 min) (**Figure 63A**). In addition, a total internalization of 5-DTAF-GM was detected in both cell subpopulations after 15 min of incubation, since almost all cells were positive for the 5-DTAF fluorochrome, specifically, 96.52% of tdTomato⁺ cells and 99.10% of tdTomato⁻ cells (**Figure 64**), even though the fluorescence intensity was greater in the tdTomato⁻ subpopulation from 30 min onwards.

For the internalization studies of labelled micelles in non-attachment conditions, MDA-MB-231 cells were cultured in low-attachment plates to allow mammosphere formation, and then incubated with 5-DTAF-GM under the same parameters of time and concentration conditions as those previously mentioned. Cytometry results indicated that a total internalization of the 5-DTAF-GM was also detected after 15 min of incubation, since 99.84% of MDA-MB-231 were positive for the 5-DTAF fluorochrome, thus coinciding with the findings in attachment conditions (**Figure 64**). Unexpectedly, the fluorescence intensity seemed to not increase in a time-dependent manner. Indeed, after 15 min of incubation with the 5-DTAF-GM no differences in fluorescence intensity were obtained when compared with the other time points tested, thus suggesting that internalization capacity of MD-MB-231 mammospheres may have reached the saturation point (**Figure 63B**). However, it should be noted that a high variability between the different replicates of the assay was obtained, and hence, statistical analysis between the different time points could not be performed to ensure these findings.

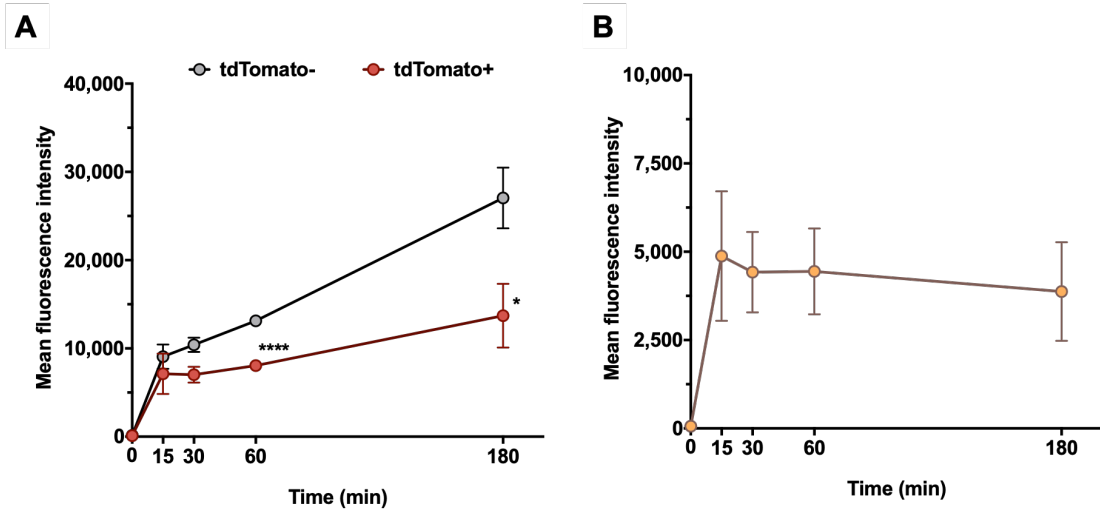


Figure 63. Internalization studies of labelled 5-DTAF-GM in CSC and non-CSC cell subpopulations in attachment and low attachment conditions. Time course of 5-DTAF-GM internalization in **(A)** CSC and non-CSC from the fluorescent MDA-MB-231 CSC model and in **(B)** CSC mammospheres. Cells were incubated with labelled micelles for the indicated times and then, the fluorescence intensity was quantified by flow cytometry. Data is represented as the mean fluorescence intensity (MFI) \pm SD of three replicates. Statistic t-test analysis was performed comparing the results between both cell subpopulations, **** $p < 0.0001$.

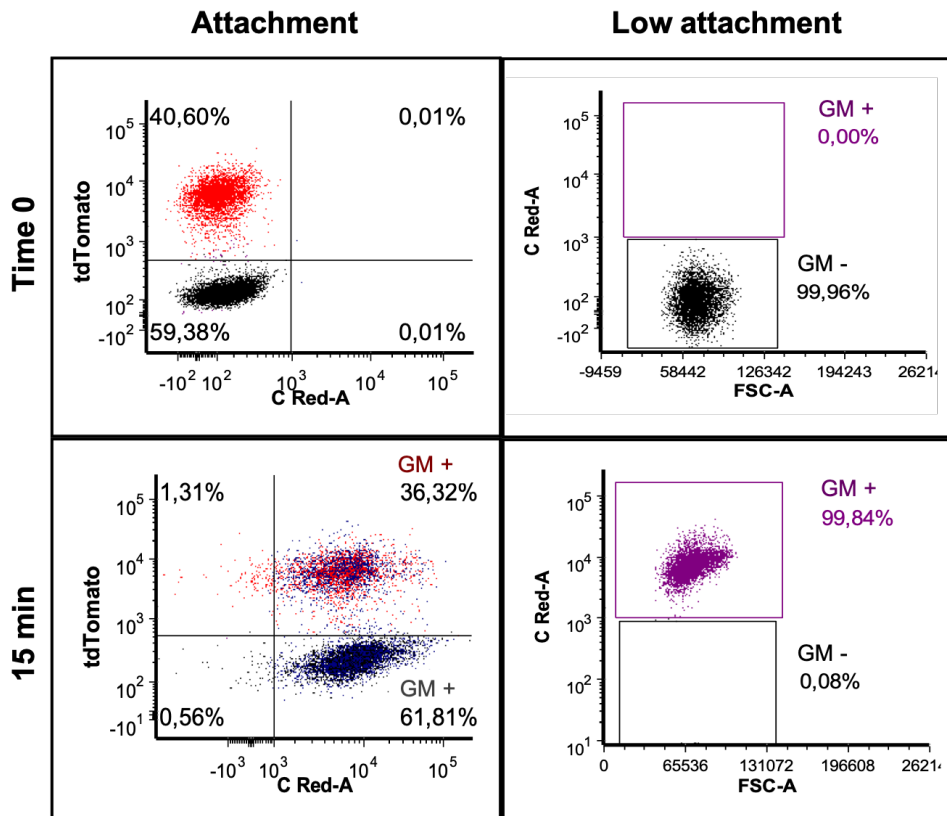


Figure 64. Flow cytometry gating analysis strategy for internalization studies used in both cell culture conditions at time 0 and after 15 min of micelles incubation. In both culture conditions, almost all cells were positive for the 5-DTAF fluorochrome after 15 min of incubation with the labelled micelles. *Clarification: 36.32% out of 37.63% results in 96,51% of tdTomato+ cells positive for 5-DTAF, while for tdTomato- cells, 61.81% out of 62.37% corresponds to 99.10% of tdTomato- cells positive for 5-DTAF.

Altogether, these findings suggested that glycosylated micelles could be considered as promising nanocarriers of anti-neoplastic drugs, since a higher and faster cellular uptake of glycosylated micelles were obtained by the entire population of BC cells in vitro.

4.4.2. Evaluation of the therapeutic efficacy in vivo of PTX-loaded glycosylated micelles towards free PTX in TNBC tumor-bearing mice

Once the validity of the PTX-GM was confirmed in vitro, we moved towards the validation in vivo using an orthotopic TNBC mice model. Considering that PTX-GM had not yet been tested in vivo, a preliminary efficacy assay was performed as a proof-of-concept. It is noteworthy to highlight that in our hands, i.v. administration of free PTX was limited to 10 mg/kg per mouse, as higher doses resulted in the death of animals caused by the use of the Cremophor EL[®] and ethanol as solubilizing agents. In this regard, the use of PTX-GM allowed doubling the PTX dose administered to animals, from 10 to 20 mg/kg per mouse in addition to allowing its i.v. administration in aqueous media (saline solution), thereby avoiding side effects associated to the use of vehicles such as Cremophor EL[®] or other organic solvents.

NOD.CB17-*Prkdc*^{scid}/NCrHsd mice with orthotopic MDA-MB-231.Fluc tumors were i.v. administered with the vehicle (n = 7), 10 mg/kg of PTX (n = 8) or 20 mg/kg PTX-loaded GM (n = 9) 3 days a week for 3-4 weeks. The treatment schedule followed is shown in **Figure 65**. Monitoring of body weight and tumor growth was performed at least twice per week. The evaluation of lung metastasis was planned at end-point. The animals were euthanized 1 h after the last treatment administration (out of a total of 9 doses for the PTX-GM group and 11 doses for the other two groups) and tumors were removed and weighted for further analyses.

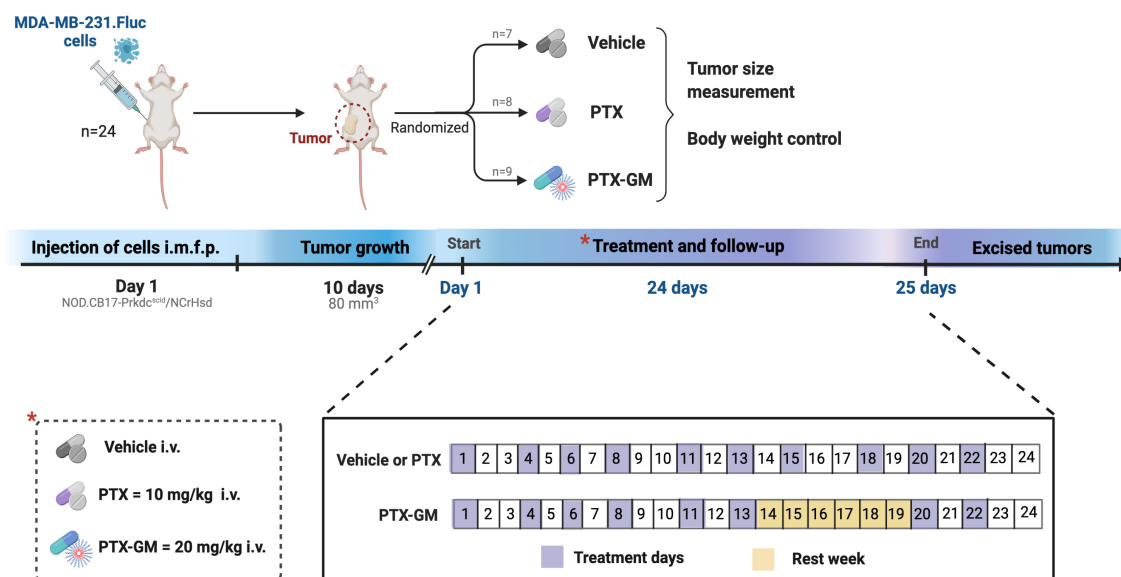


Figure 65. Experimental protocol schedule for the in vivo therapeutic efficacy assay in mice of GM-PTX. MDA-MB-231 cells were injected i.m.f.p. of NOD/SCID mice. When tumors reached volumes of 70–80 mm³, mice were randomized into three experimental groups: vehicle (n=7), PTX (n=8) or PTX-GM (n=9). The vehicle group was administered with saline solution 3 times/week; i.v.). PTX (10 mg/kg i.v.) was administered 3 times/week, while PTX-GM (20 mg/kg i.v.) was administered 3 times/week with a rest week in between. All treatments were administered over a period of 24 days. Tumor growth evaluation was performed in vivo and ex vivo at endpoint. Created with BioRender.com.

4.4.2.1. Anti-tumor proliferation efficacy of PTX-loaded glycosylated micelles in TNBC tumor-bearing mice

Unexpectedly, treatment with PTX-GM showed no improvement in tumor growth reduction when compared to PTX, since no significant differences were obtained when tumor volumes (at different time points) and weights (at the end of the experiment) were compared (**Figure 66**). Moreover, both treated-groups showed a significant efficiency in arresting MDA-MB-231 tumor growth. Those significant differences were already visible at day 6 and increased remarkably throughout the experiment (**Figure 66A**). More specifically, analysis of excised tumors at the end of the experiment showed that PTX and PTX-GM treatments reduced 9-fold tumor volumes and weights in comparison with the vehicle group (228.9 ± 36.72 mm³ and 0.396 ± 0.050 g for the vehicle; 25.31 ± 3.612 mm³ and 0.042 ± 0.004 g for PTX-treated; 25.70 ± 3.847 mm³ and 0.038 ± 0.003 g for PTX-GM-treated) (**Figure 66**).

It should be noted that mice seemed to tolerate the intravenous injection of both vehicle and PTX without overt severe signs of toxicity or significant loss of body weight (**Figure**

67). By contrast, administration of PTX-GM led to a considerable body weight loss after the first week of treatment, leading to a one-week treatment interruption in order to allow animals to recover the weight loss.

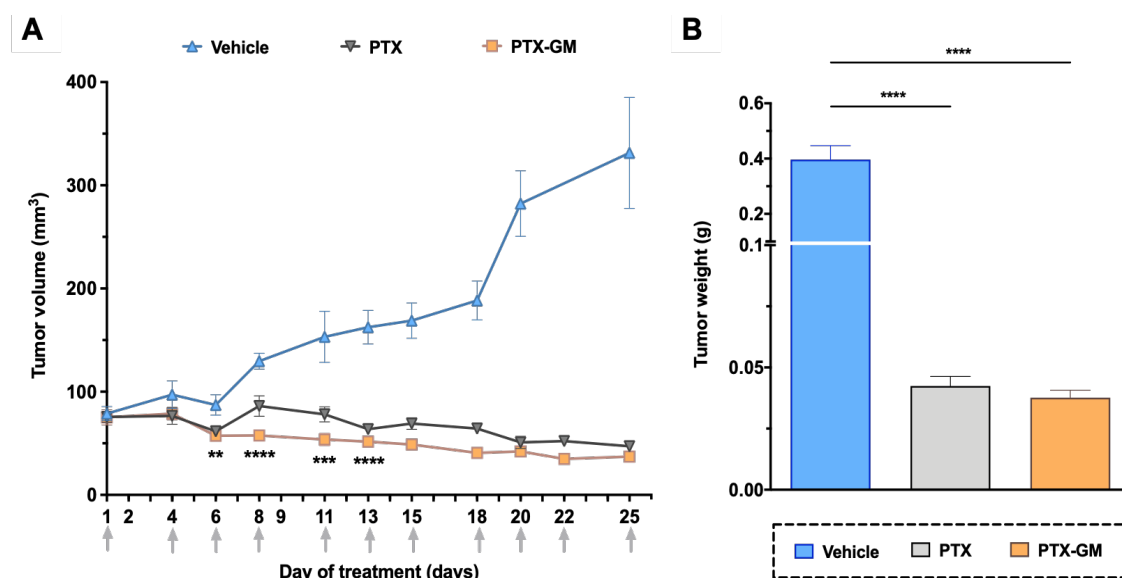


Figure 66. In vivo therapeutic efficacy of free PTX and PTX-loaded glycosylated micelles in TNBC tumor-bearing mice. A) Tumor volume measurements in different study groups during the treatment and **B)** tumor weights at the end of the experiment. Results are represented as the mean \pm SEM in both graphs (animals/group \geq 7). Statistic t-test analysis of PTX-GM treatment was performed in comparison with the vehicle group. $**p < 0.01$, $***p < 0.001$, $****p < 0.0001$.

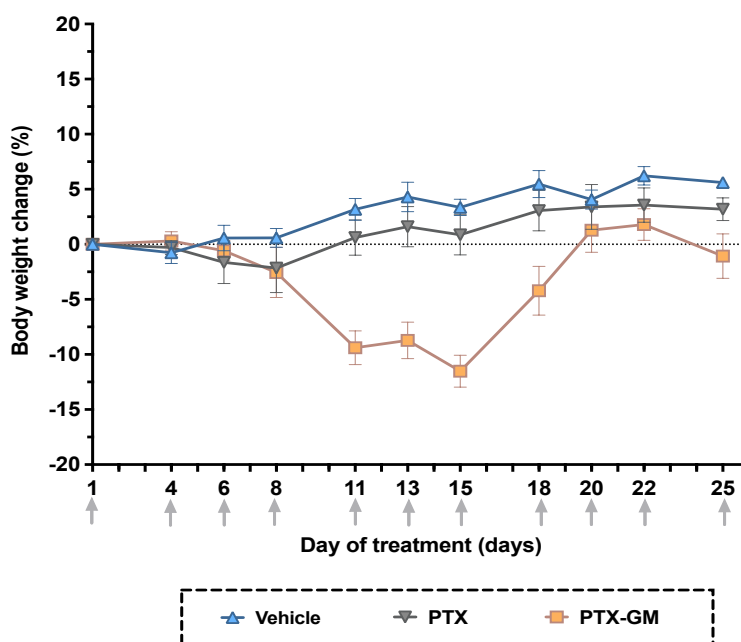


Figure 67. Body weight change (%) from all three-study groups throughout the experiment. Determination of body weight change referred to the initial weight of mice (before starting the treatments). Results are expressed as mean \pm SEM ($n \geq 7$).

Altogether, these findings proved the safety of PTX-GM as a suitable system for repeated doses intravenous administration in vivo. However, even though the use of PTX-GM allowed us to double the dose of PTX administered to animals, this increase did not translate into a greater tumor growth inhibition. Therefore, the administration of PTX at the maximum tolerated dose, either in its free form or encapsulated in glycosylated micelles, resulted in the same tumor growth inhibition efficacy. Of note, given the high antitumoral effect showed by both treatments, which almost reached a complete tumor response, the pulmonary metastasis evaluation was discarded.

4.4.3. Physicochemical characterization of drug-loaded Pluronic® F127 polymeric micelles

Different PM formulations were developed in order to select the best candidate for anti-cancer drug delivery. To this end, two different systems were generated using a polymer concentration of 50 mg/mL. Firstly, PM encapsulating single drugs, either 8Q or NCS, were developed. Afterwards, a second generation of micelles were developed by the co-encapsulation of 8Q and NCS anti-CSC drugs with PTX within the same micellar system. The methodology used for PM preparation was based on the thin-film hydration technique overcoming drug insolubility by their encapsulation into the hydrophobic core of micelles, while hydrophilic polymer blocks faced aqueous phase (**Figure 68A**). PM preparation steps and physicochemical characterization of the loaded micelles followed procedures previously published in the group [302,303]. Briefly, morphology and shape of resulting loaded PM were studied by transmission electron microscopy (TEM). Laser scattering method (DLS) revealed the characteristics of micelles such as size and distribution (referred to as polydispersity index) (NanoZS, Malvern Instruments, UK). The zeta potential was assessed by laser doppler micro-electrophoresis using a NanoZS (Malvern Instruments, UK). The drug loading capacity of PM was determined by HPLC using the previously validated high performance liquid chromatography-ultraviolet (HPLC-UV) method [304]. The stability of PM after lyophilization was also evaluated by size distribution analysis using DLS.

8Q and NCS were efficiently encapsulated into spherical shaped PM of small size (mean diameter around 24 nm), low polydispersity (< 0.21) and a slightly negative surface charge (**Figure 68B,C**) at a final anti-CSC drug concentration of 2,500 μM for PM-8Q and 400 μM for PM-NCS.

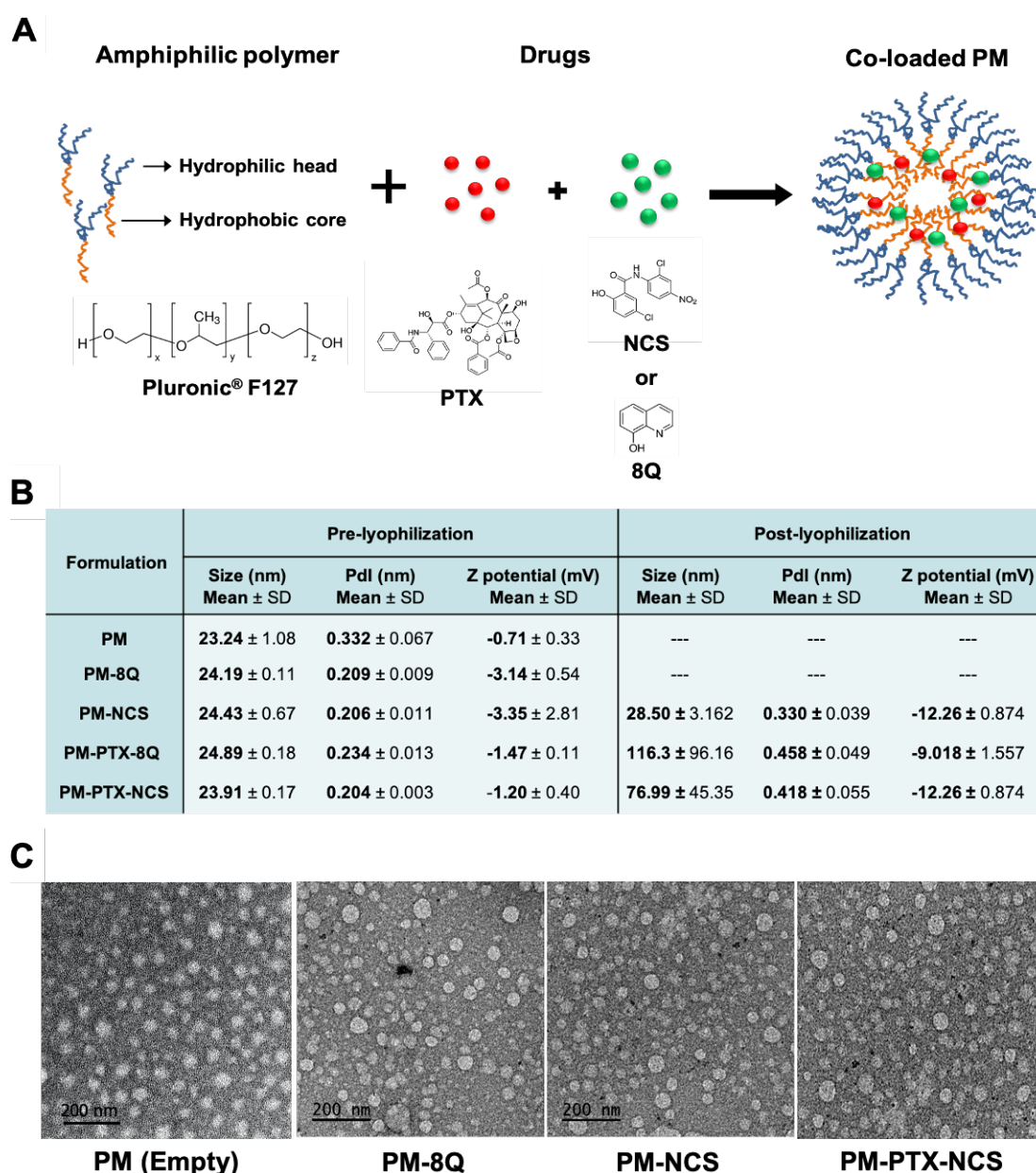


Figure 68. Physicochemical characterization of the polymeric micelles (PM). **A)** Representative diagram of co-loaded PM composition and formation. **B)** Summary of physicochemical properties of different formulations (mean diameter, polydispersity index, zeta potential) pre- and post-lyophilization (we have no available data for PM and PM-8Q). Results are expressed as mean ± SD of at least, three replicates. **C)** TEM microphotographs of the different formulations.

Same preparation method was followed for the synthesis of micelles loaded with the combination therapy. In this case, 8Q and NCS were added together with PTX agent at defined ratios. The co-loaded micelles obtained (hereinafter referred as PM-PTX-8Q and PM-PTX-NCS) also showed a mean diameter of 24 nm, with a low polydispersity index (≤ 0.23) and a slightly negative charge, which were less negative than the previous PM

(**Figure 68B,C**). For PM-PTX-8Q, resulting micelles kept the drug synergistic ratio 1:12.5 at a final concentration of 200 μM for PTX and 2,500 μM for 8Q. Furthermore, the resulting PM-PTX-NCS were efficiently co-loaded with PTX and NCS at its synergistic ratio 1:2, at a final concentration of 200 μM and 400 μM , respectively. These results indicated that presence of drugs, either alone or in combination, in the core of the micelles did not affect their physicochemical properties. To increase the storage stability and shelf-life of the system, a preliminary lyophilization process was performed and the micelles characterized regarding size and surface charge after resuspension. As observed in **Figure 68B**, the lyophilization increased the mean diameter of the micelles due to the formation of some aggregates (corresponding to approximately 20% of the particles). This phenomenon occurs mainly in PTX co-loaded micelles, as PM-NCS present a small number of aggregates. This aggregation could be avoided in the future by the use of cryoprotectants and an optimized lyophilization cycle.

Overall, these results indicated that vehiculization of 8Q or NCS in polymeric micelles was feasible, either alone or in combination with PTX. Considering that both micellar systems developed showed similar physicochemical properties, we selected the co-loaded micellar system for further experiments for its greater therapeutic potential and clinical benefit.

4.4.3.1. Combination of 8Q or NCS with PTX within the same PM increases the efficacy of the free drugs

Once the micellar nanocarriers were correctly validated, we moved towards their evaluation as potential DDS against CSCs and bulk tumor cells to treat aggressive TNBC. To evaluate whether vehiculization of selected drugs enhanced their anti-tumoral effect, co-loaded micelles cytotoxicity was evaluated compared to the free drugs, alone and in combination, by MTT assay on MDA-MB-231 cells as TNBC in vitro model.

In line with previous results, combination of drugs (free or in PM) was more efficient than single drugs. For drug free combination, cell viability after treatment was reduced up to $24.19 \pm 1.81\%$ for combined therapy of PTX and 8Q (PTX at 1 μM and 8Q at 12.5 μM ; ratio 1:12.5), and to $19.37 \pm 1.03\%$ for PTX and NCS combination (PTX at 0.5 μM and NCS at 1 μM ; ratio 1:2), hence, the cytotoxic effect was significantly higher than the produced when cells were treated individually, either with free PTX at 1 μM ($45.80 \pm 2.25\%$), with 8Q at 12.5 μM ($85.63 \pm 2.35\%$) or with NCS at 1 μM ($45.73 \pm 1.59\%$) (**Figure 69**). Of note, empty PM were inducing no toxicity, since no negative effects on cell viability were observed when empty PM were tested. Interestingly, both PM-PTX-8Q (1

μM PTX with $12.5 \mu\text{M}$ 8Q) and PM-PTX-NCS ($0.5 \mu\text{M}$ PTX with $1 \mu\text{M}$ NCS) loaded micelles inhibited the proliferation of MDA-MB-231 cell line more effectively compared to the free drug combination of PTX with 8Q and PTX with NCS, respectively (**Figure 69**). Notably, cell viability after treatment was significantly reduced up to $8.24 \pm 1.67\%$ for PM-PTX-8Q and $8.39 \pm 0.78\%$ for PM-PTX-NCS, thereby confirming that encapsulation of drugs improved their synergistic anti-tumoral activity (**Figure 69**). These findings were consistent with those described previously, thus confirming that PTX inhibited in a more efficient way cell viability when combined with anti-CSC drugs at defined ratios.

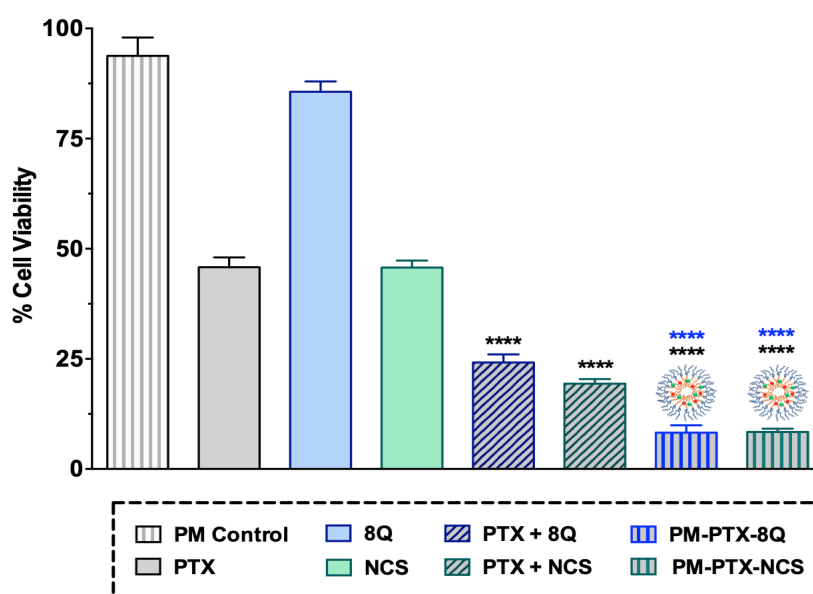


Figure 69. The anti-cancer efficacy of PM-PTX-8Q and PM-PTX-NCS in MDA-MB-231 cells. Graph shows the % of cell viability values after-treated - at equivalent doses - with individual and combination treatments, either free or within the PM. Drug concentrations tested for PM-PTX-8Q were PTX at $1 \mu\text{M}$ and 8Q at $12.5 \mu\text{M}$ (ratio 1:12.5), while for PM-PTX-NCS were $0.5 \mu\text{M}$ for PTX and $1 \mu\text{M}$ for NCS (ratio 1:2). Data is represented as the mean \pm SEM of three independent experiments. Statistic t-test analysis of PM-loaded treatments were performed in comparison with individual PTX treatment (black) as well as with their corresponding free combined therapy (blue). **** $p < 0.0001$.

4.4.3.2. Combination of 8Q or NCS with PTX within the same PM increases their anti-CSC efficacy

In order to explore if the vehiculization of combination drugs might improve its anti-CSC effect, we then tested the efficacy of co-loaded PM in reducing both MSF and MSV in MDA-MB-231 cells. Moreover, corresponding free drug treatments, individual and combined, were also included. Not surprisingly, the ability of CSCs to form mammospheres was significantly reduced in the group treated with the free drug combination of 8Q and NCS with PTX, in comparison to the single PTX exposure. Specifically, it was reduced to $36.13 \pm 1.35\%$ for PTX-8Q (PTX at $4 \mu\text{M}$ and 8Q at $50 \mu\text{M}$; ratio 1:12.5), and to $20.70 \pm 1.75\%$ for PTX-NCS combination (PTX at $4 \mu\text{M}$ and NCS at $8 \mu\text{M}$; ratio 1:2), while for PTX treatment alone ($4 \mu\text{M}$) was above 50% ($57.31 \pm 2.47\%$) (**Figure 70A**). These findings were consistent with those previously shown. Moreover, similar results were obtained when MSV was analysed after the treatment with same drug concentrations. MSV was remarkably decreased after combined free treatments ($17.63 \pm 2.90\%$ for PTX-8Q and $12.23 \pm 2.63\%$ for PTX-NCS combination) but not when treated with free PTX alone ($51.81 \pm 5.28\%$) (**Figure 70B**). This effect was already demonstrated in previous results, increasing the robustness of our work. Importantly, the inhibitory effect on both MSF and MSV was significantly enhanced when drugs were administered combined and encapsulated into the micellar systems rather than in their free form. Specifically, MSV was reduced up to $6.16 \pm 2.66\%$ after PM-PTX-8Q treatment ($4 \mu\text{M}$ PTX with $50 \mu\text{M}$ 8Q) and to $0.99 \pm 2.73\%$ after PM-PTX-NCS treatment ($4 \mu\text{M}$ PTX with $8 \mu\text{M}$ NCS), which corresponded to an almost 3-fold increased effect for PTX and 8Q treatment and 12.4-fold for PTX and NCS (**Figure 70B**). On the other hand, the MSF ability was reduced up to $10.88 \pm 1.95\%$ and $9.13 \pm 0.70\%$ for PM-PTX-8Q and PM-PTX-NCS, respectively, which means that encapsulation of drugs in PM resulted in a 3.3-fold and 2.3-fold enhanced efficacy, respectively (**Figure 70A**).

Collectively, these results indicated that encapsulation of drugs into PM increased their anti-CSC efficacy, since the capacity of CSCs to survive and grow under low attachment conditions was significantly affected.

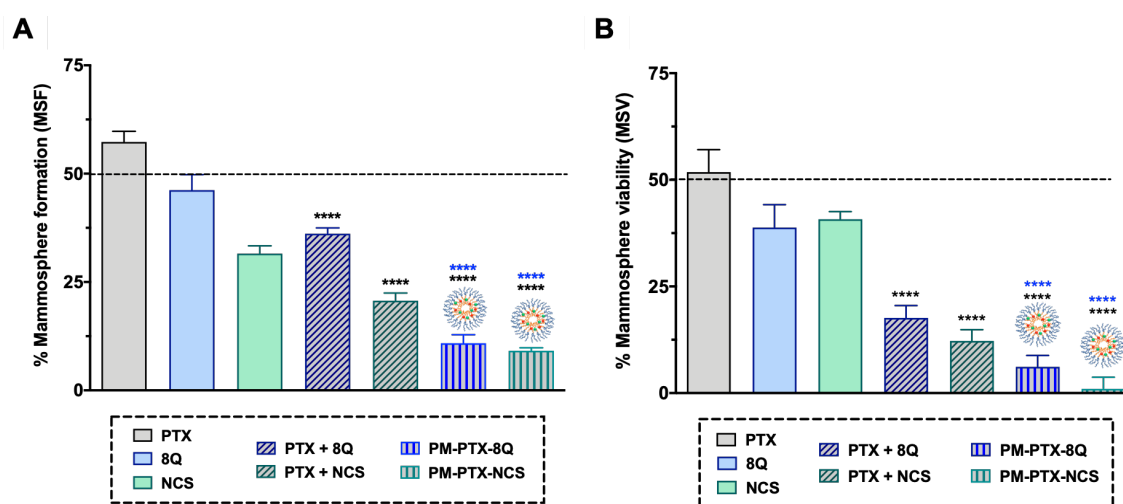


Figure 70. Combination of 8Q or NCS with PTX within the same PM enhanced their synergistic anti-CSC activity in low attachment conditions in MDA-MB-231 cell line. Effect of treatments in CSC **(A)** Mammosphere formation (MSF) ability and **(B)** mammosphere viability (MSV) once they are already formed. Drug concentrations tested for PM-PTX-8Q were PTX at 4 μ M and 8Q at 50 μ M (ratio 1:12.5), while for PM-PTX-NCS were 4 μ M for PTX and 8 μ M for NCS (ratio 1:2). Data is represented as the mean \pm SEM of three independent experiments. Statistic t-test analysis of PM-loaded treatments were performed in comparison with individual PTX treatment (black) as well as with their corresponding free combined therapy (blue). **** $p < 0.0001$.

To validate and reinforced the obtained in vitro results, we analyzed the anti-CSC potential of PM by flow cytometry analysis but this time using the fluorescent CSC MDA-MB-231 model. Consistent with previous results, following PTX exposure (1 μ M), the relative abundance of tdTomato+ cells increased in comparison with non-treated cells (**Figure 71**). On the other hand, after the individual therapy of 8Q (12.5 μ M) and NCS (2 μ M), the relative abundance of tdTomato+ cells was prevented and decreased, respectively. Moreover, combined treatments of anti-CSC drugs with PTX significantly counteracted the increase of tdTomato+ cells induced by the chemotherapeutic agent (**Figure 71**). It is worth noting that reduction in CSC presence was remarkably greater for the combination of PTX with NCS than for PTX with 8Q (**Figure 71**). As expected, the effect on cell viability was higher when drugs were administered in combination rather than as individual therapy, concurring with the synergistic activity previously described.

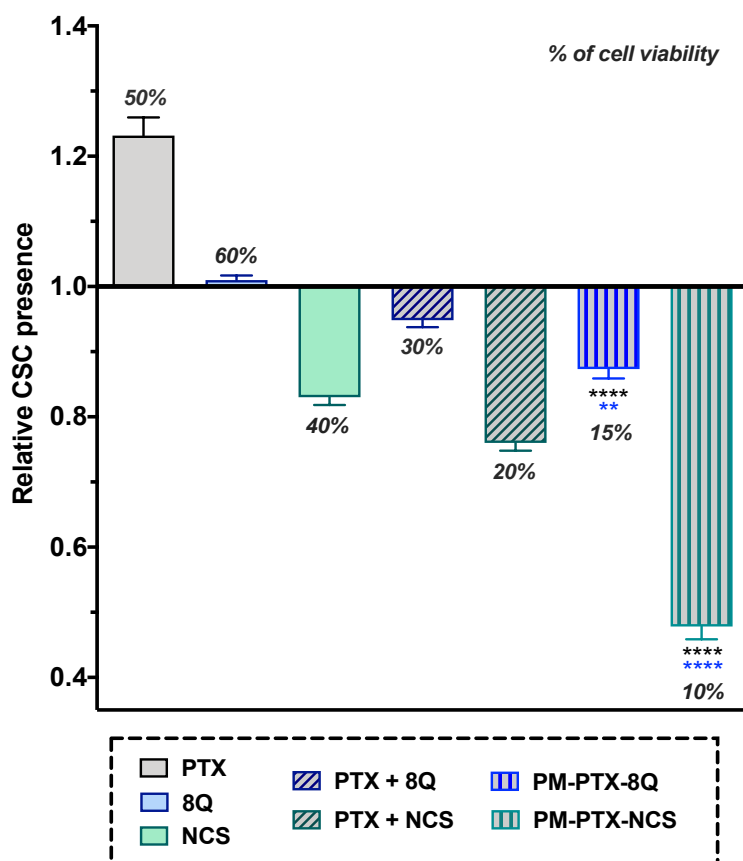


Figure 71. Anti-CSC activity of PM-PTX-8Q and PM-PTX-NCS in the MDA-MB-231 fluorescent CSC model. Relative CSC-tdTomato⁺ presence determined by flow cytometry and referred to control (non-treated cells) condition and cell viability values after-treated (% below each bar). Values below than, equal to or above than one indicated reduction, maintenance or increase of CSC-tdTomato⁺ cells within population, respectively. Drug concentrations tested for PM-PTX-8Q were PTX at 1 μ M and 8Q at 12.5 μ M (ratio 1:12.5), while for PM-PTX-NCS were 1 μ M for PTX and 2 μ M for NCS (ratio 1:2). Data is represented as the mean \pm SEM of three independent experiments. Statistic t-test analysis of PM-loaded treatments were performed in comparison with individual PTX treatment (black) as well as with their corresponding free combined therapy (blue). ** $p < 0.01$, **** $p < 0.0001$.

Importantly, combination of both drugs administered in PM reduced significantly the presence of CSC subpopulation in MDA-MB-231 cells in a more efficient way than in their free form, while keeping low cell viabilities, which were lower than the ones obtained for the free combined treatments (**Figure 71**). These results confirmed that combination of 8Q and NCS with PTX within the same PM increased the anti-CSC efficacy of the free drugs in vitro.

In conclusion, the PM co-loaded with 8Q and NCS with PTX were developed, fully characterized and its anti-cancer activity was tested in vitro. The encapsulation of drugs

into PM strongly increased its anti-proliferative effect and efficiently targeted CSC subpopulation, showing a significant improvement of combined treatment cytotoxicity on mammospheres and a reduction of the CSC presence in adherent cell cultures.

4.4.4. Evaluation of the therapeutic efficacy in vivo of combination of drugs, either free or within polymeric micelles

Having shown the potential synergistic effect of PTX with NCS in different TNBC cell lines, we then analyzed both anti-tumor and anti-CSC potential of PTX combination with NCS in an orthotopic mice model. Several studies have previously evaluated the potential of NCS as anti-cancer therapy in various cancer types in vivo, including TNBC; nevertheless, the synergistic effect of combined treatment of PTX and NCS in CSC subpopulation has not yet been clearly elucidated.

Going a step further, we also wanted to test whether PM co-loaded with PTX and NCS could enhance either anti-cancer or anti-CSC efficacy of combined treatment in vivo. For this purpose, we explored whether the developed PM could reach a therapeutic dose for intravenous administration without compromising mice safety. Given that the recommended dose of PTX for in vivo experiments is 10 mg/kg [305,306] and at least 10 mg/kg for NCS treatment [237,307], the concentration of PM should be increased at least 10 times to reach a therapeutic dose (from 0.2 mg/mL to 2 mg/mL for PTX and from 0.13 mg/mL to 2 mg/mL for NCS). With the current in vitro micellar systems, the maximum administrable dose of PTX was 1.1 mg/kg and 0.9 mg/kg for NCS, thus, falling well short of what was required to reach a therapeutic dose. In this regard, the preparation of more concentrated PM was attempted by changing different parameters of the preparation protocol of PM, in order to enhance their loading capacity and achieve the desired concentration. A short summary of the main changes tested is included below (**Table 17**).

Table 17. Summary of the main changes performed and their consequences in the preparation protocol of co-loaded micellar systems to enhance their loading capacity.

Parameters studied	Initial conditions	New formulation conditions	Concluding remarks
Polymer concentration	100 mg/mL	200 mg/mL	Risk of hyperlipidemia, [polymer] ≤ 100 mg/mL
Concentration of drugs	20 μM of PTX + 40 μM of NCS	200 μM of PTX + 400 μM of NCS	No micelle precipitation observed. Co-encapsulation is feasible. However, drugs concentration are not high enough to reach a therapeutic dose
	20 μM of PTX + 250 μM of 8Q	200 μM of PTX + 2,500 μM of 8Q	No micelle precipitation observed. Co-encapsulation is feasible. However, drugs concentration are not high enough to reach a therapeutic dose
	200 μM of PTX + 400 μM of NCS	2,000 μM of PTX + 4,000 μM of NCS	Micelle precipitation is observed
	200 μM of PTX + 2,500 μM of 8Q	2,000 μM of PTX + 25,000 μM of 8Q	Micelle precipitation is observed

Unfortunately, all these attempts failed, since precipitation of micelles was obtained as the maximum loading capacity of drugs, especially PTX, in co-loaded micelles was surpassed. Therefore, we decided to discard the co-loaded PM-PTX-NCS and work with the single PM-NCS (4 mg/kg), which have currently been validated in colorectal cancer mice model [302] and in this project.

4.4.4.1. The administration of PTX in combination with free NCS enhances the anti-tumor proliferation efficacy in TNBC tumor-bearing mice

NOD/SCID mice with orthotopic MDA-MB-231.Fluc tumors were administered with the vehicle, PTX (i.v. 10 mg/kg), the combination of free PTX and NCS (10 mg/kg i.v. and 10 mg/kg i.p., respectively) or PTX with PM-NCS combination (10 mg/kg i.v. and 4 mg/kg i.v., respectively). The treatment schedule followed (summarized in **Figure 26**) was established in accordance with previous tests performed in order to minimize drugs' side effects without compromising their therapeutic efficacy. Which consisted in the administration of both PTX and the PM-NCS 3 times a week during the first week, and then both were reduced to 2 times a week the next 2 weeks, while NCS was administered 5 times a week over 3 weeks. For PTX single treatment it was administered 3 times a week over the 3 weeks. Body weight and tumor growth was monitored at least twice a week during all the treatment period (a total of 23 days), while the number of CTCs and lung metastasis were evaluated at endpoint (day 24). Of note, PM-NCS were resuspended and filtered (0.22 μm filters) right before the i.v. administration.

As for the tumor growth, the combination of PTX with NCS had the strongest effect on reducing MDA-MB-231 tumor growth, resulting in smaller tumor volumes (**Figure 72A**) and weights (**Figure 72B**). These significant differences were already visible at day 9 and increased throughout the experiment (**Figure 72A**). Indeed, the combination treatment practically prevented tumor growth. It should be noted that on day 23, the tumoral volume for the combined treatment group was even smaller ($73.40 \pm 62.39 \text{ mm}^3$) than on day 0 when the treatment was started ($81.33 \pm 14.79 \text{ mm}^3$), while for PTX single treatment on day 23 the tumoral volumes were $371.33 \pm 338.22 \text{ mm}^3$ (**Figure 72A**). Analysis of excised tumors at the end of the experiment showed that combined treatment of PTX and NCS resulted in a reduction of 3.1-fold both tumor volumes and weights in comparison with PTX treatment. Intriguingly, although the combined treatment of PTX and NCS had a higher effect than the produced by PTX alone, when NCS was administered loaded in the PM, tumor growth was less affected compared to free combined treatment. Indeed, no differences were obtained when tumor growth was compared to PTX single treatment (**Figure 72A,B**). These results suggested that NCS dose (4 mg/kg) was not high enough to obtain an improvement in the effect on tumor growth, despite being encapsulated within micelles.

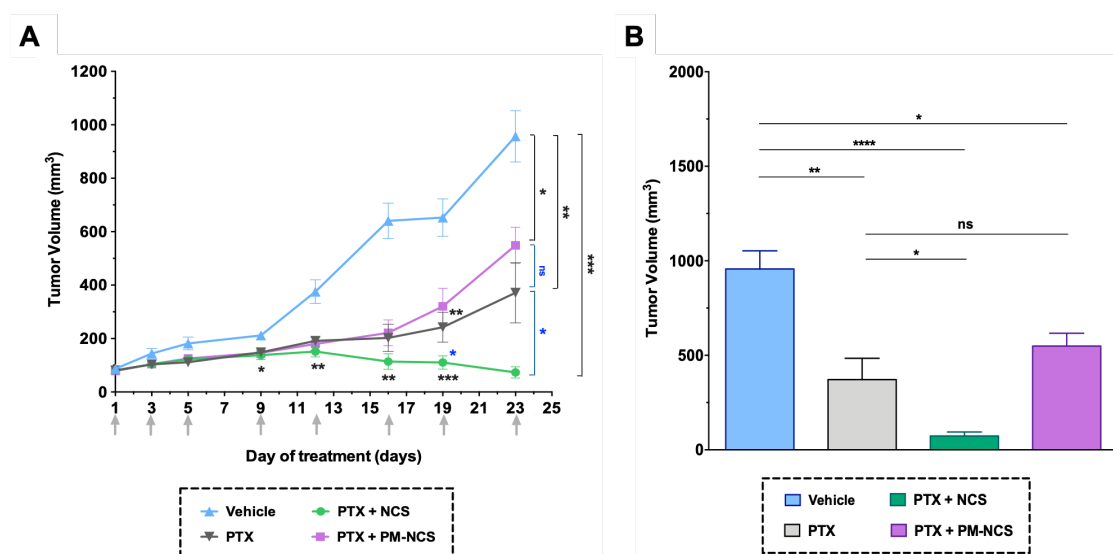


Figure 72. In vivo therapeutic efficacy of PTX in combination with NCS, either free or encapsulated in micelles in TNBC tumor-bearing mice. **A)** Tumor volume measurements in different study groups during the treatment and **B)** tumor weights at the end of the experiment. Results are represented as the mean \pm SEM in both graphs (animals/group \geq 4). Statistic t-test analyses of combined treatment were performed in comparison with vehicle (black) as well as with PTX single treatment (blue). * $p < 0.05$; ** $p < 0.01$, *** $p < 0.001$, **** $p < 0.0001$.

With regard to side effects along the treatment, a short summary is included below (**Table 18**). Animals treated with PTX alone or with free drug combination seemed to tolerate treatments without overt severe signs of toxicity or loss of body weight (**Figure 73**). Even though a slight body weight loss was obtained at the start of the treatment, especially in the group treated with the free drug combination, only 2/9 animals showed a body weight loss below 10% and was only temporary and mice recovered weight over the days. This effect was probably due to fact that treatment was initiated only 12 days after the surgery for the i.m.f.p. implantation of cells. Besides, at the end of the treatment, 1/9 animals treated with free NCS developed ulcers, while 2/9 developed ascites and/or abdominal inflammation, all three side effects associated with the use of Cremophor EL and DMSO as vehicles, and with the i.p. route of administration of NCS. Besides, almost 100% of treated animals ended up with tail injuries associated to the repeated i.v. injections of treatments (**Table 18**). On the other hand, PM-NCS treatment showed high evidence of toxicity, since 6/10 animals died after intravenous administration, and thus, reducing considerably the sample size of the experimental group. One possible explanation could be the micelle aggregation during mice inoculation.

Table 18. Summary of the main side-effects detected among the experimental groups during treatment.

Side effects along treatment	Experimental groups			
	Vehicle	PTX alone	PTX with NCS	PTX with PM-NCS
Body weight loss (>10%)	0/6	0/9	2/9	0/10
Ascites and/or abdominal inflammation	0/6	0/9	2/9	0/10
Ulcers	0/6	0/9	1/9	0/10
Tail injury	2/6	8/9	9/9	10/10
Death	0/6	0/9	0/9	6/10

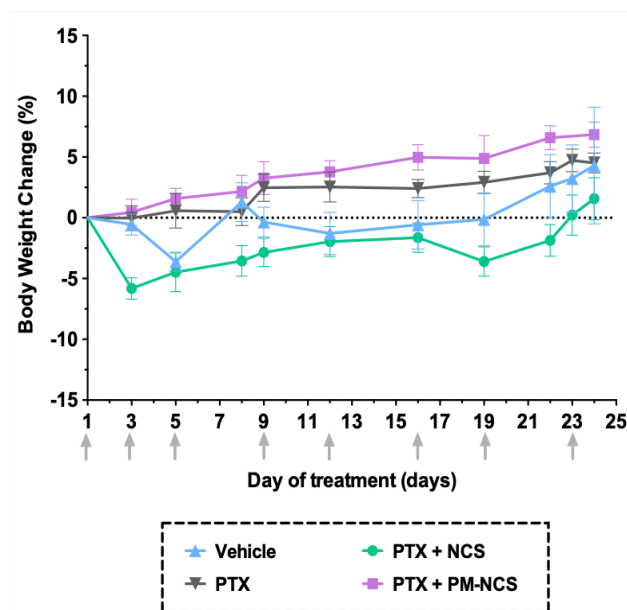


Figure 73. Body weight changes from all four-study groups throughout the therapeutic efficacy study in orthotopic TNBC mice model. Determination of body weight change referred to the initial weight of mice (before starting the treatments). Results are expressed as mean \pm SEM, $n \geq 4$.

4.4.4.2. The administration of PTX in combination with NCS reduces both intermediate and advanced stage of the metastatic process in vivo

With the aim of assessing the effect of treatments in lung metastasis initiation and development, the CTC content in mice bloodstream and lung metastasis evaluation was performed at treatment endpoint (day 24).

With regard to the CTC content, despite that the effect of PTX in primary tumors was clear, PTX-only treatment showed no significant effect on reducing CTC population when compared to vehicle (**Figure 74A**). Meanwhile, flow cytometry analysis revealed that treatment with PTX-NCS combination was more effective in eliminating the CTC in comparison to single PTX treatment or vehicle ($p = 0.0070$ and $p = 0.0124$, respectively), reducing 2.3- and 2.1-fold, respectively, the CTC content (**Figure 74A**). Similarly, a significant decrease in CTC population was also obtained for PM-NCS when compared to PTX treatment (3.6-fold; $p = 0.0181$) or vehicle (3.3-fold; $p = 0.0244$) (**Figure 74A**). Of note, the effect was lower when the PTX was combined with PM-NCS rather than with free NCS, but higher than the one produced when was administered alone. The presence of lung metastasis was evaluated by ex vivo BLI of lungs (**Figure 74B-D**). All animals treated with vehicle (6/6), PTX-only (9/9) or free PTX with PM-NCS (4/4) showed positive BLI signal in the lungs (100% incidence) while such incidence dropped down to 67%

(6/9) in the case of animals treated with the free drug combination (**Figure 74B**). Moreover, when lung BLI intensity was analyzed, free combination treatment showed a significant decrease in the BLI signal when compared to single PTX treatment ($p = 0.0492$) or the vehicle ($p = 0.0087$), reducing 8.56- and 42.83-fold the lung BLI intensity, respectively (**Figure 74C**). Moreover, combination of PTX with PM-NCS also showed significant lower BLI signal when compared with the vehicle group ($p = 0.0095$), but not when compared to PTX treatment (**Figure 74C**).

Altogether, these findings showed that combined treatment of PTX and NCS effectively arrested MDA-MB-231 tumor growth and reduced the metastatic ability of aggressive tumor cells, thereby offering a promising therapeutic approach for resistant TNBC. Moreover, combination of PTX with PM-NCS showed efficacy in inhibiting the metastatic potential of tumor cells, and thus, opens a window of opportunity to continue exploring the potential of designed micelles as a platform for drug delivery.

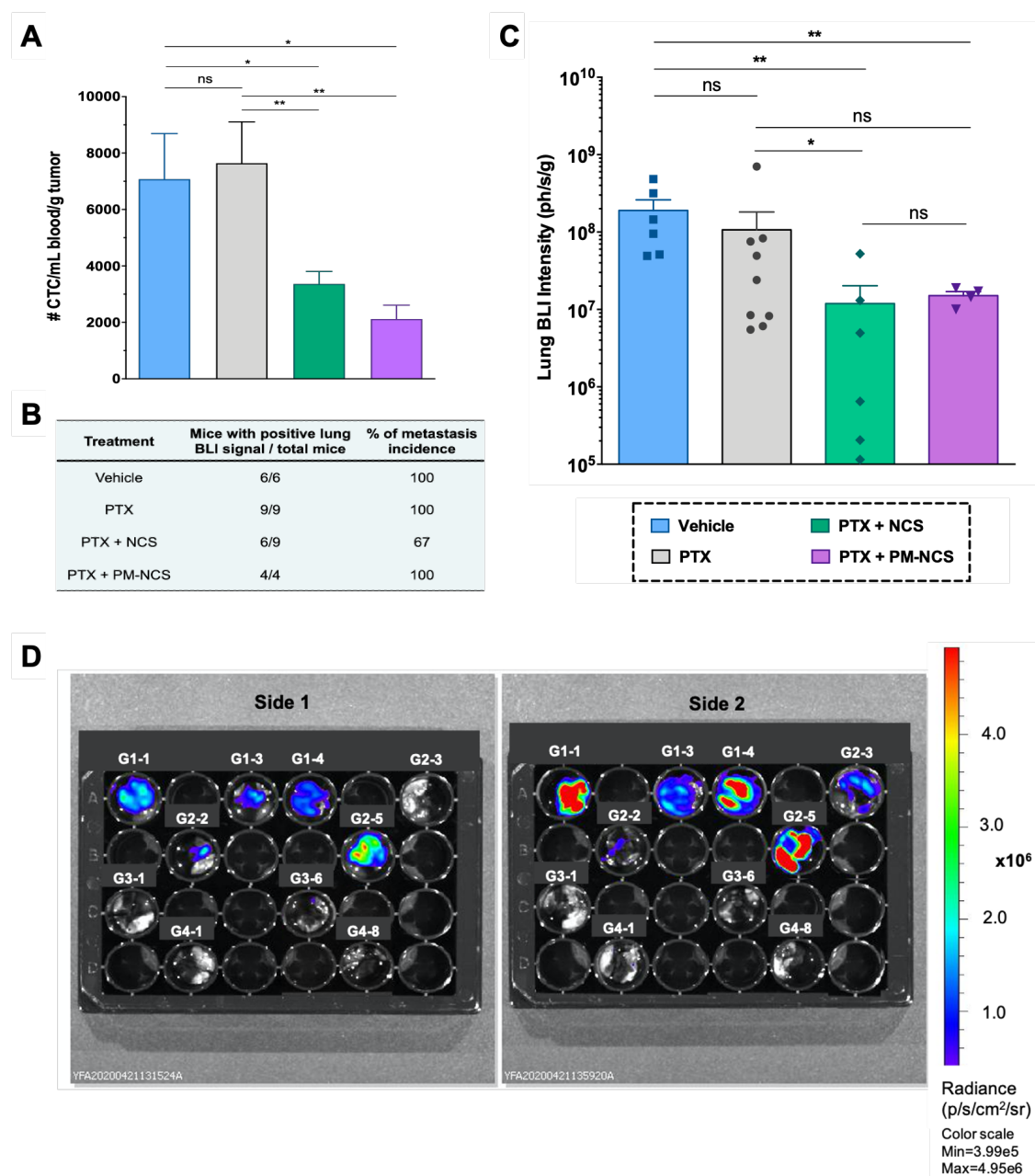


Figure 74. Analysis of intermediate and advanced stage of metastasis after treatments. **A)** Quantification of plasma circulating tumor cells (CTC) isolated from the blood of tumor-bearing mice at the end of the treatment and further analyzed by flow cytometry. Results are represented as the number of CTC events (mean \pm SEM) per mL of blood collected per gram of tumor ($n \geq 4$). Statistic t-test analysis was performed comparing the results between the study groups. **B)** Lung metastasis incidence after treatments of the study groups. **C)** Quantification of BLI signal intensity from mice lungs of all four-study groups. **D)** Representative BLI images of excised lungs (both sides) from all four-study groups (G1, vehicle; G2, free PTX; G3, free drug combination; G4, PTX with PM-NCS; followed by the number of the animal). Results are expressed as the mean \pm SEM of BLI signal (ph/s) per gram of lung tissue, ($n \geq 4$). Statistic U Mann-Whitney analysis was performed comparing the results between study groups. * $p < 0.05$, ** $p < 0.01$, *** $p < 0.001$, **** $p < 0.0001$.

DISCUSSION

DISCUSSION

5.1. Clinical challenges in the management of TNBC

Though considerable progress has been made during the past decades in the diagnosis and treatment of BC, mainly due to the development of novel diagnostic tools and therapeutic strategies, BC remains the most common form of cancer and the leading cause of death from cancer in women worldwide [1]. The continuous evolving of the genomic field and the technological advancement of high-throughput molecular techniques, have led to a shift in the paradigm of both classification and treatment of this disease [53,164]. These advances have revealed that TNBC subtype is in fact, a heterogeneous collection of cancers with distinct histology, gene-expression features and patterns of molecular alterations that along with its highly aggressive clinical course, make the disease management complex [308].

Given the heterogeneity of TNBC, different molecular studies have recently classified TNBC into different subtypes based on similar gene-expression signatures, opening the door to potential new-targeted treatment options. Massively parallel sequencing and the advancement of other 'omics' technologies, have led to the identification of potentially actionable molecular features in some TNBCs, such as germline BRCA1/2 mutations, the presence of the androgen receptor, and several molecular genomic alterations frequently affecting PI3K/mTOR or RAS/RAF/MEK pathways. The discovery of these actionable molecular alterations has provided the rationale for the development of personalized treatment strategies that could be utilized to target each disease [164,308], as PARP inhibitors for patients with BRCA-mutated tumors, or immune-checkpoint inhibitors in those advanced-stage TNBC tumors positive for PD-L1 expression [164,186,309]. However, there are still many questions that need to be addressed for a greater understanding of the molecular complexity of TNBC and for the development of better therapies to overcome drug resistance and, ultimately, to improve outcomes of patients with this challenging subtype of BC.

5.2. Cancer stem cells and their contribution to TNBC heterogeneity and treatment failure

Since CSCs were first discovered in acute myeloid leukemia in 1997 [310], their presence has been reported in different types of cancers, including BC, but also in patient derived xenografts and established cancer cell lines. The identification of CSCs has led

to a remodeling of our cancer hypothesis and played a major role in the advancement of cancer research [311]. This small pool of cells within a tumor population, has self-renewal capacity, tumorigenic and multi-lineage differentiation potential, and contribute to multiple tumor malignancies, such as multidrug and radiation resistance, metastasis, and most importantly, disease relapse and recurrence after treatment. These cells are known to be crucial in both initiation and spread of the cancer disease, and for having unique resistant mechanisms to withstand conventional anticancer therapies and progress in very harsh conditions, such as an increased expression of drug efflux pumps and an enhanced DNA repair machinery [83,85]. Interestingly, among the BC subtypes, the highest rates of CSCs are observed in TNBC patients, fact that has been correlated with its higher aggressiveness, chemo-resistance and metastatic spread [87,312,313]. Therefore, it is not surprising that CSCs have been the subject of concentrated research as potential targets to develop effective anticancer therapies.

As a consequence of phenotypic dynamism and clonal evolution during cancer treatment, breast tumors harbor a heterogeneous mixture of cancer cell populations that co-exist in distinct phenotypic states and with varying genetic patterns. Adding to this complexity, recent studies have shown that cancer cells can exhibit a high level of plasticity or the ability to dynamically switch among CSC and non-CSC states as well as between different subsets of CSCs, resulting in varied dissemination and drug resistance potential [84,95,314]. This process of CSC plasticity may be modulated by specific microenvironmental signals and intracellular and intercellular interactions arising in the tumor niche. Such factors unique to each tumor preserve the dynamic balance between CSC and non-CSC subpopulations, maintaining a controlled and finely tuned amount of CSCs within tumors [72,314]. Changes in the tumor microenvironment caused by conventional therapies, as chemotherapy, may result in a shift in this equilibrium towards a more stem-like state, leading to a more CSC-rich and aggressive tumor, thus critically influencing the clinical outcomes [315]. In this regard, eradicating only existing CSC subpopulations may be not sufficient, as the appearance of cells with CSC phenotype seems to be a bidirectional dynamic process. Accordingly, new therapeutic anticancer strategies should overcome the challenges of targeting effectively all cell populations within tumors to prevent this bidirectional interconversion process [316].

5.3. Relevant cell-based strategies for the isolation and enrichment of CSCs

The investigation of phenotypic bidirectional transitions between CSCs and non-CSCs during cancer development and/or treatment has proven technically challenging, since the use of in vitro or in vivo models for this purpose are fairly limited. Indeed, one of the major obstacles in CSC research has been the lack of experimental systems that enable the reliable enrichment of CSCs from non-CSCs for comparative analysis.

One of the most widely applied method to identify and enrich CSCs from different solid tumors and/or cell lines is by sorting the cells based on the expression of specific breast CSC surface markers, mainly CD44⁺/CD24^{-/low} [81] or by the ALDEFLUOR™ staining based on ALDH1 enzymatic activity [108,317]. Although both strategies represent two 'classical' broadly used methods in the literature for CSC enrichment, they are not universally applicable to all breast tumors [118,318]. To overcome this limitation, both markers are commonly used together, ALDH1^{high}/CD44⁺/CD24^{-/low}. Of note, detailed analysis revealed that the overlap between CD44⁺/CD24^{-/low} and ALDH1^{high} CSC phenotypes in BC was very small, as well as their distribution among intrinsic BC subtypes [319]. Breast CSCs with CD44⁺/CD24^{-/low} phenotype and high ALDH1 activity exhibit greater tumorigenicity than the cells expressing either marker alone, and are more frequently found in basal-like BC tumors than in luminal type tumors [319,320]. Correspondingly, different subtypes of BC exhibit various abundance of breast CSCs and varying proportions of breast CSC phenotypes, explaining the different patient treatment responses and clinical outcomes.

Although both isolation strategies are widely accepted approaches for CSC identification and isolation, several limitations have been described. One of the most important drawbacks of these methods is that tumor heterogeneity is not considered. The heterogeneity of CSC within breast tumors is not limited to the differential expression of surface markers but also involves various functional subsets of CSCs, which may be the result of genetic mutations and epigenetic modifications. In this regard, isolation of CSC based on CD44⁺/CD24^{-/low} cell surface expression, results in the simple segregation of subclones with low and high CSC activity, without considering the possible diversity existing between CSC derived from different subclones [110]. Besides, the markers expression could vary in vivo as a consequence of plasticity and adaptation to the microenvironment, as well as being affected by cell culture conditions. The complex procedure, time consuming and expensive processing along with low viability and a reduced number of isolated cells are other disadvantages of surface marker-dependent

isolation of CSCs, which limit clinical and research application of this method [111]. On the other hand, ALDEFLUOR staining is transient and depends on the presence of the enzymatic substrate, limiting the suitability of this approach for CSC segregation in a reduced timeframe.

Among all the alternative strategies, the use of specific CSC-reporter vectors has been regarded as a promising approach. As the CSC state is dynamic with rapid transitions between CSC to non-CSC states, the selected reporter vector should be detectable only in CSCs [121]. Several studies have already used this strategy for identifying and characterizing CSC subpopulation in human cancer cell lines, thereby demonstrating the feasibility of generating these models. In BC, most of the CSC reporter systems developed have been based on the use of GFP reporters driven by promoters for pluripotent stem cell transcription factors, such as OCT4, SOX2 and Nanog [120–126]. Of note, among these is the widely used phOCT4-EGFP reporter generated by Gerrard and Cui [321], or the flexible dual SORE6–GFP developed by Tang *et al.* [124], which both allow identifying and isolating CSCs with metastatic potential and chemo-resistance in BC, and hence, enable interrogation of CSC state in real time. However, several limitations of using this technology have been identified, such as that tumor heterogeneity might not be repopulated after initial enrichment of GFP high cells, thus impairing the CSC multi-lineage differentiation ability and the balance levels between CSCs and non-CSCs. Unexpectedly, even though GFP was expressed in CSC-enriched populations in these models, the use of the OCT4 promoter not only yielded the blocking of the CSC differentiation, but also prevented asymmetric division and non-CSC regeneration [322]. The reason why the OCT3/4-GFP vector in this model blocked the differentiation of CSCs remains unknown, however, a possible explanation might be that vector encodes one or more proteins that inhibit differentiation, or the fact that promoter might compete for one or more limiting transcriptional factors that drive CSC differentiation. In any case, these results underscore the importance of the selection of the appropriate vector and the complexity of gene expression pattern. Besides these findings, a lack of correlation between GFP+ cells and stemness markers expression was reported in tumor specimens [323]. Another important drawback is that certain cells with aggressive phenotypes, including chemotherapy resistant cell lines, might not always be efficiently enriched for CSCs based on reporter systems [324].

Considering the foregoing, our CSC models use the tdTomato as reporter gene under the control of the CSC specific promoter ALDH1A1. For this, the tdTomato reporter cDNA was cloned under the minimal ALDH1A1 promoter. Since ALDH1A1 is upregulated in CSCs, this approach enables their identification and isolation, and has proved successful

in the MCF-7 BC luminal A cell line, the highly aggressive TNBC cell line MDA-MB-231, and the HCT116 colon cancer cell line [119,127]. In these models, the expression of tdTomato correlated with the expression of various stemness markers, and the stemness nature of tdTomato-expressing cells was confirmed *in vivo* by tumorigenic assays using orthotopic cancer mice models. Contrarily to other similar models, the differentiation and dedifferentiation processes of resulting tdTomato cells were not restrained.

In this thesis, we used the same strategy to identify and trace CSCs from the TNBC cell lines HCC-1806 and MDA-MB-468. It should be noted that both CSC models generated in addition to being fluorescent are also bioluminescent, thereby being suitable for *in vivo* image-based cell tracking.

5.4. Preclinical fluorescent CSC models of TNBC cell lines for CSC identification and isolation

Here, we have developed and validated two CSC fluorescent models for direct visualization, quantitation, monitoring and isolation of tumor cells with stem-like properties, demonstrating their suitability as *in vitro* and *in vivo* preclinical tumor models. The resulting tdTomato⁺ cells showed overexpression of CSC-specific markers, highlighting the ALDH1A1, ALOX5, OCT4, ABCG2 and NANOG. Besides, tdTomato⁺ cell populations showed positive mammosphere formation and increased survival when cultured under non-attachment conditions in serum-free media. Further, red fluorescence was detected in mammospheres derived from tdTomato⁺ cells, thereby confirming their stemness nature. Importantly, both CSC models allowed CSC differentiation, since from a pure FACS-enriched CSC population is obtained a complete restoration of the tumor mother cell line *in vitro*. In cell cultures in attachment conditions, the CSC-tdTomato⁺ population divides asymmetrically leading to a gradual decrease of the % of tdTomato⁺ cells until reaches a final steady state in which the CSC population rate stabilizes in a low percentage of tdTomato⁺ cells (from 0.1 to 5%) characteristic of each cell line [325]. Therefore, as CSCs divide, the resulting more differentiate daughter cells lose their stem-like phenotype and losing in turn, their red fluorescence expression.

Interestingly, although we used the same approach to validate the *in vivo* tumorigenicity of both subpopulations from both CSC models, the inoculated cells behaved and responded in different and unexpected ways. In the case of the HCC-1806 CSC model, the tdTomato⁺ cells showed an increased tumorigenic capacity of developing tumors *in vivo*, which translated into higher tumor volumes and tumor incidence, showing both a positive correlation with the number of inoculated cells, regardless tdTomato expression.

These results were consistent with those previously published by our laboratory, thereby confirming once again the CSC nature of the tdTomato+ cells [119]. Interestingly, active CSC differentiation of the tdTomato+ cell fraction was also detected *ex vivo*. Indeed, *ex vivo* analysis of tumors showed a decrease in the tdTomato expression in all tumors of the CSC-like groups, going from the inoculated enriched-CSC population, which tdTomato+ expression was close to 100%, to only 10-15% at endpoint, thereby approaching to their steady state. These findings indicate that as cells proliferate and thus, tumor grows, the equilibrium of CSCs versus non-CSCs is re-established. Likewise, tdTomato-expressing cells were also detected in inoculated tdTomato- tumors, thereby suggesting that tdTomato- cells switched their phenotype into a stem-like phenotype, which directly induced tdTomato expression. This adaptation of the phenotype by the tdTomato fraction was also obtained in previous studies using the MDA-MB-231 CSC model, in which tdTomato- cells originated a tumor containing tdTomato+ cells and showed “*de novo*” stemness gene expression and overexpression of EMT-related genes [127].

In the case of the MDA-MB-468 CSC model, no significant differences in tumor growth nor tumor incidence were obtained between tdTomato+ and tdTomato- groups, thus preventing from fulfilling our aim of validating *in vivo* the CSC model. Indeed, it was obtained a 100% of tumor incidence rate, as well as a great tumor progression and ability to metastasize of tumors derived from MDA-MB-468-tdTomato- cells, with no significant differences between subgroups. Besides, no correlation between cell number and tumor volume was obtained, regardless of tdTomato expression. *Ex vivo* analysis of tumors - based mainly on flow cytometry and IHC assays - demonstrated a high capacity of tdTomato- cells to switch their phenotype into a stem-like phenotype. The presence of tdTomato+ cells was detected in all animals injected with tdTomato- non-CSC cells. More importantly, a higher number of CTC positive for tdTomato were detected in the blood samples from animals inoculated with tdTomato- cells than in those inoculated with the positive ones. Moreover, the interconversion process among MDA-MB-468 tumor cells was also observed *in vitro*. Gene expression analysis revealed the acquisition of a more aggressive and stem-like phenotype of tdTomato- cells after cell sorting enrichment and subsequent culture in attachment conditions. These results supported our previous work on the MDA-MB-231 model, in which tumor cells tend to recover a specific cell state equilibrium after depletion of either CSCs or non-CSCs [127]. Besides, this data fits with other reports that have evidenced that cell tumorigenicity and tumor progression strongly rely on the capacity of cancer cells to dynamically switch between CSCs and non-CSCs states or among different subsets of CSCs through intracellular and intercellular

regulatory networks [326,327]. The molecular mechanisms underlying such interconversion ability has been under extensive investigation, being the overexpression of one or more transcription factors and the activation of the transdifferentiation process of EMT considered as the major contributing factors. Moreover, accumulating evidence suggests that tumor microenvironment and epigenetic reprogramming drive such dynamic mechanisms, favoring cancer cell plasticity and tumor heterogeneity [328,329].

Considering the above, the differences obtained between both cell models are just a further demonstration of the tumor heterogeneity among tumor cell lines. Although interconversion and phenotypic changes between subpopulations were detected in both models, in the MDA-MB-468 model were such that prevented obtaining differences between the experimental groups, while in the HCC-1806 model were not decisive, allowing its validation *in vivo*. Several studies have observed genetic and phenotypic cell-to-cell variability within the same type of cancer cells and across different types of cancers and established cell lines [330]. In this regard, more in-depth characterization studies, including genomic, molecular and histological analysis, should be performed for a better understanding and interpretation of this data. For instance, given the association between the tumor heterogeneity, the CSC dynamism and the EMT process, it would be interesting to further explore if there is a positive co-relation between the expression EMT genes (SNAIL1, SLUG, ZEB1, CDH2, TWIST, VIM, etc.) and tdTomato *de novo* expression in those tumors derived from non-CSC.

These findings also underline the need to reconsider and update the experimental design for future cell model validations *in vivo*. More precisely, non-CSCs should be cultured in the presence of a minimal fraction of CSCs (1-2%) to avoid de-differentiation of the non-CSC population. Besides, the use of a dual reporter, using OCT4 and ALDH1A1 promoters, may bring out an improvement to encompass the totality of CSCs populations. This approach has already been applied by several groups, showing its potential use for the assessment of CSC plasticity and response to therapeutics [121,124].

Despite the constraints, we were able to distinguish a unique population of CSC-like cells within both tumor cell lines based on the ALDH1A1-tdTomato expression vector. Altogether, we provided two additional CSC fluorescent models of TNBC cell lines, in which these dynamic phenotypic changes could be observed both *in vitro* and *in vivo*. Therefore, the use of both CSC models should be considered as a potential tool to monitor CSC *in situ* after therapy and more importantly, for the preclinical validation of CSC-specific therapeutics before the clinical phase. A further exploration of the

mechanisms and the signaling pathways involved in this dynamic cellular conversion will allow us a better understanding of the phenotypic plasticity of CSCs, the involvement of the tumor microenvironment and its implication for cancer treatment.

5.5. Repurposed drugs for anti-CSC treatment

The identification of the CSC population has undoubtedly provided a crucial breakthrough in the understanding of cancer biology, and in particular, of the TNBC subtype. Given the evidence of the role of CSC in sustaining tumor growth, together with the molecular characterization and classification of this heterogeneous BC subtype, conventional treatment should be reconsidered and focused on targeting this minor subpopulation of resistant cells in order to prevent tumor relapse and metastasis effectively. In this context, the research on CSCs is one of the most promising ways to improve patients' survival with an understanding of the mechanisms by which CSCs are developed and maintained, and of the CSC-derived heterogeneity [117,187]. Multiple approaches have been developed and tested for efficacy in targeting CSC subpopulation. Such therapies are particularly relevant for TNBC patients due to the lack of specific treatments and the high content of CSCs in TNBC tumors [331]. Currently, conventional chemotherapy is the standard treatment for TNBC, but it spares the CSC populations, which have the ability to adapt and evolve resistant mechanisms to persist in the drug environment, causing both tumor recurrence and tumor progression [96]. In recent decades, multiple CSC-targeting strategies have shown therapeutic potential on TNBC in multiple preclinical studies [332], and although some of these strategies are currently being evaluated in clinical trials, such as the AKT inhibitor MK-2206 [333] and the chemokine receptor I/II inhibitor reparixin [208], no therapy specifically targeted against CSCs have been already approved for TNBC treatment. Therefore, the identification of novel therapeutic anti-CSC drugs is urgently needed for developing effective therapeutics for this cancer subtype. The quest to find new anti-CSC agents have resulted in drug-repositioning of old drugs for cancer therapy. Drug repositioning is a cost-effective strategy that can bypass time-consuming stages of drug development, since their pharmacokinetics and toxicity profiling are already established, thus facilitating rapid clinical translation [285]. Several studies have successfully identified non-oncology candidates targeting the hallmarks of cancer using drug repurposing, some of which are currently included in the guidelines of the European Society for Medical Oncology (ESMO) or of the National Comprehensive Cancer Network (NCCN) or approved by the FDA, as is the case of thalidomide, temsirolimus (a rapamycin analog), ATRA, zoledronic acid and non-steroidal anti-inflammatory drugs (NSAIDs).

While other compounds, such as metformin or artemisinin, or even infectious disease vaccines, have advanced to phase III and phase IV clinical trials to investigate their suitability in clinical oncology [334,335].

In this work, we focused on the validation of potential anti-CSC drugs that could inhibit CSC proliferation and downregulate signaling pathways keeping the stemness phenotype in cancer cells. As one of the main goals of this thesis was the development of drug delivery systems to enhance their antitumoral efficacy, the selection of drug candidates was made according to the following criteria: i) drugs with suitable physicochemical properties for the development of polymeric micellar systems ii) existing drugs identified as potential anti-CSC agents that were discontinued or have not progressed to clinical stages for limitations associated to bioavailability, solubility, stability, toxicity and/or side effects, with the aim of giving them, a 'third chance'.

For this purpose, a battery of 17 compounds was initially identified, all clinically non-oncology approved drugs with previously described anti-CSC activity (**Table 6**) by drug repurposing studies. A preliminary cytotoxic assay was performed using parental tumor cell lines, where CSC are found in a low and stable percentage (from 0.1 to 5%), thus mimicking the tumor situation, in order to establish the working dose range of each drug and to compare their antitumoral efficacy with the chemotherapeutic drug PTX. Besides, drugs' performance was evaluated and compared using two different BC subtypes cell lines. Despite that CSCs are known as tumor cells with a low proliferative rate, according to the bidirectional interconversion model, the non-CSC proliferating cells can dedifferentiate and acquire stem cell potential, hence drugs should efficiently inhibit proliferation of both cell subpopulations.

As expected, we detected a high heterogeneity in drugs cytotoxic efficiency depending on the cell line tested. Concordantly with previous studies, our findings revealed that MCF-7 cells were more sensitive (lower IC₅₀ values) to a large part of tested compounds -including the reference drug PTX- than MDA-MB-231 cells. These results fit with data from other studies that describe the MDA-MB-231 cell line as a model of highly aggressive TNBC, categorized as a mesenchymal stem cell-like subtype. This TNBC cell line displays chemo-resistance, high proliferation and migratory potential and representative EMT associated with BC metastasis. While the MCF-7 is a model of luminal A BC subtype showed to be more sensitive to anticancer therapies [286,336]. In order to further evaluate tumor heterogeneity in cancer cell cultures, we found interesting to study drug performance in cell lines categorized as the same BC subtype as MDA-MB-231, the TNBC. As expected, substantial differences in terms of drug cytotoxic

efficiency and treatment sensitivity were obtained when MTT results from different TNBC cell lines were compared, which is in line with previous results.

From the initial drug set, 8Q and NCS compounds emerged showing a remarkably anti-proliferative activity on CSC subpopulation, either in attachment or in low attachment culture conditions. In addition, we further demonstrated that both drugs efficiently inhibited CSC hallmarks i.e. migration, invasion and neoplastic transformation. These results were consistent with the works published by Zhou *et al.* [214] and Wang *et al.* [237], in which 8Q and NCS, respectively, were identified as having preferential activity against the breast cancer spheres, showing their effect through the downregulation of stem pathways and inducing CSC apoptosis. The 8Q compound is a metal chelator, which can form a complex with copper and induce apoptosis in cancer cells through NF- κ B signaling [214,337]. In the work by Zhou *et al.*, 8Q showed a higher inhibitory effect on NF- κ B activity in sphere cells than in MCF-7 cells [214]. In the case of NCS, several studies have already reported its in vitro efficacy in CSC through inhibition of Wnt/ β -catenin and STAT3 signaling pathways, as well as its antitumoral effect against breast CSCs in animal studies [199,237,338,339]. In our study, a strong anti-CSC potential of 8Q and NCS drugs was obtained in the CSC-like population of three different TNBC lines (MDA-MB-231, HCC-1806 and MDA-MB-468), corroborating the results from these previous studies and highlighting the potential value of using our CSC models to monitor CSC performance after treatment.

It is worth stressing that YM and PNB were considered interesting candidates too, as both showed a strong cytotoxic effect in all the TNBC cell lines tested. Based on these results, both drugs have been followed up and are being further evaluated in our laboratory.

Importantly, neither NTC, VS, DSF, FLU nor DFT drugs showed efficacy selectively in CSC population on our cell viability assays, even though all of them have proved to display a strong anti-CSC effect in the literature [220,222,227,229,239,244,245]. Discrepancies in the results might be related to differences in criteria and methodology used for CSC selection and isolation but also to differences in cell culture systems, in vitro models and experimental conditions employed for drug screening and validation assays. For instance, preferential CSC targeting of VS, FLU and DSF drugs was evaluated on isolated CSCs by CD44/CD24 markers expression, ALDEFLUOR activity and/or Hoechst dye efflux assay, while our CSC model is based on the selection of CSC-like population by the ALDH1A1-tdTomato expression system. In this context, differences observed in drugs anti-CSC efficacy could be attributed to the isolation and

subsequent in vitro testing of distinct CSC subpopulations, which translates into varying response patterns and differences in drug sensibility and behavior.

PTX is a chemotherapeutic agent commonly used to treat several kinds of cancer, especially the TNBC subtype. PTX is known as a microtubule-targeting agent with a primary molecular mechanism that disrupts the dynamics of microtubules and induces cell cycle arrest and cell death [340]. PTX usually eradicates the majority of non-CSC tumor cells, but shows low efficacy in CSCs, known as a chemo-resistant population that not only is capable of surviving after anticancer therapy, but also is responsible for tumor recurrence and metastasis [341]. In order to evaluate and confirm its lack of anti-CSC activity, PTX was also included and tested together with the rest of selected drugs. Importantly, we observed that PTX was not capable of selectively targeting the CSC subpopulation, neither in attachment nor in low attachment conditions [287,288]. Indeed, CSCs were not only chemo-resistant but also enriched after PTX treatment. Chemotherapeutic agents usually target proliferating cells, while CSCs are often dormant and evade therapy by overexpressing of multidrug resistance (MDR) transporters, such as ABCG2 or ABCB1, resulting in an enhanced cellular efflux of anti-cancer drugs, including PTX, and thereby, hampering drug retention [96,342].

Among all tested drug candidates, 8Q and NCS showed remarkable specific anti-CSC activity in terms of CSC viability, migration, invasion and anchorage independent growth reduction in the MDA-MB-231 TNBC cell model, and thus, were considered as potential candidates to target efficiently CSCs. Next, we decided to further explore their mechanism of action and to establish the most suitable CSC-targeting strategy with both compounds in order to prompt translation research for clinical application.

5.6. Combined therapy of anti-CSC drugs with the reference drug PTX leads to a synergic anti-CSC effect at specific ratios

Given the heterogeneity in tumor tissue, and the high plasticity and hierarchical complexity due to CSCs, a strategy involving combination therapy could be useful to simultaneously target both the bulk of differentiated cancer cells and the minor population of CSCs, or to simultaneously target different stemness pathways. As a starting point, combination therapy based on anti-CSC drug administration with traditional chemotherapy may yield novel chemotherapy strategies in the future and more importantly, ameliorate clinical outcomes and long-term patient survival. Thus, in the event of being evaluated in clinical trials, 8Q and NCS should be administered as combination regimens with existing chemotherapeutic modalities, rather than as

individual therapy. In this scenario, it is critical to carefully evaluate and optimize dosing and scheduling in the design of effective drug combinations from the early preclinical phases.

Various studies have concentrated on the effect of PTX to improve the therapeutic outcome of cancer patients. Although PTX is one of the most effective and frequently used chemotherapeutic drugs for the treatment of different cancers, including TNBC, its efficiency is limited due to drug resistance [341]. Therefore, novel therapeutic strategies based on the combination of PTX with other therapeutic modalities has been considered. Many trials have been carried out to determine the combinatorial benefits of PTX with distinct anticancer agents. One of the most promising combined therapies is the combined treatment of PTX with dasatinib, since not only it decreased the proportion of breast CSCs in the tumor tissue, suppressing their self-renewal capacity, but also synergistically reduced the cell viability of PTX-resistant cells [343]. Besides, preliminary evidence of the antitumor effect of this combination was observed in patients with metastatic BC [344]. The combination of sorafenib with PTX was demonstrated to have a positive effect on anti-angiogenesis in vivo in metastatic BC, along with a significant suppression of the CSCs' properties when administered at low concentrations [345,346]. Therefore, combination of sorafenib with PTX could effectively reduce the toxic side effects of chemotherapy. These are only two examples of the multiple combinations that have already been investigated in BC or are currently under way [341].

In our case, the synergistic effect of 8Q and NCS with PTX was explored through combination assays in different TNBC cell lines. Our data provided strong evidence that both anti-CSC drugs displayed a synergistic anti-proliferation activity with PTX when combined at specific ratios. It is worth noting that the synergistic ratios were drug and cell line dependent, probably due to the molecular and phenotypic heterogeneity among different cell lines. Similar findings were reported by Lohiya *et al.* In their work, they found that different clinical subtypes of BC cells responded with differential sensitivity towards NCS and doxorubicin drugs and that the extent of synergism, also varied between subtypes [347]. Interestingly, the TNBC cell line MDA-MB-231, which showed the least sensitivity towards individual drugs, demonstrated the highest sensitivity and synergism against combinatorial treatment regimens among all subtypes. In the case of the 8Q drug, Zhou *et al.* showed that the combination treatment of 8Q with PTX produced much better antitumor effects than individual treatments in both MCF-7 and MDA-MB-435 BC xenografts models [214]. However, in the case of MDA-MB-435 tumors the synergistic effect between both drugs led to higher tumor growth inhibition than in the MCF-7 tumors.

Altogether, differential drug sensitivity and the extent of synergism found between cell lines, seem to be merely another evidence of cancer complexity and heterogeneity.

There are many ongoing efforts to understand this inherent variability and resistant nature of cancer as well as to characterize the molecular differences between tumors, with the aim of developing specialized treatments for each specific subtype of cancer, mainly based on the measurement and manipulation of key patient genetic and *omic* data (transcriptomics, metabolomics, proteomics, etc.) [348]. The understanding and application of these data as tools in clinical trial design and in treatment selection have steered the field of cancer treatment toward the concept of precision and personalized medicine (PPM), in which therapy selection is tailored to each individual [348,349]. An example of such PPM approach is the well-known drug trastuzumab, which was approved years ago for the treatment of HER2 receptor positive BC [350], but also the successful use of the poly-ADP ribose polymerase inhibitor olaparib in the treatment of BRCA-mutant ovarian cancer [351]. Accordingly, clinical implementation of drug combination approaches should be considered in a personalized context to the individual patient, ensuring this way maximum performance and getting the most out of combined therapy in each case. Several studies have already demonstrated the safety, feasibility, and importance of designing precision oncology trials that emphasize personalized, individually tailored combination therapies, rather than scripted monotherapies. The targeting of a larger fraction of identified molecular alterations has been correlated with significantly improved disease control rates, as well as with longer progression-free and overall survival rates, compared to targeting just one driver mutation, according to a study published by Jason K. Sicklick *et al.* [250]. In this work, the researchers demonstrated that the use of multi-drug therapies helped to improve outcomes among patients with therapy-resistant cancers, indicating that combination drug treatments could improve precision medicine for cancer care. It is clear that integrating a PPM perspective into cancer research and tumor treatment could result in major improvements in fighting cancer, especially due to its complexity and interpatient variability.

5.7. The synergistic combination therapy prevents PTX induced CSC enrichment via inhibition crucial CSC signaling pathways

Considering that our attention was focused on finding the ideal ratio that could be combined in the same nanocarrier, we tested different drug proportions in order to find the most synergistic drug combination. Interestingly, our findings demonstrated that combination of 8Q and NCS with PTX - at established synergistic ratios - not only resulted in much greater antitumoral efficacy than individual treatments, but also was able to abrogate the relative increase of CSCs induced by PTX. As regards our 8Q results, there were consistent with the work of Zhou *et al.* [214], who showed that 8Q inhibited efficiently the NF- κ B activity of MCF-7 cells, both in attachment and in low attachment conditions. Interestingly, they found that 8Q alone showed limited antitumor activity but the combination of 8Q and PTX produced much better therapeutic effects than individual treatments, with no apparent relapse in BC xenografts models. Here, an enhanced anti-CSC effect was also demonstrated when 8Q was combined with PTX, highlighting the robustness of our study. Nevertheless, we went a step further and established the synergistic ratios of PTX-8Q combination in distinct TNBC cell lines, observing large differences among cell lines. Our study supports that PTX activated NF- κ B activity in TNBC cells, while 8Q inhibited this activation being more pronounced when combined with PTX. However, the compound 8Q shows some limitations that cannot be ignored. Its effective dose in vitro ranged from 4 to 80 μ M (IC₅₀ values) in the different cell lines tested, which means that should be administered at a relatively high concentration to obtain an efficient antitumoral effect in vitro. This limitation may become magnified if moving to clinical studies, resulting in a small therapeutic window and therapeutic index, and hence, reducing its therapeutic value. Ideally, the effective dose of a drug should be substantially less than either the toxic or lethal dose in order to be considered therapeutically relevant. The higher the effective dose, the more likely that reaches or exceeds the maximum tolerated dose [352]. Moreover, 8Q also shows limitations regarding to specificity, since its effect is not CSC selective or specific. Nevertheless, from another point of view, this latter limitation may be rated positively, since with the same treatment we could eliminate both cell subpopulations as well as to restore sensitivity to other therapeutic options. Finally, it is worth noting that limitations regarding to 8Q drug might be overcome using an appropriate strategy, as the development of DDS proposed in this thesis.

With regard to NCS drug, we found that NCS downregulated the stem cell Wnt/ β -catenin signaling pathway, inhibited the formation of mammospheres, and induced cell death in

breast CSCs, thus corroborating previous results of Wang *et al.* in MCF-7 cells [237]. More importantly, our data demonstrated that when PTX is combined with NCS produced enhanced cytotoxicity against CSCs, and potentially prevented the overactivation of Wnt/ β -catenin signaling induced by PTX when used as individual therapy. Collectively, an enhanced inhibition of both pathways was obtained when cells were treated with the established ratios of PTX with 8Q and NCS, indicating that combination therapy resulted in the suppression of bulk tumor cells proliferation but also enhanced the sensitivity of chemo-resistant cells. Based on these findings, we believed that both combination therapies were likely to affect both cell populations by inhibiting NF- κ B and Wnt/ β -catenin signaling pathways. Both signaling are overexpressed in CSC population promoting proliferation and resistance to therapy, and preserving their undifferentiated stem cell state, while in non-CSCs play a pivotal role in the transdifferentiation process of differentiate tumor cells to a stem cell-like phenotype. Although these data underline the potential therapeutic value of using 8Q and NCS in combination with PTX, more in-depth analysis should be done to elucidate their mechanism of action and to explore their potential dual benefit in preventing both resistance acquisition of CSC and the reversion of non-CSCs, strategy that could result in more clinical benefit rather than inhibiting directly the CSC subpopulation.

More importantly, our findings in combination studies showed how two drugs could move from acting synergistically to being antagonistic solely depending on their relative doses. In this regard, optimization of customized drug ratio would be vital prior to further treatment implementation.

Upon these results, we moved forward testing the efficacy of PTX-NCS treatment in vivo in an orthotopic TNBC mice model [353–355]. We believed that a strategy involving combination therapy of different anticancer agents, as the ones proposed in this work, is predicted to be more effective for improving the efficacy of conventional chemotherapy, reducing side effects and avoiding MDR. In line with the findings obtained from in vitro cell culture system, combined treatment of PTX and NCS effectively arrested MDA-MB-231 tumor growth in TNBC cancer xenograft model and significantly reduced the metastatic ability of aggressive tumor cells, indicating that combined therapy not only improved the therapeutic efficacy of treatments in bulk tumor cells but also in CSC subpopulation. Importantly, combination therapy successfully decreased the number of CTC in blood, and, more importantly, prevented the generation lung metastasis, results not observed following the treatment with PTX drug alone.

A number of studies have evaluated the potential of NCS as anticancer therapy in various cancer types *in vivo*, including TNBC and stated the ability of NCS to overcome cancer chemoresistance when combined with PTX and other frontline anticancer agents, such as cisplatin, oxaliplatin and doxorubicin [289,356,357]. However, the synergistic effect of combined treatment in CSC subpopulation has not yet been clearly elucidated. NCS is considered an effective inhibitor of multiple signaling pathways, including Notch, Wnt/ β -catenin, NF- κ B, STAT3, and mTORC1 signaling pathways, most of which are closely involved in CSC self-renewal and tumor initiation, thus, holding promise in eradicating CSCs [237,307,358]. In TNBC, Yin *et al.* reported that treatment with NCS not only suppressed constitutive Wnt/ β -catenin signaling, but also blocked ionizing radiation induced Wnt/ β -catenin signaling in TNBC cells by inhibiting Wnt3a expression, LRP6 expression and LRP6 phosphorylation [359]. Besides, Liu *et al.* demonstrated that combined NCS with cisplatin inhibits EMT and tumor growth in cisplatin-resistant TNBC cancer xenograft model with prominent suppression of Ki67 expression [236]. Therefore, suggesting that NCS might serve as a novel therapeutic strategy, either alone or in combination with cisplatin, for TNBC treatment, especially those resistant to cisplatin. Our results were consistent with the work of Wei *et al.* [289], who demonstrated the efficacy of NCS and its underlying mechanism in PTX-resistant esophageal cancer through inhibiting Wnt/ β -catenin signaling pathway. Hence, emphasizing its potential value as sensitizing candidate for overcoming chemo-resistance in esophageal cancer. Overall, these findings highlight the robustness of our study and support the potential therapeutic benefits of NCS against aggressive TNBC.

Altogether, PTX treatment combined with NCS may offer an effective therapeutic approach to improve the prognosis of TNBC by simultaneously targeting both bulk differentiated cancer cells and the minor population of CSCs. Thus, a further exploration of the signaling pathways involved in CSC therapeutic resistance and maintenance of their stem-cell phenotype will allow us to better understand the mechanism by which NCS, alone and in combination with PTX, prevents both tumor growth and CSC proliferation, to establish best treatment option for TNBC therapy. For this purpose, we would take advantage of tumor samples from the animal model and perform immunohistochemical and gene expression analysis to compare vehicle with treated groups, with the aim of identifying alterations in key signaling pathways associated with CSC chemo-resistance and tumorigenicity. Next steps will also include another orthotopic model to assess tumor relapse and metastasis generation after discontinuation of treatments.

5.8. Drug delivery systems to overcome drug resistance of CSCs

In this study, 8Q and NCS have shown promising antitumoral and specific anti-CSC activities in TNBC - either alone or in combination with PTX - although having the drawback of limited bioavailability. The poor solubility, premature degradation and high instability of both drugs because of its limited water solubility and absorption is a challenge, which has hindered its anticancer application so far [360,361]. As regards PTX chemotherapeutic, although is considered one of the most effective anticancer drugs ever developed, the current Taxol formulations have severe side effects related to the use of Cremophor EL[®] and ethanol due to its water insolubility [362,363]. Therefore, there is an urgent need for the development of alternative Taxol formulations. Moreover, the lack of specificity of common anticancer drugs to target tumor cells and their systemic biodistribution after administration, also cause undesired side effects and suboptimal therapeutic indexes. To circumvent these limitations of conventional formulations and to improve the therapeutic outcomes of anticancer drugs, nanotechnology-based drug delivery systems have been successfully used in the clinical setting to enhance their solubility, bioavailability, stability and biodistribution [364–366]. Moreover, nanoparticle-based delivery systems can take advantage of the enhanced permeability and retention (EPR) effect or the use of targeting ligands for passive or active tumor targeting, respectively. To date, the nanoparticle albumin-bound PTX (Abraxane[®]) [367] has been approved by FDA for use in patients with metastatic BC [368] and non-small-cell lung carcinoma (NSCLC) [369], and there are a number of novel PTX nanoparticle formulations in clinical trials, including polymeric micelles, lipid-based formulations and polymer conjugates [370]. Besides, several studies previously encapsulated NCS and 8Q, among them our group. A wide range of nano-based drug delivery formulations containing both NCS and 8Q have been developed, such as polymeric nanoparticles, lipid nanoparticles, nanofibers, micelles and carbon or silica nanoparticles [337,360]. In these studies, both drugs showed both in vitro and in vivo anticancer activity, and in some cases, its efficacy even improved when encapsulated in formulations. Our group has previously used PM based on the amphiphilic polymer Pluronic[®] F127 to encapsulate NCS and the surface was decorated with a Fab antibody fragment against CD44v6 using the film hydration technique [302]. Those PM-NCS:Fab effectively targeted CD44v6+ cancer cell subpopulation, showing a significant improvement of NCS cytotoxicity on colorectal CSCs and a reduction of CTC in tumor bearing mice. Besides, encapsulation of NCS into PM strongly reduced its systemic toxicity and allowed intra-tumoral accumulation for up to 48 h after i.v. administration. Considering these promising results, together with the already demonstrated effects of Pluronic in sensitization and

prevention of MDR [371], we believed that these PM-loaded with NCS were attractive candidates for simultaneous delivery of synergistic ratios of drugs to treat TNBC, particularly in the prevention of CSC-driven chemotherapy resistance.

5.9. Co-encapsulation of synergistic drug ratios increases its anti-CSC efficacy in vitro and in vivo

Moved by the positive results obtained in vitro and in vivo for both combination treatments, we next used non-targeted Pluronic® F127 PM for simultaneous delivery of drugs against TNBC [301]. In this project, two versions of PM-loaded were prepared, one in which the selected drugs were encapsulated individually (PM-8Q and PM-NCS) and a second, in which 8Q and NCS were co-encapsulated with PTX (PM-PTX-8Q and PM-PTX-NCS) at the synergistic ratios previously determined. The distinct formulations were characterized by micelle particle size and distribution, zeta potential, drug loading efficiency and stability. Physicochemical analysis depicted the feasibility of producing co-loaded PM without losing drug efficiency, being the chosen ones for further antitumoral activity studies. Regarding to anticancer efficacy, the encapsulation of combined treatments (at synergistic ratios) into micelles increased its effectiveness denoted by a decrease in the % of cell viability values. Moreover, the co-encapsulation of drugs into PM also increased the anti-CSC efficacy in MDA-MB-231 cells, by significantly reducing CSC ability to form colonies in low attachment conditions when compared with the cells treated with the free drugs, either alone or in combination. Compared with the free drug combination, NCS drug-loaded PM in combination with free PTX significantly reduced lung metastasis and circulating tumor cells in TNBC mice model.

These results emphasize the importance of therapeutic delivery systems to effectively treat resistant CSC population. The improvement of anti-CSC efficacy by PM could be explained by a combination effect of the inhibition of the Wnt and NF- κ B signaling pathways by NCS and 8Q drugs, respectively, the inhibition of drug efflux transporters' activity (as P-glycoprotein - P-gp - and ABCG2 activity) and MDR reversal by Pluronic® [372], which results in a chemosensitizing effect to PTX treatment, increasing its cytotoxic activity against both bulk tumor and CSC populations. In this regard, our results reinforced the idea that Pluronic® can sensitize CSCs to chemotherapeutic drugs, improving the efficacy of combined treatment against this population.

The biological properties of Pluronic® block copolymers, and more specifically, its MDR chemosensitization activity, make them an attractive platform for drug delivery [371,372]. Several studies have demonstrated that Pluronic display a unique set of biological

activities and have been shown to be potent sensitizers of MDR cancer cells in vitro and in vivo [371,373,374]. Moreover, data from Batrakova *et al.* revealed that Pluronics prevented the development of MDR upon selection with an anthracycline antibiotic, doxorubicin (DOX), both in vitro and in vivo in BC [375]. Alakhova *et al.* demonstrated that Pluronics in combination with DOX, SP1049C, comprising mixed micelles of Pluronic[®] F127 and L61, effectively depleted tumorigenic cell subpopulations, suppressing tumorigenicity and tumor aggressiveness upon treatment in vivo [376]. In their work, DOX/Pluronic combination drastically changed the gene expression profiles and DNA methylation patterns upon in vivo treatment of cancer cells. Considering that misregulation of DNA methylation/demethylation plays an important role in cancer origin, progression, angiogenesis, metastasis, and MDR development [377–379], the use of Pluronic (and similar polymers)-based drug delivery systems offer significant advantages for the development of new formulations of approved and/or experimental therapeutics for effective cancer therapy [380]. However, we are still far from complete understanding of the complexity of the tumor MDR and its multiple correlated resistance mechanisms, and the potential role that Pluronic-based PM can play in addressing these challenges.

5.10. Promising PTX-targeted BC chemotherapy to overcome MDR based on glycolytic PM

As an effective chemotherapeutic agent, PTX has been formulated in various nano-delivery systems which have several advantages over the standard-of-care therapy. A major achievement on 2005 was the US FDA approval of Abraxane[®] for the treatment of metastatic BC in patients who fail other chemotherapy or relapse [381,382]. Years later, in October 2012, was approved to treat non-small cell lung cancer, the most common form of lung cancer [369]. Abraxane[®] has demonstrated some advantages in terms of reduced toxicity compared to Taxol, since this NP formulation completely eliminates Cremophor EL[®] and ethanol [368]. However, whether Abraxane[®] could improve survival and address Pgp-mediated drug resistance is still unclear. Genexol-PM is a novel PM formulation of PTX that has been FDA approved for use in patients with BC [383]. In phase II studies, Genexol-PM was found to be effective and safe with high response rates in patients suffering from metastatic BC and advanced pancreatic cancer [273]. Several studies are currently underway, including a phase III and IV study in patients with recurrent BC [384–386]. Both nanotechnological strategies are passively targeted micelle products that were focused on Cremophor EL[®] replacement for a safer PTX intravenous administration for cancer therapy. However, there are still some drawbacks that should be addressed to improve chemotherapy outcome.

Among them, acquired resistance to PTX is considered one of the main clinical challenges to be coped with if we wish to succeed in cancer therapy. To date, the possibility to specifically target (due to ligand–receptor interactions) genes and antineoplastic drugs to certain cancer tissues/cells represents a milestone in cancer chemotherapy. In this regard and taking advantage of the over-expression of glucose (Glu) membrane transporters in breast cancer cells [387], we proposed a novel nano-delivery system based on mixed micelles using two biocompatible copolymers, Soluplus and TPGS to encapsulate PTX, which surface was decorated with Glu moieties. The designed glycosylated micelles (PTX-GM) showed the potential to administer the double of PTX dose, allowing a higher dose of chemotherapeutic treatment without increasing undesirable side-effects. In vitro cytotoxic studies of PTX-GM confirmed that this system enhanced the cytotoxic effect of PTX against tumor cells. Moreover, the encapsulation of PTX into micelles also increased the anti-CSC efficacy in MDA-MB-231 cells, by significantly reducing CSC ability to form colonies in low attachment conditions when compared with the cells treated with PTX free drug. Besides, a higher and faster cellular uptake of GM was obtained by the entire population of breast cancer cells in vitro. TPGS has been recognized as a potent inhibitor of the efflux pump P-gp and responsible for mediating MDR in tumor cells, following a similar mechanism as the one of Pluronic® [388]. Moreover, it has been reported that TPGS exhibited in vitro and in vivo cytotoxic activity on different cancer cell lines by promoting cellular apoptosis [389]. This data was consistent with previous results of these PM designed by Moretton *et al.* [298]. In their work they demonstrated the feasibility of using this strategy to design novel PTX delivery system based on nanocarrier glycosylation with Glu residues for a potential active targeting to breast cancer cells. Importantly, the in vitro antitumoral activity as well as the PTX intracellular levels were significantly improved in comparison with Genexol in MCF-7 and MDA-MB-231 cancer cell lines, confirming the potential of this micellar formulation as an intelligent nanocarrier for PTX-targeted BC chemotherapy.

Unexpectedly, the PTX-GM did not show any improvement in tumor growth inhibition over the free drug PTX in tumor bearing mice. PTX showed an effect much higher than expected at the administered dose, preventing nanoparticle superiority assessment in vivo. A possible explanation to this lack of improvement regarding PTX-GM and free drug PTX treatment might be that preparation and subsequent implantation of the cells may have seriously affected their tumorigenic ability, giving rise to tumors more sensitive to the treatments administered. In any case, for future assays it would be interesting to assess PTX-GM in resistant-PTX cell lines or to discontinue the treatment to evaluate if

encapsulation of PTX into GM provides an advantage to overcome chemotherapeutic resistance and/or tumor relapse.

Altogether, these results open a window of opportunity to continue exploring the potential of both designed micellar formulations as platforms for both active and passive drug delivery to overcome multidrug resistance, to efficiently target CSC and hence, to improve TNBC therapy.

CONCLUSIONS

CONCLUSIONS

First: The generation of fluorescent CSC models in HCC-1806 and MDA-MB-468 TNBC cell lines, using the ALDH1A1-tdTomato expression vector, is a suitable method for visualizing these cells in heterogeneous tumor population and for monitoring CSC biological performance after therapy.

Second: The processes of CSC differentiation and un-differentiation are not restrained and longitudinal studies are feasible in both CSC fluorescent models generated.

Third: Both HCC-1806 and MDA-MB-468 fluorescent models generated allow the study of the bidirectional interconversion process between CSCs and non-CSCs in vitro and in vivo.

Fourth: 8Q and NCS show a remarkable anti-CSC activity in terms of CSC viability and overall inhibition of migration, invasion and anchorage independent growth of TNBC in vitro, thus highlighting both drugs as potential candidates for CSC targeting.

Fifth: Synergistic combination therapy of 8Q and NCS with the chemotherapeutic agent PTX prevented PTX induced CSC enrichment by inhibiting the NF- κ B and Wnt/ β -Catenin signaling pathways, respectively.

Sixth: The combined treatment of PTX and NCS effectively inhibits triple negative breast tumor growth and reduces the metastatic ability of aggressive tumor cells in vivo in NOD/SCID mice with orthotopic MDA-MB-231 tumors, thereby offering a promising therapeutic approach for resistant TNBC.

Seventh: The Pluronic-based PM are suitable nanocarriers for the in vitro administration of drug combinations, by enhancing their synergistic effect against CSC population and providing evidence of a chemosensitizing effect to PTX on tumor cells.

Eighth: NCS-loaded PMs lead to a reduction of CTC and the likelihood of metastatic spread in vivo when combined with free PTX.

Ninth: The encapsulation of PTX into Glu-decorated PM enhances its in vitro anti-CSC efficacy, confirming the potential of this novel formulation as a promising PTX-targeted BC chemotherapy to overcome MDR.

REFERENCES

REFERENCES

1. Ferlay J, Ervik M, Lam F, Colombet M, Mery L, Piñeros M, et al. Global Cancer Observatory: Cancer Today 2020. *Int. Agency Res. Cancer*. 2020.
2. American Cancer Society. *Cancer Facts and Figures 2021*. Am Cancer Soc. Atlanta, Ga: Atlanta, Ga; 2021.
3. Konduri S, Singh M, Bobustuc G, Rovin R, Kassam A. Epidemiology of male breast cancer. *Breast*. 2020/08/22. Elsevier; 2020;54:8–14.
4. Harbeck N, Penault-Llorca F, Cortes J, Gnant M, Houssami N, Poortmans P, et al. Breast cancer. *Nat Rev Dis Prim*. 2019;5.
5. Dumitrescu RG, Cotarla I. Understanding breast cancer risk - Where do we stand in 2005? *J Cell Mol Med*. 2005;9:208–21.
6. Danaei G, Vander Hoorn S, Lopez AD, Murray CJL, Ezzati M. Causes of cancer in the world: Comparative risk assessment of nine behavioural and environmental risk factors. *Lancet*. 2005;366:1784–93.
7. Collins A, Politopoulos I. The genetics of breast cancer: Risk factors for disease. *Appl Clin Genet*. 2011;4:11–9.
8. Kuchenbaecker KB, Hopper JL, Barnes DR, Phillips KA, Mooij TM, Roos-Blom MJ, et al. Risks of breast, ovarian, and contralateral breast cancer for BRCA1 and BRCA2 mutation carriers. *JAMA - J Am Med Assoc*. 2017;317:2402–16.
9. Pinamonti M, Zanconati F. Normal Breast. *Monogr Clin Cytol*. 2018;24:20–4.
10. Wellings SR. A Hypothesis of the Origin of Human Breast Cancer from the Terminal Ductal Lobular Unit. *Pathol Res Pract*. 1980;166:515–35.
11. Makki J. Diversity of breast carcinoma: Histological subtypes and clinical relevance. *Clin Med Insights Pathol*. 2015;8:23–31.
12. Barba D, León-Sosa A, Lugo P, Suquillo D, Torres F, Surre F, et al. Breast cancer, screening and diagnostic tools: All you need to know. *Crit Rev Oncol Hematol*. 2021;157:103174.
13. Song JL, Chen C, Yuan JP, Sun SR. Progress in the clinical detection of heterogeneity in breast cancer. *Cancer Med*. 2016;5:3475–88.
14. Becker S. A historic and scientific review of breast cancer: The next global healthcare challenge. *Int J Gynecol Obstet*. 2015;131:S36–9.
15. Bevers TB, Anderson BO, Bonaccio E, Buys S, Daly MB, Dempsey PJ, et al. Breast Cancer Screening and Diagnosis. *J Natl Compr Cancer Netw J Natl Compr Canc Netw*. 2009;7:1060–96.

16. Peairs KS, Choi Y, Stewart RW, Sateia HF. Screening for breast cancer. *Semin Oncol.* 2017;44:60–72.
17. Baltzer PAT, Kapetas P, Marino MA, Clauser P. New diagnostic tools for breast cancer. *Memo.* 2017;10:175–80.
18. Rakha EA, Reis-Filho JS, Baehner F, Dabbs DJ, Decker T, Eusebi V, et al. Breast cancer prognostic classification in the molecular era: The role of histological grade. *Breast Cancer Res.* 2010;12.
19. Weigelt B, Geyer FC, Reis-Filho JS. Histological types of breast cancer: How special are they? *Mol Oncol.* 2010;4:192–208.
20. Viale G. The current state of breast cancer classification. *Ann Oncol.* 2012;23.
21. Vuong D, Simpson PT, Green B, Cummings MC, Lakhani SR. Molecular classification of breast cancer. *Virchows Arch.* 2014;465:1–14.
22. Boughey JC, Gonzalez RJ, Bonner E, Kuerer HM. Current treatment and clinical trial developments for ductal carcinoma in situ of the breast. *Oncologist.* 2007;12:1276–87.
23. Goldhirsch A, Ingle JN, Gelber RD, Coates AS, Thürlimann B, Senn HJ. Thresholds for therapies: Highlights of the St Gallen international expert consensus on the primary therapy of early breast cancer 2009. *Ann Oncol.* 2009;20:1319–29.
24. Eliyatkin N, Yalcin E, Zengel B, Aktaş S, Vardar E. Molecular Classification of Breast Carcinoma: From Traditional, Old-Fashioned Way to A New Age, and A New Way. *J Breast Heal.* 2015;11:59–66.
25. Perou CM, Sørile T, Eisen MB, Van De Rijn M, Jeffrey SS, Ress CA, et al. Molecular portraits of human breast tumours. *Nature.* 2000;406:747–52.
26. Sørilie T, Perou CM, Tibshirani R, Aas T, Geisler S, Johnsen H, et al. Gene expression patterns of breast carcinomas distinguish tumor subclasses with clinical implications. *Proc Natl Acad Sci U S A.* 2001;98:10869–74.
27. Parker JS, Bernard PS, Mullins M, Cheung MCU, Leung S, Voduc D, et al. Supervised risk predictor of breast cancer based on intrinsic subtypes. *J Clin Oncol.* 2009;27:1160–7.
28. Prat A, Perou CM. Deconstructing the molecular portraits of breast cancer. *Mol Oncol.* 2011;5:5–23.
29. Prat A, Pineda E, Adamo B, Galván P, Fernández A, Gaba L, et al. Clinical implications of the intrinsic molecular subtypes of breast cancer. *Breast.* 2015;24:S26–35.
30. Nascimento RG do, Otoni KM. Histological and molecular classification of breast cancer: what do we know? *Mastology.* 2020;30:1–8.
31. Vieira AF, Schmitt F. An Update on Breast Cancer Multigene Prognostic Tests-Emergent Clinical Biomarkers. *Front Med.* 2018;5:248.

32. Huang S, Murphy L, Xu W. Genes and functions from breast cancer signatures. *BMC Cancer*. 2018;18:473.
33. Van't Veer LJ, Dai H, Van de Vijver MJ, He YD, Hart AAM, Mao M, et al. Gene expression profiling predicts clinical outcome of breast cancer. *Nature*. 2002;415:530–6.
34. Sotiriou C, Pusztai L. Gene-Expression Signatures in Breast Cancer. *N Engl J Med*. 2009;360:790–800.
35. Ayers M, Symmans WF, Stec J, Damokosh AI, Clark E, Hess K, et al. Gene expression profiles predict complete pathologic response to neoadjuvant paclitaxel and fluorouracil, doxorubicin, and cyclophosphamide chemotherapy in breast cancer. *J Clin Oncol*. 2004;22:2284–93.
36. Szymiczek A, Lone A, Akbari MR. Molecular intrinsic versus clinical subtyping in breast cancer: A comprehensive review. *Clin Genet*. 2021;99:613–37.
37. Gao JJ, Swain SM. Luminal A Breast Cancer and Molecular Assays: A Review. *Oncologist*. 2018;23:556–65.
38. Goldhirsch A, Winer EP, Coates AS, Gelber RD, Piccart-Gebhart M, Thürlimann B, et al. Personalizing the treatment of women with early breast cancer: Highlights of the st gallen international expert consensus on the primary therapy of early breast Cancer 2013. *Ann Oncol*. 2013;24:2206–23.
39. Brenton JD, Carey LA, Ahmed A, Caldas C. Molecular classification and molecular forecasting of breast cancer: Ready for clinical application? *J Clin Oncol*. 2005;23:7350–60.
40. Fragomeni SM, Sciallis A, Jeruss JS. Molecular subtypes and local-regional control of breast cancer. *Surg Oncol Clin N Am*. 2019;27:95–120.
41. Ennis S, Lamon DJ, Rian Eyland -j, Ones BL, Teven Hak SS, Ank Uchs HF, Irginia Aton VP, Harm PD, et al. Use of chemotherapy plus a monoclonal antibody against HER2 for metastatic breast cancer that overexpress HER2. *N Engl J Med*. 2001;344:783–92.
42. Alexandrou S, George SM, Ormandy CJ, Lim E, Oakes SR, Elizabeth Caldon C. The proliferative and apoptotic landscape of basal-like breast cancer. *Int J Mol Sci*. 2019;20:1–30.
43. Rakha EA, Reis-Filho JS, Ellis IO. Basal-like breast cancer: A critical review. *J Clin Oncol*. 2008;26:2568–81.
44. Bosch A, Eroles P, Zaragoza R, Viña JR, Lluch A. Triple-negative breast cancer: Molecular features, pathogenesis, treatment and current lines of research. *Cancer Treat Rev*. Elsevier Ltd; 2010;36:206–15.
45. Kennecke H, Yerushalmi R, Woods R, Cheang MCU, Voduc D, Speers CH, et al. Metastatic behavior of breast cancer subtypes. *J Clin Oncol*. 2010;28:3271–7.

46. Palma G, Frasci G, Chirico A, Esposito E, Siani C, Saturnino C, et al. Triple negative breast cancer: Looking for the missing link between biology and treatments. *Oncotarget*. 2015;6:26560–74.
47. Kreike B, van Kouwenhove M, Horlings H, Weigelt B, Peterse H, Bartelink H, et al. Gene expression profiling and histopathological characterization of triple-negative/basal-like breast carcinomas. *Breast Cancer Res*. 2007;9:1–14.
48. Herschkowitz JI, Simin K, Weigman VJ, Mikaelian I, Usary J, Hu Z, et al. Identification of conserved gene expression features between murine mammary carcinoma models and human breast tumors. *Genome Biol*. 2007;8:1–17.
49. Prat A, Parker JS, Karginova O, Fan C, Livasy C, Herschkowitz JI, et al. Phenotypic and molecular characterization of the claudin-low intrinsic subtype of breast cancer. *Breast Cancer Res*. 2010;12.
50. Dias K, Dvorkin-Gheva A, Hallett RM, Wu Y, Hassell J, Pond GR, et al. Claudin-low breast cancer; clinical & pathological characteristics. *PLoS One*. 2017;12:1–17.
51. Fougner C, Bergholtz H, Norum JH, Sørli T. Re-definition of claudin-low as a breast cancer phenotype. *Nat Commun*. 2020;11:1–11.
52. Weigelt B, Mackay A, A'hern R, Natrajan R, Tan DSP, Dowsett M, et al. Breast cancer molecular profiling with single sample predictors: a retrospective analysis. *Lancet Oncol*. 2010;11:339–49.
53. Yersal O, Barutca S. Biological subtypes of breast cancer: Prognostic and therapeutic implications. *World J Clin Oncol*. 2014;5:412–24.
54. Foulkes WD, Smith IE, Reis-Filho JS. Triple-Negative Breast Cancer. *N Engl J Med*. 2010;363:1938–48.
55. Pareja F, Geyer FC, Marchiò C, Burke KA, Weigelt B, Reis-Filho JS. Triple-negative breast cancer: The importance of molecular and histologic subtyping, and recognition of low-grade variants. *npj Breast Cancer*. 2016;2:1–11.
56. Turner NC, Reis-Filho JS. Tackling the diversity of Triple-negative breast cancer. *Clin Cancer Res*. 2013;19:6380–8.
57. Hirshfield KM, Ganesan S. Triple-negative breast cancer: Molecular subtypes and targeted therapy. *Curr Opin Obstet Gynecol*. 2014;26:34–40.
58. Lehmann BD, Bauer JA, Chen X, Sanders ME, Chakravarthy AB, Shyr Y, et al. Identification of human triple-negative breast cancer subtypes and preclinical models for selection of targeted therapies. *J Clin Invest*. 2011;121:2750–2767.
59. Lehmann BD, Jovanović B, Chen X, Estrada M V., Johnson KN, Shyr Y, et al. Refinement of triple-negative breast cancer molecular subtypes: Implications for neoadjuvant chemotherapy selection. *PLoS One*. 2016;11:1–22.

60. Lehmann B, Pietschmann J. Identification and use of biomarkers in treatment strategies for triple negative breast cancer subtypes. *J Pathol.* 2014;232:142–50.
61. Teschendorff AE, Miremadi A, Pinder SE, Ellis IO, Caldas C. An immune response gene expression module identifies a good prognosis subtype in estrogen receptor negative breast cancer. *Genome Biol.* 2007;8:R157.
62. Omarini C, Guaitoli G, Pipitone S, Moschetti L, Cortesi L, Cascinu S, et al. Neoadjuvant treatments in triple-negative breast cancer patients: where we are now and where we are going. *Cancer Manag Res.* 2018;10:91–103.
63. Martelotto LG, Ng CKY, Piscuoglio S, Weigelt B, Reis-filho JS. Breast cancer intra-tumor heterogeneity. *Breast Cancer Res.* 2014;16:210.
64. Prat A, Perou CM. Mammary development meets cancer genomics. *Nat Med.* 2009;15:842–4.
65. Skibinski A, Kuperwasser C. The origin of breast tumor heterogeneity. *Oncogene.* 2015;34:5309–16.
66. Meyer DS, Brinkhaus H, Müller U, Müller M, Cardiff RD, Bentires-Alj M. Luminal expression of PIK3CA mutant H1047R in the mammary gland induces heterogeneous tumors. *Cancer Res.* 2011;71:4344–51.
67. Van Keymeulen A, Lee MY, Ousset M, Brohée S, Rorive S, Girardi RR, et al. Reactivation of multipotency by oncogenic PIK3CA induces breast tumour heterogeneity. *Nature.* 2015;525:119–23.
68. Greaves M, Maley CC. Clonal evolution in cancer. *Nature.* 2012;481:306–13.
69. Meacham CE, Morrison SJ. Tumour heterogeneity and cancer cell plasticity. *Nature.* 2013;501:328–37.
70. Turner NC, Reis-Filho JS. Genetic heterogeneity and cancer drug resistance. *Lancet Oncol.* 2012;13:e178–85.
71. Shibata M, Shen MM. The roots of cancer: Stem cells and the basis for tumor heterogeneity. *BioEssays.* 2013;35:253–60.
72. Cabrera MC. Cancer stem cell plasticity and tumor hierarchy. *World J Stem Cells.* 2015;7:27.
73. Zhang M, Lee A V., Rosen JM. The cellular origin and evolution of breast cancer. *Cold Spring Harb Perspect Med.* 2017;7:1–14.
74. van Neerven SM, Tiekens M, Vermeulen L, Bijlsma MF. Bidirectional interconversion of stem and non-stem cancer cell populations: A reassessment of theoretical models for tumor heterogeneity. *Mol Cell Oncol.* 2016;3:1–9.
75. Plaks V, Kong N, Werb Z. The Cancer Stem Cell Niche: How Essential is the Niche in Regulating Stemness of Tumor Cells? *Cell Stem Cell.* 2015;16:225–38.

76. Prasetyanti PR, Medema JP. Intra-tumor heterogeneity from a cancer stem cell perspective. *Mol Cancer. BioMed Central*; 2017;16:41.
77. Campbell LL, Polyak K. Breast tumor heterogeneity: Cancer stem cells or clonal evolution? *Cell Cycle*. 2007;6:2332–8.
78. Feng Y, Spezia M, Huang S, Yuan C, Zeng Z, Zhang L, et al. Breast cancer development and progression: Risk factors, cancer stem cells, signaling pathways, genomics, and molecular pathogenesis. *Genes Dis*. 2018;5:77–106.
79. Place AE, Jin Huh S, Polyak K. The microenvironment in breast cancer progression: Biology and implications for treatment. *Breast Cancer Res*. 2011;13.
80. Lapidot T, Sirard C, Vormoor J, Murdoch B, Hoang T, Caceres-Cortes J, et al. A cell initiating human acute myeloid leukaemia after transplantation into SCID mice. *Nature*. 1994;367:645–8.
81. Al-Hajj M, Wicha MS, Benito-Hernandez A, Morrison SJ, Clarke MF. Prospective Identification of Tumorigenic Breast Cancer Cells. *Proc Natl Acad Sci U S A*. 2003;100:3983–8.
82. Visvader JE, Lindeman GJ. Cancer stem cells in solid tumours: accumulating evidence and unresolved questions. *Nat Rev Cancer*. 2008;8:755–68.
83. Yang F, Xu J, Tang L, Guan X. Breast cancer stem cell: the roles and therapeutic implications. *Cell Mol Life Sci*. 2017;74:951–66.
84. Visvader JE, Lindeman GJ. Cancer stem cells: Current status and evolving complexities. *Cell Stem Cell*. 2012;10:717–28.
85. Saeg F, Anbalagan M. Breast cancer stem cells and the challenges of eradication: a review of novel therapies. *Stem Cell Investig*. 2018;5:39–39.
86. Clarke MF, Dick JE, Dirks PB, Eaves CJ, Jamieson CHM, Jones DL, et al. Cancer stem cells - Perspectives on current status and future directions: AACR workshop on cancer stem cells. *Cancer Res*. 2006;66:9339–44.
87. Butti R, Gunasekaran VP, Kumar TVS, Banerjee P, Kundu GC. Breast cancer stem cells: Biology and therapeutic implications. *Int J Biochem Cell Biol*. 2019;107:38–52.
88. Sancho P, Barneda D, Heeschen C. Hallmarks of cancer stem cell metabolism. *Br J Cancer*. 2016;114:1305–12.
89. Yadav UP, Singh T, Kumar P, Sharma P, Kaur H, Sharma S, et al. Metabolic Adaptations in Cancer Stem Cells. *Front Oncol*. 2020;10.
90. Peixoto J, Lima J. Metabolic traits of cancer stem cells. *DMM Dis Model Mech*. 2018;11:1–13.
91. Zhu X, Chen HH, Gao CY, Zhang XX, Jiang JX, Zhang Y, et al. Energy metabolism in cancer stem cells. *World J Stem Cells*. 2020;12:448–61.

92. Tanabe A, Sahara H. The metabolic heterogeneity and flexibility of cancer stem cells. *Cancers (Basel)*. 2020;12:1–22.
93. Ancey PB, Contat C, Meylan E. Glucose transporters in cancer – from tumor cells to the tumor microenvironment. *FEBS J*. 2018;285:2926–43.
94. Hussein YR, Bandyopadhyay S, Semaan A, Ahmed Q, Albashiti B, Jazaerly T, et al. Glut-1 Expression Correlates with Basal-like Breast Cancer. *Transl Oncol*. 2011;4:321–7.
95. Gener P, De Sousa Rafael DF, Fernández Y, Ortega JS, Arango D, Abasolo I, et al. Cancer stem cells and personalized cancer nanomedicine. *Nanomedicine*. 2016;11:307–20.
96. Dean M, Fojo T, Bates S. Tumour stem cells and drug resistance. *Nat Rev Cancer*. 2005;5:275–84.
97. Zhou J, Chen Q, Zou Y, Chen H, Qi L, Chen Y. Stem cells and cellular origins of breast cancer: Updates in the rationale, controversies, and therapeutic implications. *Front Oncol*. 2019;9:1–12.
98. Ginestier C, Hur MH, Charafe-Jauffret E, Monville F, Dutcher J, Brown M, et al. ALDH1 Is a Marker of Normal and Malignant Human Mammary Stem Cells and a Predictor of Poor Clinical Outcome. *Cell Stem Cell*. 2007;1:555–67.
99. Bane A, Vilorio-Petit A, Pinnaduwege D, Mulligan AM, O'Malley FP, Andrulis IL. Clinical-pathologic significance of cancer stem cell marker expression in familial breast cancers. *Breast Cancer Res Treat*. 2013;140:195–205.
100. Li W, Ma H, Zhang J, Zhu L, Wang C, Yang Y. Unraveling the roles of CD44/CD24 and ALDH1 as cancer stem cell markers in tumorigenesis and metastasis. *Sci Rep*. 2017;7:1–15.
101. Zhou L, Sheng D, Wang D, Ma W, Deng Q, Deng L, et al. Identification of cancer-type specific expression patterns for active aldehyde dehydrogenase (ALDH) isoforms in ALDEFLUOR assay. *Cell Biol Toxicol*. 2019;35:161–77.
102. Miraglia S, Godfrey W, Yin AH, Atkins K, Warnke R, Holden JT, et al. A novel five-transmembrane hematopoietic stem cell antigen: Isolation, characterization, and molecular cloning. *Blood*. 1997;90:5013–21.
103. Brugnoli F, Grassilli S, Al-Qassab Y, Capitani S, Bertagnolo V. CD133 in Breast Cancer Cells: More than a Stem Cell Marker. *J Oncol*. 2019;2019.
104. Zhao W, Li Y, Zhang X. Stemness-related markers in cancer. *Cancer Transl Med*. 2017;3:87.
105. Finicelli M, Benedetti G, Squillaro T, Pistilli B, Marcellusi A, Mariani P, et al. Expression of stemness genes in primary breast cancer tissues: The role of SOX2 as a prognostic marker for detection of early recurrence. *Oncotarget*. 2014;5:9678–88.
106. Da Cruz Paula A, Lopes C. Implications of different cancer stem cell phenotypes in breast cancer. *Anticancer Res*. 2017;37:2173–83.

107. Akbarzadeh M, Maroufi NF, Tazehkand AP, Akbarzadeh M, Bastani S, Safdari R, et al. Current approaches in identification and isolation of cancer stem cells. *J Cell Physiol.* 2019;234:14759–72.
108. Tirino V, Desiderio V, Paino F, De Rosa A, Papaccio F, La Noce M, et al. Cancer stem cells in solid tumors: an overview and new approaches for their isolation and characterization. *FASEB J.* 2013;27:13–24.
109. Duan J-J, Qiu W, Xu S-L, Wang B, Ye X-Z, Ping Y-F, et al. Strategies for isolating and enriching cancer stem cells: well begun is half done. *Stem Cells Dev.* 2013/05/09. Mary Ann Liebert, Inc.; 2013;22:2221–39.
110. Renovanz M, Kim EL. Intratumoral heterogeneity, its contribution to therapy resistance and methodological caveats to assessment. *Front Oncol.* 2014;4:142.
111. Zhang X, Powell K, Li L. Breast Cancer Stem Cells: Biomarkers, Identification and Isolation Methods, Regulating Mechanisms, Cellular Origin, and Beyond. *Cancers (Basel).* MDPI; 2020;12:3765.
112. Begicevic R-R, Falasca M. ABC Transporters in Cancer Stem Cells: Beyond Chemoresistance. *Int J Mol Sci.* MDPI; 2017;18:2362.
113. Dontu G, Abdallah WM, Foley JM, Jackson KW, Clarke MF, Kawamura MJ, et al. In vitro propagation and transcriptional profiling of human mammary stem/progenitor cells. *Genes Dev.* 2003;17:1253–70.
114. Ponti D, Costa A, Zaffaroni N, Pratesi G, Petrangolini G, Coradini D, et al. Isolation and in vitro propagation of tumorigenic breast cancer cells with stem/progenitor cell properties. *Cancer Res.* 2005;65:5506–11.
115. Lombardo Y, de Giorgio A, Coombes CR, Stebbing J, Castellano L. Mammosphere formation assay from human breast cancer tissues and cell lines. *J Vis Exp.* 2015;2015:1–5.
116. Justus CR, Leffler N, Ruiz-Echevarria M, Yang L V. In vitro cell migration and invasion assays. *J Vis Exp.* 2014;1–8.
117. Han L, Shi S, Gong T, Zhang Z, Sun X. Cancer stem cells: therapeutic implications and perspectives in cancer therapy. *Acta Pharm Sin B.* 2013;3:65–75.
118. S. Franco S, Szczesna K, Iliou MS, Al-Qahtani M, Mobasheri A, Kobolák J, et al. In vitro models of cancer stem cells and clinical applications. *BMC Cancer.* 2016;16:738.
119. Gener P, Gouveia LP, Sabat GR, de Sousa Rafael DF, Fort NB, Arranja A, et al. Fluorescent CSC models evidence that targeted nanomedicines improve treatment sensitivity of breast and colon cancer stem cells. *Nanomedicine Nanotechnology, Biol Med.* 2015;11:1883–92.
120. Patel SA, Ramkissoon SH, Bryan M, Pliner LF, Dontu G, Patel PS, et al. Delineation of breast cancer cell hierarchy identifies the subset responsible for dormancy. *Sci Rep.* 2012;2:906.

121. Mohan A, Raj R. R, Mohan G, K. P. P, Thomas Maliekal T. Reporters of Cancer Stem Cells as a Tool for Drug Discovery. *Front Oncol.* 2021;11:1–16.
122. Iglesias JM, Leis O, Pérez Ruiz E, Gumuzio Barrie J, Garcia-Garcia F, Aduriz A, et al. The Activation of the Sox2 RR2 Pluripotency Transcriptional Reporter in Human Breast Cancer Cell Lines is Dynamic and Labels Cells with Higher Tumorigenic Potential. *Front Oncol.* 2014;4:1–10.
123. Wu F, Zhang J, Wang P, Ye X, Jung K, Bone KM, et al. Identification of two novel phenotypically distinct breast cancer cell subsets based on Sox2 transcription activity. *Cell Signal.* Elsevier Inc.; 2012;24:1989–98.
124. Tang B, Raviv A, Esposito D, Flanders KC, Daniel C, Nghiem BT, et al. A flexible reporter system for direct observation and isolation of cancer stem cells. *Stem Cell Reports.* The Authors; 2015;4:155–69.
125. Thiagarajan PS, Hitomi M, Hale JS, Alvarado AG, Otvos B, Sinyuk M, et al. Development of a Fluorescent Reporter System to Delineate Cancer Stem Cells in Triple-Negative Breast Cancer. *Stem Cells.* 2015;33:2114–25.
126. Shanmugam G, Mohan A, Kumari K, Louis JM, Soumya Krishnan U, Balagopal PG, et al. A novel reporter construct for screening small molecule inhibitors that specifically target self-renewing cancer cells. *Exp Cell Res.* Elsevier Inc.; 2019;383:111551.
127. Gener P, Rafael D, Seras-franzoso J, Perez A, Pindado LA, Casas G, et al. Pivotal role of AKT2 during dynamic phenotypic change of breast cancer stem cells. *Cancers (Basel).* 2019;11:1–18.
128. Dey P, Rathod M, De A. Targeting stem cells in the realm of drug-resistant breast cancer. *Breast Cancer Targets Ther.* 2019;11:115–35.
129. Takebe N, Harris PJ, Warren RQ, Ivy SP. Targeting cancer stem cells by inhibiting Wnt, Notch, and Hedgehog pathways. *Nat Rev Clin Oncol.* 2011;8:97–106.
130. M. PM, Simeone C, Ribot EJ, Foster PJ, Palmieri D, Steeg PS, et al. Notch1 inhibition alters the CD44^{hi} /CD24^{lo} population and reduces the formation of brain metastases from breast cancer. *Mol Cancer Res.* 2011;9:834–44.
131. Fultang N, Chakraborty M, Peethambaran B. Regulation of cancer stem cells in triple negative breast cancer. *Cancer Drug Resist.* 2021;4:321–42.
132. Xu L, Zhang L, Hu C, Liang S, Fei X, Yan N, et al. WNT pathway inhibitor pyrvinium pamoate inhibits the self-renewal and metastasis of breast cancer stem cells. *Int J Oncol.* 2016;48:1175–86.
133. Monkkonen T, Lewis MT. New Paradigms for the Hedgehog Signaling Network in Mammary Gland Development and Breast Cancer. *Biochim Biophys Acta.* 2017;1868:315–32.

134. Valenti G, Quinn HM, Heynen GJJE, Lan L, Holland JD, Vogel R, et al. Cancer stem cells regulate cancer-associated fibroblasts via activation of hedgehog signaling in mammary gland tumors. *Cancer Res.* 2017;77:2134–47.
135. Porta C, Paglino C, Mosca A. Targeting PI3K/Akt/mTOR signaling in cancer. *Front Oncol.* 2014;4:1–11.
136. Butti R, Das S, Gunasekaran VP, Yadav AS, Kumar D, Kundu GC. Receptor tyrosine kinases (RTKs) in breast cancer: Signaling, therapeutic implications and challenges. *Mol Cancer.* 2018;17:1–18.
137. Yu JSL, Cui W. Proliferation, survival and metabolism: The role of PI3K/AKT/ mTOR signalling in pluripotency and cell fate determination. *Dev.* 2016;143:3050–60.
138. Moustakas A, de Herreros AG. Epithelial–mesenchymal transition in cancer. *Mol Oncol.* 2017;11:715–7.
139. Sarrio D, Franklin CK, Mackay A, Reis-Filho JS, Isacke CM. Epithelial and mesenchymal subpopulations within normal basal breast cell lines exhibit distinct stem cell/progenitor properties. *Stem Cells.* 2012;30:292–303.
140. Jolly MK, Boareto M, Huang B, Jia D, Lu M, Onuchic JN, et al. Implications of the hybrid epithelial/mesenchymal phenotype in metastasis. *Front Oncol.* 2015;5:1–19.
141. Wang SS, Jiang J, Liang XH, Tang YL. Links between cancer stem cells and epithelial–mesenchymal transition. *Onco Targets Ther.* 2015;8:2973–80.
142. Mani SA, Guo W, Liao MJ, Eaton EN, Ayyanan A, Zhou AY, et al. The Epithelial-Mesenchymal Transition Generates Cells with Properties of Stem Cells. *Cell.* 2008;133:704–15.
143. Gener P, Seras-Franzoso J, Callejo PG, Andrade F, Rafael D, Martínez F, et al. Dynamism, sensitivity, and consequences of mesenchymal and stem-like phenotype of cancer cells. *Stem Cells Int.* 2018;2018.
144. Battula VL, Evans KW, Hollier BG, Shi Y, Marini FC, Ayyanan A, et al. Epithelial-mesenchymal transition-derived cells exhibit multi-lineage differentiation potential similar to mesenchymal stem cells. *Stem Cells.* 2010;28:1435–45.
145. Morel AP, Lièvre M, Thomas C, Hinkal G, Ansieau S, Puisieux A. Generation of breast cancer stem cells through epithelial-mesenchymal transition. *PLoS One.* 2008;3:1–7.
146. Brooks MD, Burness ML, Wicha MS. Therapeutic Implications of Cellular Heterogeneity and Plasticity in Breast Cancer. *Cell Stem Cell.* 2015;17:260–71.
147. Dongre A, Weinberg RA. New insights into the mechanisms of epithelial–mesenchymal transition and implications for cancer. *Nat Rev Mol Cell Biol.* 2019;20:69–84.

148. Celià-Terrassa T, Meca-Cortés Ó, Mateo F, De Paz AM, Rubio N, Arnal-Estapé A, et al. Epithelial-mesenchymal transition can suppress major attributes of human epithelial tumor-initiating cells. *J Clin Invest*. 2012;122:1849–68.
149. Armstrong AJ, Marengo MS, Oltean S, Kemeny G, Bitting RL, Turnbull JD, et al. Circulating tumor cells from patients with advanced prostate and breast cancer display both epithelial and mesenchymal markers. *Mol Cancer Res*. 2011;9:997–1007.
150. Catherine A-P, Pantel K. Challenges in circulating tumour cell research. *Nat Rev Cancer*. 2014;14:623–31.
151. Grosse-Wilde A, D'Hérouël AF, McIntosh E, Ertaylan G, Skupin A, Kuestner RE, et al. Stemness of the hybrid epithelial/mesenchymal state in breast cancer and its association with poor survival. *PLoS One*. 2015;10:1–28.
152. May CD, Sphyris N, Evans KW, Werden SJ, Guo W, Mani SA. Epithelial-mesenchymal transition and cancer stem cells: A dangerously dynamic duo in breast cancer progression. *Breast Cancer Res*. 2011;13:1–10.
153. Cho H, Kim J, Song H, Sohn KY, Jeon M, Han K-H. Microfluidic technologies for circulating tumor cell isolation. *Analyst*. 2018;143:2936–70.
154. Chaffer CL, Brueckmann I, Scheel C, Kaestli AJ, Wiggins PA, Rodrigues LO, et al. Normal and neoplastic nonstem cells can spontaneously convert to a stem-like state. *Proc Natl Acad Sci U S A*. 2011;108:7950–5.
155. Klevebring D, Rosin G, Ma R, Lindberg J, Czene K, Kere J, et al. Sequencing of breast cancer stem cell populations indicates a dynamic conversion between differentiation states in vivo. *Breast Cancer Res*. 2014;16:1–7.
156. Gilkes DM, Semenza GL. Role of hypoxia-inducible factors in breast cancer metastasis. *Futur Oncol*. 2013;9:1623–36.
157. Peiró CHF, Encina JA, Perez MM, Aquino GSA, Veiga GL, Fonseca F, et al. The role of hypoxia-induced factor 1 α in breast cancer. *J Cancer Metastasis Treat*. 2019;2019.
158. Moriyama H, Moriyama M, Ozawa T, Tsuruta D, Iguchi T, Tamada S, et al. Notch Signaling Enhances Stemness by Regulating Metabolic Pathways Through Modifying p53, NF- κ B, and HIF-1 α . *Stem Cells Dev*. 2018;27:935–47.
159. Mancini P, Angeloni A, Risi E, Orsi E, Mezi S. Standard of care and promising new agents for triple negative metastatic breast cancer. *Cancers (Basel)*. 2014;6:2187–223.
160. Carey LA, Dees EC, Sawyer L, Gatti L, Moore DT, Collichio F, et al. The triple negative paradox: Primary tumor chemosensitivity of breast cancer subtypes. *Clin Cancer Res*. 2007;13:2329–34.

161. Cortazar P, Zhang L, Untch M, Mehta K, Costantino JP, Wolmark N, et al. Pathological complete response and long-term clinical benefit in breast cancer: The CTNeoBC pooled analysis. *Lancet*. 2014;384:164–72.
162. Von Minckwitz G, Untch M, Blohmer JU, Costa SD, Eidtmann H, Fasching PA, et al. Definition and impact of pathologic complete response on prognosis after neoadjuvant chemotherapy in various intrinsic breast cancer subtypes. *J Clin Oncol*. 2012;30:1796–804.
163. Bonotto M, Gerratana L, Poletto E, Driol P, Giangreco M, Russo S, et al. Measures of Outcome in Metastatic Breast Cancer: Insights From a Real-World Scenario. *Oncologist*. 2014;19:608–15.
164. Bianchini G, Balko JM, Mayer IA, Sanders ME, Gianni L. Triple-negative breast cancer: Challenges and opportunities of a heterogeneous disease. *Nat Rev Clin Oncol*. 2016;13:674–90.
165. Won KA, Spruck C. Triple-negative breast cancer therapy: Current and future perspectives. *Int J Oncol*. 2020;57:1245–61.
166. Mayer LD, Janoff AS. Optimizing combination chemotherapy by controlling drug ratios. *Mol Interv*. 2007;7:216–23.
167. Cardoso F, Paluch-Shimon S, Senkus E, Curigliano G, Aapro MS, André F, et al. 5th ESO-ESMO international consensus guidelines for advanced breast cancer (ABC 5). *Ann Oncol Off J Eur Soc Med Oncol*. 2020/09/23. 2020;31:1623–49.
168. Yadav BS, Sharma SC, Chanana P, Jhamb S. Systemic treatment strategies for triple-negative breast cancer. *World J Clin Oncol*. 2014;5:125–33.
169. Mylavarapu S, Das A, Roy M. Role of BRCA mutations in the modulation of response to platinum therapy. *Front Oncol*. 2018;8:1–11.
170. Balko JM, Giltane JM, Wang K, Schwarz LJ, Christian D, Cook RS, et al. Molecular profiling of the residual disease of triple-negative breast cancers after neoadjuvant chemotherapy identifies actionable therapeutic targets. *Cancer discov*. 2014;4:232–45.
171. Lyons TG. Targeted Therapies for Triple-Negative Breast Cancer. *Curr Treat Options Oncol. Current Treatment Options in Oncology*; 2019;20.
172. Banerjee S, Kaye S. PARP inhibitors in BRCA gene-mutated ovarian cancer and beyond. *Curr Oncol Rep*. 2011;13:442–9.
173. Okuma HS, Yonemori K. BRCA Gene Mutations and Poly(ADP-Ribose) Polymerase Inhibitors in Triple-Negative Breast Cancer BT - Translational Research in Breast Cancer: Biomarker Diagnosis, Targeted Therapies and Approaches to Precision Medicine. In: Song E, Hu H, editors. Singapore: Springer Singapore; 2017. p. 271–86.
174. Bürkle A. Poly(APD-ribosyl)ation, a DNA damage-driven protein modification and regulator of genomic instability. *Cancer Lett*. 2001;163:1–5.

175. Farmer H, McCabe N, Lord CJ, Tutt ANJ, Johnson DA, Richardson TB, et al. Targeting the DNA repair defect in BRCA mutant cells as a therapeutic strategy. *Nature*. 2005;434:917–21.
176. Kaufman B, Shapira-Frommer R, Schmutzler RK, Audeh MW, Friedlander M, Balmaña J, et al. Olaparib monotherapy in patients with advanced cancer and a germline BRCA1/2 mutation. *J Clin Oncol*. 2015;33:244–50.
177. Robson M, Im S-A, Senkus E, Xu B, Domchek SM, Masuda N, et al. Olaparib for Metastatic Breast Cancer in Patients with a Germline BRCA Mutation. *N Engl J Med*. 2017;377:523–33.
178. Litton JK, Rugo HS, Ettl J, Hurvitz SA, Gonçalves A, Lee K-H, et al. Talazoparib in Patients with Advanced Breast Cancer and a Germline BRCA Mutation. *N Engl J Med*. 2018;379:753–63.
179. Schmid P, Adams S, Rugo HS, Schneeweiss A, Barrios CH, Iwata H, et al. Atezolizumab and Nab-Paclitaxel in Advanced Triple-Negative Breast Cancer. *N Engl J Med*. Massachusetts Medical Society; 2018;379:2108–21.
180. Bardia A, Mayer IA, Diamond JR, Moroosse RL, Isakoff SJ, Starodub AN, et al. Efficacy and Safety of Anti-Trop-2 Antibody Drug Conjugate Sacituzumab Govitecan (IMMU-132) in Heavily Pretreated Patients With Metastatic Triple-Negative Breast Cancer. *J Clin Oncol*. 2017/03/14. American Society of Clinical Oncology; 2017;35:2141–8.
181. Modi S, Puzstai L, Forero A, Mita M, Miller KD, Weise A, et al. Phase 1 study of the antibody-drug conjugate SGN-LIV1A in patients with heavily pretreated triple-negative metastatic breast cancer. *Cancer Res*. 2018;78:PD3-14.
182. Zardavas D, te Marvelde L, Milne RL, Fumagalli D, Fountzilias G, Kotoula V, et al. Tumor PIK3CA Genotype and Prognosis in Early-Stage Breast Cancer: A Pooled Analysis of Individual Patient Data. *J Clin Oncol*. 2018;36:981–90.
183. Kim S-B, Dent R, Im S-A, Espié M, Blau S, Tan AR, et al. Ipatasertib plus paclitaxel versus placebo plus paclitaxel as first-line therapy for metastatic triple-negative breast cancer (LOTUS): a multicentre, randomised, double-blind, placebo-controlled, phase 2 trial. *Lancet Oncol*. Elsevier; 2017;18:1360–72.
184. Dent R, Im S-A, Espie M, Blau S, Tan AR, Isakoff SJ, et al. Overall survival (OS) update of the double-blind placebo (PBO)-controlled randomized phase 2 LOTUS trial of first-line ipatasertib (IPAT) + paclitaxel (PAC) for locally advanced/metastatic triple-negative breast cancer (mTNBC). *J Clin Oncol*. Wolters Kluwer; 2018;36:1008.
185. Schmid P, Abraham J, Chan S, Wheatley D, Brunt M, Nemsadze G, et al. AZD5363 plus paclitaxel versus placebo plus paclitaxel as first-line therapy for metastatic triple-negative breast cancer (PAKT): A randomised, double-blind, placebo-controlled, phase II trial. *J Clin Oncol*. Wolters Kluwer; 2018;36:1007.
186. Gupta GK, Collier AL, Lee D, Hofer RA, Zheleva V, van Reesema LLS, et al. Perspectives on triple-negative breast cancer: Current treatment strategies, unmet needs, and potential targets for future therapies. *Cancers (Basel)*. 2020;12:1–33.

187. Park S-Y, Choi J-H, Nam J-S. Targeting cancer stem cells in TNBC. *Cancers (Basel)*. 2019;11.
188. Voon DC, Huang RY, Jackson RA, Thiery JP. The EMT spectrum and therapeutic opportunities. *Mol Oncol*. 2017;11:878–91.
189. Van Phuc P, Nhan PLC, Nhung TH, Tam NT, Hoang NM, Tue VG, et al. Downregulation of CD44 reduces doxorubicin resistance of CD44+CD24- breast cancer cells. *Onco Targets Ther*. 2011;4:71–8.
190. Pham P V., Phan NLC, Nguyen NT, Truong NH, Duong TT, Le D V., et al. Differentiation of breast cancer stem cells by knockdown of CD44: Promising differentiation therapy. *J Transl Med*. 2011;9:209.
191. Ohlfest JR, Zellmer DM, Panyam J, Swaminathan SK, Oh S, Waldron NN, et al. Immunotoxin targeting CD133+ breast carcinoma cells. *Drug Deliv Transl Res*. 2013;3:195–204.
192. Croker AK, Allan AL. Inhibition of aldehyde dehydrogenase (ALDH) activity reduces chemotherapy and radiation resistance of stem-like ALDH hiCD44 + human breast cancer cells. *Breast Cancer Res Treat*. 2012;133:75–87.
193. Kim S-H, Singh S V. Mammary cancer chemoprevention by withaferin A is accompanied by in vivo suppression of self-renewal of cancer stem cells. *Cancer Prev Res (Phila)*. 2014;7:738–47.
194. Schott AF, Landis MD, Dontu G, Griffith KA, Layman RM, Krop I, et al. Preclinical and clinical studies of gamma secretase inhibitors with docetaxel on human breast tumors. *Clin Cancer Res*. 2013;19:1512–24.
195. Krop I, Demuth T, Guthrie T, Wen PY, Mason WP, Chinnaiyan P, et al. Phase I pharmacologic and pharmacodynamic study of the gamma secretase (Notch) inhibitor MK-0752 in adult patients with advanced solid tumors. *J Clin Oncol*. 2012;30:2307–13.
196. Shan NL, Wahler J, Lee HJ, Bak MJ, Gupta S Das, Maehr H, et al. Vitamin D compounds inhibit cancer stem-like cells and induce differentiation in triple negative breast cancer. *J Steroid Biochem Mol Biol*. 2017;173:122–9.
197. Huang C, Chen Y, Liu H, Yang J, Song X, Zhao J, et al. Celecoxib targets breast cancer stem cells by inhibiting the synthesis of prostaglandin E2 and down-regulating the Wnt pathway activity. *Oncotarget*. 2017;8:115254–69.
198. Gurney A, Axelrod F, Bond CJ, Cain J, Chartier C, Donigan L, et al. Wnt pathway inhibition via the targeting of Frizzled receptors results in decreased growth and tumorigenicity of human tumors. *Proc Natl Acad Sci U S A*. 2012;109:11717–22.
199. Zhang Y, Wang X. Targeting the Wnt/ β -catenin signaling pathway in cancer. *J Hematol Oncol*. 2020;13:1–16.

200. Bhateja P, Cherian M, Majumder S, Ramaswamy B. The Hedgehog Signaling Pathway: A Viable Target in Breast Cancer? *Cancers (Basel)*. 2019;11.
201. Mukherjee S, Frolova N, Sadlonova A, Novak Z, Steg A, Page GP, et al. Hedgehog signaling and response to cyclopamine differ in epithelial and stromal cells in benign breast and breast cancer. *Cancer Biol Ther*. 2006;5:674–83.
202. Merchant AA, Matsui W. Targeting Hedgehog - A cancer stem cell pathway. *Clin Cancer Res*. 2010;16:3130–40.
203. Cazet AS, Hui MN, Elsworth BL, Wu SZ, Roden D, Chan CL, et al. Targeting stromal remodeling and cancer stem cell plasticity overcomes chemoresistance in triple negative breast cancer. *Nat Commun*. 2018;9:1–18.
204. Koike Y, Ohta Y, Saitoh W, Yamashita T, Kanomata N, Moriya T, et al. Anti-cell growth and anti-cancer stem cell activities of the non-canonical hedgehog inhibitor GANT61 in triple-negative breast cancer cells. *Breast Cancer*. 2017;24:683–93.
205. Dragu DL, Necula LG, Bleotu C, Diaconu CC, Chivu-Economescu M. Therapies targeting cancer stem cells: Current trends and future challenges. *World J Stem Cells*. 2015;7:1185–201.
206. Moitra K. Overcoming Multidrug Resistance in Cancer Stem Cells. *Biomed Res Int*. 2015;2015.
207. Cho Y, Kim YK. Cancer Stem Cells as a Potential Target to Overcome Multidrug Resistance. *Front Oncol*. 2020;10:1–10.
208. Schott AF, Goldstein LJ, Cristofanilli M, Ruffini PA, McCanna S, Reuben JM, et al. Phase Ib pilot study to evaluate reparixin in combination with weekly paclitaxel in patients with HER-2–negative metastatic breast cancer. *Clin Cancer Res*. 2017;23:5358–65.
209. Ginestier C, Liu S, Diebel ME, Korkaya H, Luo M, Brown M, et al. CXCR1 blockade selectively targets human breast cancer stem cells in vitro and in xenografts. *J Clin Invest*. 2010;120:485–97.
210. Jin X, Jin X, Kim H. Cancer stem cells and differentiation therapy. *Tumor Biol*. 2017;39:1–11.
211. He YC, Zhou FL, Shen Y, Liao DF, Cao D. Apoptotic death of cancer stem cells for cancer therapy. *Int J Mol Sci*. 2014;15:8335–51.
212. Ray A, Vasudevan S, Sengupta S. 6-Shogaol Inhibits Breast Cancer Cells and Stem Cell-Like Spheroids By Modulation of Notch Signaling Pathway and Induction of Autophagic Cell Death. *PLoS One*. 2015;10:1–23.
213. Wu CH, Hong BH, Ho CT, Yen GC. Targeting cancer stem cells in breast cancer: Potential anticancer properties of 6-shogaol and pterostilbene. *J Agric Food Chem*. 2015;63:2432–41.

214. Zhou J, Zhang H, Gu P, Margolick JB, Yin D, Zhang Y. Cancer stem/progenitor cell active compound 8-quinolinol in combination with paclitaxel achieves an improved cure of breast cancer in the mouse model. *Breast Cancer Res Treat.* 2009;115:269–77.
215. Martirosyan A, Leonard S, Shi X, Griffith B, Gannett P, Strobl J. Actions of a histone deacetylase inhibitor NSC3852 (5-nitroso-8-quinolinol) link reactive oxygen species to cell differentiation and apoptosis in MCF-7 human mammary tumor cells. *J Pharmacol Exp Ther.* 2006;317:546–52.
216. Ahmed M, Jinks N, Babaei-Jadidi R, Kashfi H, Castellanosuribe M, May ST, et al. Repurposing antibacterial AM404 as a potential anticancer drug for targeting colorectal cancer stem-like cells. *Cancers (Basel).* 2020;12.
217. Takehara M, Hoshino T, Namba T, Yamakawa N, Mizushima T. Acetaminophen-induced differentiation of human breast cancer stem cells and inhibition of tumor xenograft growth in mice. *Biochem Pharmacol.* 2011;81:1124–35.
218. Nigjeh SE, Yeap SK, Nordin N, Rahman H, Rosli R. In vivo anti-tumor effects of citral on 4T1 breast cancer cells via induction of apoptosis and downregulation of aldehyde dehydrogenase activity. *Molecules.* 2019;24.
219. Thomas ML, de Antueno R, Coyle KM, Sultan M, Cruickshank BM, Giacomantonio MA, et al. Citral reduces breast tumor growth by inhibiting the cancer stem cell marker ALDH1A3. *Mol Oncol.* 2016;10:1485–96.
220. Kolev VN, Tam WF, Wright QG, McDermott SP, Vidal CM, Shapiro IM, et al. Inhibition of FAK kinase activity preferentially targets cancer stem cells. *Oncotarget.* 2017;8:51733–47.
221. Navas T, Pfister TD, Colantonio S, Aziz A, Dieckman L, Saul RG, et al. Novel antibody reagents for characterization of drug- and tumor microenvironment-induced changes in epithelial-mesenchymal transition and cancer stem cells. *PLoS One.* 2018;13:1–25.
222. Yip NC, Fombon IS, Liu P, Brown S, Kannappan V, Armesilla AL, et al. Disulfiram modulated ROS-MAPK and NFB pathways and targeted breast cancer cells with cancer stem cell-like properties. *Br J Cancer.* 2011;104:1564–74.
223. Kim YJ, Kim JY, Lee N, Oh E, Sung D, Cho TM, et al. Disulfiram suppresses cancer stem-like properties and STAT3 signaling in triple-negative breast cancer cells. *Biochem Biophys Res Commun.* 2017;486:1069–76.
224. Yang Z, Guo F, Albers AE, Sehoul J, Kaufmann AM. Disulfiram modulates ROS accumulation and overcomes synergistically cisplatin resistance in breast cancer cell lines. *Biomed Pharmacother.* 2019;113:108727.
225. Yunokawa M, Koizumi F, Kitamura Y, Katanasaka Y, Okamoto N, Kodaira M, et al. Efficacy of everolimus, a novel mTOR inhibitor, against basal-like triple-negative breast cancer cells. *Cancer Sci.* 2012;103:1665–71.

226. Chen L, Yang G, Dong H. Everolimus reverses palbociclib resistance in ER+ human breast cancer cells by inhibiting phosphatidylinositol 3-kinase(PI3K)/Akt/ mammalian target of rapamycin (mTOR) pathway. *Med Sci Monit.* 2019;25:77–86.
227. Oh E, Kim YJ, An H, Sung D, Cho TM, Farrand L, et al. Flubendazole elicits anti-metastatic effects in triple-negative breast cancer via STAT3 inhibition. *Int J Cancer.* 2018;143:1978–93.
228. Kim YJ, Sung D, Oh E, Cho Y, Cho TM, Farrand L, et al. Flubendazole overcomes trastuzumab resistance by targeting cancer stem-like properties and HER2 signaling in HER2-positive breast cancer. *Cancer Lett.* 2018;412:118–30.
229. Hou ZJ, Luo X, Zhang W, Peng F, Cui B, Wu SJ, et al. Flubendazole, FDA-approved anthelmintic, targets breast cancer stem-like cells. *Oncotarget.* 2015;6:6326–40.
230. Jiang F, Li Y, Mu J, Hu C, Zhou M, Wang X, et al. Glabridin inhibits cancer stem cell-like properties of human breast cancer cells: An epigenetic regulation of miR-148a/SMAd2 signaling. *Mol Carcinog.* 2016;55:929–40.
231. Qian J, Xia M, Liu W, Li L, Yang J, Mei Y, et al. Glabridin resensitizes p-glycoprotein-overexpressing multidrug-resistant cancer cells to conventional chemotherapeutic agents. *Eur J Pharmacol.* 2019;852:231–43.
232. Lin PH, Chiang YF, Shieh TM, Chen HY, Shih CK, Wang TH, et al. Dietary compound isoliquiritigenin, an antioxidant from licorice, suppresses triple-negative breast tumor growth via apoptotic death program activation in cell and xenograft animal models. *Antioxidants.* 2020;9.
233. Peng F, Tang H, Liu P, Shen J, Guan X, Xie X, et al. Isoliquiritigenin modulates MIR-374a/PTEN/Akt axis to suppress breast cancer tumorigenesis and metastasis. *Sci Rep.* 2017;7:1–14.
234. Jung JW, Park SB, Lee SJ, Seo MS, Trosko JE, Kang KS. Metformin represses self-renewal of the human breast carcinoma stem cells via inhibition of estrogen receptor-mediated OCT4 expression. *PLoS One.* 2011;6:1–9.
235. Vazquez-Martin A, Oliveras-Ferraros C, Del Barco S, Martin-Castillo B, Menendez JA. The anti-diabetic drug metformin suppresses self-renewal and proliferation of trastuzumab-resistant tumor-initiating breast cancer stem cells. *Breast Cancer Res Treat.* 2011;126:355–64.
236. Liu J, Chen X, Ward T, Pegram M, Shen K. Combined niclosamide with cisplatin inhibits epithelial-mesenchymal transition and tumor growth in cisplatin-resistant triple-negative breast cancer. *Tumor Biol.* 2016;37:9825–35.
237. Wang YC, Chao TK, Chang CC, Yo Y Te, Yu MH, Lai HC. Drug Screening Identifies Niclosamide as an Inhibitor of Breast Cancer Stem-Like Cells. *PLoS One.* 2013;8.
238. Sun M, Zhang N, Wang X, Li Y, Qi W, Zhang H, et al. Hedgehog pathway is involved in nitidine chloride induced inhibition of epithelial-mesenchymal transition and cancer stem cells-like properties in breast cancer cells. *Cell Biosci.* 2016;6:1–14.

239. Pan X, Han H, Wang L, Yang L, Li R, Li Z, et al. Nitidine Chloride inhibits breast cancer cells migration and invasion by suppressing c-Src/FAK associated signaling pathway. *Cancer Lett.* 2011;313:181–91.
240. Qin G, Li Y, Xu X, Wang X, Zhang K, Tang Y, et al. Panobinostat (LBH589) inhibits Wnt/ β -catenin signaling pathway via upregulating APC expression in breast cancer. *Cell Signal.* 2019;59:62–75.
241. Kai M, Kanaya N, Wu S V., Mendez C, Nguyen D, Luu T, et al. Targeting breast cancer stem cells in triple-negative breast cancer using a combination of LBH589 and salinomycin. *Breast Cancer Res Treat.* 2015;151:281–94.
242. Tyagi M, Patro BS. Salinomycin reduces growth, proliferation and metastasis of cisplatin resistant breast cancer cells via NF- κ B deregulation. *Toxicol Vitro.* 2019;60:125–33.
243. Kamlund S, Janicke B, Alm K, Oredsson S. Salinomycin treatment specifically inhibits cell proliferation of cancer stem cells revealed by longitudinal single cell tracking in combination with fluorescence microscopy. *Appl Sci.* 2020;10.
244. Kolev VN, Wright QG, Vidal CM, Ring JE, Shapiro IM, Ricono J, et al. PI3K/mTOR dual inhibitor VS-5584 preferentially targets cancer stem cells. *Cancer Res.* 2015;75:446–55.
245. Hart S, Novotny-Diermayr V, Goh KC, Williams M, Tan YC, Ong LC, et al. VS-5584, a novel and highly selective PI3K/mTOR kinase inhibitor for the treatment of cancer. *Mol Cancer Ther.* 2013;12:151–61.
246. Ookura M, Fujii T, Yagi H, Ogawa T, Kishi S, Hosono N, et al. YM155 exerts potent cytotoxic activity against quiescent (G0/G1) multiple myeloma and bortezomib resistant cells via inhibition of survivin and Mcl-1. *Oncotarget.* 2017;8:111535–50.
247. Véquaud E, Séveno C, Loussouarn D, Engelhart L, Campone M, Juin P, et al. YM155 potently triggers cell death in breast cancer cells through an autophagy-NF- κ B network. *Oncotarget.* 2015;6:13476–86.
248. Mokhtari RB, Homayouni TS, Baluch N, Morgatskaya E, Kumar S, Das B, et al. Combination therapy in combating cancer. *Oncotarget.* 2017;8:38022–43.
249. Fisusi FA, Akala EO. Drug Combinations in Breast Cancer Therapy. *Pharm Nanotechnol.* 2019;7:3–23.
250. Sicklick JK, Kato S, Okamura R, Schwaederle M, Hahn ME, Williams CB, et al. Molecular profiling of cancer patients enables personalized combination therapy: the I-PREDICT study. *Nat Med.* 2019;25:744–50.
251. Ligibel JA, Winer EP. Trastuzumab/chemotherapy combinations in metastatic breast cancer. *Semin Oncol.* 2002;29:38–43.
252. Wang X, Zhang H, Chen X. Drug resistance and combating drug resistance in cancer. *Cancer Drug Resist.* 2019;

253. Yao Y, Zhou Y, Liu L, Xu Y, Chen Q, Wang Y, et al. Nanoparticle-Based Drug Delivery in Cancer Therapy and Its Role in Overcoming Drug Resistance. *Front Mol Biosci.* 2020;7:193.
254. Shi J, Kantoff PW, Wooster R, Farokhzad OC. Cancer nanomedicine: progress, challenges and opportunities. *Nat Rev Cancer.* 2017;17:20–37.
255. Pearce AK, O'Reilly RK. Insights into Active Targeting of Nanoparticles in Drug Delivery: Advances in Clinical Studies and Design Considerations for Cancer Nanomedicine. *Bioconjug Chem.* 2019;30:2300–11.
256. O'Reilly EA, Gubbins L, Sharma S, Tully R, Guang MHZ, Weiner-Gorzal K, et al. The fate of chemoresistance in triple negative breast cancer (TNBC). *BBA Clin.* 2015;3:257–75.
257. Wicki A, Witzigmann D, Balasubramanian V, Huwyler J. Nanomedicine in cancer therapy: challenges, opportunities, and clinical applications. *J Control Release.* 2015;200:138–57.
258. Boix-Montesinos P, Soriano-Teruel PM, Armiñán A, Orzáez M, Vicent MJ. The past, present, and future of breast cancer models for nanomedicine development. *Adv Drug Deliv Rev.* 2021;173:306–30.
259. Gabizon AA. Pegylated liposomal doxorubicin: Metamorphosis of an old drug into a new form of chemotherapy. *Cancer Invest.* 2001;19:424–36.
260. Henderson IC, Bhatia V. Nab-paclitaxel for breast cancer: a new formulation with an improved safety profile and greater efficacy. *Expert Rev Anticancer Ther.* 2007;7:919–43.
261. Tran S, DeGiovanni P-J, Piel B, Rai P. Cancer nanomedicine: a review of recent success in drug delivery. *Clin Transl Med.* 2017;6:44.
262. Attia MF, Anton N, Wallyn J, Omran Z, Vandamme TF. An overview of active and passive targeting strategies to improve the nanocarriers efficiency to tumour sites. *J Pharm Pharmacol.* John Wiley & Sons, Ltd; 2019;71:1185–98.
263. Wu D, Si M, Xue HY, Wong HL. Nanomedicine applications in the treatment of breast cancer: Current state of the art. *Int J Nanomedicine.* 2017;12:5879–92.
264. Barenholz Y. Doxil®--the first FDA-approved nano-drug: lessons learned. *J Control Release.* 2012;160:117–34.
265. Gradishar WJ, Tjulandin S, Davidson N, Shaw H, Desai N, Bhar P, et al. Phase III trial of nanoparticle albumin-bound paclitaxel compared with polyethylated castor oil-based paclitaxel in women with breast cancer. *J Clin Oncol.* 2005;23:7794–803.
266. Lluch A, Álvarez I, Muñoz M, Seguí MÁ, Tusquets I, García-Estévez L. Treatment innovations for metastatic breast cancer: Nanoparticle albumin-bound (NAB) technology targeted to tumors. *Crit Rev Oncol Hematol.* 2014;89:62–72.

267. Guo Z, Wang F, Di Y, Yao L, Yu X, Fu D, et al. Antitumor effect of gemcitabine-loaded albumin nanoparticle on gemcitabine-resistant pancreatic cancer induced by low hENT1 expression. *Int J Nanomedicine*. 2018;13:4869–80.
268. Amiri-Kordestani L, Blumenthal GM, Xu QC, Zhang L, Tang SW, Ha L, et al. FDA Approval: Ado-Trastuzumab Emtansine for the Treatment of Patients with HER2-Positive Metastatic Breast Cancer. *Clin Cancer Res*. 2014;20:4436 LP – 4441.
269. von Minckwitz G, Huang C-S, Mano MS, Loibl S, Mamounas EP, Untch M, et al. Trastuzumab Emtansine for Residual Invasive HER2-Positive Breast Cancer. *N Engl J Med*. 2019;380:617–28.
270. Biswas S, Kumari P, Lakhani PM, Ghosh B. Recent advances in polymeric micelles for anti-cancer drug delivery. *Eur J Pharm Sci*. 2016;83:184–202.
271. Aliabadi HM, Lavasanifar A. Polymeric micelles for drug delivery. *Expert Opin Drug Deliv*. 2006;3:139–62.
272. Avramović N, Mandić B, Savić-Radojević A, Simić T. Polymeric nanocarriers of drug delivery systems in cancer therapy. *Pharmaceutics*. 2020;12:1–17.
273. Oerlemans C, Bult W, Bos M, Storm G, Nijssen JFW, Hennink WE. Polymeric micelles in anticancer therapy: Targeting, imaging and triggered release. *Pharm Res*. 2010;27:2569–89.
274. Chou T-C. Theoretical basis, experimental design, and computerized simulation of synergism and antagonism in drug combination studies. *Pharmacol Rev*. 2006;58:621–81.
275. Hellemans J, Mortier G, De Paepe A, Speleman F, Vandesomepele J. qBase relative quantification framework and software for management and automated analysis of real-time quantitative PCR data. *Genome Biol. BioMed Central*; 2007;8:R19.
276. Jenkins DE, Hornig YS, Oei Y, Dusich J, Purchio T. Bioluminescent human breast cancer cell lines that permit rapid and sensitive in vivo detection of mammary tumors and multiple metastases in immune deficient mice. *Breast Cancer Res*. 2005/04/08. *BioMed Central*; 2005;7:R444–54.
277. Byrne FL, McCarroll JA, Kavallaris M. Analyses of Tumor Burden In Vivo and Metastasis Ex Vivo Using Luciferase-Expressing Cancer Cells in an Orthotopic Mouse Model of Neuroblastoma BT - RNA Imaging: Methods and Protocols. In: Medarova Z, editor. New York, NY: Springer New York; 2016. p. 61–77.
278. Simmons JK, Hildreth 3rd BE, Supsavhad W, Elshafae SM, Hassan BB, Dirksen WP, et al. Animal Models of Bone Metastasis. *Vet Pathol*. 2015/05/28. 2015;52:827–41.
279. Yeh H-W, Karmach O, Ji A, Carter D, Martins-Green MM, Ai H-W. Red-shifted luciferase-luciferin pairs for enhanced bioluminescence imaging. *Nat Methods*. 2017/09/04. 2017;14:971–4.

280. Kim JE, Kalimuthu S, Ahn B-C. In vivo cell tracking with bioluminescence imaging. *Nucl Med Mol Imaging* (2010). 2014/11/26. Springer Berlin Heidelberg; 2015;49:3–10.
281. Adams Jr ST, Miller SC. Beyond D-luciferin: expanding the scope of bioluminescence imaging in vivo. *Curr Opin Chem Biol*. 2014/08/01. 2014;21:112–20.
282. Baklaushev VP, Kilpeläinen A, Petkov S, Abakumov MA, Grinenko NF, Yusubalieva GM, et al. Luciferase Expression Allows Bioluminescence Imaging But Imposes Limitations on the Orthotopic Mouse (4T1) Model of Breast Cancer. *Sci Rep*. 2017;7:7715.
283. Al-Hajj M, Wicha MS, Benito-Hernandez A, Morrison SJ, Clarke MF. Prospective identification of tumorigenic breast cancer cells. *Proc Natl Acad Sci U S A*. 2003;100:3983–8.
284. Jin L, Han B, Siegel E, Cui Y, Giuliano A, Cui X. Breast cancer lung metastasis: Molecular biology and therapeutic implications. *Cancer Biol Ther*. 2018/04/30. Taylor & Francis; 2018;19:858–68.
285. Pushpakom S, Iorio F, Eyers PA, Escott KJ, Hopper S, Wells A, et al. Drug repurposing: Progress, challenges and recommendations. *Nat Rev Drug Discov*. 2018;18:41–58.
286. Kathryn JC, Sireesha V G, Stanley L. Triple Negative Breast Cancer Cell Lines: One Tool in the Search for Better Treatment of Triple Negative Breast Cancer. *Breast Dis*. 2012;32:35–48.
287. Balko JM, Bhola NE, Dugger TC, Kuba MG, Sánchez V, Sanders M, et al. TGF- β inhibition enhances chemotherapy.pdf. *J Clin Invest*. 2013;123:1348–58.
288. Creighton CJ, Li X, Landis M, Dixon JM, Neumeister VM, Sjolund A, et al. Residual breast cancers after conventional therapy display mesenchymal as well as tumor-initiating features. *Proc Natl Acad Sci U S A*. 2009;106:13820–5.
289. Wei W, Liu H, Yuan J, Yao Y. Targeting Wnt/ β -catenin by anthelmintic drug niclosamide overcomes paclitaxel resistance in esophageal cancer. *Fundam Clin Pharmacol*. 2020;0–1.
290. Gener P, Rafael D, Schwartz S, Andrade F. The Emerging Role of Nanomedicine in the Advances of Oncological Treatment. *Nanoparticles Life Sci Biomed*. 1st Editio. Pan Stanford Publishing; 2018. p. 42.
291. Lu B, Huang X, Mo J, Zhao W. Drug Delivery Using Nanoparticles for Cancer Stem-Like Cell Targeting. *Front Pharmacol*. Frontiers Media S.A.; 2016;7:84.
292. Cagel M, Tesan FC, Bernabeu E, Salgueiro MJ, Zubillaga MB, Moretton MA, et al. Polymeric mixed micelles as nanomedicines: Achievements and perspectives. *Eur J Pharm Biopharm*. 2017;113:211–28.
293. Pignatello R, Corsaro R. Polymeric Nanomicelles of Soluplus® as a Strategy for Enhancing the Solubility, Bioavailability and Efficacy of Poorly Soluble Active Compounds. *Curr Nanomedicine*. 2019;09.

294. Linn M, Collnot E-M, Djuric D, Hempel K, Fabian E, Kolter K, et al. Soluplus® as an effective absorption enhancer of poorly soluble drugs in vitro and in vivo. *Eur J Pharm Sci.* 2012;45:336–43.
295. Miller DW, Batrakova E V, Kabanov A V. Inhibition of multidrug resistance-associated protein (MRP) functional activity with pluronic block copolymers. *Pharm Res.* 1999;16:396–401.
296. Bogman K, Erne-Brand F, Alsenz J, Drewe J. The Role of Surfactants in the Reversal of Active Transport Mediated by Multidrug Resistance Proteins. *J Pharm Sci. Elsevier;* 2003;92:1250–61.
297. Collnot E-M, Baldes C, Wempe M, Kappl R, Hüttermann J, Hyatt J, et al. Mechanism of Inhibition of P-Glycoprotein Mediated Efflux by Vitamin E TPGS: Influence on ATPase Activity and Membrane Fluidity. *Mol Pharm.* 2007;4:465–74.
298. Moretton MA, Bernabeu E, Grotz E, Gonzalez L, Zubillaga M, Chiappetta DA. A glucose-targeted mixed micellar formulation outperforms Genexol in breast cancer cells. *Eur J Pharm Biopharm.* 2017;114:305–16.
299. Wegmann M, Parola L, Bertera FM, Taira CA, Cagel M, Buontempo F, et al. Novel carvedilol paediatric nanomicelle formulation: in-vitro characterization and in-vivo evaluation. *J Pharm Pharmacol.* 2017;69:544–53.
300. Rafael D, Martínez F, Andrade F, Seras-Franzoso J, Garcia-Aranda N, Gener P, et al. Efficient EGFR mediated siRNA delivery to breast cancer cells by Cetuximab functionalized Pluronic® F127/Gelatin. *Chem Eng J.* 2018;340:81–93.
301. Rafael D, Gener P, Andrade F, Seras-Franzoso J, Montero S, Fernandez Y, et al. AKT2 siRNA delivery with amphiphilic-based polymeric micelles show efficacy against cancer stem cells. *Drug Deliv.* 2018;25:961–72.
302. Andrade F, Rafael D, Vilar-Hernández M, Montero S, Martínez-Trucharte F, Seras-Franzoso J, et al. Polymeric micelles targeted against CD44v6 receptor increase niclosamide efficacy against colorectal cancer stem cells and reduce circulating tumor cells in vivo. *J Control Release.* 2021;331:198–212.
303. Gener P, Montero S, Xandri-Monje H, Díaz-Riascos Z V., Rafael D, Andrade F, et al. Zileuton™ loaded in polymer micelles effectively reduce breast cancer circulating tumor cells and intratumoral cancer stem cells. *Nanomedicine Nanotechnology, Biol Med.* 2020;24:102106.
304. Shantier S, Garelnabi E, Gadkariem E. Development of derivative spectrophotometric and HPLC methods for determination of niclosamide. *J Harmon Res Pharm.* 2015;4:87–92.
305. Falah M, Rayan M, Rayan A. A Novel Paclitaxel Conjugate with Higher Efficiency and Lower Toxicity: A New Drug Candidate for Cancer Treatment. *Int J Mol Sci. MDPI;* 2019;20:4965.
306. Huehnchen P, Boehmerle W, Springer A, Freyer D, Endres M. A novel preventive therapy for paclitaxel-induced cognitive deficits: preclinical evidence from C57BL/6 mice. *Transl Psychiatry.* 2017;7:e1185–e1185.

307. Yo Y-T, Lin Y-W, Wang Y-C, Balch C, Huang R-L, Chan MWY, et al. Growth inhibition of ovarian tumor-initiating cells by niclosamide. *Mol Cancer Ther.* 2012;11:1703–12.
308. Garrido-Castro AC, Lin NU, Polyak K. Insights into molecular classifications of triple-negative breast cancer: Improving patient selection for treatment. *Cancer Discov.* 2019;9:176–98.
309. Mehanna J, Haddad FGH, Eid R, Lambertini M, Kourie HR. Triple-negative breast cancer: Current perspective on the evolving therapeutic landscape. *Int J Womens Health.* 2019;11:431–7.
310. Bonnet D, Dick JE. Human acute myeloid leukemia is organized as a hierarchy that originates from a primitive hematopoietic cell. *Nat Med.* 1997;3:730–7.
311. Al-Hajj M, Clarke MF. Self-renewal and solid tumor stem cells. *Oncogene.* 2004;23:7274–82.
312. Lee KL, Kuo YC, Ho YS, Huang YH. Triple-negative breast cancer: Current understanding and future therapeutic breakthrough targeting cancer stemness. *Cancers (Basel).* 2019;11.
313. Wang H, Wang L, Song Y, Wang S, Huang X, Xuan Q, et al. CD44+/CD24- phenotype predicts a poor prognosis in triple-negative breast cancer. *Oncol Lett.* 2017;14:5890–8.
314. Lee G, Hall RR, Ahmed AU. Cancer Stem Cells: Cellular Plasticity, Niche, and its Clinical Relevance. *J Stem Cell Res Ther.* OMICS Publishing Group; 2016;6.
315. Iliopoulos D, Hirsch HA, Wang G, Struhl K. Inducible formation of breast cancer stem cells and their dynamic equilibrium with non-stem cancer cells via IL6 secretion. *Proc Natl Acad Sci U S A.* 2011/01/10. National Academy of Sciences; 2011;108:1397–402.
316. Shibue T, Weinberg RA. EMT, CSCs, and drug resistance: the mechanistic link and clinical implications. *Nat Rev Clin Oncol.* 2017;14:611–29.
317. Yoshioka T, Umekita Y, Ohi Y, Souda M, Sagara Y, Sagara Y, et al. Aldehyde dehydrogenase 1 expression is a predictor of poor prognosis in node-positive breast cancers: a long-term follow-up study. *Histopathology.* 2011;58:608–16.
318. Jaggupilli A, Elkord E. Significance of CD44 and CD24 as cancer stem cell markers: an enduring ambiguity. *Clin Dev Immunol.* 2012;2012:708036.
319. Ricardo S, Vieira AF, Gerhard R, Leitão D, Pinto R, Cameselle-Teijeiro JF, et al. Breast cancer stem cell markers CD44, CD24 and ALDH1: expression distribution within intrinsic molecular subtype. *J Clin Pathol.* 2011;64:937 LP – 946.
320. Honeth G, Bendahl P-O, Ringnér M, Saal LH, Gruvberger-Saal SK, Lövgren K, et al. The CD44+/CD24- phenotype is enriched in basal-like breast tumors. *Breast Cancer Res.* 2008/06/17. *BioMed Central;* 2008;10:R53–R53.

321. Gerrard L, Zhao D, Clark AJ, Cui W. Stably Transfected Human Embryonic Stem Cell Clones Express OCT4-Specific Green Fluorescent Protein and Maintain Self-Renewal and Pluripotency. *Stem Cells*. 2005;23:124–33.
322. Sajithlal GB, Rothermund K, Zhang F, Dabbs DJ, Latimer JJ, Grant SG, et al. Permanently blocked stem cells derived from breast cancer cell lines. *Stem Cells*. 2010;28:1008–18.
323. Darini CY, Pisani D, Hofman P, Pedeutour F, Sudaka I, Chomienne C, et al. Self-renewal gene tracking to identify tumour-initiating cells associated with metastatic potential. *Oncogene*. 2011;31:2438–49.
324. Turksen K. *Stem Cell Heterogeneity*. Turksen K, editor. 4th Int. Conf. Stem Cell Eng. 2014. New York, NY: Humana Press, New York, NY; 2016.
325. Gener P, Callejo PG, Seras-Franzoso J, Andrade F, Rafael D, Abasolo I, et al. The potential of nanomedicine to alter cancer stem cell dynamics: The impact of extracellular vesicles. *Nanomedicine*. 2020;15:2785–800.
326. Capp J-P. Cancer Stem Cells: From Historical Roots to a New Perspective. *J Oncol*. 2019;2019:1–10.
327. Thankamony AP, Saxena K, Murali R, Jolly MK, Nair R. Cancer Stem Cell Plasticity - A Deadly Deal. *Front Mol Biosci*. 2020;7:79.
328. Poli V, Fagnocchi L, Zippo A. Tumorigenic cell reprogramming and cancer plasticity: Interplay between signaling, microenvironment, and epigenetics. *Stem Cells Int*. Hindawi Limited; 2018.
329. Battle E, Clevers H. Cancer stem cells revisited. *Nat Med*. Nature Publishing Group; 2017;23:1124–34.
330. Shen Y, Schmidt BUS, Kubitschke H, Morawetz EW, Wolf B, Käs JA, et al. Detecting heterogeneity in and between breast cancer cell lines. *Cancer Converg*. Cancer Convergence; 2020;4:1.
331. O’Conor CJ, Chen T, González I, Cao D, Peng Y. Cancer stem cells in triple-negative breast cancer: A potential target and prognostic marker. *Biomark Med*. 2018;12:813–20.
332. Desai A, Yan Y, Gerson SL. Concise Reviews: Cancer Stem Cell Targeted Therapies: Toward Clinical Success. *Stem Cells Transl Med*. 2019;8:75–81.
333. Xing Y, Lin NU, Maurer MA, Chen H, Mahvash A, Sahin A, et al. Phase II trial of AKT inhibitor MK-2206 in patients with advanced breast cancer who have tumors with PIK3CA or AKT mutations, and/or PTEN loss/PTEN mutation. *Breast Cancer Res*. 2019;21:1–12.
334. Zhang Z, Zhou L, Xie N, Nice EC, Zhang T, Cui Y, et al. Overcoming cancer therapeutic bottleneck by drug repurposing. *Signal Transduct Target Ther*. Springer US; 2020;5.

335. Correia AS, Gärtner F, Vale N. Drug combination and repurposing for cancer therapy: the example of breast cancer. *Heliyon*. 2021;7.
336. Dai X, Cheng H, Bai Z, Li J. Breast Cancer Cell Line Classification and Its Relevance with Breast Tumor Subtyping. *J Cancer*. 2017;8:3131–41.
337. Wang D, Huang J, Wang X, Yu Y, Zhang H, Chen Y, et al. The eradication of breast cancer cells and stem cells by 8-hydroxyquinoline-loaded hyaluronan modified mesoporous silica nanoparticle-supported lipid bilayers containing docetaxel. *Biomaterials*. Elsevier Ltd; 2013;34:7662–73.
338. Londoño-Joshi AI, Arend RC, Aristizabal L, Lu W, Samant RS, Metge BJ, et al. Effect of niclosamide on basal-like breast cancers. *Mol Cancer Ther*. 2014;13:800–11.
339. Ye T, Xiong Y, Yan Y, Xia Y, Song X, Liu L, et al. The anthelmintic drug niclosamide induces apoptosis, impairs metastasis and reduces immunosuppressive cells in breast cancer model. *PLoS One*. 2014;9.
340. Jordan MA, Wilson L. Microtubules as a target for anticancer drugs. *Nat Rev Cancer*. 2004;4:253–65.
341. Nawara HM, Afify SM, Hassan G, Zahra MH, Seno A, Seno M. Paclitaxel-Based Chemotherapy Targeting Cancer Stem Cells from Mono- to Combination Therapy. *Biomedicines*. 2021;9:1–17.
342. Huang Y, Sadée W. Membrane transporters and channels in chemoresistance and -sensitivity of tumor cells. *Cancer Lett*. 2006;239:168–82.
343. Tian J, Lo C, Raffa F AI, Dai M, Lebrun J-J. Abstract 144: Dasatinib enhances the effects of paclitaxel on chemotherapy-resistant breast cancer through targeting breast cancer stem cells. *Cancer Res*. 2018;78:144 LP – 144.
344. Fornier MN, Morris PG, Abbruzzi A, D'Andrea G, Gilewski T, Bromberg J, et al. A phase I study of dasatinib and weekly paclitaxel for metastatic breast cancer. *Ann Oncol Off J Eur Soc Med Oncol*. 2011;22:2575–81.
345. Merz M, Komljenovic D, Zwick S, Semmler W, Bäuerle T. Sorafenib tosylate and paclitaxel induce anti-angiogenic, anti-tumour and anti-resorptive effects in experimental breast cancer bone metastases. *Eur J Cancer*. 2011;47:277–86.
346. Nawara HM, Afify SM, Hassan G, Zahra MH, Atallah MN, Mansour H, et al. Paclitaxel and sorafenib: The effective combination of suppressing the self-renewal of cancer stem cells. *Cancers (Basel)*. 2020;12:1–16.
347. Lohiya G, Katti DS. A synergistic combination of niclosamide and doxorubicin as an efficacious therapy for all clinical subtypes of breast cancer. *Cancers (Basel)*. 2021;13:1–24.

348. Krzyszczyk P, Acevedo A, Davidoff EJ, Timmins LM, Marrero-Berrios I, Patel M, et al. The growing role of precision and personalized medicine for cancer treatment. *Technology*. 2020;6:79–100.
349. Gambardella V, Tarazona N, Cejalvo JM, Lombardi P, Huerta M, Roselló S, et al. Personalized Medicine: Recent Progress in Cancer Therapy. *Cancers (Basel)*. 2020;12:1–3.
350. Gajria D, Chandarlapaty S. HER2-amplified breast cancer: Mechanisms of trastuzumab resistance and novel targeted therapies. *Expert Rev Anticancer Ther*. 2011;11:263–75.
351. Ledermann J, Harter P, Gourley C, Friedlander M, Vergote I, Rustin G, et al. Olaparib maintenance therapy in patients with platinum-sensitive relapsed serous ovarian cancer: A preplanned retrospective analysis of outcomes by BRCA status in a randomised phase 2 trial. *Lancet Oncol*. 2014;15:852–61.
352. McCallum L, Lip S, Padmanabhan S. Chapter 18 - Pharmacodynamic Pharmacogenomics. In: Padmanabhan SBT-H of P and SM, editor. San Diego: Academic Press; 2014. p. 365–83.
353. Shangguan F, Liu Y, Ma L, Qu G, Lv Q, An J, et al. Niclosamide inhibits ovarian carcinoma growth by interrupting cellular bioenergetics. *J Cancer*. 2020;11:3454–66.
354. Jin Y, Lu Z, Ding K, Li J, Du X, Chen C, et al. Antineoplastic mechanisms of niclosamide in acute myelogenous leukemia stem cells: Inactivation of the NF- κ B pathway and generation of reactive oxygen species. *Cancer Res*. 2010;70:2516–27.
355. Luo F, Luo M, Rong QX, Zhang H, Chen Z, Wang F, et al. Niclosamide, an antihelmintic drug, enhances efficacy of PD-1/PD-L1 immune checkpoint blockade in non-small cell lung cancer. *J Immunother Cancer*. 2019;7:1–13.
356. Liu C, Armstrong C, Zhu Y, Lou W, Gao AC. Niclosamide enhances abiraterone treatment via inhibition of androgen receptor variants in castration resistant prostate cancer. *Oncotarget*. 2016;7:32210–20.
357. Chen L, Wang L, Shen H, Lin H, Li D. Anthelmintic drug niclosamide sensitizes the responsiveness of cervical cancer cells to paclitaxel via oxidative stress-mediated mTOR inhibition. *Biochem Biophys Res Commun*. 2017;484:416–21.
358. Park IH, Sohn JH, Kim SB, Lee KS, Chung JS, Lee SH, et al. An Open-Label, Randomized, Parallel, Phase III Trial Evaluating the Efficacy and Safety of Polymeric Micelle-Formulated Paclitaxel Compared to Conventional Cremophor EL-Based Paclitaxel for Recurrent or Metastatic HER2-Negative Breast Cancer. *Cancer Res Treat*. 2017;49:569–77.
359. Yin L, Gao Y, Zhang X, Wang J, Ding D, Zhang Y, et al. Niclosamide sensitizes triple-negative breast cancer cells to ionizing radiation in association with the inhibition of Wnt/ β -catenin signaling. *Oncotarget*. 2016;7:42126–38.
360. Barbosa EJ, Löbenberg R, de Araujo GLB, Bou-Chacra NA. Niclosamide repositioning for treating cancer: Challenges and nano-based drug delivery opportunities. *Eur J Pharm Biopharm*. Elsevier B.V.; 2019;141:58–69.

361. Gupta R, Luxami V, Paul K. Insights of 8-hydroxyquinolines: A novel target in medicinal chemistry. *Bioorg Chem.* 2021;108:104633.
362. Gelderblom H, Verweij J, Nooter K, Sparreboom A. Cremophor EL: the drawbacks and advantages of vehicle selection for drug formulation. *Eur J Cancer.* 2001;37:1590–8.
363. Sparreboom A, van Tellingen O, Nooijen WJ, Beijnen JH. Nonlinear pharmacokinetics of paclitaxel in mice results from the pharmaceutical vehicle Cremophor EL. *Cancer Res.* 1996;56:2112–5.
364. Suri SS, Fenniri H, Singh B. Nanotechnology-based drug delivery systems. *J Occup Med Toxicol.* 2007;2:16.
365. Senapati S, Mahanta AK, Kumar S, Maiti P. Controlled drug delivery vehicles for cancer treatment and their performance. *Signal Transduct Target Ther.* 2018;3:7.
366. Frank A, Eric M P, Robert L, Omid C F. Nanoparticles Technologies for Cancer Therapy. *Handb. Exp. Pharmacol.* 2010.
367. Desai N. Nanoparticle Albumin-Bound Paclitaxel (Abraxane®). *Albumin Med Pathol Clin Appl.* 2016. p. 101–19.
368. Sparreboom A, Scripture CD, Trieu V, Williams PJ, De T, Yang A, et al. Comparative preclinical and clinical pharmacokinetics of a cremophor-free, nanoparticle albumin-bound paclitaxel (ABI-007) and paclitaxel formulated in Cremophor (Taxol). *Clin Cancer Res.* 2005;11:4136–43.
369. Green MR, Manikhas GM, Orlov S, Afanasyev B, Makhson AM, Bhar P, et al. Abraxane®, a novel Cremophor®-free, albumin-bound particle form of paclitaxel for the treatment of advanced non-small-cell lung cancer. *Ann Oncol. Elsevier Masson SAS;* 2006;17:1263–8.
370. Ma P, Mumper RJ. Paclitaxel nano-delivery systems: A comprehensive review. *J Nanomedicine Nanotechnol.* 2013;4:6.
371. Alakhova DY, Kabanov A V. Pluronic and MDR reversal: An update. *Mol Pharm.* 2014;11:2566–78.
372. Chowdhury P, Nagesh PKB, Kumar S, Jaggi M, Chauhan SC, Yallapu MM. Pluronic Nanotechnology for Overcoming Drug Resistance BT - Bioactivity of Engineered Nanoparticles. In: Yan B, Zhou H, Gardea-Torresdey JL, editors. Springer Singapore; 2017. p. 207–37.
373. Batrakova E V, Kabanov A V. Pluronic block copolymers: evolution of drug delivery concept from inert nanocarriers to biological response modifiers. *J Control Release.* 2008;130:98–106.
374. Batrakova E V., Li S, Elmquist WF, Miller DW, Alakhov VY, Kabanov A V. Mechanism of sensitization of MDR cancer cells by Pluronic block copolymers: Selective energy depletion. *Br J Cancer.* 2001;85:1987–97.

375. Batrakova E V, Kelly DL, Li S, Li Y, Yang Z, Xiao L, et al. Alteration of genomic responses to doxorubicin and prevention of MDR in breast cancer cells by a polymer excipient: pluronic P85. *Mol Pharm*. 2008;3:113–23.
376. Alakhova DY, Zhao Y, Li S, Kabanov A V. Effect of doxorubicin/pluronic SP1049C on tumorigenicity, aggressiveness, DNA methylation and stem cell markers in murine leukemia. *PLoS One*. 2013;8:e72238.
377. Lujambio A, Esteller M. How epigenetics can explain human metastasis: A new role for microRNAs. *Cell Cycle*. 2009;8:377–82.
378. Rodenhiser DI. Epigenetic contributions to cancer metastasis. *Clin Exp Metastasis*. 2009;26:5–18.
379. Sharma S, Kelly TK, Jones PA. Epigenetics in cancer. *Carcinogenesis*. 2009;31:27–36.
380. Yu J, Qiu H, Yin S, Wang H, Li Y. Polymeric drug delivery system based on pluronics for cancer treatment. *Molecules*. 2021;26:1–23.
381. Miele E, Spinelli GP, Miele E, Tomao F, Tomao S. Albumin-bound formulation of paclitaxel (Abraxane ABI-007) in the treatment of breast cancer. *Int J Nanomedicine*. 2009;4:99–105.
382. Gradishar WJ. Albumin-bound paclitaxel: a next-generation taxane. *Expert Opin Pharmacother*. Taylor & Francis; 2006;7:1041–53.
383. Kim SC, Kim DW, Shim YH, Bang JS, Oh HS, Wan Kim S, et al. In vivo evaluation of polymeric micellar paclitaxel formulation: toxicity and efficacy. *J Control Release*. 2001;72:191–202.
384. Lee KS, Chung HC, Im SA, Park YH, Kim CS, Kim S-B, et al. Multicenter phase II trial of Genexol-PM, a Cremophor-free, polymeric micelle formulation of paclitaxel, in patients with metastatic breast cancer. *Breast Cancer Res Treat*. 2008;108:241–50.
385. Saif MW, Podoltsev NA, Rubin MS, Figueroa JA, Lee MY, Kwon J, et al. Phase II clinical trial of paclitaxel loaded polymeric micelle in patients with advanced pancreatic cancer. *Cancer Invest*. 2010;28:186–94.
386. Park IH, Sohn JH, Kim SB, Lee KS, Chung JS, Lee SH, et al. An open-label, randomized, parallel, phase III trial evaluating the efficacy and safety of polymeric micelle-formulated paclitaxel compared to conventional Cremophor EL-Based paclitaxel for recurrent or metastatic HER2-negative breast cancer. *Cancer Res Treat*. 2017;49:569–77.
387. Barbosa AM, Martel F. Targeting Glucose Transporters for Breast Cancer Therapy: The Effect of Natural and Synthetic Compounds. *Cancers (Basel)*. 2020;12.
388. Varma MVS, Panchagnula R. Enhanced oral paclitaxel absorption with vitamin E-TPGS: effect on solubility and permeability in vitro, in situ and in vivo. *Eur J Pharm Sci*. 2005;25:445–53.
389. Neophytou CM, Constantinou C, Papageorgis P, Constantinou AI. D-alpha-tocopheryl polyethylene glycol succinate (TPGS) induces cell cycle arrest and apoptosis selectively in Survivin-overexpressing breast cancer cells. *Biochem Pharmacol*. 2014;89:31–42.

